Pharmacological and Functional Regulation of Two-Pore Domain Potassium Channels

Louisa-Jane Ping Ping Evans

A thesis submitted in the fulfilment of the requirements for the degree of Doctor of Philosophy of the University of London and the Diploma of Imperial College London

October 2007

Biophysics Section

Blackett Laboratory

Imperial College

London

SW7 2AZ

BRITISH LIBRARY

IMAGING SERVICES NORTH

Boston Spa, Wetherby
West Yorkshire, LS23 7BQ
www.bl.uk

ORIGINAL COPY TIGHTLY BOUND

BRITISH LIBRARY HSIL

IMAGING SERVICES NORTH

Boston Spa, Wetherby
West Yorkshire, LS23 7BQ
www.bl.uk

PAGINATED BLANK PAGES ARE SCANNED AS FOUND IN ORIGINAL THESIS

NO INFORMATION IS MISSING

Abstract

Two pore domain potassium (K2P) channels underlie the background potassium leak currents of excitable cells. In this study, the whole cell patch clamp technique was used with transiently transfected human embryonic kidney cells, and cerebellar granule neurones (CGNs) in primary culture, to compare the pharmacological properties of acid sensitive K2P channels.

Zn^{2+}, La^{3+}, Cu^{2+}, ruthenium red and Ru-360 blocked TASK-1 and TASK-3 channel currents. Substitution of external sodium ions with N-methyl-D-glucamine and choline also caused a significant reduction in TASK-1 and TASK-3 currents, demonstrating that maximal conductance through these potassium channels requires the presence of external sodium ions.

Whilst Cu^{2+} blocked TASK-1 and TASK-3 channel currents, TASK-2 currents were not affected by the ion. Mannitol, a scavenger of hydroxyl radicals, did not alter Cu^{2+} block of TASK-3 currents showing hydroxyl radical production was not the underlying mechanism. Application of thiol oxidant, DTNB (5',5'-dithio-bis(2 nitrobenzoic acid)), showed a potent block, mimicking that of Cu^{2+} in size and reversibility. DTNB and Cu^{2+} block were reversed by disulphide-reducing DTT (dithiothreitol), suggesting thiol rich cysteine residues played a fundamental role in TASK-3 current block by Cu^{2+}. The standing-outward, voltage-insensitive potassium current in CGNs also showed DTNB and copper sensitivity.

Substitutions of TASK-3 cysteine residues to alanine and serine retained copper sensitivity while whole cell current amplitude diminished and a sensitivity to alkaline

pH (8.4) was introduced to TASK-3. Point mutation of cysteine 110 was found to be key in facilitating the pH 8.4 potentiation of current. Cu^{2+} and DTNB were applied to a TASK-2/TASK-3 chimera channel where a robust, albeit reduced, block was observed.

The central role of the TASK channels in neuronal excitability is demonstrated by their extensive physiological and cross-species distribution and varied mechanisms of regulation. In this study, the interaction of essential trace element Cu^{2+} was shown to be a significant mechanism of TASK regulation.

In memory

Grandmother

Ione Merle Evans

(1919 – 2007)

&

Mother-in-Law

Yvonne Murphy

(1951 – 2004)

Inspiring women who are sorely missed.

Acknowledgements

Firstly, I must thank all of the members of my lab' that have taught and supported me so much, particularly during the writing of this thesis: Alistair Mathie, my supervisor, Emma Veale, research assistant and patch-clamper extraordinaire, and Louise Kennard my sometime partner in crime. Thanks also go to Stephen Brickley, my second supervisor, and Damian Bright, for bring patient and brilliant at explaining things when I interrupted with queries unannounced and Raquel Yustos for her technical expertise and support throughout the study.

I would also like to thank Sarah Hopwood for making me laugh so much I cried nearly every time I was with her, Stefan Trapp for his terrible jokes and even worse taste in music and lab' members, Anna Zecharia, Ale Caley, Christian Robledo, Sadaf-Ahmahni Hussain, Mark Coburn and Isabelle Andres Enguix for making my time in the Biophysics Section both memorable and enjoyable.

My acknowledgements are not complete without the mention of my husband, Christian Murphy, who has not only bank-rolled the thesis writing period but has been an unwavering support and source of discipline throughout the course of the PhD, for which he has my unending gratitude.

Table of Contents

Table of Figures

1 Introduction

1.1 Ion channels - Mediators of neuronal excitability

The cell membrane comprises a phospholipid bilayer in which, and attached to which, protein molecules serve different functions in maintaining the living cell and communicating with its environment. The integral proteins can be mobile within the plane of the membrane, traverse both leaflets, while others, embedded only within one membrane layer, may flip from one to the other. Since Singer and Nicolson first proposed the 'fluid mosaic model' of membrane structure (Singer & Nicolson, 1972), there have been a number of refinements; proteins have been found to be less randomly dispersed across the cell membrane than initially proposed, more densely packed, with the bilayers varying in thickness (Figure 1-1) (Engelman, 2005).

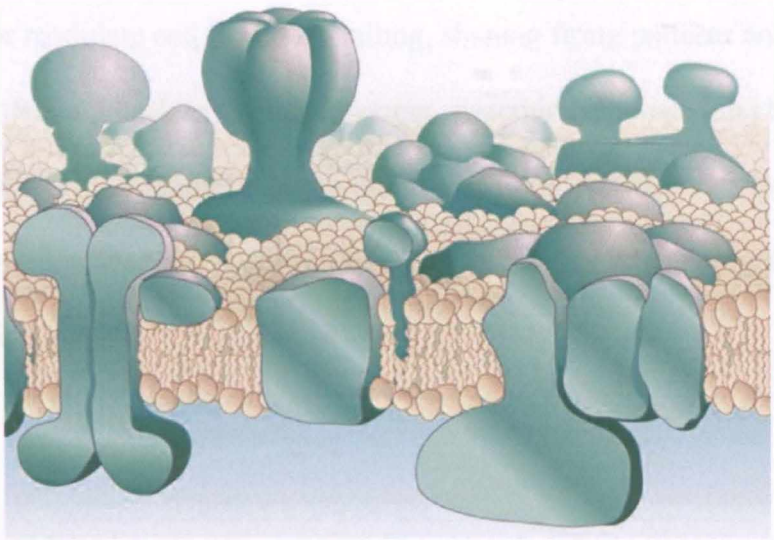

Figure 1-1 Fluid-mosaic model of the plasma membrane *(From Engelman, 2005)* The more sparsely populated phospholipid bilayer has become more densely packed with a greater number of associated proteins and integral protein complexes than the original membrane structure proposed by Singer and Nicholson in 1972.

Ion channels are an example of integral proteins that allow the passage of ions across the membrane. They form water filled pores that can be open or shut and are the fundamental elements of the excitable cell (Hille, 2001; Aidley, 1998). The two key functional features of the ion channel are its gating properties and its selectivity. Gating of ion channels varies greatly; some open in response to changes in the voltage across the membrane (voltage gated ion channels), while others are opened by intracellular or extracellular combination (or binding) with various molecules (ligand gated ion channels) while others still may respond to mechanical stimuli (e.g. stretch) or physicochemical factors (e.g. pH). Non-gated channels that are always open also exist and these contribute significantly to the resting potential.

As with the gating, so a range of selectivity can be demonstrated with ion channels. The most selective permit only particular ions to pass through, while others will admit the general passage of broad groups of ions. This broad spectrum of ion channels confers a great flexibility in the response of the excitable cell. Multiple stimuli can initiate or modulate cell to cell signalling, shaping firing patterns and strength of neurons, feeding back to the macroscopic, systemic response. Ion channels also play an important role in signal transduction; amplifying cell response by facilitating a messaging cascade (e.g. G protein linked channels), or attenuating a signal (e.g. desensitization).

The action potential and membrane permeability

The electrical nature of nerve impulse was first demonstrated experimentally by Luigi Galvani in 1791 (Verkhratsky *et al.*, 2006). Using a preparation of a connected spinal cord and lower limbs of a frog, he demonstrated a relationship between stimulus intensity and muscle contraction that ended in saturation (a plateau of contraction force of muscle occurred with increasing intensity of stimulus) and exhibited refraction (repeated stimulation eventually stopped inducing contraction). He was also able to demonstrate conduction of the nerve impulse when, having fixed two preparations together by means of their sciatic nerves, contraction in both sets of limbs could be elicited by stimulation of the nerve of the first preparation. To describe his data, Galvani postulated the existence of water-filled channels that penetrated the surface of the nerve fibres and allowed electrical excitability by the movement of accumulated positive and negative charges on the internal and external surfaces of the nerve and muscle.

The first action potential was recorded by Julius Bernstein in 1868 (Figure 1-2) with the nerve interior being 60mV more negative than the exterior. It was over 30 years later (1902) that he applied the electrolytic theory of Walther Nernst[1] to ions across a semi permeable membrane (Seyfarth, 2006). He hypothesized that the potassium permeability of the membrane was likely to underlie the generation of the negative

[1] The Nernst equation describes a relationship between ionic equilibrium potentials (E) and ion concentration ratio. For an ion, X, it is written;

$$E_X = \frac{RT}{zF} \ln \frac{[X]_2}{[X]_1}$$

Where R = the gas constant (8.314 $JK^{-1}mol^{-1}$), T = absolute temperature (K), z = charge number for that ion, and F is the Faraday constant (96500 C mol^{-1}). $[X]_2$ and $[X]_1$ are the activities or concentrations of ion X in two compartments. Physiological convention dictates for cations that 2 is outside (extracellular) while 1 is inside (intracellular), and all membrane potentials are to be measured inside minus outside.

resting potential for two reasons. He applied the equation to the variety of known concentrations of inorganic substances inside and outside of nerves and found that the electrical ('equilibrium', *E*) potentials predicted for the potassium gradients lay closest to his experimental observations. He also found that the current in both nerve and muscle of a frog leg preparation increased linearly with temperature, also predicted by Nernst.

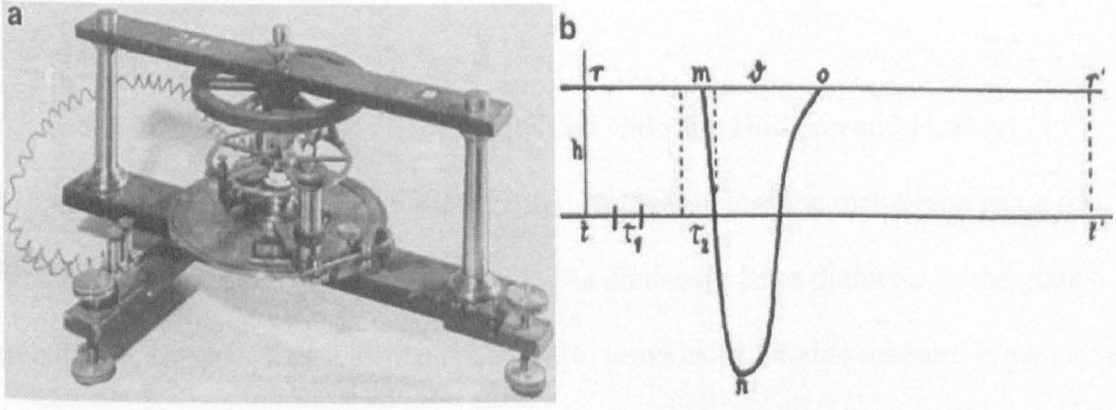

Figure 1-2 The apparatus and trace of the first recorded action potential *(Adapted from Verkhratsky et al., 2006)* (a) shows the recording apparatus, the Bernstein rheotome. Briefly, a rotating cam closes a circuit for electrical stimulation of nerve or muscle via two electrodes. A second circuit, in which a galvanometer is connected to a pair of recording electrodes, is closed as the wheel spins round, recording 'negative variation' after stimulation. The speed of the spinning wheel determines sampling interval. (b) The recorded action potential. τ_1 and τ_2 indicate sampling intervals, *n* is the 'sign reversal', *m* and *o* indicate the duration of the action potential while *v* is the point of *n*, the negative '*Schwankung*' (fluctuation).

Bernstein's 'membrane hypothesis' was the first plausible physico-chemical model of bio-electrical events. It described the dependency of the membrane potential on the differential distribution of positively charged ions across the membrane with positively charged ions being at a high concentration in the cytoplasm and lower outside the cell, and attributed excitation to the passage of those ions through the membrane, so losing the internal negativity (Hille, 2001).

In 1939, Kenneth Cole and Howard Curtis used extracellular electrodes to measure impedance in axons isolated from the giant squid, *Loligo pealii* (Cole & Curtis, 1939).

They found that each action potential was accompanied by a dramatic decrease in impedance corresponding to a 40-fold increase in membrane conductance without a significant change in membrane capacity. This fitted well with Bernstein's membrane theory and they hypothesized that if the conductance was a reflection of membrane permeability, then the change in the membrane properties upon excitation must be 'delicate' if it occurred homogeneously across the entire membrane or, tantalizingly, "it must be confined to a very small area" (Hille, 2001).

Around the beginning of the 1940s, Curtis and Cole and Hodgkin and Huxley independently began to analyse the potential changes across the membrane using the first intracellular electrodes (Hille, 2001). The unusually large diameter of the giant squid axon, described by J. Z. Young in 1936, provided a suitable medium in which to investigate the action potential more clearly.

A glass capillary tube, 100μm in diameter, was filled with a salt solution. For Hodgkin and Huxley this was sea water, for Curtis and Cole, this was a potassium salt solution isotonic with sea water. The tissue was also bathed in sea water. The electrode was inserted into the cut end of an axon until it was sufficiently far from the damaged end, and, while external electrodes electrically stimulated the axon, the potential difference between an electrode in the bathing solution and the intracellular electrode was recorded.

The resultant trace showed unexpected results. The resting potential arose from a negative voltage measurement intracellularly, in line with Bernstein's original paper. However, during the action potential, the internal electrode measured an increase that

rose above 0mV, unlike that which had been predicted by the original theory where the membrane was expected to become permeable to all ions.

In 1949, Hodgkin and Huxley returned to equilibrium potentials predicted by Nernst, in the context of the resting membrane potential (E_{mem}). $E_{mem,}$ was not equal to the equilibrium potential for sodium (E_{Na} = +55mV) or potassium (E_K = -75mV), but lay somewhere in between (-60mV, from squid axon data after Hodgkin, 1958- Aidley, 1998). D. E. Goldman, in 1943, had developed an adaptation of the Nernst equation for determining membrane potential when it is permeable to more than one ion. This was known as the constant field theory, commonly known now as the Goldman-Hodgkin-Katz equation;

$$E = \frac{RT}{zF} \ln \frac{P_K[K^+]_o + P_{Na}[Na^+]_o + P_{Cl}[Cl^-]_i}{P_K[K^+]_i + P_{Na}[Na^+]_i + P_{Cl}[Cl^-]_o}$$

Where 'P_x' is the ion's permeability constant. Hodgkin and Huxley assessed the changes in E_{mem} in response to altered external ion concentrations and discovered that the order of relative permeabilities of the resting membrane to the three ions was:

$$P_K > P_{Cl} >> P_{Na} = 1: 0.45: 0.04$$

While the membrane permeabilities at the peak of the action potential were ordered:

$$P_{Na} >> P_K > P_{Cl} = 20 : 1 : 0.45$$

Making the most significant ion at the peak of the action potential sodium (hence 'sodium' theory) instead of potassium, and moving E_{mem} towards E_{Na} (+55mV). Several follow up experiments validated the theory; removal of external sodium ions prevented the generation of action potential, reduction in sodium decreased the amplitude of the action potential and increasing external sodium had the opposing effect.

The end of the 1940s brought with it the most significant technological advance in the field; the development of the voltage clamp. An assessment of the changing permeabilities of the membrane to sodium and potassium ions necessitated a technique that could facilitate the dissection of the currents at any given voltage. Until then any change in the membrane potential was accompanied by an ion flow that in turn, altered the membrane potential- posing a problem for the early electrophysiologists when trying to assess the voltage dependency. Cole and colleagues overcame this with the voltage clamp technique in 1949 (Aidley, 1998). He designed an electronic feedback system that held the membrane potential constant by injecting a compensating current that matched that of the transmembrane ion movement. Early forms of this negative feedback loop consisted of two electrodes each connected to an amplifier one measuring transmembrane voltage and the other passing current. A feedback amplifier joined the two systems and compared the voltage set (V_{CMD} – command voltage) to the measured membrane voltage (V_m). The difference between the two (known as the error signal) drove the feedback system to inject current via the current passing electrode, keeping the error signal as close to zero as possible. In this setup, the current injected is therefore equal to the macroscopic current flowing across the membrane (I) and consequently, the command voltage controlled by the experimenter is the same as the transmembrane voltage and the voltage dependency of the macroscopic, whole cell current could be quantified.

Hodgkin and Huxley used this technique to great effect and in 1952 published a series of papers (Hodgkin & Huxley, 1952 a-f) that detailed the current and voltage relations

that made up the action potential. This model, now known as the Hodgkin and Huxley model, was developed from a crucial concept- by replacing or changing concentrations of ions in the external solution, currents across the membrane could be separated into their constituent ionic components. Further to this, as the ions seemed only to move down their electrochemical gradients, by using the Nernst equation and the known ion concentrations internally and externally, the direction of the net movement of a particular ion could be predicted at a given membrane potential.

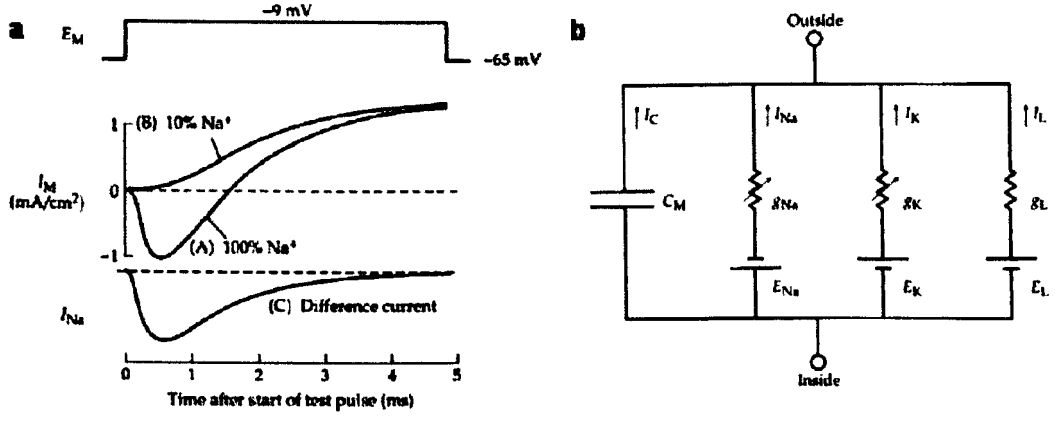

Figure 1-3 Currents of the action potential (a) Ion substitution was used to distinguish sodium and potassium currents from squid giant axon; (A) shows action potential while axon was bathed in seawater, (B) 90% of bathing sodium chloride replaced by choline chloride (low sodium) (C) An algebraic subtraction of (B) from (A) leaves the 'difference current', the potassium contribution. (b) Equivalent circuit of an axon membrane as described by the Hodgkin and Huxley model. C_m = the membrane capacitance; the lipid of the bilayer acts as an electrical insulator between two conducting 'surfaces', the intracellular and extracellular media, I_x = ionic current through the membrane, g_x = ion conductance of membrane, E_x = electromotive force for ion, provided by the electrochemical gradient of the ion across the membrane. $_L$ = leak (described as a miscellaneous cation leak by Hodgkin and Huxley (1952e) The variable resistors labelled g_{Na} and g_K represent the voltage and time sensitivity of these conductances. g_L denotes the standing outward cation leak current, which is both voltage and time insensitive. *Figure adapted from Hille, 2001, after Hodgkin and Huxley 1952e and 1952b)*

Voltage clamp studies in the squid giant axon were immediately illuminating (Figure 1-3). Hodgkin and Huxley depolarised the squid axon membrane by 56mV to -9mV. The resultant action potential was recorded under two conditions, (a) with the axon in sea water and (b) in 10% sea water with 90% isotonic choline chloride solution. At -9mV E_{mem} is closer to E_{Na} which decreases the sodium current to a minimum. When

combined with a low external sodium concentration, the electromotive force driving the sodium influx is close to zero, thus only leaving the outward potassium current recorded (Figure 1-3(a) Trace B. With E_{mem} not equal to E_{Na}, it had to be assumed that the small sodium current remaining was a constant fraction of full Na^+ influx in order to make it possible to calculate the K^+ currents). An algebraic subtraction was made of the low sodium trace from the original trace. With the former being representative of the potassium ion movements (outward), the 'difference current' showed the sodium ion movements, inwards (negative deflection) before automatically decreasing after a delay. Thus the action potential was shown to comprise a rapid increase in sodium conductance (inwards), followed by a slow decrease in sodium conductance (sodium inactivation) with a slow increase in potassium conductance (outwards) (Aidley, 1998).

We now know that the channels underlying the action potential conductances are the voltage gated sodium and potassium channels. The longer lasting outward current is the delayed potassium current so named for its slow increase in size. The faster component is mediated by the voltage gated sodium channel. The time sensitivity of this channel brings about inactivation, capping sodium conductance after the inward current strongly depolarizes the membrane, bringing its potential closer to E_{Na}. Repolarisation is brought about by potassium efflux through leak channels (voltage insensitive standing outward current) as well as through their voltage-gated counterparts. This tandem of pathways for potassium efflux speeds up repolarisation and with an electro-motive force generated by the electrochemical gradients of K^+, drives an overshoot, a hyperpolarisation. This in turn accelerates the inactivation of

the voltage gated potassium channels and as the larger conductances diminish, the standing outward potassium currents dominate, returning the membrane potential to its resting voltage near E_K.

Hodgkin and Huxley defined their model in terms of Ohm's law ($V = IR$, Figure 1-3), including the role of the potassium leak current. The membrane bilayer was modelled as an insulating layer between two conductors, the intracellular and external solutions. The driving force of the currents, represented by batteries, is derived from the electrochemical gradients of the ions across the membrane, while the conductance of the ions dependent on membrane voltage and time are represented by variable resistors. The potassium leak current driven only by the ion distribution across the membrane was modelled with a constant conductance.

The late 70's and early 80's brought a further leap in the field of electrophysiology with the development of the patch-clamp technique by Neher and Sakmann. Using fire polished glass pipettes they were able to record currents moving across a patch of membrane. They found that a high resistance giga-ohm seal could be formed between the cell membrane and the glass micropipette greatly increasing the mechanical stability of the recording set-up and facilitating new configurations with which to test ion channel activity (Hille, 2001).

In 1976 they reported the first single channel recordings of an acetylcholine activated channel (Neher & Sakmann, 1976), followed, in 1981, with a breakthrough paper outlining the gigaseal patch-clamping technique (Hamill *et al.*, 1981). The new

technique facilitated new recording configurations with which to measure currents under test solutions; the stability of the system allowed the sealed patch of membrane to be pulled from the cell with its internal surface being continuous with either the internal surface of the pipette (outside-out, see Figure 1-4) or with the bathing solution (inside-out).

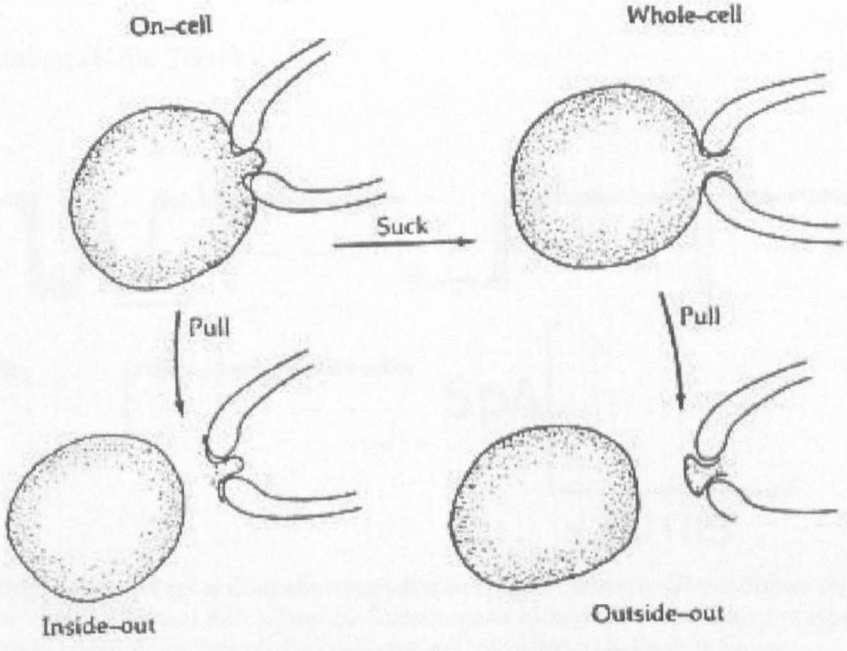

Figure 1-4 Four patch clamp microeclectrode pipette configurations *(From Hille, 2001)*

On-cell recordings or cell attached patch recordings were made with the micropipette sealed against the cell membrane, the membrane potential being controlled by a voltage clamp. Whole cell recordings, such as those used in this study, could also be made with the rupture of the cell membrane at the pipette tip while keeping the remainder of the cell intact.

These techniques have now become the mainstay of the electrophysiology toolkit. The significant advantages of the patch clamp method lie in the ability to access and control the ionic contents within the cell as well as its external bathing solutions. It also facilitates the recording of unitary current steps carried by single channels

revealing both the abrupt "on" and "off" of current flow (Figure 1-5). We now associate these current patterns with ion channel gating. It was found that depolarizing steps elicited different patterns of openings so the kinetic description of this stochastic channel gating had to be altered to terms of open probabilities. Summation of multiple records showed the smoother traces akin to those seen by Hogkin and Huxley and the current amplitudes of a single channel (several picoamperes) necessitated an aqueous pore mechanism (Hille 2001).

Figure 1-5 Single channel recording showing sample channel activity *(From Sigworth, F. J., Chapter 14 in 'Single Channel Recording' by Sakmann and Neher)* The ion channel is closed when the trace is 'up' and current flows though the open channel, recorded as a dip in the trace.

Structural and biophysical information continues to be forthcoming with this technique and coupled with advances in molecular biology, newly discovered channels (such as the two pore domain potassium channels analysed here) are being characterised to a greater depth and at a faster rate than ever before. In 1991 Neher and Sakmann received a Nobel Prize "for their discoveries concerning single ion channels in cells", following their academic fore-fathers Hodgkin and Huxley, who shared the Nobel Prize in Physiology or Medicine in 1963 "for their discoveries concerning the ionic mechanism ... of the nerve cell membrane" (Hille 2001).

1.2 The potassium channel family

The interplay of Na^+, Ca^{2+}, Cl^- and K^+ ions in modulating the firing behaviour of the excitable cell was demonstrated from the earliest voltage clamp studies (see 1.2), with a significant role for the transmembrane conductance of K^+ being initially proposed by Bernstein in his studies of 1902 (Hille, 2001, see 1.1).

The key structural components of the potassium channel family members are two transmembrane helices (2TM) interconnected by a loop of amino acids that dips into the membrane known as the P loop (Choe, 2002). The pore forming subunit is also referred to as the α subunit. Auxillary (β) subunits may also interact with the pore forming subunits to modify its function.

The P loop contains the highly conserved selectivity filter, a 'signature sequence' of five amino acids, TXGXG (where T represents threonine, G, Glycine, and X is usually a valine residue following the threonine and a tyrosine residue between the glycines, but can also be other amino acids) (Doyle *et al,* 1998). The functional potassium channel has a tetrameric formation (MacKinnon, 1991), with the TXGXG residues of 4 P loops coming together, lining the narrowest part of the pore which functions as a selectivity filter, facilitating the permeation of K^+ over other ions (Miller, 2000).

The mechanism of the K^+ channel selectivity and permeation has recently been elucidated following the crystallisation of the bacterial KcsA channel from *Streptomyces lividans* (Doyle *et al,* 1998). The TXGXG residues of the selectivity filter extend carbonyl groups into the pore. Before the selectivity filter is a water filled cavity into which the K^+ ions can readily pass, owing to the hydrophilic environment.

The carbonyl groups of the selectivity filter residues are arranged in such as way as to mimic the coordination of water molecules to the K^+ ion in its hydrated form, as would be present in the cavity. As the ions approach the pore, the coordinated water molecules are substituted for a coordination with the pore's carbonyl groups. Electrostatic repulsion of one coordinated K^+ ion with the next, in combination with the K^+ concentration gradient across the membrane, drives the ions from one carbonyl group to the next, through the rest of the pore. The alignment of the carbonyl groups is essential for the specific permeation of K^+ ions. The dehydrated Na^+ ion, for example, is too small to coordinate with the extended carbonyl groups (Doyle *et al*, 1998). Further, as the association of K^+ with the carbonyl groups is as energetically favourable as association with water molecules, the rate passage of the ion through the membrane remains close to the free diffusion limit (Doyle *et al*, 1998).

The K^+ channels are very diverse, occurring across phyla, in every fully sequenced genome to date, suggesting a very early evolution (Miller, 2000). Over 80 mammalian genes for K^+ subunits have been identified (Hille, 2001) since the cloning of the first potassium channel in 1987 (Jan and Jan, 1987). The 'superfamily' of potassium channels can be divided into three families by the amino acid sequences of their pore - forming α subunits. The most basic of channel subtypes are the inward-rectifier K^+ channels with two transmembrane (2TM) domains per subunit. The K^+ current flow mediated by these channels is blocked at depolarised potentials by intracellular polyamines (such as spermine and spermidine) and or Mg^{2+} ions. K^+ currents of these channels increase with hyperpolarisation. The bacterial KcsA channel, recently structurally resolved using an X-ray analysis by Mackinnon and others at Rockefeller University, has this basic 2TM and single pore structure (Doyle, 1998).

K^+ channels with six transmembrane domains (6TM) mediate outward K^+ currents at depolarised membrane potentials as well as outward Ca^{2+} dependent K^+ currents. The transmembrane helices are labelled S1-6, with the P loop between S5 and S6. S4 contains a number of positively charged amino acid residues that act as a voltage sensing region. The currents these channels facilitate include delayed rectifier (K_V) K^+ currents, which inactivate slowly after activation at depolarised potentials and transient currents (e.g. 'K_A' currents), which inactivate quickly after activation, also at depolarised membrane potentials. K^+ currents activated after an increase of Ca^{2+} inside the cell (e.g. 'BK' currents) as well as those inhibited by activation of muscarinic acetylcholine receptors ('M' currents) are also mediated by 6TM configured K^+ channels.

The K^+ channels of particular interest to this study have four transmembrane domains (4TM). These 4TM channels are known as the tandem or two-pore channels as they have two basic subunits (one P loop between two transmembrane helices) in tandem at the subunit level. Unusual among the K^+ channels, the subunits come together as dimers to form functional potassium channels, the two pore domains of both arranged in the tetrameric formation of the selectivity filter. The currents mediated by these channels are known as K^+ leak currents as the channels are open at all membrane potentials and, as a consequence, determine the resting membrane potential of the excitable cell.

1.3 Two pore domain potassium channel family

A new type of potassium channel

Despite the early identification of a central role for a standing outward potassium conductance, a molecular correlate remained, until recently, undiscovered. In 1995 however, the first two-pore domain potassium channel exhibiting a potassium current with biophysical characteristics matching those discussed in earliest models of the resting membrane potential.

The channel, TOK1 (**T**wo pore domain **O**utwardly rectifying $\mathbf{K}^+$ channel-**1**), was identified by searching the *Saccharomyces cerevisiae* DNA databases for sequences homologous to the pore sequence conserved across many K^+ channels (Ketchum *et al.*, 1995). It was the first potassium channel that had two pore domains in a single polypeptide sequence. With a length of 691 amino acids, the sequence also bore 8 transmembrane regions and when heterologously expressed in *Xenopus laevis* oocytes, TOK1 currents were outwardly rectifying, preferentially passing outward potassium currents determined by extracellular potassium concentrations. The identification of a second two pore domain potassium channel, d-ORK1 (**d**rosophila **O**pen **R**ectifier $\mathbf{K}^+$ channel), soon followed (Goldstein *et al.*, 1996). Isolated from *Drosophila melanogaster*, this channel exhibited open rectifying (leak) currents, but only 4 transmembrane regions. To date, TOK1 has been the only two pore domain potassium channel that has 8 transmembrane regions.

The first human two-pore domain potassium channel to be found was identified again using P domains of potassium channels with the BLAST sequence alignment program with the GenBank database (Lesage *et al.*, 1996). This channel had inwardly rectifying potassium currents, a 4TM/2P (4 transmembrane and 2 pore region) arrangement, and was 336 amino acids long. Due to its structure and biophysical characteristics it was named TWIK-1 (**T**andem pore **W**eak **I**nward rectifying $\mathbf{K}^+$ channel). Hydrophobicity analysis of the polypeptide revealed the two pore regions to be inserted into the membrane from the outside with intracellular amino and carboxy terminals (Figure 1-6), with an extended large loop of 59 amino acids between M1 and P1 that contained one potential glycosylation site.

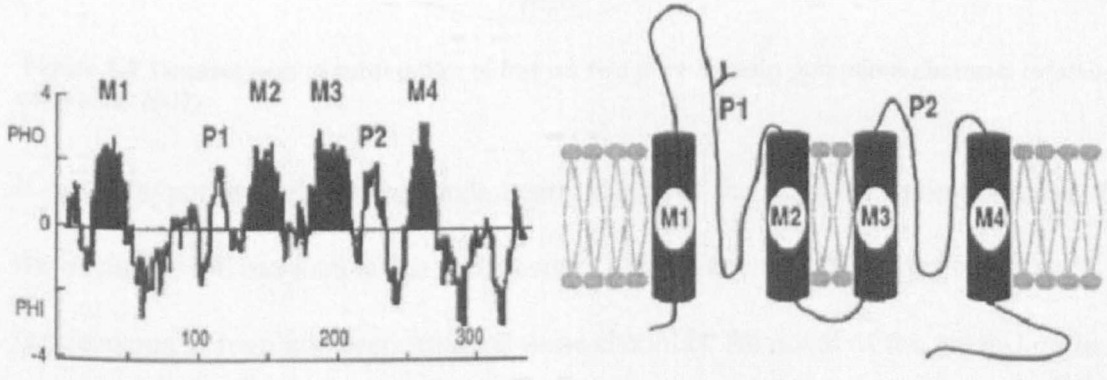

Figure 1-6 Hydrophobicity analysis derived structure of TWIK-1 *(Adapted from Lesage et al, 1996)* Hydrophobicity values were plotted against amino acid position revealing 4 transmembrane regions (denoted M1-4), intracellular amino and carboxy terminals and two pore regions P1 and P2 that dip into the membrane from the extracellular side, formed by regions of the M1M2 and M3M4 loops.

To date, 15 two-pore domain potassium channels have been identified. They have been divided into six structural subfamilies, the TWIK, THIK, TRESK, TREK, TALK and TASK subfamilies (Figure 1-7), and a recent revision of the nomenclature designated the prefix *K2P1.1* for mammalian gene names (Goldstein *et al.*, 2005; Talley *et al.*, 2003).

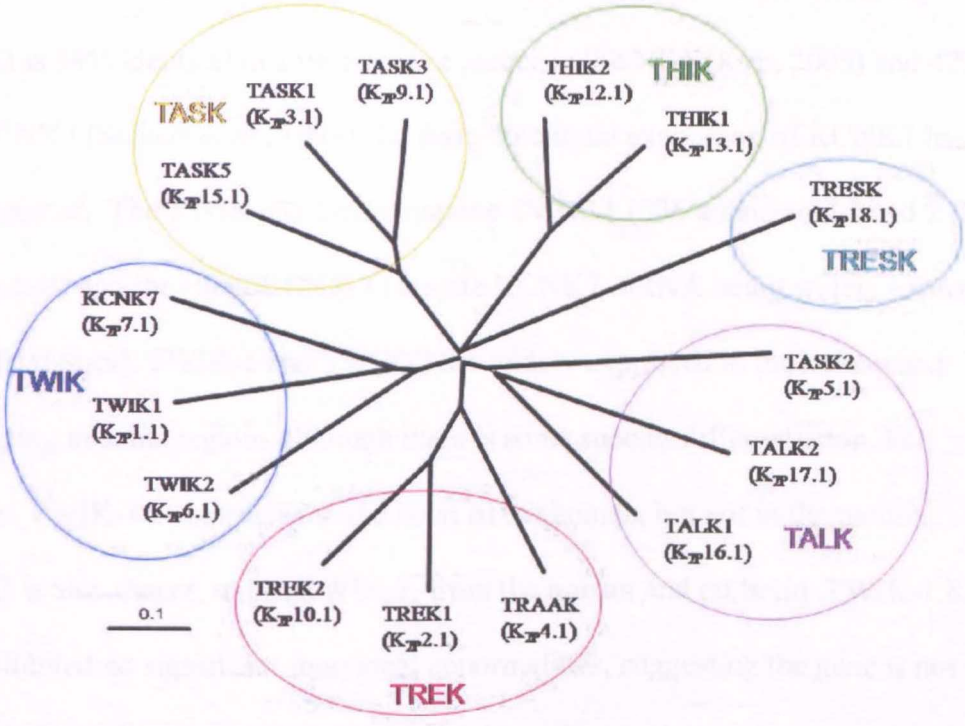

Figure 1-7 Dendrogram of subfamilies of human two pore domain potassium channels *(Mathie and Veale, 2007)*

It can be hypothesized that the fundamental nature of the negative resting potential for the excitable cell has lead to the evolutionary development of the very diverse mechanisms of regulation reported for these channels. Removal of the potassium leak current by blocking the two pore domain potassium channel leads to a depolarization of the cell, moving the membrane potential away from E_K, towards the threshold for action potential firing, therefore increasing cell excitability. Various forms of modulation of these channels continue to be investigated, to date the list includes neurotransmitters, physicochemical stimuli such as pH, temperature, oxygen tension and osmolarity to clinical compounds such as anaesthetics (Talley *et al.*, 2003).

1.3.1 TWIK subfamily

TWIK-1 has now been joined by TWIK-2 and KCNK7 in the TWIK subfamily. TWIK-2 is 54% identical in amino acid sequence to TWIK-1 (Kim, 2005) and 42% with KCNK7 (Salinas *et al.*, 1999). To date, functional expression of KCNK7 has yet to be reported. The TWIK channels comprise TWIK-1 (336 amino acids) and 2 (313 amino acids) and the silent KCNK 7 (despite KCNK7 mRNA being widely expressed in human tissues). TWIK-1 and TWIK-2 are widely expressed in the human and overlapping in some regions although there is some species differentiation. For example, TWIK-1 is expressed in the heart of the human, but not in the mouse. TWIK-2 is also absent, unlike TWIK-1, from the human and rat brain. TWIK-1 K/O mice exhibited no significant functional abnormalities, suggesting the gene is not essential although some renal dysfunction lead to abnormal phosphate retention in a low phosphate diet (Aller *et al.*, 2005; Lesage & Lazdunski, 2000; Arrighi *et al.*, 1998; Lesage *et al.*, 1997; Orias *et al.*, 1997; Lesage *et al.*, 1996).

TWIK-1 and TWIK-2 currents are hard to distinguish, with conflicting properties being reported (Rajan *et al.*, 2005; Lesage *et al.* 1996, 1997). Furthermore the lack of clarity in the literature means that the channels' currents are hard to separate from other K2P channels properties.

One particular characteristic of TWIK channels is unclear. TWIK-1 was reported to have small inwardly rectifying currents at its initial identification (Lesage *et al.*, 1997, 1996), a property shared by TWIK-2 (Chavez *et al.*, 1999). Later analysis (Rajan *et al.*, 2005) indicated that hTWIK-1 currents could be greatly increased when it was prevented from conjugating with a small Ubiquitin-like polypeptide, SUMO. De-

SUMOylation (through mutation (K274E/R) or proteolytic action) of channels elicited openly rectifying currents, in contrast to the initial characterisation. They were also sensitive to extracellular pH (Rajan *et al.*, 2005) unlike their unmodified counterparts (Lesage *et al.*, 1997, 1996). Very recently, the importance of SUMOylation/de-SUMOylation of TWIK-1 channels has been questioned (Feliciangeli *et al.*, 2007).

hTWIK-2 has also proved controversial with studies reporting that Ba^{2+} and quinidine both inhibited (Patel *et al.*, 2001) and had no effect (Chavez *et al.*, 1999) on channel currents. The main distinguishing feature between TWIK-1 and TWIK-2 may lie in the reported sensitivity of TWIK-1 to cytosolic Mg^{2+}, 3mM of the ion reduced the outward conductance from 34 to 19pS (Lesage *et al.*, 1996) an effect not seen in TWIK-2 (Chavez *et al.*, 1999).

1.3.2 THIK subfamily

The THIK subfamily comprises two isoforms, THIK-1 and THIK-2, 408 and 430 aminoacid polypeptides respectively, that share a 63% sequence homology. The topology of the THIK channel conforms to that of the rest of the family, with the exception that it does not contain cysteine residues for disulphide bridge formation in the M1- P1 linker. With TWIK-2 (and possibly TWIK-1) THIK-1 exhibits inwardly rectifying currents under symmetrical K+ distribution although a physiological gradient elicits an outwardly rectifying IV relationship (Rajan *et al.*, 2001); (Campanucci *et al.*, 2005), although to date, only macroscopic currents of the rat orthologue have been described. Both isoforms are unduly expressed while in the rat TWIK-2 mRNA was absent from skeletal muscle, heart and testes (Rajan *et al.*, 2001). The THIK family is named from its inhibition by halothane (**T**andem-pore domain **H**alothane **I**nhibited **K**+ channel) although this property is shared by TWIK-2, TALK-1 and TALK-2. They also share an arachadonic acid sensitivity with TWIK-2 and a weak inhibition by hypoxia with TASK channels (see below). The channel subfamily remains poorly characterised, sharing a number of its biophysical and pharmacological characteristics with other two pore domain potassium channels, and its unitary currents still awaiting description.

1.3.3 TRESK subfamily

The TRESK family has only one member identified from the human genome (Sano *et al.*, 2003). A murine TRESK channel was initially named TRESK-2 due to its sharing only a 65% amino acid identity with the human TRESK. However, it was discovered that there was only one TRESK gene in the rat and mouse (Keshavaprasad *et al.*, 2005).

The TRESK channel was named after expression seemed to be localised solely to the spinal cord (TWIK-related spinal cord potassium channel) (Sano *et al.*, 2003), but a follow-up study detected brain expression also (Liu *et al.*, 2004). The species difference in expression was substantial, however, with murine TRESK being reported in testes (from which it had been originally cloned), spleen and thymus as well as the mouse cortex, cerebellum and dorsal root ganglion.
Unlike the two pore domain potassium channels, the predicted topology for TRESK included a 91 amino acid long cytostolic M2-M3 linker with a short C-terminal. The polypeptide also contained two cysteines suitable for formation of disulphide bridges as well as two asparagine residues which could serve as glycosylation sites within the M1-P1 linker domain.

Key biophysical and pharmacological features of the human TRESK channel differ in the rodent orthologues, likely to stem from the significant differences in the amino acid sequences. (Rat and mice TRESK share a 92% amino acid sequence identity (Keshavaprasad *et al.*, 2005)).While all mice channels exhibit outwardly rectifying currents under physiological K^+ distribution (Kang *et al.*, 2004; Liu *et al.*, 2004), K^+ TRESK currents exhibited the instantaneous kinetics common to all three orthologues

as well as a time-dependant activation component followed by a slower inactivation of outward currents (Liu *et al.*, 2004; Sano *et al.*, 2003).

Human TRESK was also only weakly sensitive or insensitive to extracellular pH (Keshavaprasad *et al.*, 2005; Liu *et al.*, 2004; Sano *et al.*, 2003); while mouse and rat orthologs were strongly modulated by pH (Keshavaprasad *et al.*, 2005; Sano *et al.*, 2003). Human TRESK was also insensitive to Zn^{2+} (Keshavaprasad *et al.*, 2005) while rodent TRESK channel were potently inhibited by the ion (Czirjak & Enyedi, 2006).

Three orthologs do, however, share a sensitivity to block by mercuric ions (onset and recovery of which was slow) (Czirjak & Enyedi, 2006) as well as potentiation by volatile anaesthetics including halothane, isoflurane and chloroform (Liu *et al.*, 2004) and both mouse and human TRESK channels are unique among K2P channels to exhibit a large Ca^{2+} dependent stimulation upon activation of G_q- coupled receptors (Czirjak & Enyedi, 2006; Czirjak *et al.*, 2004).

Mutation of 3 potential phosphorylation sites S274A, S276A and S279A abolished Ca^{2+} dependant stimulation of channel activity with S276A producing the greatest effect. When glutamate was substituted for the residue at this position basal channel activity was lowered as would be predicted by the molecular mimicry of the phosphorylated state.

Further studies are needed to elucidate the exact molecular mechanisms of this TRESK regulation though Ca^{2+}/calmodulin-dependant phosphatase calcineurin (phosphatase2b) is thought to play a significant role (Czirjak *et al.*, 2004).

1.3.4 TREK subfamily

The TREK subfamily of two pore domain potassium channels have, owing to their diverse regulatory and modulatory mechanisms, elicited a significant amount of interest. The subfamily has 3 members, TREK (**T**WIK-**r**elated $\mathbf{K}^+$ channels)-1 and 2, which share a 63% sequence identity (Lesage *et al.*, 2000) and TRAAK (**T**WIK **r**elated **a**rachadonic **a**cid-stimulated $\mathbf{K}^+$ channel), which has a 39% sequence identity with the TREK channels (Ozaita & Vega-Saenz de, 2002). Splice variants of all three have been described; 2 for TREK-1, short (411 amino acids) and long (426 amino acids, 15 amino acid (N terminal extension)) variants; 3 for TREK-2 (TREK-2a, 2b, 2c, each containing one of three alternative first-exons (Gu *et al.*, 2002), and 2 for TRAAK, again a long (b) and a short (a) variant. All have been found to be expressed widely and with some overlap, with some species-specific differences in distribution. Human TREK-1, for example, is abundantly expressed in the brain and GI tract but not in the heart, while its mouse orthologs could be found in all three regions, as well as the lung and kidney (Aller *et al.*, 2005; Talley *et al.*, 2001; Fink *et al.*, 1996). TREK-2 splice variants exhibited organ specific expression in humans, 2b in kidney and pancreas, 2c in the brain, while 2a was nearly undetectable in all tissues studied (Gu *et al.*, 2002). TRAAK expression has yet to be distinguished at the splice variant level, although it has been found to overlap TREK-1 and 2 in the mouse, rat and human, being found in the brain, heart, liver, kidney, pancreas, and placenta (Ozaita & Vega-Saenz de, 2002; Kim *et al.*, 2001; Meadows & Randall, 2001).

Under symmetrical K^+ distribution, TREK-1 and TREK-2 channels show an outwardly rectifying current to voltage relationship, attributed to both an external Mg^{2+} block present at negative membrane potentials and a weakly voltage dependant channel gating (Maingret *et al.*, 2002; Bockenhauer *et al.*, 2001; Patel *et al.*, 1998). TREK channels also share a large unitary conductance, although the isoforms have differing IV relationships and mean open times. The steady-state current voltage relationship for TRAAK channels has been reported to differ from that of TREK-1 and TREK-2 in that it approximates Goldman-Hodgkin-Katz predictions (Ozaita & Vega-Saenz de, 2002; Meadows & Randall, 2001; Meadows *et al.*, 2001; Fink *et al.*, 1998), modulated by some voltage dependency.

TREK channels are modulated by a diverse range of physio-chemical, endogenous and clinical factors. A mechosensitivity with a thermosensitivity distinguish the subfamily from all other two-pore domain potassium channels. Hypotonic extracellular solutions that cause swelling, as well as laminar shear force, stimulate TREK-1 currents, while cell shrinkage inhibits TREK-1 activity (Patel *et al.*, 1998). Lipids that can enter the lipid bilayer leaflets have also been shown to modulate TREK currents via changing the curvature of the cell. Insertion into the external leaflet causes an outward curvature, which has been shown to stimulate TREK-1 and TRAAK in a similar fashion to an outward membrane stretch (that can be brought about with a negative pressure applied in cell-attached or whole cell patch clamp configurations). Trinitrophenol elicited a suction effect, categorizing it as a "crenator". "Cup formers" such as chlorpromazine, inserted into the inner leaflet of the membrane bilayer and inhibited the channel (Patel *et al.*, 2001, 1998).

Temperature sensitivity has been demonstrated in heterologously expressed TREK channels in *Xenopous* oocytes, in cells between temperatures of 14 and 42°C. Basal channel activity greatly increased, making the contribution of the channel currents to the resting membrane potential much more significant; $Q10^2$ values up to 14 were obtained over 24-37°C for TREK-2, compared with 2 or less for TASK-1 and 3, THIK-1 or TRESK channels (Kang *et al.*, 2005; Rajan *et al.*, 2001 Maingret *et al.*, 2000).

Other modulators of TREK channels have been identified as pH, phosphorylation, zinc, copper, general anaesthetics and other pharmological agents. Cytosolic acidification (<pH 7) increased both the spontaneous activity of TREK-1 and 2, as well as their sensitivity to stretch (Kim *et al.*, 2001; Maingret *et al.*, 1999). TRAAK currents can only be potentiated by cytostolic alkalinisation (> pH 7), which also potentiated mechanosensitivity of the channel (Kim *et al.*, 2001).

General anaesthetics such as chloroform, halothane and isoflurane have all been shown to potentiate TREK-1 currents in the mouse (Patel *et al.*, 1999, 1998) and TREK-2 currents in humans (Lesage *et al.*, 2000) with chloroform eliciting the most significant response in TREK-1 (250% increase at 0.8mM), while isoflurane elicited a 90% current increase in TREK-2 (Gu *et al.*, 2002). Murine TRAAK channels investigated with the general anaesthetics have exhibited no or little (inhibitory) sensitivity however.

---

[2] Q10 values refer to the increase in the rate of a process produced by raising the temperature 10°C. A process that doubles in rate with a 10°C rise in temperature has a Q10 value of 2.

Like some other two pore domain potassium channels, the TREK family all have currents with voltage and time dependent components, shifting the I-V relation from a complete Goldman-Hodgkin and Katz (GHK) fit. Phosphorylation of serine-333 of the long TREK-1 splice variant by Protein kinase A (PKA) was found to regulate voltage and time dependent gating. Channel gating was inhibited- an increase in voltage dependency manifested in a decrease in channel open probability at negative membrane potentials (Bockenhauer *et al.*, 2001; Maylie & Adelman, 2001).
In other studies, however, a serine 333 substitution by alanine (mimicking the dephosphorylated state of the channel) generated a functional mutant channel with currents that displayed comparable activation kinetics to the wild type indicating that the numbers of active channels may being regulated by phosphorylation (Maingret *et al.*, 2001; Patel *et al.*, 1998).

The complexity of TREK regulation strongly suggests an integrating function for this subfamily. Control of membrane potential and cell excitability by virtue of whole cell potassium conductance comes about via a variety of physico-chemical factors introduced here. Coupled with a widespread distribution in multiple tissues, the TREK channels have generated considerable interest. Native conductances thought to be due to TREK channel isoforms have been identified through the cloned channel phenotypes in multiple cell types. In the rat, TREK channels are thought to underlie background potassium conductances of dordal root ganglion cells, magnocellular cells and cardiac myocytes (Kang *et al.*, 2005; Tan *et al.*, 2002; Terrenoire *et al.*, 2001). Murine straital neurones and colonic smooth muscle cells also exhibit TREK like conductances and TREK-2 channel currents are present in cerebella granule neurones

as well as magnocellular neurones (Chemin *et al.*, 2005a-b; Kang *et al.*, 2005; Han *et al.*, 2003, 2002).

1.3.5 TALK subfamily

Of the TALK family, TASK-2 is possibly the most well characterized member. All three clone TALK channels, TALK-1. TALK-2 and TASK-2 are sensitive to extracellular pH changes, being inhibited by decreases in pH and potentiated by alkalinity. Indeed it was this property of TASK-2 that, upon initial identification, caused it to be classified as a member of the TASK family. TALK-2 was also named TASK-4 for the same reason.

TALK-1, TALK-2 and TASK-2 genes in the human encode genes of 309, 332 and 499 amino acids respectively (Girard *et al.*, 2001; Reyes *et al.*, 1998), with TALK-1 splice variants being cloned from human pancreas although only two of these could be functionally expressed (Han *et al.*, 2003). Unlike some other two pore domain potassium subfamilies, the TALK channels share little sequence identity around 35% between each of them (Lotshaw, 2007). The channels do, however, have a predicted topology in line with the rest of the superfamily with cysteine residues for disulphide bridge formation and phosphorylation and glycosylation sites in the M1-P1 linker (Han *et al.*, 2003; Decher *et al.*, 2001; Girard *et al.*, 2001; Reyes *et al.*, 1998) of potential PKA and PKC phosphorylation sites however, none of the channels have been shown to be modulated by the kinases.

Species difference exist in expression patterns, mouse TASK-2 being found in lung and uterus which showed low to no expression levels in the human (Reyes *et al.*,

1998). TALK-1 overlaps some TASK-2 expression in the rat and mouse, mRNA being identified as present in the small intestine of both, along with TASK-2, although the human orthologs of TASK-1 has only been found in the pancreas (Duprat *et al.*, 2005; Kang & Kim, 2004; Decher *et al.*, 2001; Girard *et al.*, 2001). TASK-2 was recently postulated to underlie a leak current in rat cerebella granule neurones (Cotten *et al.*, 2004) and some studies reported TASK-2 in human dorsal root ganglion and spinal cord (Medhurst *et al.*, 2001). This conclusion is controversial as TASK-2 mRNA has also been reported as absent from the rodent and human CNS (Brickley *et al.*, 2007; Aller *et al.*, 2005; Warth *et al.*, 2004; Reyes *et al.*, 1998).

TALK channels are so named because of their current potentiation by increasing pH (**T**WIK related **A**lkaline pH Activated $\mathbf{K}^+$ channel (Girard *et al.*, 2001). TASK-2 has also been found to share a mechano-type sensitivity with TREK channels in its activation by cell swelling (hypotonic extracellular solution) and inhibition with cell shrinkage (Niemeyer *et al.*, 2001) although stretch activation did not elicit a TREK like response. For this reason, TASK-2 has been implicated in cell volume regulation (Barriere *et al.*, 2003; Niemeyer *et al.*, 2001). Indeed a TASK-2 knockout mouse lacked a volume sensitive K^+ leak current in the proximal tubules of the kidney where TASK-2 had been shown to be strongly expressed (Barriere *et al.*, 2003).

TALK currents are outwardly rectifying under physiological K^+ gradients although human TALK-1 macroscopic currents exhibited open rectifier under symmetric K^+ distribution (Duprat *et al.*, 2005; Han *et al.*, 2003; Girard *et al.*, 2001). The pharmacology of the channels appears as yet, to be common to all of them for the most part. The restricted expression of human TALK-1 in the pancreas may be its

main characterisation feature, while human TALK-2 currents may be identified from other TALK currents by its potentiation by nitric oxide and reactive oxygen species (Duprat *et al.*, 2005). The full complement of tandem pore channel subunits await testing with these although a similar TREK-1 nitric oxide sensitivity has been reported (Koh *et al.*, 2001)

TASK-2 currents are also stimulated by volatile anaesthetics halothane, isoflurane and chloroform (Gray *et al.*, 2000) unlike TALK-1 and 2 isoforms but akin to THIK-1. However, the TASK-2 knockout mouse exhibited no change in its sensitivity to volatile anaesthetics (Gerstin *et al.*, 2003) suggesting no significant role for TASK-2 in mediating their effects. Local anaesthetic bupivacaine inhibited TASK-2 channel although TALK-1 was relatively insensitive (Decher *et al.*, 2001). TALK-1, TALK-2 and TASK-2 can also be distinguished through their differing responses to reactive oxygen species. While TALK-2 and TALK-1 were stimulated by chloromine T and O·, the response of TALK-2 was much more significant while TASK-2 was inhibited by them. Superoxide anion strongly stimulated all TALK channel currents.

1.3.6 TASK subfamily

Of particular interest in this study are the TASK channels 1 and 3, along with the TALK isoform TASK-2. TASK channels are a subfamily of the two pore domain channels, the human genes encoding proteins of 394 amino acids (TASK-1, (Duprat *et al.*, 1997)), 374 amino acids (TASK-3, (Vega-Saenz de *et al.*, 2001; Rajan *et al.*, 2000)) and 330 amino acids (TASK-5, (Vega-Saenz de *et al.*, 2001; Ashmole *et al.*, 2001; Karschin *et al.*, 2001; Kim & Gnatenco, 2001)). TASK-5 remains to be functionally expressed; it is unknown whether this is due to the requirement for auxiliary subunits, a silencing mechanism at the membrane or the retention of the channel on internal membranes.

The human TASK-1 and 3 isoforms share a 58% amino acid identity and the predicted topology of both channels is that of the general two pore domain superfamily; four transmembrane domains with two pore domains in a single polypeptide with intracellular amino and carboxy terminals, a large M1-P1 linker and the pore domains on the extracellular side of the membrane embedded in outer leaflet. Unlike other members of the subfamily however, there is evidence for heteromeric dimerization between TASK-1 and TASK-3. Co-expression of the two subunits results in functional expression of a channel with properties distinct from TASK-1 and TASK-3 (Berg *et al.*, 2004; Clarke *et al.*, 2004; Kang *et al.*, 2004; Czirjak & Enyedi, 2002).

The distribution of the channels has been studied in the human and rodent and mRNA for all three TASK channels have been found throughout the body, often overlapping with other two pore domain potassium channels as well as other TASK isoforms. Electrophysiological studies following the analysis of expression patterns of the TASK channels have confirmed TASK-like conductances in many neuronal cell groups including cerebellar granule neurones (see below), locus coeruleus and raohe neurones (Washburn *et al.*, 2002; Sirois *et al.*, 2000), magnocellular neurones of the supraoptic nucleus (SON) (Han *et al.*, 2003) and motoneurones (Sirois *et al.*, 2000; Talley *et al.*, 2000). In the periphery, native TASK conductances have been identified in the adrenal glomerulosa cells (Czirjak & Enyedi, 2002; Czirjak *et al.*, 2000) as well as in the carotid body glomus cells (Williams & Buckler, 2004; Buckler *et al.*, 2000), where the sensitivity of the channels to oxygen tension is implicated in chemoreceptor responses.

Species differences do exist in terms of distribution; TASK-1 mRNA is present in the brain, lung, pancreas and placenta with some expression in the heart while TASK-1 mRNA in the rodent is most significant in the heart (Karschin *et al.*, 2001; Lopes *et al.*, 2000; Kim *et al.*, 1999; Leonoudakis *et al.*, 1998; Duprat *et al.*, 1997). TASK-3 mRNA has also been identified in the central nervous system as well as the peripheral organs (Aller *et al.*, 2005; Bayliss *et al.*, 2003; Karschin *et al.*, 2001; Talley *et al.*, 2001; Vega-Saenz de *et al.*, 2001; Kim *et al.*, 2000; Rajan *et al.*, 2000).

TASK channels were named after their pH sensitivity (**T**WIK related **A**cid **S**ensitive $\mathbf{K}^+$ channels) but using pH sensitivity to distinguish these channel currents from others of the two pore domain potassium channel family is complicated by the pH

sensitivity of TWIK-1, TALK-1, TALK-2 and TASK-2 as well as rodent orthologs of TRESK (Lotshaw, 2007; Morton *et al.*, 2003; Lopes *et al.*, 2001; Kim *et al.*, 2000; Rajan *et al.*, 2000). However, while TASK-1 channel currents can be potentiated and inhibited by pH changes (increasing and decreasing pH from 7.4 respectively), TASK-3 currents cannot be potentiated by extracellular alkalinisation (Berg *et al.*, 2004; Morton *et al.*, 2003; Talley *et al.*, 2000; Duprat *et al.*, 1997) and TASK-1/3 heterodimers have an intermediate sensitivity to pH changes (Berg *et al.*, 2004; Czirjak & Enyedi, 2002). The pH sensitivity is dependent on extracellular K^+ concentration, TASK-1, TASK-3 and heterodimer channel currents becoming less sensitive to H^+ inhibition with increasing K^+ (Morton *et al.*, 2003; Czirjak & Enyedi, 2002a-b; Lopes *et al.*, 2001, 2000). H^+ inhibition of the channel is hypothesized to be state dependent- increasing extracellular K^+ increases the open probability, decreasing the opportunity for H^+ ions to inhibit channel gating (Lotshaw, 2006; Lopes *et al.*, 2001).

Zn^{2+} has been hypothesized to inhibit TASK-3 in a similar way with involvement from H98 and E70. Site-directed mutation of these two residues decreased hTASK-3 sensitivity and a speculative quaternary zinc co-ordination site utilizing the two residues from both subunits was proposed (Clarke *et al.*, 2004). Zinc inhibition of TASK-3 like currents in the rat adrenal glomerulosa cells was attributed to a decreased open probability without a decrease in unitary conductance or mean open time suggesting again, in a fashion akin to H^+ inhibition, alteration of channel gating was likely to underlie zinc effect. Indeed zinc is not the only divalent cation that the TASK channels are sensitive to. Mercuric ions have been reported to potentiate both TASK-1 (30%, 3μM) and TASK-3 (70%, 3μM) (Czirjak & Enyedi, 2006) while a

voltage dependent block of guinea pig TASK-3 was brought about by extracellular Mg^{2+} and Ca^{2+} ions (Kang *et al.*, 2004; Rajan *et al.*, 2002, 2000; Maingret *et al.*, 1999).

In contrast to this, the polycationic dye ruthenium red has been reported to block TASK-1, TASK-3 and the TASK-1/TASK-3 heterodimer (Musset *et al.*, 2006; Aller *et al.*, 2005; Kang *et al.*, 2004; Han *et al.*, 2003; Czirjak & Enyedi, 2002) with TASK-3 being the most sensitive ($IC_{50} = 0.7\mu M$) and as a consequence has most widely been used to distinguish TASK-3 currents in a number of species. It is also purported to be useful in distinguishing TASK-3 currents from other two pore domain potassium channel currents despite the sensitivity of several other ion channels to the dye (Berg *et al.*, 2004; Szabadkai *et al.*, 1999). Ruthenium red block of TASK-3 has been characterized as voltage independent with an inhibition of unitary conductance and mean open time (Musset *et al.*, 2006; Kang *et al.*, 2004; Czirjak & Enyedi, 2002). Channel sensitivity to ruthenium red was abolished by site directed mutagenesis of glutamate at position 70 (E70) in the M1-P1 linker. Low sensitivity to the dye in TASK-1 was reversed with substitution of a lysine in the same position by a glutamate (K70E), strongly suggesting this residue played a crucial role in TASK channel ruthenium red sensitivity.

Both ruthenium red sensitivity and spermine (a polyamine) block of TASK-3 was inhibited at the unitary conductance level by increasing extracellular Ca^{2+} ions. TASK-1 and TASK-3 E70K (the latter mimicking the former) were both insensitive to ruthenium red and spermine block also. This suggested that the divalent cations competed with the polycationic compounds for a shared mechanism and location of

action. It has been hypothesized that the cations, via E70, shield the negative surface charge in the outer pore (Musset *et al.*, 2006; Kang *et al.*, 2004).

Like other two pore domain potassium channels the TASK channels can be modulated by general anaesthetics, specifically the volatile anaesthetics halothane, isoflurane, chloroform and diethyl ether. TASK-1 currents are moderately inhibited by chloroform (10-15% inhibition, 0.8-1.3mM) (Lopes *et al.*, 2000; Patel *et al.*, 1999,1998) and diethyl ether (40% inhibition, 0.6mM (Patel *et al.*, 1999)) and the rat TASK-1 currents are also inhibited by isoflurane (15%, 0.8mM (Berg *et al.*, 2004)). The human ortholog currents are potentiated by isoflurane however (20%, 2mM (Patel *et al.*, 1999)), as are human and rodent ortholog currents by halothane (up to 60% increase 0.1-1mM) (Talley & Bayliss, 2002; Lopes *et al.*, 2000; Sirois *et al.*, 2000; Patel *et al.*, 1999). TASK-3 human and rat orthologs are also potentiated by halothane and isoflurane (hTASK-3 66% increase 1mM halothane (Talley & Bayliss, 2002; Meadows & Randall, 2001) rat TASK-3 134% increase, rat TASK-3, 138% increase (0.8mM (Berg *et al.*, 2004)) as well as the rat TASK-1/TASK-3 heterodimer currents (150% increase with 0.3mM halothane (Berg *et al.*, 2004;Talley & Bayliss, 2002), 106% increase 0.8mM isoflurane (Berg *et al.*, 2004).

Further evidence for TASK sensitivity to general anaesthetics came about from analysis of TASK-1 knockout mice, which exhibited a decrease in sensitivity to inhalational anaesthetics (Linden *et al.*, 2006).

Potentiation of TASK-1 and 3 currents by halothane was voltage independent (Chemin *et al.*, 2005; Berg *et al.*, 2004; Talley & Bayliss, 2002; Meadows & Randall,

2001; Patel *et al.*, 1999), with an increased single channel open probability in hTASK-1. Unitary current amplitude was unchanged, suggesting a direct effect on the protein. Indeed a conserved six amino acid sequence (VLRFM/LT) was found to be required for halothane sensitivity of rat and human TASK-1, TASK-3 and TASK-1/TASK-3 heterodimers (Talley & Bayliss, 2002; Patel *et al.*, 1999).

The VLRFLT sequence at the final transmembrane domain and the cytoplasmic C terminus has recently been reported to play a key role in methanandamide block of TASK-1 and TASK-3 channels (Veale *et al.*, 2007a). In the same study, 3μM methandamide applied extracellularly potently blocked heterologously expressed human TASK-3 channel currents over hTASK-1 and mouse TASK-3, corroborating previous findings in human and rodent TASK orthologs (Czirjak & Enyedi, 2006; Berg *et al.*, 2004; Maingret *et al.*, 2001). Deletion of the VLRFLT residues however resulted in functional channels insensitive to the cannabinoid. Interestingly this was accompanied by an insensitivity to action by G protein coupled receptors (Veale *et al.*, 2007). Anandamide also inhibits TASK currents, with inhibition of hTASK-1 currents more potent than block of hTASK-3 or rat TASK-3 (inhibition by 3μM 90%, 20% and 9% respectively (Berg *et al.*, 2004; Maingret *et al.*, 2001).

The final major class of modulators of TASK channels are the G protein coupled receptors TASK-like native conductances in a number of cell types are inhibited by Gq/11 coupled neurotransmitter receptors (Talley *et al.*, 2000; Watkins & Mathie, 1996) corroborated by the results of mechanistic investigations of cloned TASK-1, TASK-3 and TASK-1/TASK-3 currents (Chemin *et al.*, 2003; Czirjak & Enyedi, 2002a-b; Talley & Bayliss, 2002). Two possible mechanisms have been proposed to

date the first owing inhibition to phospholipase-C activation and depletion of membrane PIP2 by hydrolysis (Lopes *et al.*, 2005; Chemin *et al.*, 2003; Czirjak *et al.*, 2001) while the second mechanism is PLC independent, inhibition being mediated instead by $G_{\alpha q}$ binding directly with TASK-1 and TASK-3 (Chen *et al.*, 2006). Evidence for both hypotheses has been reported. 3μM wortmannin which inhibits PIP_2 synthesis and, after receptor mediated inhibition, impeded TASK-1 channel current recovery. PIP_2 scavengers also inhibited TASK-1 and TASK-3 currents (Lopes *et al.*, 2005; Chemin *et al.*, 2003).

TASK channel current inhibition via direct action of G_q, independent of phospholipase C activation has also been supported in the literature. Phospholipase C inhibitor U-73122, for example, only partially reduced TASK current GPCR mediated inhibition (Talley & Bayliss, 2002). Others reported that TASK channel current modulation could be elicited by a mutant G_q protein that was unable to activate PLC (Chen *et al.*, 2006).

The regions required for G protein receptor coupled channel modulation have been investigated using sequence deletion and site directed mutagenesis. Inhibition of TASK-3 by $G_{q/11}$ was significantly reduced after C terminus truncation (Lotshaw, 2007; Veale *et al.*, 2007; Lopes *et al.*, 2005) and the aforementioned conserved sequence VLRFLT (residues 243 to 248) at the end of the M4 domain was necessary for hormone reduced inhibition (Talley & Bayliss, 2002).

This apparent convergence of anaesthetic methanandamide and GPCR modulation at the same sequence is noteworthy, a layered sensitivity can facilitate an adaptable closely regulated response of the K^+ current (and so excitability) of the cell.

1.4 The cerebellum

Functional anatomy and neural networks of the cerebellum

The cerebellum is located at the base of the brain, rostral and dorsal to the occipital lobe and the brain stem respectively, in the human. It comprises two highly folded hemispheres, joined at the middle with the vermis and sits in the posterior cranial fossa of the skull. Structurally, the cerebellum is akin to its larger, less tightly folded counterpart, the cerebrum, in that it has a cortex of grey matter overlaying the white matter of its medulla. It forms part of the hindbrain (rhombencephalon), with the medulla (myelencephalon) and pons (metencephalon), connected by two pairs of peduncles (inferior and middle), while the superior peduncles connect it to the midbrain.

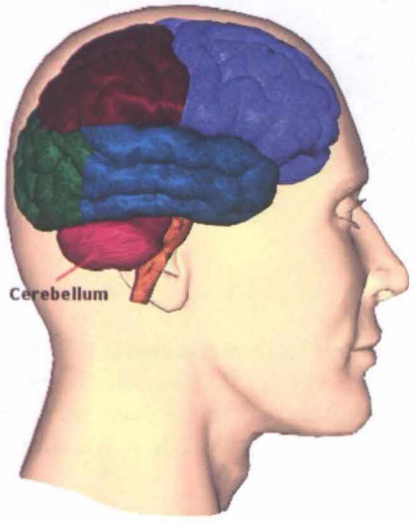

Figure 1-8 Location of the human cerebellum *in situ* *(Reproduced from* www.neuroskills.com*)*

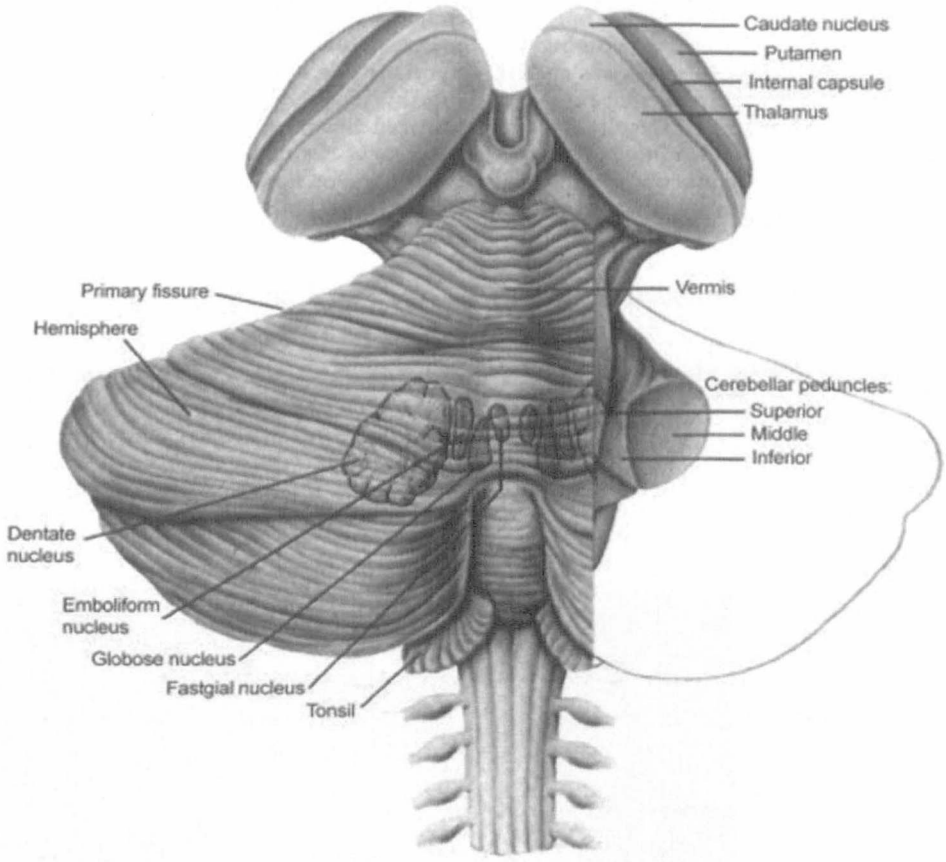

Figure 1-9 Gross anatomy of the cerebellum and brainstem The location cerebellar peduncles can be viewed underneath the right hemisphere (cut out). The cerebellar nuclei sit within the white matter core of the cerebellum; their outlines are projected onto the folia to indicate their position. *(Adapted from Kandel et al. 2000)*

Embedded within the white matter core are the cerebellar nuclei on each side of the midline (Figure 1-9). The medial (fastigial) nucleus projects chiefly to the nuclei of the lower brain stem and spinal cord, the interpositus (globus and emboliform) nucleus projects to the midbrain while the lateral (dentate) nucleus projects to the thalamus and cerebral cortex (Voogd, 2003).

From a neural network perspective, the cerebellum has two main divisions; the cortex and the cerebellar nuclei. The cortex is specialised for processing large amounts of information about the state of the body (muscle contraction force, length etc). It also receives information from proprioceptors, tactile receptors and visual and auditory

cues about the body's environment and assimilates this with neural inputs from parts of the brain associated with goal oriented behaviour, problem solving and motor commands (Nicholls *et al,* 1992; Ghez C, 1991; Llinás & Walton, 1998).

The deep nuclei of the cerebellum have been found to co-ordinate specific types of function; posture, gaze and locomotion (vermis and flocculus), voluntary reaching and grasping movements with the hands and arms (intermediate zones) and more complex movements and cognition (lateral zones) (Figure 1-9).

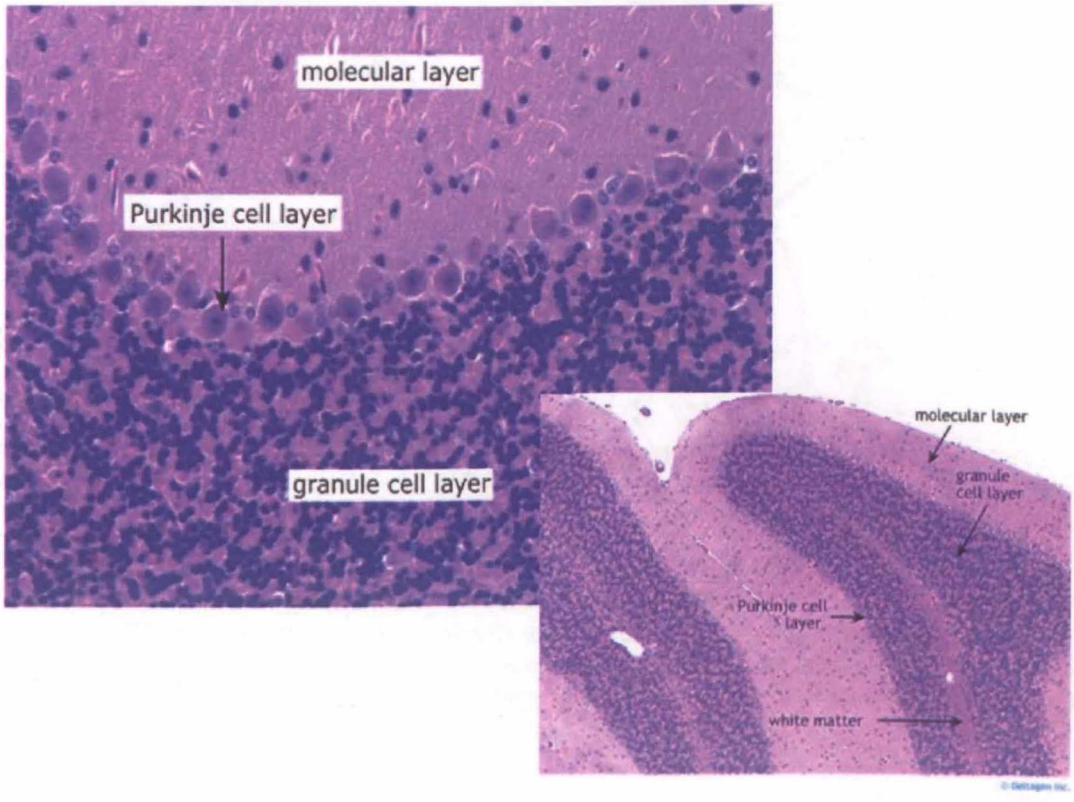

Figure 1-10 Cerebellum cortex, low (inset, right, x10) and high (top, left, x40) magnification *(Adapted from Deltabase Histology Atlas http://www.deltagen.com/target/histologyatlas/atlas_files/nervous/cerebellum_cortex_10X.jpg)*

The cerebellum, histologically, is seen to have three distinct layers (Figure 1-10) determined by the neuronal types present. From surface to medulla, the cortical layers are the molecular layer, populated by basket and stellate cells and the axons of granule

neurones known as parallel fibres, the piriform layer, comprising of large Purkinje cells, and the granular layer, consisting chiefly of cerebellar granule neurons (Figure 1-11). The only efferent of the cerebellar cortex is the Purkinje cell axon.

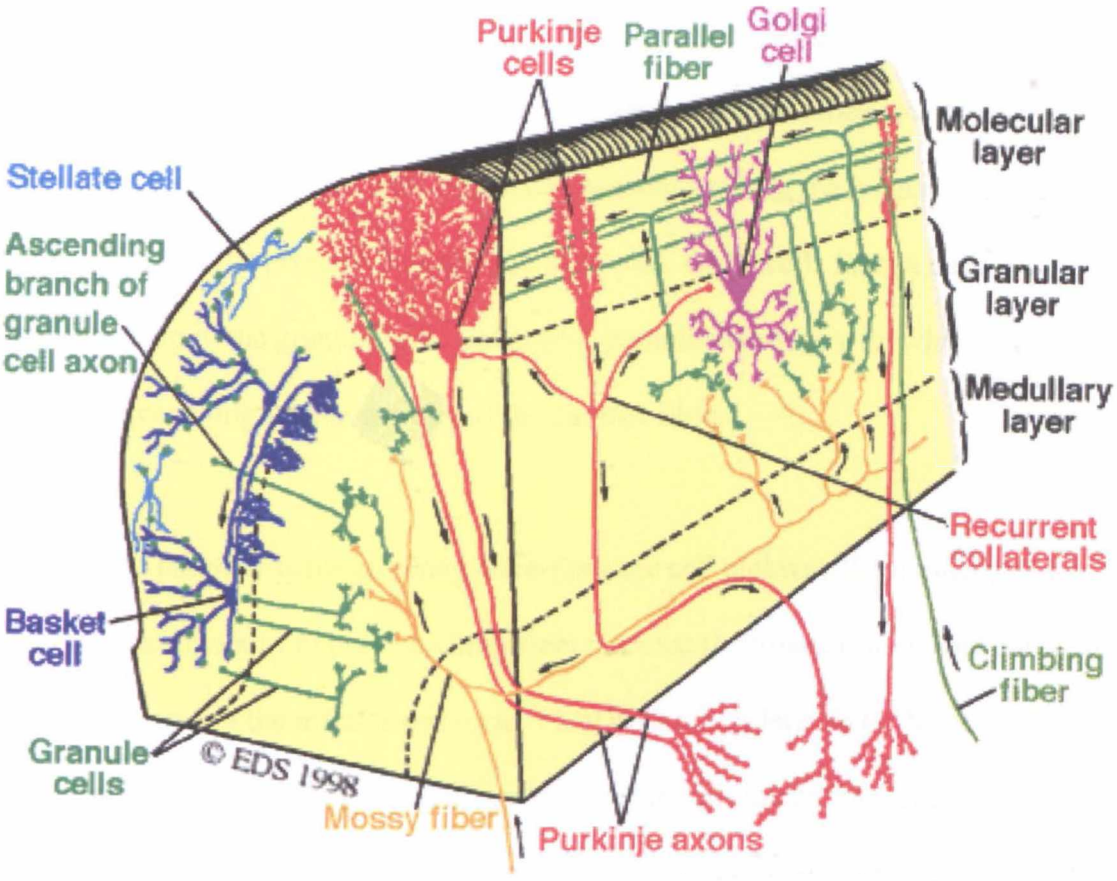

Figure 1-11 Three layer organisation of the cerebellar cortex This transverse and longitudinal representation of the cerebellar cortex outlines its three fundamental circuits. Mossy and climbing fibres are the main afferents of the cerebellum, receiving information from across the CNS (in the case of the mossy fibres) and the inferior olive (climbing fibres). Purkinje fibres are the only efferents of the cerebellar cortex. *(Reproduced from http://www.tnb.ua.ac.be/models/index.shtml)*

There are three main components of cerebellar circuitry (Nicholls *et al,* 1992; Kandel *et al,* 1991; Zigmond, 1999; Shepard, 1998), the primary pathway being the mossy fibre-granule neurone- Purkinje cell pathway. Mossy fibres receive their inputs from many CNS regions, the chief among them being the pontocerebellar pathway. Others

include the spinal cord, the vestibular nucleus and tract and the cerebellar nuclei, these fibres entering the cerebellum via the middle and inferior peduncles.

The mossy fibres then synapse on granule cells, which, via their parallel fibres, terminate on an array of Purkinje cells, as well as inhibitory basket, stellate and Golgi cells. Activation of the basket and stellate inhibitory interneurones results in strong suppression of the Purkinje cells they are connected to along the length of the parallel fibre, as well as the primary Purkinje cell activated. Golgi cells form a negative feedback loop in the granule layer and inhibit granule neurones with which they synapse, quenching further activity of the parallel fibre.

The second pathway is the climbing fibre-Purkinje cell pathway. Climbing fibres receive their inputs from only one brainstem nucleus; the inferior olive, and enter with the cerebellum via the inferior peduncle. They give off collaterals to the cerebellar nuclei and pass through the granule layer before terminating on Purkinje cell dendrites in the molecular layer. Each Purkinje cell receives inputs from a single climbing fibre, although a single cell of the inferior olive may synapse with several climbing fibres.

When activated, the climbing fibres elicit a prolonged burst of high-frequency potentials that dominate Purkinje cell inputs. The spatial localisation of activation by climbing fibres occurs in a similar fashion to the mossy fibre-granule neurone-Purkinje cell pathway; Golgi cells activated by the climbing fibres inhibit mossy fibre input, while climbing fibre innervated basket and stellate cells inhibit activation of surrounding Purkinje cells.

The final major circuit of the cerebellar neurones is between the cerebellar cortex and the cerebellar nuclei. The nuclei are directly innervated by mossy fibre collaterals feeding the same information to them as to the cortex. The Purkinje cells are, as previously noted, inhibitory efferent cells, projecting to the nuclei. Stimulation of the mossy fibre-granule neurone-Purkinje circuit therefore feeds back to an inhibition of the cerebellar nuclei. The nuclei inhibition is followed by an increase in excitability from a basket/stellate/Golgi cell mediated inhibition of Purkinje cell activity.

Motor learning in the cerebellum

The cerebellum, while not necessary for the initiation or perception of muscle contraction, has a comparator role that indirectly regulates movement and posture by adjusting the major descending motor systems of the brain (Zigmond, 1999). By comparing intention with performance, it is able to correct errors in movement. The cerebellum also participates in motor learning, laying down minute to minute corrections for the long term enhancement of performance. The memory function theory of the cerebellum was first proposed by David Marr and James Albus in the early 1970s (Albus, 1971; Marr, 1969). They suggested that the function of the climbing fibre input was to alter Purkinje cell response to mossy fibre stimulation. Ito had also postulated that processing of information coming into the cerebellum was modulated by changing levels of Purkinje cell inhibition (Ito, 1970). This activity dependent modifiability became known as 'synaptic plasticity' and it wasn't until the 1980's when long term depression (LTD) was first discovered that a suitable neuronal circuit was found that matched the properties hypothesised to be necessary for memory.

LTD was found to occur when climbing fibres activated Purkinje cells in conjunction with the parallel fibres from cerebellar granule cell neurones. The result was a decrease in the sensitivity of the postsynaptic Purkinje cell to glutamate, later identified as the result of removal of AMPA (α-amino-3-hydroxy-5-methyl-4-isoxazolone propionate) receptors by endocytosis (Ito & Kano, 1982; for review, see Ito, 2006). Around the same time it was found that long term [postsynaptic] potentiation (LTP) at the same neuronal interface also occurred; LTP was observed to take place when parallel fibres were stimulated independently of climbing fibres (Sakurai, 1987) confirming previous theories of the existence of a necessary balance between LTD and LTP to prevent global depression of all cerebellar synapses (Sejnowski, 1977).

The cerebellar granule neuron

Of particular interest in this study are the cerebellar granule neurons (CGNs). The smallest neurones in the brain, they are also the most plentiful (Zagon *et al.*, 1977; Braitenberg & Atwood, 1958) and via their axonal projections into the molecular layer as parallel fibres they play a fundamental role of integration and signal definition in the cerebellum. It has also recently been shown that the previously overlooked ascending portions of the granule cell axon are also important inputs to Purkinje cells, being selectively resistant to cerebellar LTD and releasing greater amounts of transmitter with a higher frequency (Sims & Hartell, 2005). This latest finding adds a further layer of functionality to the granule neurone, expanding its significance in cerebellar processing.

The granule cell layer has been proposed as sparse coding system – i.e. each granule cell represents an integration of a small convergence (3 -5) of mossy fibres (Ito, 2006; Chadderton *et al.*, 2004; Albus, 1971) and the granule cell's filtering function comes about by selective responses to temporally separated stimuli.

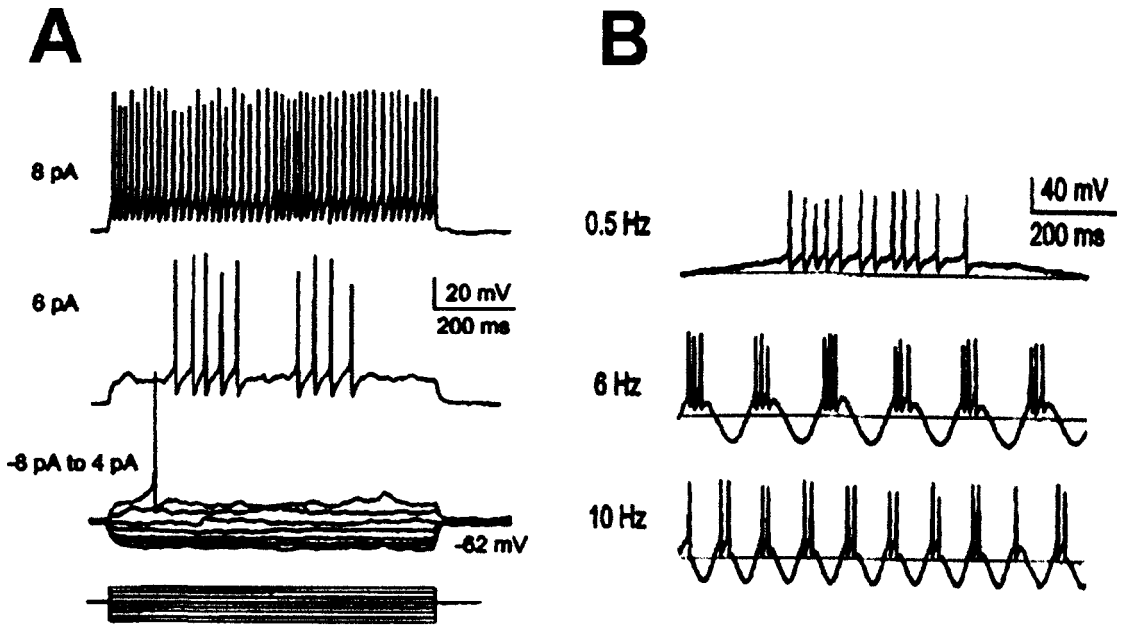

Figure 1-12 Rat cerebellar granule cell responses to stepped current injection *(Adapted from D'Angelo et al 2001).* (A) Current steps were from -8 to 6pA. Resting membrane potential was -62mV, spikes activated around -40mV. The tracing shows a single spike at 4pA, two clustered spike bursts at 6pA and regular repetitive firing can be seen at 8pA. (B) Injection of sinusoidal currents at various frequencies reveals resonance in spike burst frequency; further analysis (not shown here) showed the greatest number of spikes occurred at a frequency of 6Hz, decreasing at higher current injection frequencies. Recording shown were made in the presence of bicuculline to prevent granule cell rhythmic inhibition by Golgi cells.

Granule cells exhibit a variety of responses to excitatory stimulation; repetitive firing (D'Angelo *et al.*, 1995; Gabbiani *et al.*, 1994), spike bursting, oscillations and resonance (D'Angelo *et al.*, 2001) (Figure 1-12). Mossy fibres have long been known to fire at frequencies exceeding 100Hz (Kase *et al.*, 1980) in response to limb and eye movements, and these provide excitatory synapses tc granule cell dendrites (majority being glutaminergic). These excitatory stimuli are balanced with inhibitory (GABAergic) synapses from Golgi cells.

Recent analysis of sensory processing *in vivo* (Chadderton *et al.*, 2004) has demonstrated that sensory stimulation of the vibrissae in ketamine / urethane anaesthetised rat evoked bursts of excitatory postsynaptic currents (EPSCs) in mossy fibres that, in a course of three or more, evoked a burst of action potentials in the granule neurone. This frequency dependency of the granule cells effectively ensures reliable relay of sensory evoked mossy fibre input to the Purkinje cell, while filtering out stimulations not associated with sensory input.

A large convergence of granule cells is required to stimulate the Pukinje cell, ensuring that the sparse coding system is one of low noise too. In cerebellar slices, simultaneous whole cell recordings were made of connected Purkinje and granule cells (Barbour, 1993), and single granule cells evoked EPSCs of 2-60pA. From this, it was calculated that in the order of 50 granule cells would be required to be activated to excite a single Purkinje cell.

Chadderton found that single EPSCs were unable to elicit the action potential bursts in the granule neurone (Chadderton *et al* 2004). This was largely due to a dampening of excitability caused by a hyperpolarized membrane potential and a tonic inhibitory conductance mediated by $GABA_A$ receptors. Only a reduction in the inhibition (application of gabazine, a $GABA_A$ selective blocker) was able to facilitate action potential firing in the granule cell after a single EPSC. The tonic inhibition of cerebellar granule neurones by $GABA_A$ conductances and the cerebellar granule neurone hyperpolarized membrane has been frequently reported and is critical for normal cerebellar function (Eccles *et al.*, 1966).

In 1996, Watkins and Mathie identified a non-inactivating potassium current sensitive to muscarinic receptor activation in cultured rat cerebellar granule neurones that developed with days in culture, making the resting membrane potential much more hyperpolarized (Watkins & Mathie, 1996). Pharmacological and biophysical characterisation revealed the standing outward potassium current ($I_{K(SO)}$) was not blocked by conventional potassium channel blocker TEA, was outwardly rectifying, and was reduced by La^{3+}, Zn^{2+} and Ba^{2+}. Inhibition of $I_{K(SO)}$ caused a depolarization in granule neurones. Functionally, $I_{K(SO)}$ was similar to the $GABA_A$ conductance in that its inhibition would increase the excitability of the granule neurone, allowing it to respond readily to mossy fibre EPSCs.

Indeed, in an analysis using murine cerebellar slices (Brickley *et al.*, 2001), a knockout of the $GABA_A$ subunits $\alpha 6$ ($\alpha 6$-/-) abolished the $GABA_A$ mediated tonic conductance in the granule neurones, but the response of the cells to excitatory input remained unaltered, compensated for by an increase in a potassium 'leak' conductance. This standing outward conductance shared characteristics with the previously identified $I_{K(SO)}$ and its increased presence in the knockout highlighted both the dynamic interplay of the ion channels in these cells, as well as the importance of maintenance of the hyperpolarised membrane potential for normal cerebellar granule neurone behaviour.

The potassium conductance increases potassium permeability and thus moves the membrane potential away from action potential threshold- an important regulator of excitability in the cerebellar granule neurone as previously discussed. Further to this,

a recent paper analysing high frequency firing in the cerebellar granule neurone and two pore domain potassium channel, TASK-3 postulates a role for the potassium conductance *during* the action potential propagation (Brickley *et al.*, 2007). The increased membrane permeability brought about by the potassium channels reduces the membrane time constant, allowing voltage gated sodium channels, the purveyors of the action potential, to recover from inactivation faster, speedily readying the cell for successive firing. This reduction in the depolarization block would facilitate the high-frequency, burst firing seen in the CGN. In addition to this, the more hyperpolarised membrane potential will, owing to the intrinsic voltage dependent properties of the voltage gated sodium channel, increase the amplitude of the action potential by making more available for activation in the steady state.

In conclusion, the CGN plays an important integration and transduction role in signal processing of the cerebellum, and motor function overall. The *weaver* mouse, for example, exhibits a mutation in the inwardly rectifying G-protein activated K^+ channel, GIRK2 which gives rise to CGN death shortly after birth. This mouse displays an uneven, weaving gait, ataxia, some locomoter hyperactivity and occasionally tonic-clonic seizures along with a depletion in dopaminergic neurones in the substantia nigra (Harkins & Fox, 2002). Underlying the functionality of the CGN is its membrane excitability and consequently the channel currents that make up $I_{K(SO)}$.

1.5 Characterising $I_{K(SO)}$

The identification of the standing outward potassium current in cerebellar granule neurones was accompanied by the description a number of biophysical and pharmacological properties; the current was non-inactivating, exhibited outward rectification and reversed close to the potassium equilibrium potential (Watkins and Mathie, 1996, see above). It was also inhibited by muscarine, 10μM lanthanum, 10μM zinc and 1mM barium, while it remained unaffected by classical potassium channel blocker tetra-ethylammonium, 5-hydroxy-trytamine, noradrenaline and 2-chloroadenosine.

Since this early characterisation, $I_{K(SO)}$ has also been found to be blocked by external acidification (Millar *et al.*, 2000), anandamide (Maingret *et al.*, 2001), enhanced by the volatile anaesthetic halothane (Maingret *et al.*, 2001) and insensitive to 4-amino pyridine (Millar *et al.*, 2000).

These features of $I_{K(SO)}$ were compared to the properties of concurrently emerging family of two pore domain potassium channels, and their expression patterns. TASK-1 was the primary molecular candidate for $I_{K(SO)}$ (Millar *et al.*, 2000), for the channel's lack of a voltage threshold for activation, and its matching muscarine and pH sensitivities. *In situ* hybridization studies and RT-PCR localised TASK-1 mRNA to the cerebellar granule neurones (Millar *et al.*, 2000; Duprat *et al.*, 1997).

With the cloning of TASK-3 a second candidate came to the fore (Kim *et al.*, 2000; Rajan *et al.*, 2000). With similar properties to TASK-1 and expression in the cerebellar granule neurones (Brickley *et al.*, 2001; Talley *et al.*, 2001; Karschin *et al.*,

2001), and an ability to form functional heterodimers with TASK-1 (Czirjak & Enyedi, 2002; Kang *et al.*, 2004) these studies suggested that $I_{K(SO)}$ might be composed of more than one 'leak' channel current. TASK-3 was also found to be sensitive to zinc, one of the traits originally reported with $I_{K(SO)}$ identification (Clarke *et al.*, 2004).

Three other two-pore domain potassium channels have also been found to be expressed in the cerebellar granule neurone; TWIK-1, TREK-2c and THIK-2 (Aller *et al.*, 2005; Talley *et al.*, 2001) (Figure 1-13) and are all thought to contribute to the standing outward potassium current (Kang *et al.*, 2007; Brickley *et al.*, 2007; Han *et al.*, 2002). This is supported by TREK-2, TASK-1 and TASK-3 also sharing a sensitivity to volatile anaesthetics with $I_{K(SO)}$, being potentiated by halothane (Maingret *et al.*, 2001; Patel *et al.*, 1999), and TASK-1 expressing rat somatic motoneurones and locus coeruleus cells exhibiting a halothane sensitive potassium conductance potentiation, similar to cerebellar $I_{K(SO)}$ (Sirois *et al.*, 2000).

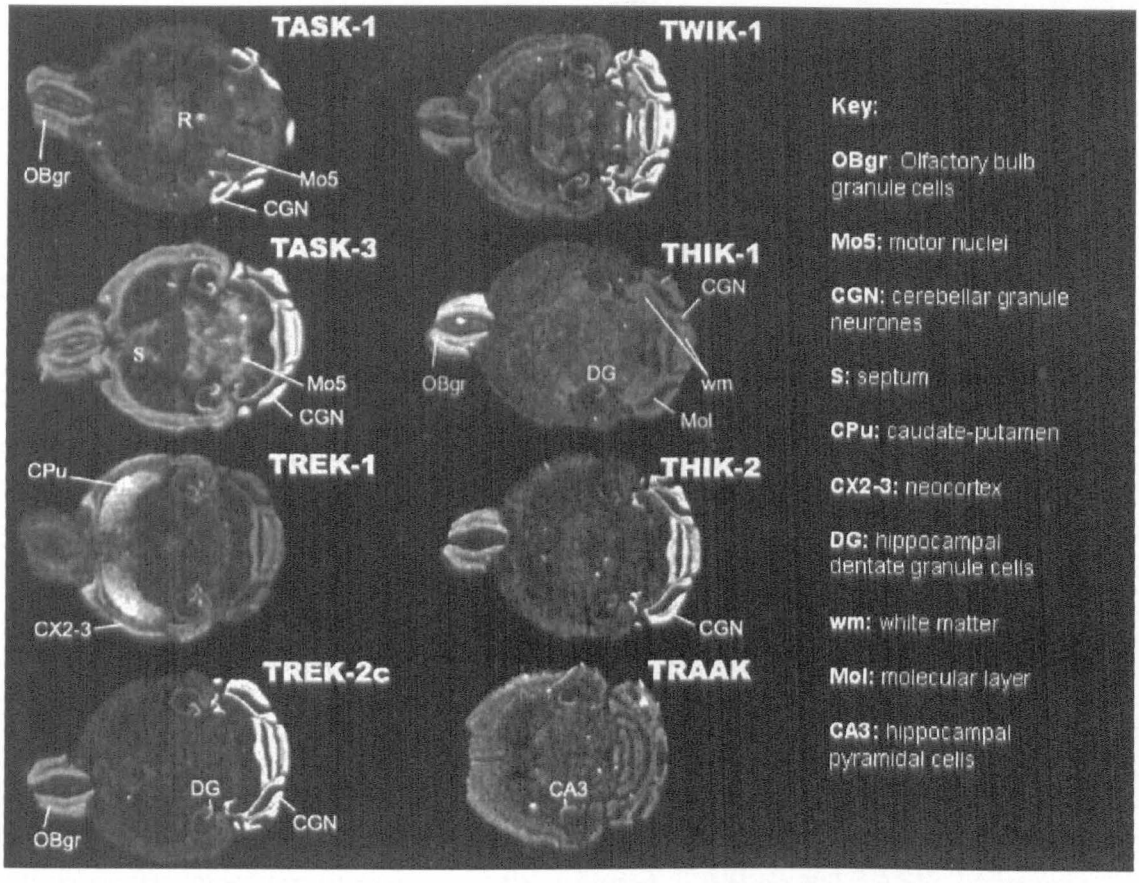

Figure 1-13 ***In situ*** **hybridization of two pore domain potassium channels** ***(Adapted from Aller et al., 2005)*** **Axial slices of C57BL/6 mice brains were hybridized with ^{35}S-labelled oligonucleotide probes and images were generated from a 4 week exposure to x-ray film (TRAAK took 12 weeks). THIK-1, TREK-1 and TRAAK were less well expressed than TWIK-1, TASK-1, TASK-3, TREK-2c or THIK-2 in the cerebellar granule neurones.**

In conclusion, there is strong biophysical, pharmacological and expression pattern evidence to date suggesting the molecular correlates for the cerebellar granule neurone $I_{K(SO)}$ are the TASK-1, TASK-3 and TREK-2c two-pore domain potassium channels.

1.6 Rationale for current study

From this discussion of the available literature it can be seen that the two pore domain channels have very diverse modulators and expression patterns. Therefore, owing to their mediation of background K^+ currents it can be hypothesized that they play a fundamental role in general physiology and consequently may prove valuable therapeutic targets in drug development. In order for this direction to become more viable however, analysis of native two pore domain currents in situ is needed and in order to identify which channels form the molecular basis for native conductances biophysical and pharmacological characteristics that distinguish the different channels must be established in the cloned channel.

Of particular interest in this study are the TASK-1, TASK-3 and TASK-2 channels. Key pharmacological features are shared by all three; pH and Zn^{2+} sensitivity, potentiation by general anaesthetics and anandamide inhibition. Biophysically their macroscopic currents are also not easily distinguished, with TASK-2 and TASK-3 being reported as outward rectifiers while TASK-1 bears open rectifying currents (Morton *et al*, 2003; Czirjak & Enyedi, 2002; Goldstein *et al.*, 2001; Lopes *et al,* 2000; Rajan *et al*, 2000; Gray *et al.*, 1998; Leonoudakis *et al.*, 1998; Reyes *et al*, 1998; Duprat *et al.*, 1997). Further, despite the established properties of these channels being quantifiably different, a heterogeneous two pore domain channel population would be hard to dissect without agents that produce markedly different responses in the channel currents. The aims of this study, therefore, are to seek out new pharmacological agents that differentiate between cloned TASK-1, 2 and 3 channel properties and to test them against native TASK like conductances.

The identification of the standing outward potassium currents, $I_{K(SO)}$, of the cerebellar granule neurone (Watkins and Mathie, 1996) with the localization of TASK-1 and TASK-3 mRNA expression in the cells provides a suitable native system for testing the agents. A further aim would be to establish, where possible, a molecular mechanism underlying the channel responses that could be used to predict sensitivities in other two pore domain channels.

In this study the heterologous expression in modified human embryonic kidney cells of TASK-1, TASK-2 and TASK-3 was used to characterise established pharmacology and seek out novel agents. Investigations of the potential mechanisms underlying the newly identified sensitivities (Chapters 4 and 5). With a transfer to the cultured murine cerebellar granule neurone (Chapter 4) comparing the native conductance with the cloned channel properties.

2 Methods

In order to compare the functional properties of the TASK and TALK channels, the cDNA of the specific channels of interest was incorporated into vector plasmids, transiently transfected into tsA-201 cells and studied using the whole-cell patch clamping technique. Studies were also carried out on primary cultures of murine cerebellar granule neurons using the same electrophysiological technique. All cell culture procedures were carried out under a laminar flow hood (heraSafe, Heraeus) sterilized by spraying all surfaces with 70% ethanol. Everything introduced to the laminar flow hood was sprayed with 70% ethanol also, and solutions were warmed to 37°C in a water bath before use.

2.1 tsA-201 cell growth and maintenance

In this study, two cell types have been used; the neonatal murine cerebellar granule neuron (see section 3.5) and tsA-201 cells. The latter are modified human embryonic kidney (HEK) cell line from the European Collection of Cell Cultures (ECACC, Sigma-Aldrich). The tsA-201 cells have an epithelial morphology and were first generated by transformation of cultures of normal human embryonic kidney cells with sheared adenovirus 5 DNA by Frank Graham in 1977 (Graham *et al.*, 1977) These cells are reputed to be one of the most straightforward to culture and transfect by the calcium phosphate method (see 3.3). A significant feature of this cell line is its possession of the SV40 large T antigen that allows for episomal replication of

transfected plasmids containing the SV40 replication origin, facilitating high production levels of recombinant proteins.

Cell culture and passage

tsA cell cultures were grown in 25cm^2 vented tissue culture flasks maintained in humidified incubators (Heraeus, Germany) at 37°C with 5% CO_2. The incubators were disassembled and had each internal component disinfected monthly using Barrycidal (Barry, Italy), and access to them was with nitrile or latex gloves sprayed with 70% ethanol solution at all times.

Each culture flask contained 5ml of culture medium comprising minimum essential media Eagle (MEM) with Earle's salts and L-glutamine, 10% heat-inactivated foetal bovine serum (HIFBS), 100 units ml^{-1} penicillin, 100μg ml^{-1} streptomycin and 10% non-essential amino acids. Cell growth was checked twice a week and at 80% confluency, the cells were passaged and plated.

To passage the cells, the culture medium was decanted from the flasks, and the cells washed twice with cold phosphate buffer solution (PBS, 4.3mM Na_2HPO_4, 1.47mM KH_2PO_4, 2.7mM KCl and 137mM NaCl). The cell monolayers were then dislodged from the surface by a 3 minute incubation at 37°C with 0.5ml of trypsin/EDTA (0.25%(w/v)) solution added at room temperature.1.5ml of culture medium was added to quench the action of trypsin before being triturated to break up any cell clusters. A cell pellet was formed by transferring the solution to a 15ml Falcon tube and, in turn, a centrifuge at 1200 rpm for 4 minutes at 4°C. The supernatant was removed and 5ml of culture media was added and the pellet was resuspended.

The cell density could now be determined using 50μl of cell suspension and a haemocytometer (Webber Scientific International), diluting the cell suspension 1:4 with 150μl of Trypan Blue Dye. The dyed solution was drawn under a coverslip and those cells that excluded the dye were counted (see 3.5.2). Flasks were seeded at a density of 1.5 x 10^5 cells ml^{-1}, making them suitably confluent for passaging after 3 days. Remaining cell suspension was cryopreserved at low numbers of passage cycles, or plated out for electrophysiology.

Cell plating for electrophysiology

Both tsA-201 and CGN cells were plated onto 13mm diameter plates coated with poly-D-lysine (poly-D-lysine Hrdrobromide, Sigma Aldrich) and incubated in 4 well cell culture plates.

The glass coverslips were stored in 100% ethanol, sonicated in ultra-filtered Mili-q water to remove particulate contaminates, then rinsed alternately in 100% ethanol and Mili-q water twice before being individually flame sterilized using a blue, roaring flame of a Bunsen burner. Once so cleaned, the glass coverslips were transferred to the 4-well culture plates under an extraction hood to avoid contamination with dust.

Plates were handled aseptically at all times, using fine forceps.

Poly-D lysine (PDL, 1mg ml^{-1}) was applied to each plate using a sterile glass Pasteur pipette which had had its tip flame polished for sterilization. The PDL was left for 20mins to form a film over the plate to which the cells would adhere. Excess PDL was

then removed using a new pipette and the plates were transferred to a closed UV plexiglass chamber for 1-2 hours for further sterilization.

Plates were stored aseptically at -4°C in sealed bags of four, and prior to use, were returned to the plexiglass chamber for a minimum of 2 hours of UV sterilization.

tsA-201 cells were plated at a moderate density (7 x 10^4 per ml) owing to their growth capacity. 0.5ml of cell suspension was used to seed the plates. CGN primary culture survival was found to be extremely density dependant. The optimum cell density was from a ratio of one cerebellum for 4 plates; 0.5x10^6 cells per ml.

Cryopreservation and resuscitation of cells

Transfection efficiency was found to decrease with repeated passage of cells over time (some months) and the cells became less tolerant of the whole cell patch configuration. It was therefore necessary to maintain a frozen stock of fresh cells which had been subjected to few passage cycles. Three 25cm^2 tissue culture flasks seeded with these optimum tsA-201 cells were used to produce two 1ml cryovials (Nunc, Denmark). Once the cells were 70-80% confluent, the culture medium was discarded and the cells washed twice with cold phosphate buffer solution (PBS) before detaching them from the flask using 0.5ml trypsin/EDTA (0.25%(w/v)) solution, added at room temperature. The flasks were then incubated for 3 minutes at 37°C (5% CO_2) and a gentle tapping ensured all cells were dislodged from the flask surfaces.

The cell suspension was then supplemented with 1.5ml of culture medium, quenching the action of trypsin, and transferred to a 15ml Falcon tube and centrifuged at 1200 rpm for 4 minutes at 4°C. The supernatant was then discarded and the pellet resuspended in 5ml PBS and the centrifugation repeated. On completion, the cell pellet was extracted and gently triturated in a cryopreservation medium of 90% heat-inactivated foetal bovine serum (HIFBS, Invitrogen) and 10% dimethylsulfoxide (DMSO), immediately transferred to 1ml cryovials and transferred to a cryocontainer and stored at -80°C.

Resuscitation of the cells was performed quickly as the DMSO of the cryopreservation medium is toxic at room temperature. Vials were warmed to 37°C in a water bath and, immediately upon thawing, the cell suspension was transferred to a 15ml Falcon tube and centrifuged for 4 minutes at 1200rpm with 10mls of culture medium. The supernatant was discarded and the cell pellet resuspended in 5ml of culture medium for seeding new culture flasks.

2.2 Molecular Biology

Wild-type human TASK-1, TASK-2 and TASK-3 channels were obtained as gifts from Dr Helen Meadows (GlaxoSmithKline) (See Chapman *et al.*, 2000 for methods on how TASK-3 was produced). The chimaeric TASK channel was a kind gift from Dr Catherine Clarke (University of New South Wales, Sydney, NSW, Australia). The chimaeric TASK channel was constructed by swapping the M1-P1 loop of TASK-3 (serine 31 to proline 71) with that of TASK-2 (glutamate 28 to glycine 77) channels, by the introduction of silent mutations to create unique restriction sites, Xho 1 and

BamH 1, on either side of the M1-P1 regions, as determined by SwissProt, using standard PCR techniques (Figure 2-1). Chimaeras were then formed by a simple "cutting and pasting" of this region using standard ligation procedures. The replacement TASK-2 M1-P1 region exceeded the TASK-3 M1-P1 region by four amino acids. All clones were in pcDNA3.1 expression vector (Invitrogen).

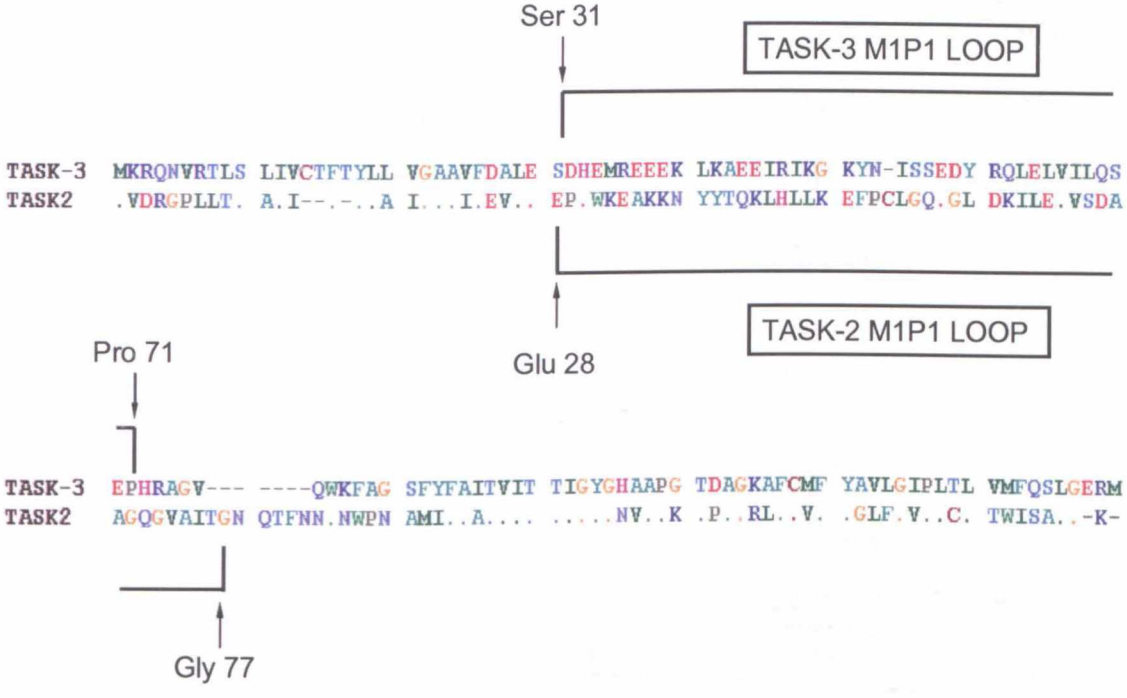

Figure 2-1 Chimeric TASK-2 TASK-3 channel The M1P1 loop of TASK-3 (residues 31 to 71) was replaced with that of TASK-2 (residues 28 to 77).

2.2.1 TASK channel expression vectors

The TASK DNA was incorporated into a pcDNA3.1 vector for expression (Invitrogen). This contained 4 key elements; the human cytomegalovirus (CMV) promoter (permits high level expression of channel), multiple cloning sites ((MCS) for gene insertion, facilitating cloning), neomycin resistance gene (for selection of stable transfectants in HEK cells) and SV40 elelments (early promoter and origin – for high level expression of the neomycin resistance gene – and polyadenylation signal – for transcription termination and polyadenylation of mRNA (Information sheet *pcDNA3.1(+), pcDNA3.1(-)*, Version 1, *www.invitrogen.com*)).

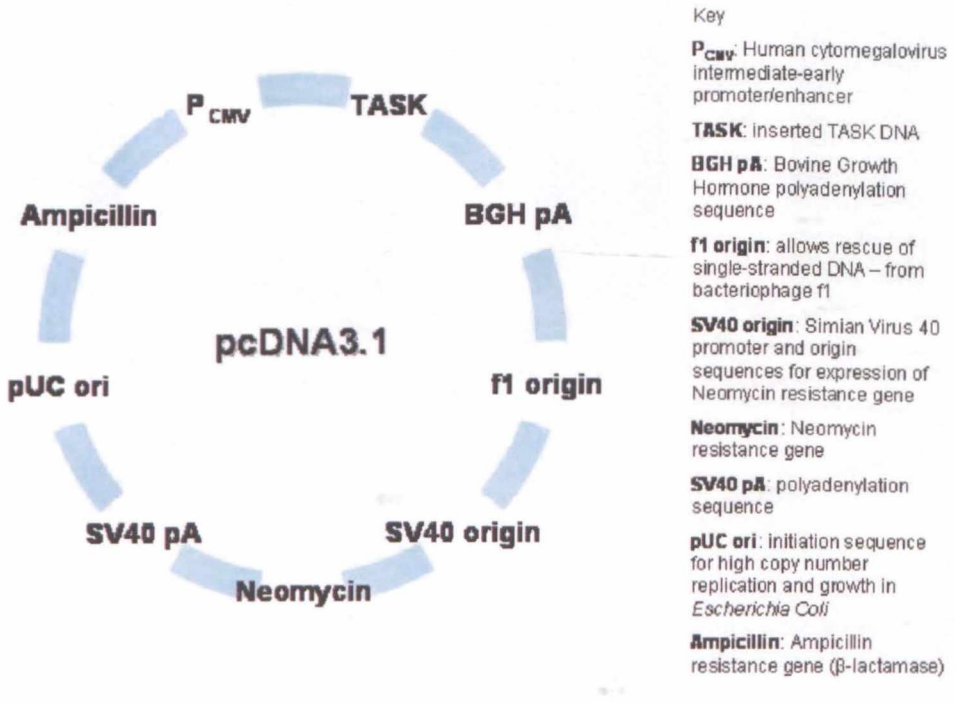

Figure 2-2 Map of vector pcDNA3.1 summarising features

2.2.2 Production of mutant and truncated channels

Mutant and truncated channels were created by Emma Veale using the QuikChange® Site-Directed Mutagenesis Kit (Stratagene, Amsterdam, The Netherlands). Individual or multiple amino acid point mutations were introduced using site-directed mutagenesis. Naturally occurring cysteine residues mostly present on the extracellular surface or transmembrane regions of the TASK-3 channel were mutated to alanine or serine residues (Figure 2-3). A truncated TASK-3 channel was also produced, where the last 124 amino acids of the channel were removed, was generated by the insertion of a stop codon (TAG) at position 250.

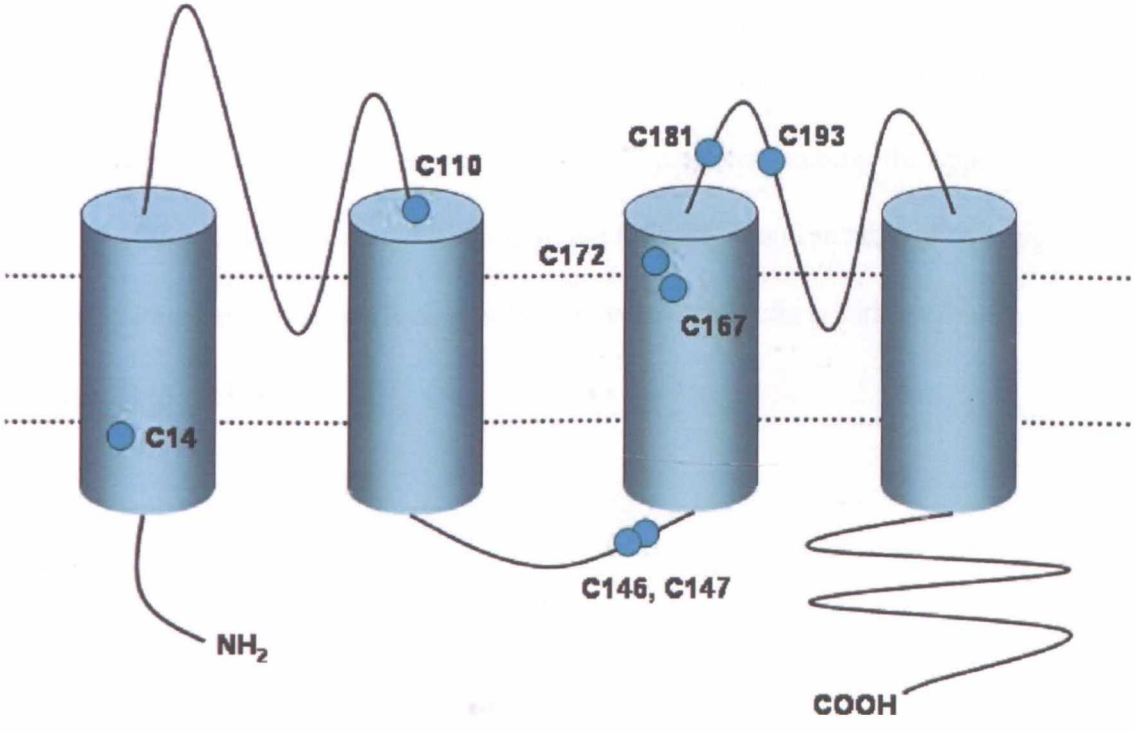

Figure 2-3 TASK-3 cysteine residues Naturally occurring cysteine residues were substituted for by alanine and serine. Single and multiple mutants were constructed, with a maximum of all eight cysteine residues shown substituted for serine residues.

Using *PfuTurbo*® DNA polymerase (Stratagene) in a temperature cycling process, the plasmids were denatured and the primers containing the desired mutation were annealed and incorporated, after which digestion (of the methylated, nonmutated parental DNA with *Dpn*I) and transformation cycles were completed to produce the mutated plasmid. The *Dpn*I treated DNA from each PCR reaction was transformed into XL1-Blue supercompetant cells (Stratagene), using a heat-shock-protocol. 50μl aliquots of supercompetant cells were defrosted on ice to which 1μl of the *Dpn*I treated DNA was added. Transformation reactions were mixed gently and then incubated on ice for 30minutes. The transformation reaction mixture was then heat-shocked at 42°C for 45 seconds and placed immediately on ice for 2 minutes. Following this incubation, 0.5μl of NZY^+ nutrient broth (preheated to 45°C) was added. It was then incubated at 37°C for 1 hour with shaking (225-250rpm). The transformation mixture was then plated onto agar plates containing the appropriate antibiotic (ampicillin, neomycin or kanamycin ($50mgl^{-1}$)) and incubated overnight at 37°C allowing only those cells containing the vector (therefore with antibiotic resistance) to proliferate.

2.2.3 Preparation of cDNA

Well separated single colonies of transformed cells were used to inoculate 5ml LB broth (Sigma, UK) cultures containing the appropriate antibiotic. After overnight incubation at 37°C (with gentle agitation), the bacterial cultures were divided and spun down (at 12,000g, 4°C for 10 minutes), the supernatant dispensed with and the bacterial pellet frozen at -80°C. Plasmid DNA was later removed from the cells using miniprep kits (Sigma) and stored, diluted with nuclease-free water, at -18°C.

1μl of the DNA was digested using specific restriction enzymes (Roche) to confirm correct banding pattern for the insert pre-freezing. Purity and concentrations were calculated using ultraviolet spectrophotometry (Beckmann DU530 spectrophotometer). All constructs and mutants were sequenced (MWG-biotech) to ensure correct base sequence, confirmation of the correct point mutation and to confirm absence of any non-specific sequence changes using pcDNA3.1_forward (GGC TAA CTA GAG AAC CCA CTG) and pcDNA3.1_reverse (GGC AAC TAG AAG GCA CAG TC) sequencing primers. All DNA clones were kept at -18°C in <1ml aliquots between 200 and 1000ng/l between uses.

2.3 Calcium Phosphate Transfection Protocol

tsA 201 cells were transiently transfected using a modified calcium-phosphate protocol (Batard *et al.*, 2001; Chen & Okayama, 1987). The primary expression construct comprised a pcDNA3.1 vector and the cloned DNA encoding the human TASK channel protein of interest; TASK-1, 2, 3, TASK-3-STOP, TASK-2 TASK-3 M1 P1 or a cysteine substitution mutant thereof (Figure 2-1). A plasmid containing the cDNA of green fluorescent protein (GFP) was co-transfected with the hTASK-cDNA, to fluorescently identify cells containing the TASK constructs. Those cells that had expressed the proteins were identified by their bright green fluorescence under the ultraviolet light source (mercury bulb, see *Experimental set-up*). Typically, over 80% of cells that express one protein will also express the other using this method (Phillips, 1997).

The expression constructs containing cDNA were added to the calcium chloride solution below, which was, in turn, gently vortexed with the phosphate solution. This mixture was then incubated for a maximum of 20 minutes at room temperature to allow calcium phosphate crystals to form, before being pippetting onto the plated HEK cells (cells were plated a minimum of 4 hours ahead of transfection). These crystals, containing the plasmid, adhered to the cells surfaces and the DNA was taken up into the nucleus where it was translated and expressed.

The cells were then transferred to a 3% CO_2 incubator at 37°C for 15 to 17 hours after which they were washed with phosphate buffered saline (PBS). Replacement fresh

growth media was added (0.5ml per well) and the cells were transferred to a 5% CO_2 incubator. Cells were then used for electrophysiology 24 to 48 hours later.

Solutions for Calcium-Phosphate Transfection

All cDNA solutions were stored frozen in aliquots while transfection solutions were refrigerated between use, and only applied to actively dividing cells for optimal take-up and expression of the plasmid cDNA.

Calcium Chloride solution

1000ng TASK cDNA construct

1440ng GFP cDNA construct

25μl 2M $CaCl_2$

+ H_2O to volume of 98.2μl (depending on concentrations of cDNA, ~67μl)

Phosphate solution

75μl Phosphate-free HEPES buffered Saline (see below)

1.35μl 100ml Na_2HPO_4 (titrated to pH 7.4 with HCl)

Phosphate-free, HEPES buffered saline – titrated with NaOH to pH 74

2M $CaCl_2$

280μM NaCl

50mM HEPES

100mM Na_2HPO_4

2.4 Whole cell patch clamping

2.4.1 Experimental setup

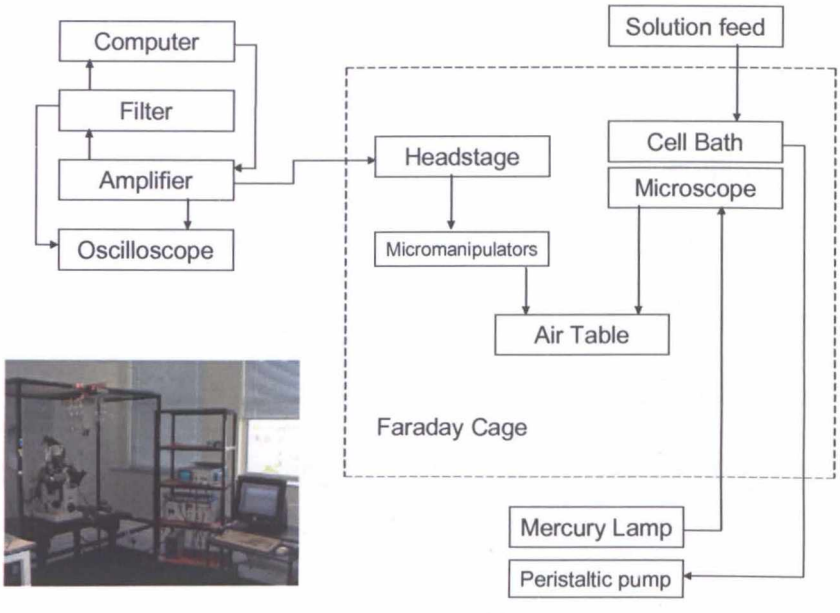

Figure 2-4 Block diagram of the patch clamp setup and photograph of equipment (inset). The experimental setup comprises three distinct systems, the data capture and processing equipment (computer with on-board oscilloscope, amplifier, headstage), the patching hardware (micromanipulators, air table, microscope, mercury lamp and Faraday cage) and the perfusion system (solution feed, cell bath and peristaltic pump) (*Adapted from Levis & Rae "Constructing a Patch Clamp Setup", chapter 2, Methods in Enzymology, vol 207).*

Experimental setup for whole cell patch clamp recording comprises three functional systems illustrated in figure 4-1; the data capture and processing equipment (computer, amplifier, headstage), the patching hardware (micromanipulators, mercury lamp, microscope and mercury lamp on the air table, in the Faraday cage) and the perfusion system. They provide a mechanically and electrically isolated system with which to measure and record transmembrane currents arising from the command voltages applied to the cell. The voltage protocols applied are designed to distinguish TASK channel currents from endogenous transmembrane currents of the native tsA-201 cell (see 2.4.4).

Mechanical isolation was provided by the air table (Technical Menu Corporation) to which the microscope and manipulators were fixed. The air pressure in the table was maintained by a pneumatic pump kept at 90p.s.i. The ambient room temperature was 22-24°C. All equipment was electrically grounded via the Faraday cage (minimizing the possibility for ground-loop noise) and the power supply to the microscope and lamp housings were shielded by being loosely (but securely) wrapped with foil. The apparatus was physically withdrawn from once recording was underway to minimize interference by stray capacitative charges. Recordings were further protected from interference from sixty-hertz frequency signals (for example from lights, the mains electric supply or electronic equipment in the room) by directly grounding the bath stabilizing pins on the stage.

Plates of cells were placed into the bath in the primary recording chamber, perfused with external solution and secured to the base of the chamber using Vaseline. An inverted microscope (Diaphot, Nikon) was used to visualize the cells through the glass bottom of the bath (20mm coverslip) and could be brought into very close proximity of the cells. It was fitted with both a standard light source and a Halogen lamp (Microscope light source Osram Low voltage Tungsten Halogen lamp 64610 HLX)

The custom built, perspex bath comprised two chambers, the primary recording chamber and the secondary waste reservoir chamber from which solutions were drawn using a peristaltic pump. The second chamber also housed the earthing electrode, a silver wire ended with a silver chloride pellet (Harvard Apparatus, UK), which, via the reversible electrochemical reaction, $Ag + Cl^- \leftrightarrow AgCl + e^-$, converted ion flow in

the bath solution to be converted to electron flow in the electrode. The two chambers were connected by a narrow, open channel through which flowed the perfusing solutions (external or test), from the 60ml plastic syringes (without plungers) of the gravity feed, at a rate of approximately 1ml per minute. A flow switch connected six syringes to the bath via a single line of PTFE tubing that allowed a quick change from external to test solution and back again.

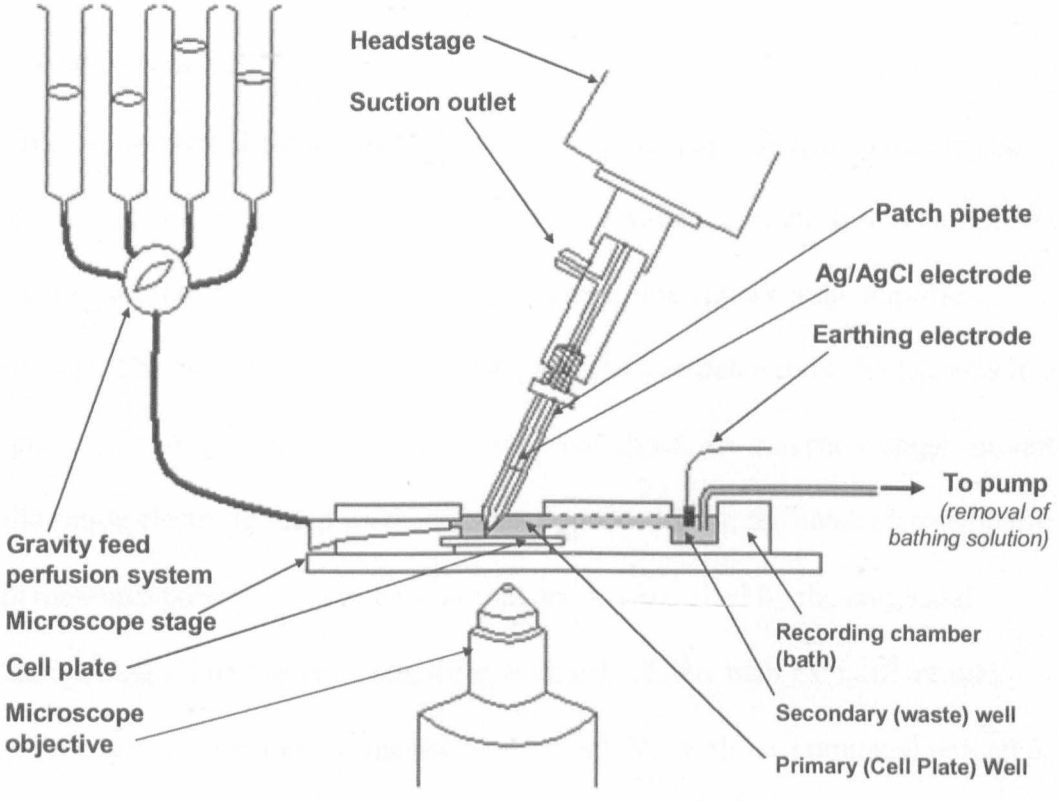

Figure 2-5 Schematic of experimental setup for whole cell patching The filled patch pipette tip was manoeuvred into close proximity of the cell chosen for patching using a hydraulic micro-manipulator. The cell plate was secured with Vaseline to the base of the primary recording chamber and was constantly perfused with external or test solutions from the gravity feed perfusion syringes mounted at the top of the Faraday cage. The second chamber of the Perspex recording bath was connected to the primary with a channel, through which the external solution was drawn by a vacuum created by a peristaltic pump outside of the Faraday cage. From the secondary chamber solutions were expelled into a waste reservoir. This chamber also housed the earthing electrode, comprising a silver wire ended with a silver/silver chloride pellet. The suction outlet was connected to an empty syringe via PTFE tubing, a closed system to allow the seal to be made.

The microelectrode pipette was brought into close proximity to the cells using coarse (Axon Instruments) and fine (Water Robot Micromanipulator, Narishige Scientific Instruments) micromanipulators mounted together. It was found that the safest and quickest way for the pipette to be manoeuvred into position was by initially focusing on the cell, defocusing to a point above the cell, and then bringing the microelectrode tip into focus by adjusting the micromanipulator. These steps were repeated until the cell surface and the pipette were in focus in the same plane. The fine micromanipulators were used to bring the pipette into mechanical contact with the cell.

Recording electronics

In order to measure the changes of the TASK channel currents in response to test solutions, the cell membrane is clamped and the resultant current flow is compensated for and measured via a resistive feedback circuit of the patch clamp amplifier headstage. This is done within the headstage of the microelectrode pipette, which, by outputting a voltage that corresponds to a current input, are current-voltage converters. In the single electrode setup used here, the electrode within the patch clamp pipette both measures potential and injects current and is controlled by the command potential, V_{CMD}. The feedback amplifier, with gain A, is a high gain differential amplifier, and it compares the measured potential, V_P, with the command potential, V_{CMD}, Its output is proportional to the difference between the two. V_{CMD} is fed into the non-inverting input of the amplifier (i.e. the input with the same polarity as the output), while V_P is fed into the inverting input. The output voltage (V_O) of the amplifier is a function of the difference between the two inputs ($V_O = A(V_{CMD} - V_P)$). This is fed back by the output being connected to the inverting input, therefore minimizing the difference between the two inputs.

When a cell is clamped, and the V_{CMD} is set such that a current (I_P) starts to flow through the cell membrane, the membrane potential will change, altering measured potential of the pipette, V_P. The feedback arrangement around the amplifier injects an opposing and equal current to I_P (I_F) via the pipette, minimising the difference between V_P and V_{CMD}, holding the cell at the desired potential.

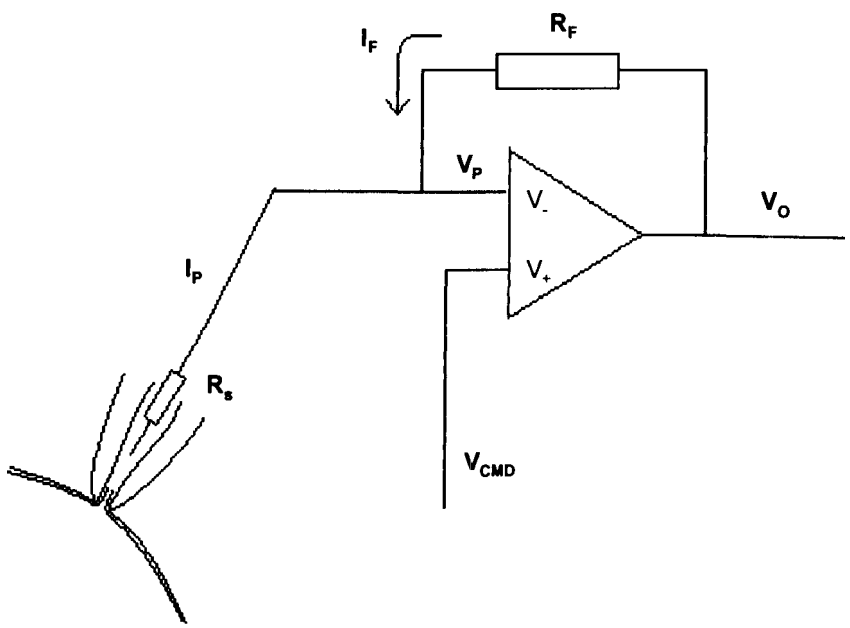

Figure 2-6 The Patch Clamp Headstage Circuit Diagram The differential amplifier of the patch clamp headstage has two differential inputs, V_-, and V_+. V_- is known as the *inverting* input to the amplifier as its polarity is opposite to the amplifier output. The output of the amplifier is proportional to the difference (hence *differential*) of the inputs, in the form, $V_o = A (V_+ - V_-)$ where A is the gain. V_{CMD} is controlled by the experimenter, V_P is the voltage measured by the pipette and V_O drives a feedback circuit by providing a current, I_F, through a resistor, R_F, that compensates for any current change needed to maintain the cell membrane at a constant membrane potential, making $V_P = V_{CMD}$.

Voltage clamp data were low-pass filtered at 5kHz and sampled at 2-10kHz. Currents were amplified with an Axopatch-1D patch clamp amplifier (Axon Instruments) equipped with a CV-4 headstage (Axon Instuments, Foster City, CA, USA). Data was stored on the hard drive of a standard Pentium 2 Dell PC, digitized with a DigiData

1200 Series Interface. The "'scope view" function within the pClamp software enabled the visualization of cell responses to the command voltage protocols during recordings, and a separate oscilloscope (2221A 100MHz Digital Storage oscilloscope, Tecktronix) was used to achieve whole cell patch clamp and monitoring and spontaneous changes in cell stability (leak, series resistance, capacitative transients).

Electrode Manufacture

The command voltage was applied to the cell membrane by way of a silver wire electrode coated with silver chloride, in a boroscillate glass pipette that was back-filled with the internal salt solution.

The glass pipettes were pulled from glass capillaries (using a two-stage vertical Narishige PC-10 puller) which had an internal diameter of 0.86mm and external diameter of 1.5mm, the relatively thick walls generating low electrical noise. For successful gigaseal formation, the pipette tips were fire-polished using a microforge (Narishige MF-83) under direct visualization using magnifications of 100x. Fire polishing of the pipette tip consisted of loading the pulled capillary into the microforge under high magnification and bringing it into close proximity to a short loop of platinum iridium wire. The wire loop was heated yellow-hot very briefly (manually controlled) and the brief pulse melted the pipette tip, rounding any jagged edges and smoothing any rough surfaces ensuring a clean and smooth finish.

2.4.2 Practical considerations of the whole cell voltage clamp recording

Series Resistance Compensation

The whole cell patch clamp described and used in this study is also known as a continuous single electrode voltage clamp. The same electrode is used for current passing and voltage recording, and the voltage at the top of the pipette is controlled by the voltage clamp circuit within the headstage, as opposed to the tip. Two main factors alter the voltage recorded at the top of the pipette; the residual resistance of the ruptured cell membrane, and the pipette itself. It is from their being in series with the membrane that these resistances get their name, and the extent of their influence is also determined by the size of the currents that must flow through them. Series resistance is therefore problematic as it causes errors in membrane potential when large membrane currents flow ($V = IR$) and its presence necessarily means that the charging of the membrane capacitance is slowed as it impedes the flow of capacitative charging currents when a voltage step is applied to the electrode.

Series resistance compensation is the addition of a signal, proportional to the measured current, to the command potential. This limits errors in the I-V curves recorded and improves the effective speed of the voltage clamp. It relies on the accurate determination of R_S throughout the experiment (which is subject to spontaneous change).

Whole Cell Capacitance Compensation

At the onset of voltage changes high-amplitude currents are generated comprising two components, a slow component for charging the cell membrane (cell membrane capacitative current) and a fast current (so called because the time constant of the corresponding current is very fast) caused by charging the pipette capacitance. Both the cell membrane and the pipette act as capacitors because they are thin insulators separating the conducting solutions of the internal milieu of the cell and the bath solution. Compensation of the currents avoids saturating any amplifiers of the recording circuit. It is done by feeding an adjustable signal (V_{shaped}) to the negative input of the headstage amplifier. The corresponding current flow cancels the capacitative current so that no net current is recorded by the amplifier.

Pipette capacitance is distributed along the length of the pipette and time courses of the transients will reflect dielectric relaxation in the material of the pipette holder and glass. Each element of capacitance has a different amount of resistance in series with it so that a single value of the time constant will not provide perfect cancellation. Using pipette glass with low dielectric loss helps minimize the error.

The cell capacitance component of the transient can also be reduced to a fraction of its original amplitude if the chosen cell is round. However, a cell with many processes or a long, cylindrical morphology will have a complex capacitative transient will, not a single exponential, and the cancellation will not be as complete. Such cells were avoided, as were those in close proximity to or in contact with neighbouring cells.

In this study, whole cell capacitance and series resistance compensation were monitored by adjusting the controls on the amplifier immediately after achieving a tight gigaseal and rupturing the cell membrane. Turning up the gain on the oscilloscope allowed the visualisation of capacitative transients and facilitated the manual balancing of compensation. Whole cell capacitance and series resistance compensation was recorded for every cell.

Liquid Junction Potentials

Liquid junction potentials exist between two solutions of differing compositions at their apposing boundaries owing to differing ionic mobilities. During whole cell recording, the internal and external (bath) solutions are separated by the cell membrane, but an error can be introduced when the pipette current is nulled by adjusting the offset to show zero current and voltage prior to seal formation, while the pipette solution is in contact with the external solution. Doing so also compensates for the junction potential. When the whole cell configuration is achieved, the solutions are separated and the compensated potential is no longer necessary, so the command voltage is distorted.

In this study, the use of KCl as the predominant salt in the internal solution apposing the physiological salt solution of the bath helps minimize the offset. Liquid junction potentials were measured using a simple protocol. A zero junction potential was set up by having the pipette and bath loaded with internal solution only. The patch clamp amplifier was set to current clamp, and the voltage was monitored and the current zeroed by use of the null controls on the amplifier. The bath solution was then replaced with external solution and the resultant change in voltage while maintaining

zero current flow was measured. Using this method, the potential was recorded as 1mV. This offset would be present in the pipette after seal formation. As it was less than a 1% contribution to the command potentials (maximum range of voltage protocol is -110mV to +20mV), it was therefore an insignificant source of error. Data presented here is without liquid junction potential correction throughout.

Choosing suitable cells

As described previously, the tsA-201 cells were co-transfected with both the TASK channel cDNA of interest, and the cDNA of green fluorescent protein (GFP) to identify which cells were suitable for experiments. The mercury lamp (with HB10104 Superhigh Pressure Mercury Lamp Power supply) provided a broad spectrum of UV light which excited the GFP at around 395nm, causing it to fluoresce in the visible spectrum at 509nm (Chalfie *et al.*, 1994) appearing green.

Very large cells, those in contact with neighboring cells, those which had poorly defined margins and those that fluoresced excessively were discarded. Very bright cells tended to exhibit much larger currents than would normally be expected. They would run-down rapidly and not stabilize, or the cell would be extremely short-lived. Conversely, poorly fluorescing cells generally had very low levels of TASK channel expression. Both were avoided where possible. Ideal cells were of moderate brightness under UV light, and isolated, adhering well to the plate and oval and displayed strong phase contrast around their perimeter.

Cells also had to be discarded 72 hours after transfection as their fast growth rate, although optimal for protein expression, led to >70% confluence if left incubated for any length of time after this.

Patching cells

Once a suitable cell for patching has been identified, a fire-polished, borosilicate glass pipette, back-filled with intracellular solution, (see 3.4.3) was inserted into the pipette holder of the headstage amplifier (see 3.4.1), the contained solution just immersing the tip of the electrode. The tip of the pipette was then lowered into the bath and, using the coarse and fine micromanipulators, brought into close apposition to the cell. While the electrode remained immersed in the bath, the amplifier was set to apply a 5mV square-wave to the pipette, with a holding potential of 0mV. Upon contact with the cell membrane, the increase in pipette resistance was signified by a step up in amplitude of the square wave. Pulling out the plunger of the syringe, with which the electrode pipette was continuous, applied a gentle negative pressure which brought the cell and pipette tip into contact, verified visually, and on the oscilloscope by the amplitude of the square waves diminishing to a straight line. The holding potential at this point was taken down to -60mV to aid the formation of a tight seal, to keep calcium channels closed to avoid calcium loading the cell and to avoid depolarizing the cell when breaking the patch. For whole cell recording, the membrane was ruptured in one of two ways. A further, manual draw on the plunger could rupture the cell membrane sufficiently gently avoiding unnecessary damage, or the cell could be 'zapped' (application of a large potential to the membrane patch) via the amplifier. Doing so created capacitative transients as the pipette became continuous with the cell membrane, the intracellular solution now being in contact with the internal milieu of

the cell. The transients were then cancelled on the amplifier by adjusting the whole cell capacitance and series resistance compensation. Once cancelled, the amplifier square wave was cancelled to avoid introducing artifacts, and the cell allowed to stabilize at a holding potential of -60mV.

Leak

A significant source of error, 'leak' can be exhibited by the patched cell once accessed by the pipette, masking the current flow through the channels of interest. In this setup, it manifested in a small proportion of cells as a non-specific, frequently increasing (and subsequently fatal), inward current present at all voltages, but easiest to identify at the -80mV step episode. According to the Nernst equation, the reversal potential for potassium with the concentrations used should be near -100mV. Consequently, it is to be expected that a small outward current (positive) should be resent at -80mV. Absence of such a current or indeed presence of an inward (negative) current at this point of the recorded trace indicated a 'leaky' cell to be discarded. Such cells were found to have low-resistance pipette-membrane seal resistance, allowing ion influx through this glass-membrane junction. It was found that keeping cells hyperpolarised (at-60mV), while going whole-cell, significantly facilitated the formation of seals with resistance greater or equal to 1GΩ. Seal resistance could be easily monitored in real time during the patching process on the patch amplifier.

Other, more general sources of leak can be persistent native ion channel activity. This was minimised through careful design of the stimulus waveform (see 3.4.4), analyzing data at potentials where minimal voltage dependant ion channel activity is present (-40 to -80mV and avoiding calcium loading of the cell. Calcium loading of the cell can

open calcium-activated calcium release channels (releasing calcium from internal stores) and keep calcium activated chloride and potassium channels active, masking TASK channel responses. 5mM ethylene glycol bis beta aminoethyl ether tetra-acetic acid (EGTA) was included in the internal pipette solution to chelate excess Ca^{2+}.

2.4.3 Experimental Solutions

All chemicals were purchased from Sigma Aldrich Ltd (UK) unless otherwise stated.

External, bathing solution, comprised 145mM NaCl, 2.5mM KCl, 3mM $MgCl_2$, 1mM $CaCl_2$, 10mM HEPES buffer solution, titrated to pH 7.4 with 10M NaOH. Internal pipette solution comprised 150mM KCl, 3mM $MgCl_2$, 5mM EGTA and 10mM HEPES buffer, titrated to pH 7.4 with 5M KOH. These concentrations were chosen to supplement the pipette solution for as long as possible to maintain the normal function of the cells and particularly the normal function of the TASK channels, minimizing run-down.

External solution was made up in 10x concentration batches and diluted before experimentation daily. Internal solutions were made up in batches, and frozen in 1ml aliquots. Both solutions were discarded monthly and remade.

2.4.4 Data Acquisition and Voltage protocols

The pClamp software used for data acquisition was Clampex 8 (Axon Instruments) was used while Clampfit 8.1 and Origin 5.0 (Microcal ™ Origin™, Microcal Software, Inc, Northampton, MA, USA) were used for offline analysis of data.

Voltage protocol was designed to isolate TASK channel currents from endogenous potassium currents of the tsA-201 cells. The cells were held at -60mV before going through the 6 epoch step and ramp protocol, the step comprising a voltage shift down to -80mV for 100ms then up to -40mV for 500ms. The ramp ran from -110mV to +20mV over 500ms before a brief 100ms step at -80mV before returning to the holding potential of -60mV. In a single cycle it was possible to record both the held current and an IV relation with the ramp. Using this protocol, between -80 and -40mV supplementary conductance contribution by endogenous K_v currents (which make significant contributions to whole cell currents at and above -20mV) were minimised.

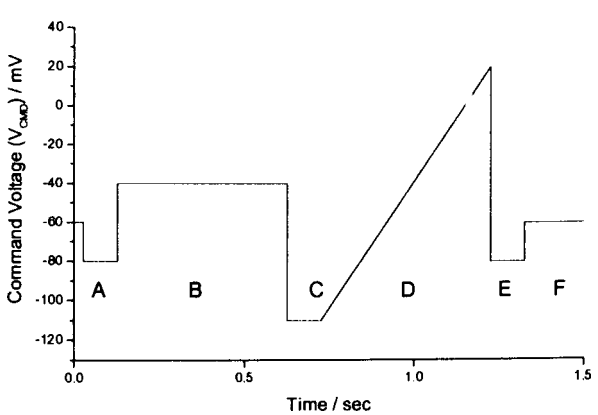

Figure 2-7 Waveform of command voltage protocol for tsA-201 cells. This step-ramp protocol was used to isolate TASK channel currents from endogenous potassium currents in of the tsA cells once patched (A) initial step down form the holding potential of -60mV to -80mVfor 100ms (B) 40mV step up to -40mV for 500ms (C) Step down to -110mV for 100ms (D) voltage ramp from -110mV up to +20mV over 500ms (E) final step at -80mV for 100ms (F) holding potential of -60mV. The entire protocol cycled once every 5 seconds when initiated, and recordings consisted of 40 step-ramp sweeps.

2.5 Primary Culture of Murine Cerebellar Granule Neurons

TASK channels were found to be highly expressed in the cerebellum, particularly within the granule cell layer (Rusznak *et al.*, 2004; Karschin *et al.*, 2001; Medhurst *et al.*, 2001; Talley *et al.*, 2001) and a TASK-like conductance, IK_{SO}, was identified by Watkins and Mathie (Watkins & Mathie, 1996) in cerebellar granule neurons. It is now thought that the TASK-1 and TASK-3 channels are directly responsible for this standing outward potassium current of granule cells (Aller *et al.*, 2005; Kang *et al.*, 2004; Millar *et al.*, 2000; Talley *et al.*, 2000). To complement the studies here and provide a valuable comparison with the murine wild-type, a protocol for primary culture of cerebellar granule neurones was refined and optimized for electrophysiology as described here.

All solutions were filtered through a 0.22μm Millipore syringe filters (Sarstedt) prior to use, and made in a laminar flow hood prepared by washing down with 100% ethanol where possible. All solutions were stored at 4°C and obtained from Sigma unless otherwise noted.

2.5.1 Tissue Dissection

P7-P8 C57Black6 mice pups were decapitated, rinsed in ethanol and washed with ice cold Hanks Balanced Salt Solution (Basal Salt Mixture, Sigma-Aldrich). The tissue was handled as little as possible to minimize temperature elevation and damage while the cells were being separated from the connective membranes.

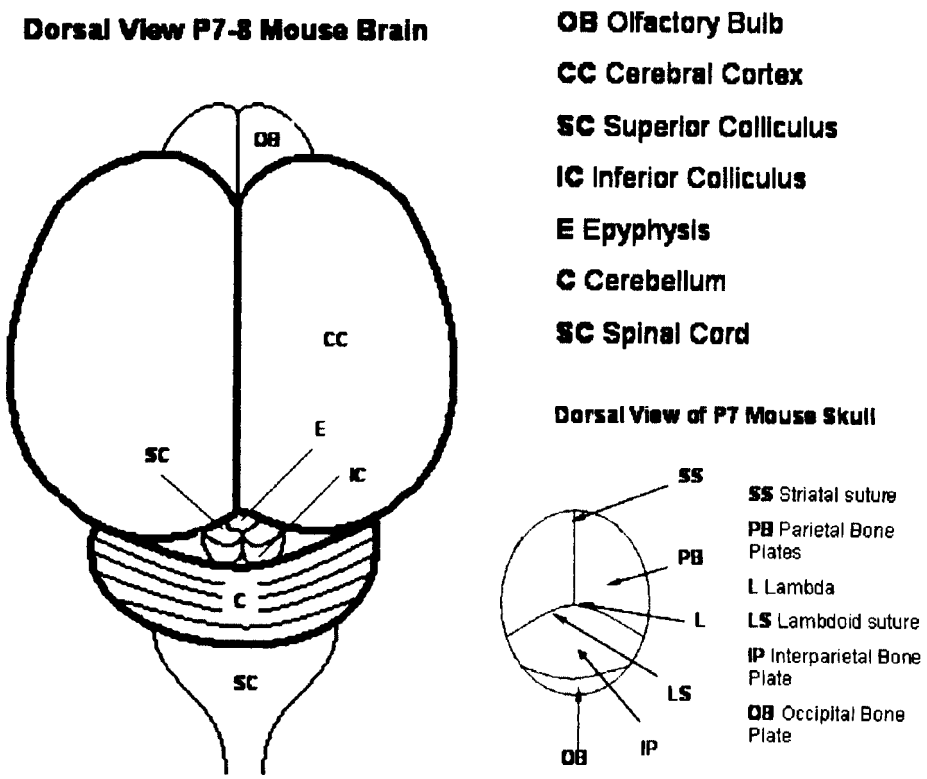

Figure 2-8 Surface anatomy of the P7 C57Black6 mouse brain (Skull surface anatomy inset)

A sagittal incision through the dermal layers to the skull surface was made by inserting dissection scissors at the base of the skull and bisecting the skin over the back of the head along the sagittal suture of the skull. Once peeled and pinned forward, the dissection scissors were inserted into the foramen magnum and the cranial cartilage was cut through along the lateral part of the skull from the occipital plate forwards, until the base of each ear on both sides. A sharp scalpel was then used to cut through the cartilage along the lambdoid suture, down towards the base of the ears, allowing the immature occipital plates to be removed entirely, exposing the cerebellum, epiphysis colliculi superiors and colliculi inferiors of the hindbrain (see fig 5.1). Curved forceps were then inserted around the cerebellum, which could be gently separated from the rest of the brain. The dura mater, arachnoid mater and meninges were then pulled away from the tissue where possible and the cerebellum

was then stored in ice cold cerebella granule neuron culture medium (Minimum essential media eagle (MEM) supplemented with 2% Heat inactivated foetal bovine serum, 25mM KCl, 30mM glucose, 60units/ml penicillin, 60μg/ml streptomycin, 5mls ITS supplement) until required. One mouse pup cerebellum was found to provide the optimum density of cells for 4 plates (10mm diameter, 1ml growth medium). Longevity of the cells is crucial in primary culture and it was found that the dissection must be done as quickly as possible, minimizing the time between animal sacrifice and disaggregation of the cells.

2.5.2 CGN culture and maintenance

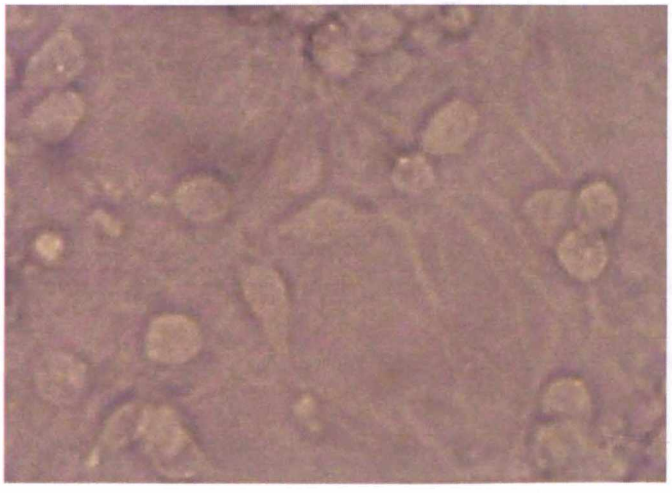

Figure 2-9 Cerebellar granule neuron culture taken at culture day 7 using an S7000 SLR-type Fujifilm digital camera through the Diaphot Inverted Nikon microscope. The image has been enhanced using Paint Shop Pro 5.

Immediately after dissection, cerebella were transferred to a laminar flow cell culture hood prepared by spraying with 70% ethanol and placed onto a 100% ethanol soaked tissue to maintain sterile environment for tissue manipulation. Growth medium was removed from the dish using a sterile disposable Pasteur pipette, carefully reserving the tissue. Cerebella were then rinsed with ice cold HBSS and chopped finely with a sterile razor blade (prepared by soaking in 100% ethanol).

Trypsin was added in excess (~2ml per cerebella) to digest the tissue and the suspension was triturated using a fire polished glass Pasteur pipette, before being incubated at 37°C (5% CO_2) to allow the enzyme to gradually disaggregate the tissue. Trituration and incubation was repeated and the solution was transferred to a sterile 15ml falcon tube with excess minimal essential media (MEM) to quench the action of the enzyme.

The coarse cell suspension was triturated again before being centrifuged at 2800 RPM for 8 minutes. This high speed and prolonged centrifugation time was found to be optimum for pelleting the small granule neurons.

After centrifugation, the supernatant was carefully removed and discarded, the pellet resuspended in 3ml MEM by trituration. Large clumps of cells were discarded after allowing them to settle. The remaining cloudy suspension was drawn up (leaving the larger tissue debris behind) into a sterile disposable stripette. The cells suspension was then transferred to prepared 4 well culture plates, allowing 0.5ml for each cell plate.

CGN cultures were then transferred to 37°C (5% CO_2) incubators overnight. It was found that neurite growth could be seen within 24 hours of plating. CGN cultures were maintained for a maximum of 3 weeks, replacing growth media once every five days and were ready for electrophysiology after 7 days in culture.

Plating density

It was found that the plating density of the CGN cells was a fundamental environmental factor in the success and longevity of the culture. The density of several successful cultures (good neurite growth, minimal cells death, extensive CGN

migration from starting cell clusters, good cell adhesion) were measured. Optimum plating density was found to correlate with approximately one cerebellum per four wells (each containing 0.5ml cell suspension. This was calculated to be $0.5x10^6$ cells per ml.

Cell counts were performed using a haemocytometer and Trypan Blue dye (Sigma). 50μl of cell suspension was expelled into an Eppendorf tube. Trypan Blue (150μl) was added to the Eppendorf, diluting the cell suspension 1:4. The haemocytometer (Webber Scientific International) was prepared for the microscope using a coverslip and the dyed cell suspension solution was drawn under it, forming a monolayer of cells. Total cells in four quadrants of the cytometer were counted, and the density of the cell suspension was calculated from the following equation;

$$\text{Cell suspension density} = 4 \times 1 \times 10^3 x\bar{\delta}$$

Where $\bar{\delta}$ is the mean cell count (mean cells of four quadrants), 4 corresponds to the dilution factor and 1×10^3 converts the volume to ml from μl.

2.5.3 Recording CGN currents

CGN currents were recorded using the same experimental set up as previously described. CGNs were held at -20mV and stepping to -60mV for 250ms every six seconds. The standing outward potassium current, IK_{SO} was taken as the average current over 200ms at -20mV. Micropipettes where found to be more successful when pulled at a higher temperature creating a finer tip with a higher resistance.

2.6 Analysis

All cells were continuously perfused to avoid any build-up of test solution and to maintain control of the concentration of test solutions applied. Cell responses were found to be maximal at 10-15 sweeps (50-75 seconds) after the perfusing chamber had been changed from the control using the switch. Test solutions were only applied once the patched cell had reached stability upon achieving whole cell patch clamp and were typically applied for 50 seconds, variation determined by the stability of the cell once maximal effect was achieved. Second applications of test solutions occurred only if full wash-out of the initial solution was accompanied by a full recovery of the control response where appropriate.

Offline analysis was conducted using Microcal™ Origin™ 5.0 (Microcal Software Inc, USA) data analysis software importing whole cell currents recorded with Clampex (online) via Clampfit version 8.1.0.12 (Axon Instruments Inc.) and Excel (Microsoft Office).

Percentage inhibitions were calculated using a plot of time course of drug response (current against time). The mean current over the maximal cell response was subtracted from mean of the current before and after (upon full recovery) test solution application, avoiding skewing of data if run down was present. Time courses were constructed as a ratio of the mean current at -40mV divided by the mean current at -80mV.

Error bars were plotted as the standard error of the mean (SEM = sd/$\sqrt{n}$ where sd = standard deviation of the population and n = number of variables). The Student t test was used to determine the significance of difference between two populations of data. The t test used was a two population independent t test where normal distribution of the data was assumed and differences were considered significant probability, $p < 0.05$.

Current voltage relations were calculated using the ramp from the step-ramp protocol, taking the mean of five traces before the drug response, and five on maximal drug response, and plotting as a line graph between -110mV and +20mV to avoid K_V current contributions.

Where responses to a range of test concentrations were available, these were fitted to the Hill equation using Origin where all parameters were allowed to vary.

$$y = V_{\max}\left(\frac{x^n}{k^n + x^n}\right)$$

Where V_{max} is the maximal response, k is the concentration at 50% of maximal response and n is the Hill coefficient.

3 Results

3.1 Characterisation of TASK-1 and TASK-3 channel currents

In this chapter, the functional properties of TASK-1 and TASK-3 channels expressed in tsA-201 cells and recorded under whole cell voltage clamp conditions are described.

3.1.1 Current size and IV

The differing amplitude of whole cell currents through expressed TASK-1 and TASK-3 channels can be seen in Figure 3-1. Cells were held at a holding potential of -60mV, and stepped to various voltages. The mean difference current between that measured at -40 mV and that at -80 mV is substantially less for TASK-1 transfected cells (218.7 ± 31.2ρA, n = 33) compared to TASK-3 transfected cells (1210.3 ± 76.1ρA, n = 109) (Figure 3-1). In previous studies, in symmetric K^+ solutions (100 – 150mM), single channel recording of TASK-1 channel currents show inward and outward unitary conductances of 14 and 10ρS respectively, almost half those of TASK-3 under the same conditions, 30 and 17ρS (Han *et al.*, 2002; Kim *et al.*, 2000; Lopes *et al.*, 2000; Leonoudakis *et al.*, 1998) reflecting the whole cell data The difference in whole cell conductance has also been attributed to differences in trafficking of the channels to the membrane (Renigunta *et al.*, 2006; Rajan *et al.*, 2002) as well as differing open times (Kang *et al.*, 2004; Han *et al.*, 2002), and is likely due to a combination of all three factors. (See Discussion).

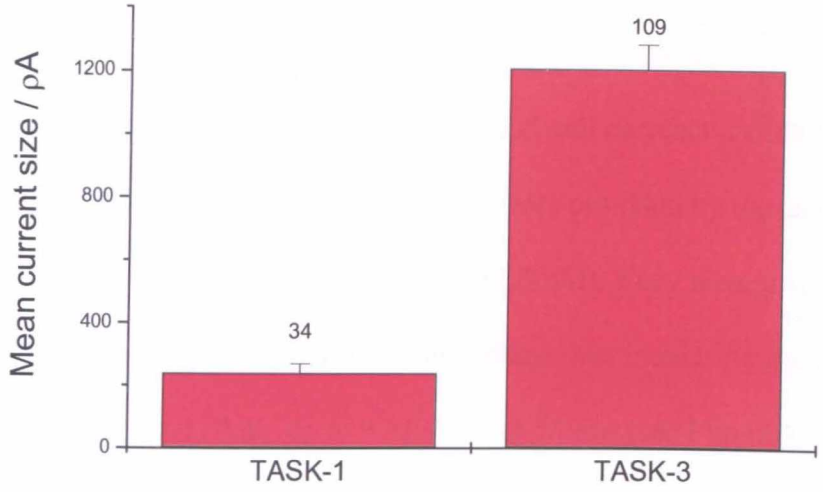

Figure 3-1 Mean whole cell TASK-1 and TASK-3 currents. Transfected HEK whole cell currents represented here are a difference between I_a - I_b where I_a was the whole cell current at -40mV and I_b was the whole cell current at -80mV. Error bars represent standard error of the mean (S.E.M.) values.

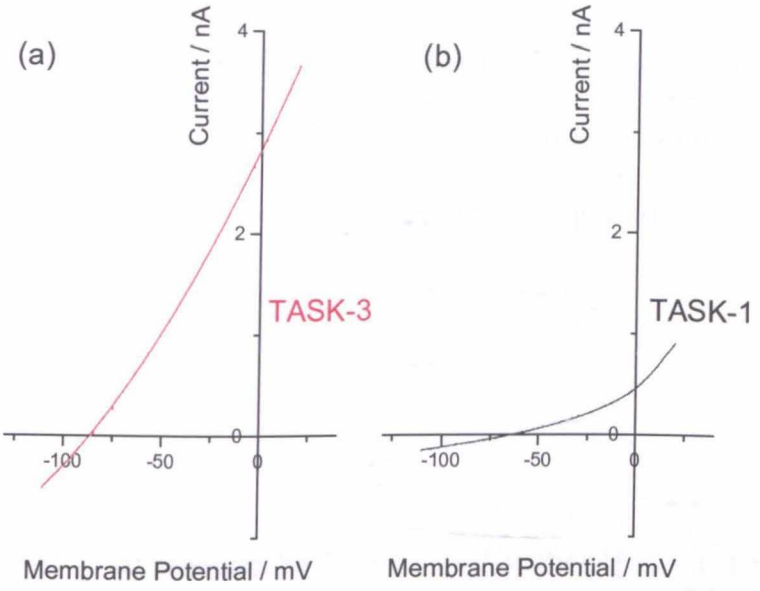

Figure 3-2 Mean I-V relations for (a) TASK-3 and (b) TASK-1 currents of transfected HEK cells Figure shows mean current – membrane potential relationship for n = 8 exemplar TASK-1 cells and n = 9 exemplar TASK-3 cells, each cell providing three IV traces.

The *I/V* plots (Figure 3-2) of TASK transfected HEK cell currents are outwardly rectifying in the physiological potassium ion gradients provided by the concentrations within the pipette (150mM KCl) and in the bath (2.5mM). They were generated by holding the membrane potential at -110mV for 100ms then increasing the potential in a continuous ramp from -110mV up to +20mV over 500ms (see Figure 4, Methods). Both TASK-1 and TASK-3 currents reverse around -70 mV, akin to previously reported reversal potentials for the channels (Clarke *et al.*, 2004) although more positive to the predicted E_K (-103.4mV). This difference is most likely explained both by the presence of a non-selective leak conductance which reverses around 0 mV and the fact that the channels are not completely selective for K ions. The greater whole cell current amplitude in the TASK-3 transfected cells over that of the TASK-1 counterparts is reflected in the steeper gradient of the I-V plot of the former, consistent with previous findings (Renigunta *et al.*, 2006).

3.1.2 pH sensitivity

TASK-1 and TASK-3 currents can be distinguished by the pH at which they are half-maximally activated (pK), being near pH 7.3 for TASK-1 currents and pH 6.6 for TASK-3 (Clarke *et al.*, 2004; Kim *et al.*, 2000; Rajan *et al.*, 2000; Talley *et al.*, 2000; Lopes *et al.*, 2000; Leonoudakis *et al.*, 1998; Duprat *et al.*, 1997).

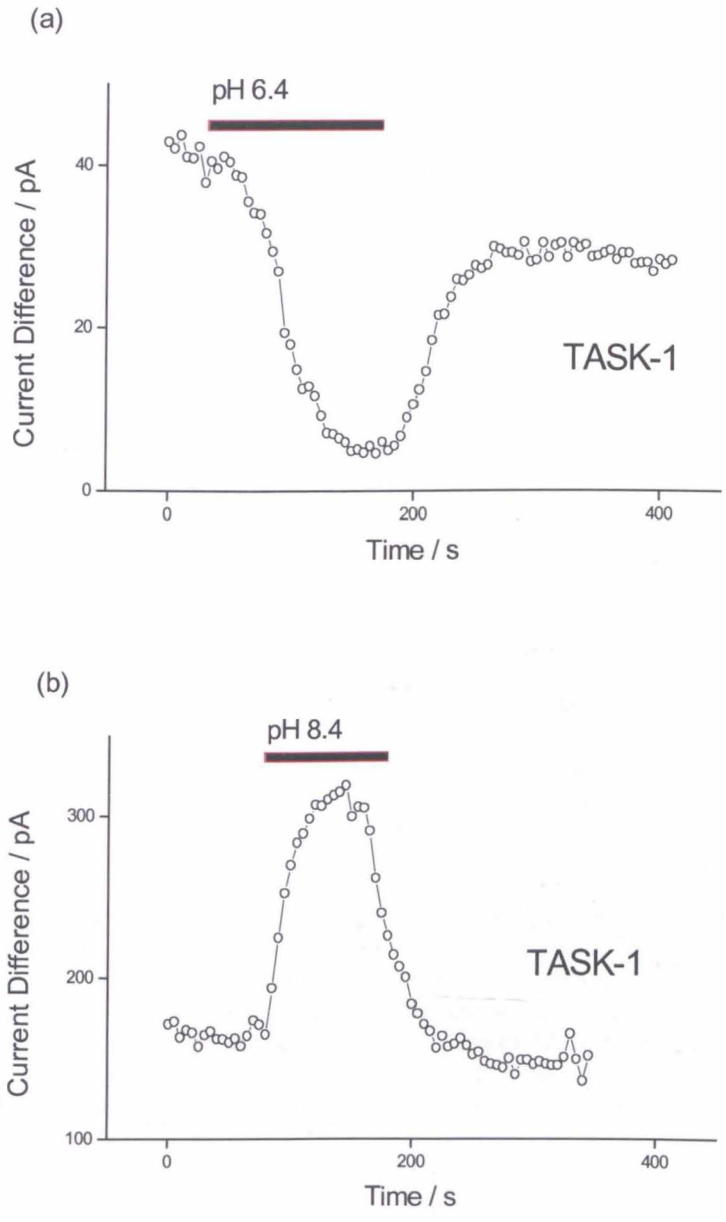

Figure 3-3 Time course plots of pH responses of TASK-1 channel currents to (a) pH 6.4 from pH 7.4 and (b) pH 8.4 from pH 7.4. Bathing solutions of different pH were applied to the cell at a holding potential of -60mV, traces were generated by measuring the current difference between that at -40mV and that at -80mV and plotting against time.

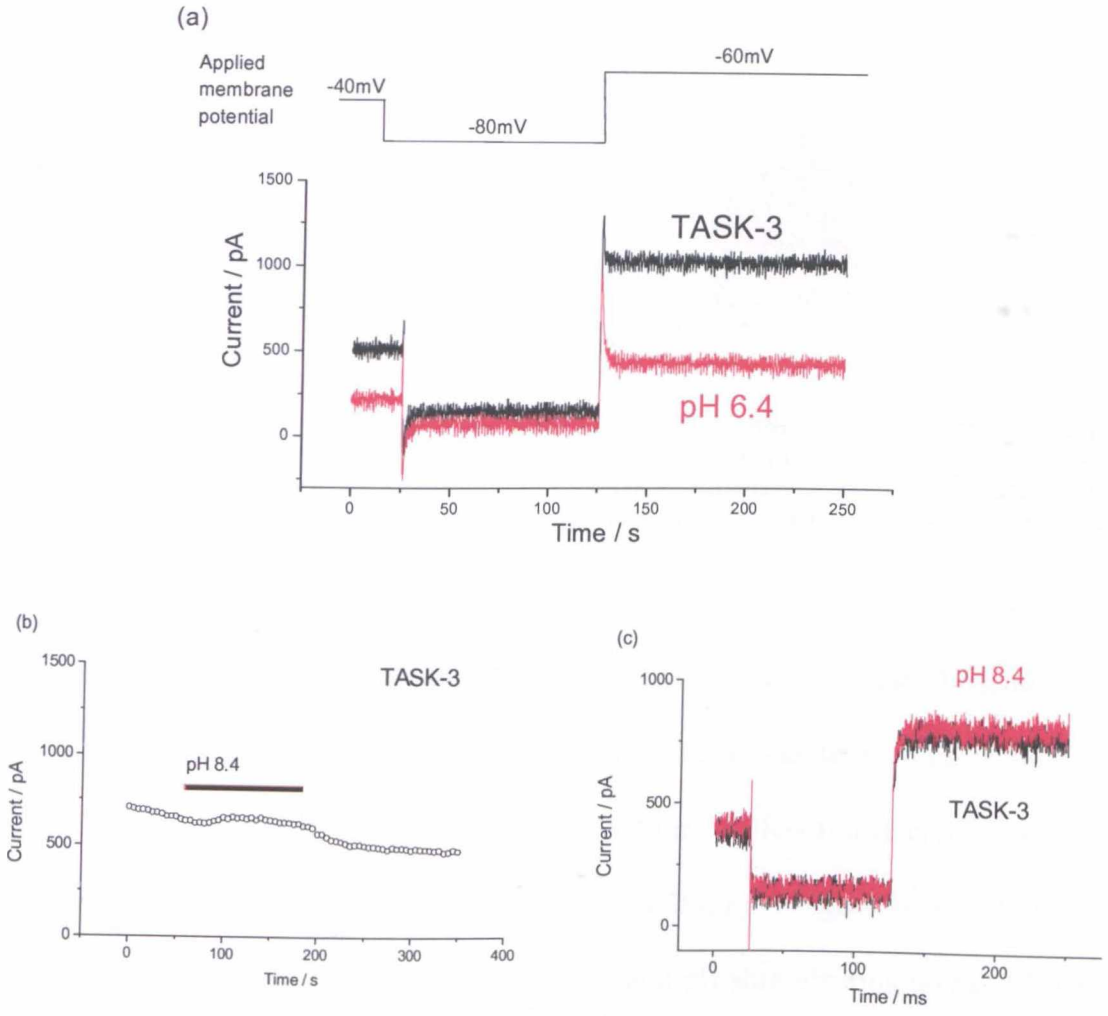

Figure 3-4 TASK-3 channel current response to pH 6.4 (a) and pH 8.4 (b) + (c). (a) shows the data traces generated while applying a holding potential of -60mV, stepping to -80mV for 50ms, then stepping up to -40m. The protocol repeated every 5s. The traces shown here are the mean of 5 traces of the whole cell current before application of pH6.4 (t=0-5s) and at maximum block by pH 6.4 (t=175-200s). (b) Time course plot illustrating the minimal potentiation of TASK-3 currents in response to application of pH 8.4 bathing solution from pH 7.4. (c) Mean data trace generated as in (a) of TASK-3 current response to pH 8.4. *N.B.(b) and(c) do not come from the same whole-cell recording.*

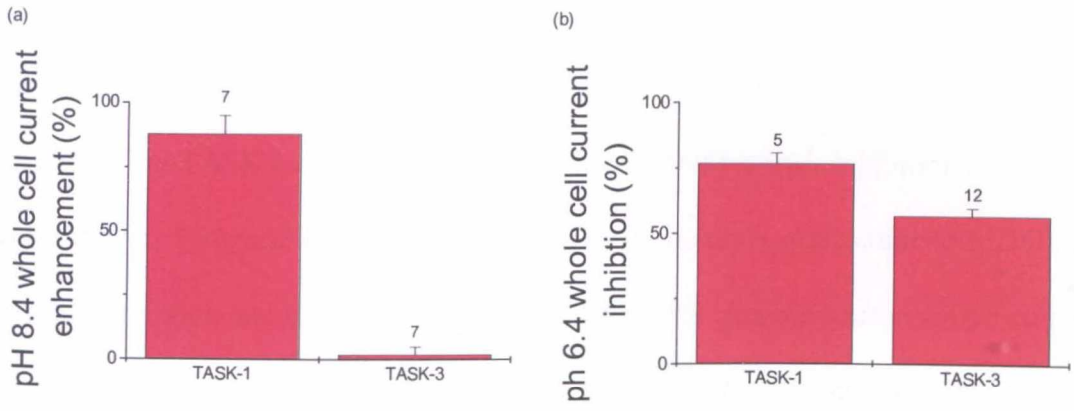

Figure 3-5 Mean % change of TASK-3 and TASK-1 currents in response to a shift in external pH from pH 7.4 to pH 6.4 and pH 8.4. from percentage change in current from time course plots. TASK-3 currents were inhibited by extracellular pH 6.4 (-57 ± 2%, n=12) relativeto pH 7.4, but unaffected by pH 8.4 (2 ± 3%, n=7) while TASK-1 currents were significantly potentiated by pH 8.4 (88 ± 7%, n=7) and inhibited by pH 6.4 (-77 ± 4%, n=5) relative to pH 7.4.

The effects of changing the external pH on currents of TASK-1 (Figure 3-3)and TASK-3 (Figure 3-4) transfected HEK cells were measured under voltage clamp conditions. Increasing external pH from 7.4 to 8.4 for TASK-1 transfected cells substantially increased the whole cell current (88 ± 7%, n=7, Figure 3-5a). TASK-3 currents were maximal at pH 7.4, with the same unit pH shift eliciting no significant potentiation (2 ± 3%, n=7, Figure 3-5a). Inhibition of both TASK-1 and TASK-3 channel currents was found with application of pH 6.4, causing a 77 ± 4% (n=5) inhibition with TASK-1 and a 57 ± 2% (n=12) inhibition with TASK-3 (Figure 3-5b). Further work on pH response was conducted in the lab as part of an analysis of mouse TASK-3 currents in comparison with the human counterpart. These data showed no potentiation on current in response to pH 8.4 (2 ± 1% reduction, n=7 (Aller *et al.*, 2005)). These recordings corroborate previous findings (Kang *et al.*, 2004; Kim *et al.*, 2000; Duprat *et al.*, 1997) and demonstrate that changes in external pH are a useful biophysical characteristic of the channels that can be used to distinguish them as TASK-3 channels are purveying their maximal current at pH 7.4, while TASK-1 channel currents are not, being potentiated by alkaline pH.

3.1.3 $Na^+_{(ext)}$ substitution by NMDG and Choline

An interesting property reported for heterologously expressed TREK-1 (Fink *et al.*, 1996) and rat TASK currents (Leonoudakis *et al.*, 1998) is their inhibition by substitution of extracellular sodium ($Na^+_{(ext)}$) by *N*- methyl D-glucamine (NMDG). A similar inhibition has also been observed for cerebellar granule neuron native current $I_{K(SO)}$ (Millar *et al.*, 2000). This sensitivity is of interest for a number of reasons. Firstly, the apparent dependence of a potassium current on extracellular sodium ion concentration could be argued to be unexpected, especially as the potassium ion concentrations across the membrane are maintained. Secondly, the $Na^+_{(ext)}$ sensitivity has yet to be established across the two pore domain potassium channel family and may prove to bear some selectivity.

The dependence of human TREK-1 conductance on external sodium was first considered and tested in the *Xenopus laevis* heterologous expression system (Fink *et al.*, 1996), and was subsequently followed up by Leonoudakis *et al* in the same expression system with rat TASK cDNA (Leonoudakis *et al.*, 1998). Fink et al assessed the biophysical properties of TREK-1, noting the channel's instantaneous activation kinetics and outwardly rectifying current-voltage (I-V) relationship and observed a rightward and downward shift in the I-V curve with substitution of $Na^+_{(ext)}$ with K^+.

Assessing the separate effects of external K^+ and Na^+ by substituting with NMDG, they found that the currents were inhibited in a voltage dependent fashion when the Na^+ substitution was made. The reversal potential was not affected significantly. The same inhibition was also observed with Li^+ substitution for $Na^+_{(ext)}$. Leonoudakis

substituted $Na^{+}_{(ext)}$ for NMDG in characterizing rat TASK channel currents and observed a weak inhibition of outward K^{+} currents (28 ± 2%), while Goldstein noted ORK1 (a *Drosophila Melanogaster* potassium sensitive leak channel cloned by complementation in *Saccharomyces cerevisiae*) K^{+} currents were unaffected by NMDG substitution when heterologously expressed in *Xenopus laevis* oocytes (Goldstein *et al.*, 1996).

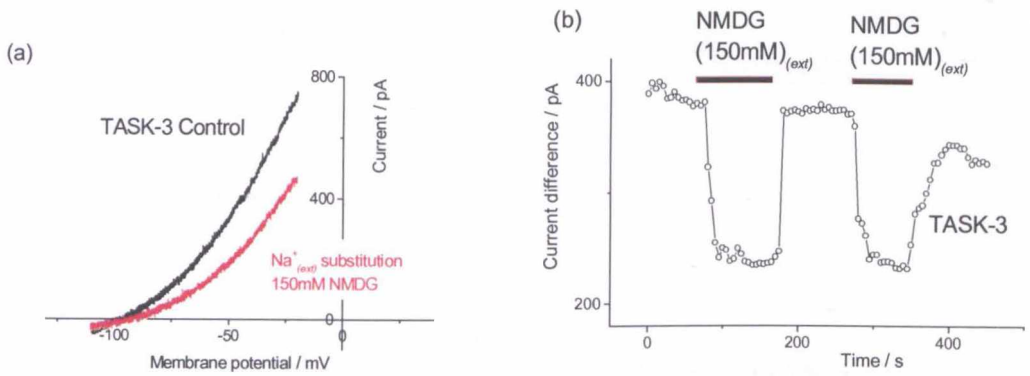

Figure 3-6 External Na^{+} substitution by 150mM NMDG. NMDG experiments were performed with a perfusion solution where external Na^{+} was replaced by the same molar concentration of *N*-methyl D-glucamine. (a) I-V relationship of TASK-3 potassium current in control and Na substituted conditions, (b) shows the time course plot of the same cell with two consecutive NMDG perfusions, measured as previous, with a holding potential of -60mV.

$NMDG^{+}$ substitution of Na^{+} ions was tested on TASK-3 and TASK-1 currents in the tsA-201 expression system. In this study, 150mM $NMDG^{+}$ substituting for Na^{+}_{ext} inhibited TASK-3 reversibly with a mean current change of -27.7 ± 1.9% (n=14) (Figure 3-6). Time courses were plotted as current against time, using the standard step-ramp protocol. Percentage current changes were taken from each time course, as the difference of the whole cell current at -80mV and -40mV, before and during $NMDG^{+}$ solution was applied. TASK-1 currents were also blocked under Na^{+} free conditions (approx -38%) (Figure 3-7) although the smaller whole cell currents made this less reproducible. Increasing the TASK-1 whole cell current by perfusion with pH 8.4 external solution followed by Na^{+} substitution solution at the same pH revealed a

comparable block to that of TASK-3 at pH 7.4 (-32.0 ± 16.1%, n=3, Figure 3-7(b)). A follow-up study substituting $Na^+_{(ext)}$ for 150mM choline on TASK-1 (at pH 7.4) and TASK-3 currents produced an increased block of both TASK-1 and TASK-3 currents

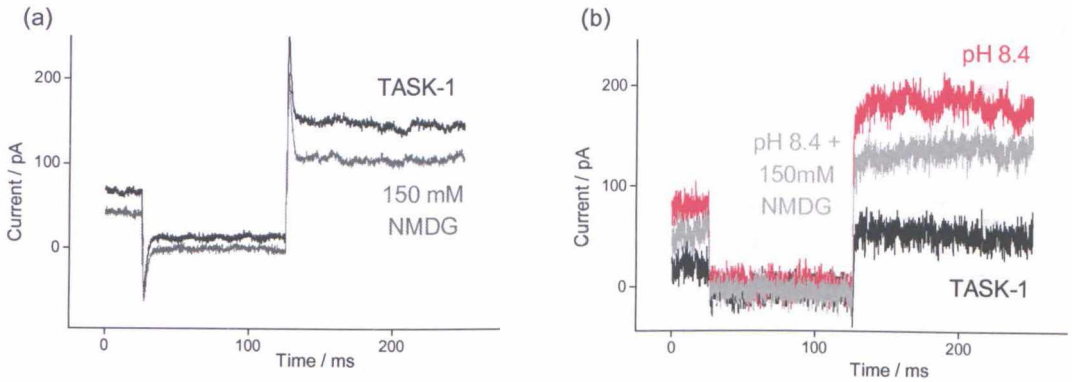

(-52.4 ± 10.0, n=3; -53.3 ± 9.2, n=6 respectively (Figure 3-8)).

Figure 3-7 TASK-1 current block produced on $Na^+_{(ext)}$ substitution by 150mM NMDG Raw traces show representative data from two separate cells. (a) Cell perfused with NMDG solution at pH 7.4 (b) TASK-1 currents increased by perfusion with pH 8.4 external solution followed by a perfusion of NMDG solution at pH 8.4.

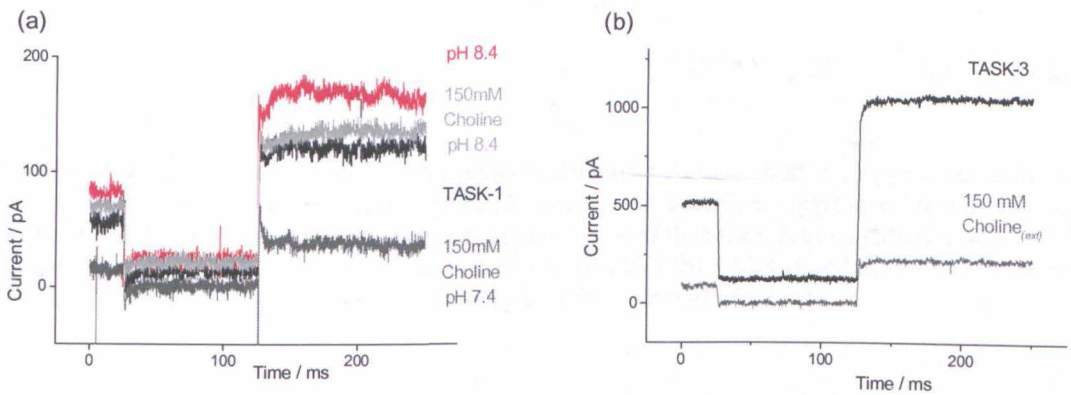

Figure 3-8 TASK-1 and TASK-3 currents are diminished in the presence of 0mM Na^+ / 150mM choline$_{(ext)}$ (a) Raw data traces of TASK-1 currents inhibited by $Na^+_{(ext)}$ substitution with 150mM choline in pH 7.4 and 8.4 bathing and test solutions (b) Raw trace of maximal block of TASK-3 currents by $Na^+_{(ext)}$ substitution with 150mM choline in pH 7.4

3.1.4 Zinc

Zinc, a 'trace' element, has a concentration of 15μM in the blood (Mathie *et al.*, 2006), while being found at concentration ten times that in the brain (Kozma *et al.*, 1981; Ono *et al.*, 1997). It is also found in nerve terminals and the synaptic cleft, into which it is released after depolarization where it can achieve concentrations of 100μM or more (Takeda, 2000; Frederickson & Moncrieff, 1994; Assaf & Chung, 1984).

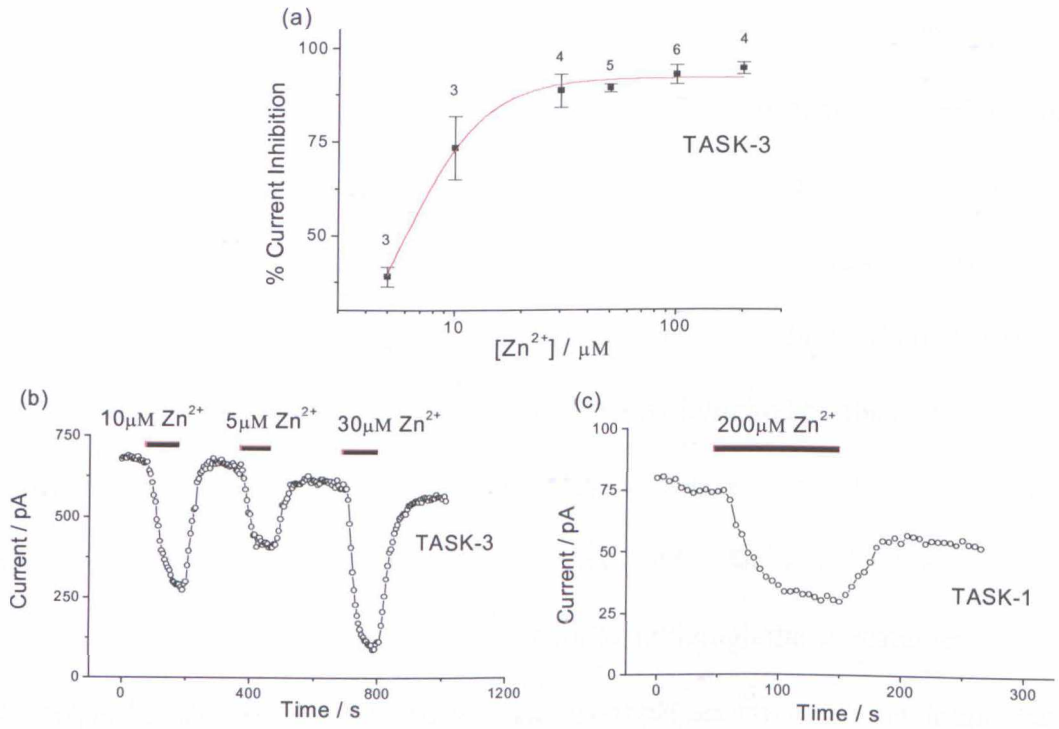

Figure 3-9 Zinc block of TASK-3 and TASK-1 currents. (a) concentration-response curve for zinc inhibition of TASK-3 channel currents. % block measured as described previously. Data means from between 3 and 6 cells, error bars in terms of standard error of the mean. Fit to a Hill plot, IC_{50} = 5.7 ± 0.4μM (b) and (c) Time course exemplar plot of zinc block of (b) TASK-3 and (c) TASK-1 currents. Whole cell recording is from a single cell with a holding potential of -60mV

Homomeric human TASK-1 channels expressed in cell lines have been reported to display little sensitivity to 100μM Zinc while TASK-3 channels are substantially blocked (-70%) at this concentration (Clarke *et al.*, 2004; Leonoudakis *et al.*, 1998). These data are corroborated here in the HEK cell lines used with zinc block of TASK-1 only achieving a maximal block of -52% at 200μM Zinc (Figure 3-9(c)), while TASK-3 was blocked almost completely by 100μM Zinc (-92.8 ± 2.6%, n=6). The

best fit of the pooled TASK-3 current block by zinc data to the Hill equation[3] yielded an IC_{50} of 5.7 ± 0.4μM (Figure 3-9(a)), while the Hill coefficient (n) was 2.3±0.4.

3.1.5 Ruthenium Red and Ru-360

Ruthenium red (RR), a polycationic dye originally used for histological staining, was first shown to inhibit the resting potassium conductance in rat adrenal glomerulosa cells (and so depolarize them) by (Szabadkai *et al.*, 1999) Northern blot analyses and RT-PCR determined the presence of TASK-1 and TASK-3 in the cell type, which could account for the leak current. Block of the channel conductances was also investigated in *Xenopus laevis* oocytes (Czirjak & Enyedi, 2002a-b) where it was found that the TASK-3 homodimer was more potently inhibited by the compound over the TASK-1 homodimer and a TASK-1/TASK-3 heterodimer. The creation of a TASK-3 – TASK-3 concatamer (Czirjak & Enyedi, 2003) facilitated a closer structural study of the molecular basis of RR block (although the concatamer exhibited a slightly altered functionality in terms of pH sensitivity). They found that mutation of a glutamate at position 70 to a positively charged arginine or an uncharged cysteine rendered the artificial TASK-3 dimer insensitive to RR. TASK-1

---

[3] The Hill equation was derived in 1909 by A.V. Hill in his analysis of drug concentration to receptor occupancy. His application of the Law of Mass Action (which states that the rate of reaction is proportional to the product of the concentrations of the reactants) describes the relationship between drug concentration and receptor occupancy by the drug at equilibrium and models the rate at which that equilibrium is reached. It is stated:

$$p_{AR} = \frac{[A]^n}{K_A + [A]^n}$$

where [A] is the agonist (drug) concentration, p_{AR} is the proportion of receptors occupied by the drug and K_A is the dissociation equilibrium constant. K_A = dissociation rate constant (s^{-1}) / association rate constant ($M^{-1}s^{-1}$). n is the Hill coefficient, which indicates the degree of cooperativity between agonist molecules binding to the receptor. A Hill coefficient of 1 indicates completely independent binding, irrespective of the numbers of agonist molecules already bound. IC_{50} stated above refers to the drug concentration at which half of the available receptors are occupied and is used as a comparison figure across different drugs and receptors.

has a positively charged lysine at position 70 and mutation to the negatively charged glutamate conferred RR sensitivity to their previously insensitive TASK-1 dimer. They then adapted their TASK-3 concatamer and created a wild-type-E70R tandem construct. The general functionality of this channel altered comparably to the original concatamer in terms pH sensitivity (though it yielded smaller currents), and it exhibited no sensitivity to RR, supporting their hypothesis of the action of RR being dependent on glutamate at position 70.

In this study, RR was applied to the bath solution of tsA-201 cells expressing pure TASK-1 and TASK-3, each self-dimerised. TASK-1 showed little sensitivity to RR (for 10μM RR, current change was -17%, Figure 3-10(b)) while a more robust block was observed of the TASK-3 currents (10μM RR, current change of -73.2 ± 3.3 %, n=6). Fitting the TASK-3 data to the Hill equation gives a maximum block, V_{max}, of 84.2 % (S.D. = 12.4), half maximal block at 3.5 μM RR (S.D. = 1.4) with a Hill coefficient ~1.

Figure 3-10 Ruthenium Red blocks TASK-1 and TASK-3 currents differently. (a) Concentration-

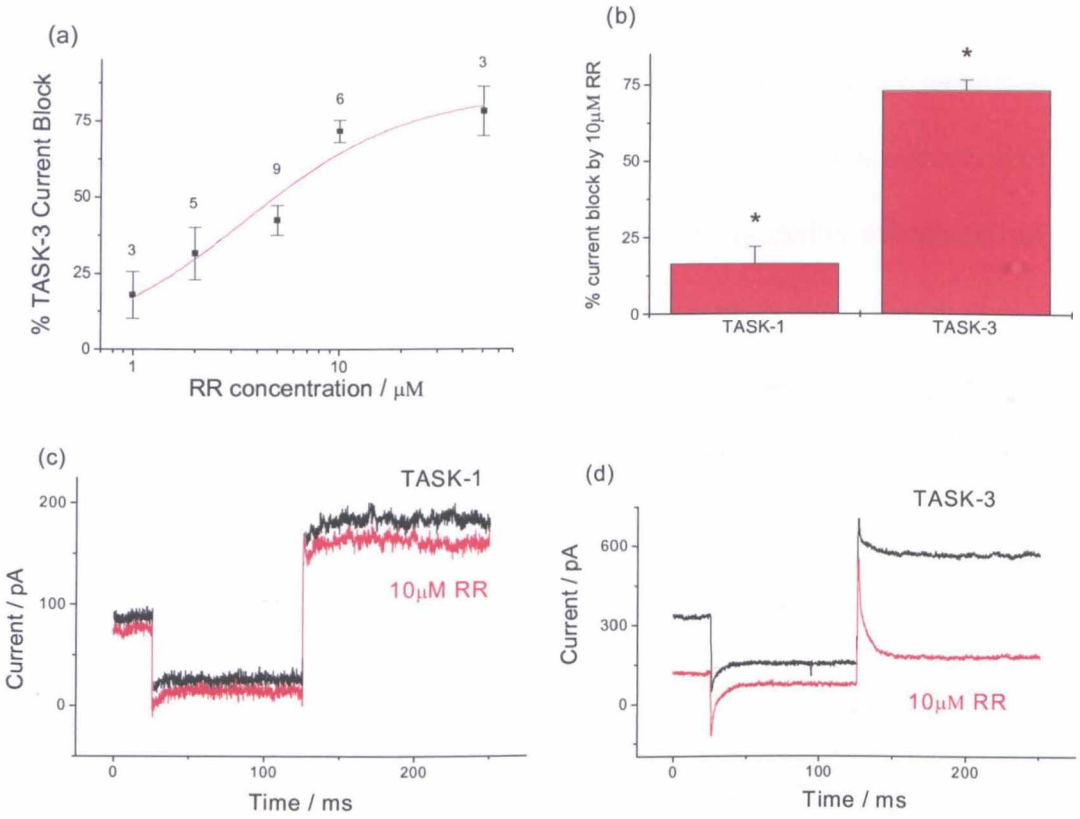

Response curve of RR block of TASK-3 currents, V_{max} = 84.2% SD = 12.4 when fitted to the Hill equation. Data point labels refer to n numbers of cells tested at each concentration. (b) RR block of whole cell currents from TASK-1 transfected cells compared to those of TASK-3 transfected cells. Mean block for 10μM RR is shown here, TASK-1 current change was -16.5 ± 5.5 % (n=2), TASK-3 current change was -73.2 ± 3.3 % (n=6) (c) and (d) show example raw data traces before and with 10μM $RR_{(ext)}$ for comparison.

When Szabadkai et al (1999) embarked on their initial analysis of ruthenium red in rat adrenal glomerulosa cells, the dye was only commercially available in an impure form (See Methods, (Szabadkai *et al.*, 1999)). One of the three ruthenium contaminants was Ru-360, a dinuclear ruthenium-amine complex, with an absorption maximum of 360nm. When purified from $RuCl_3$, Ru-360 was shown to inhibit mitochondrial calcium ion transport *in vivo* (Ying *et al.*, 1991) and later *in vitro* (Matlib *et al.*, 1998), the delay in transferring to the cultured cell arising from the compound's inhibitory effects on sarcoplasmic reticulum Ca^{2+} release and a wide range of ion transporters.

Here, Ru-360 was tested as a potentially more potent blocker of TASK-1 or TASK-3 than ruthenium red. Despite the statistically significant difference of the block between TASK-1 (-5.175 ± 0.9%, n = 4) and TASK-3 currents (see Figure 3-11(a)), with the block of TASK-3 currents being the greater (-13.3%, n = 2), the overall extent of the block was very small and the difference not significant enough to consistently differentiate between the two channel currents. Coupled with its instability (light-sensitive) and non-specificity, Ru-360 has limited use in this context.

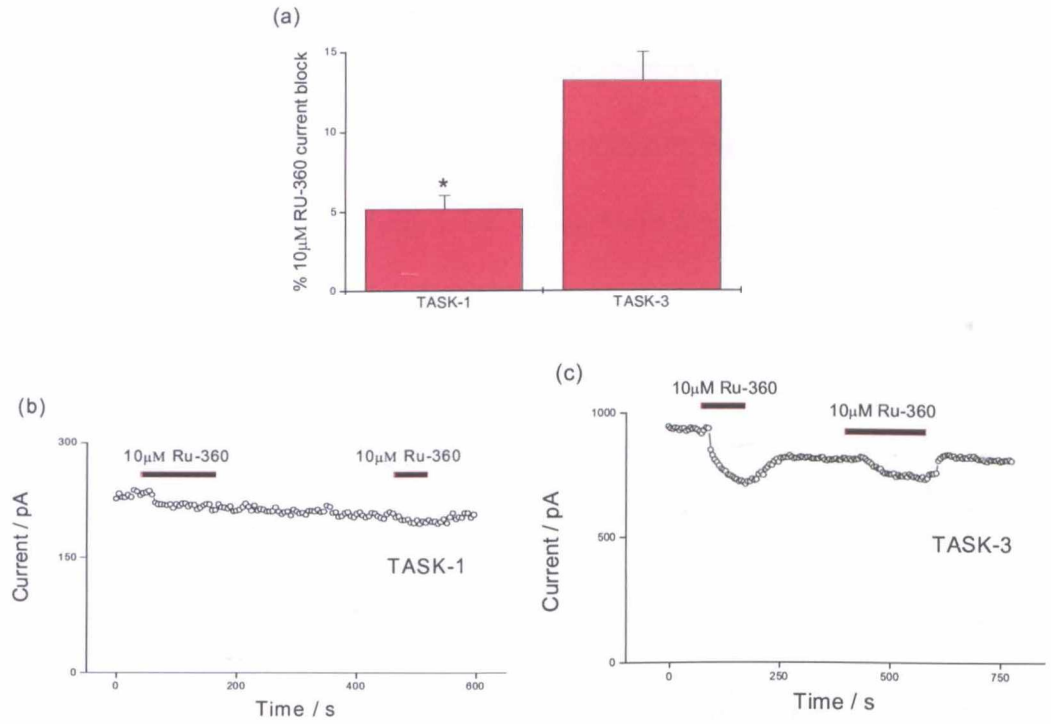

Figure 3-11 Ru-360 blocks TASK-1 and TASK-3 whole cell currents differently, but less potently than RR. (a) TASK-3 currents block is significantly greater (-13.3 ± 1.8 %, n = 2) than block of TASK-1 currents by RU-360 (5.175 ± 0.9%, n = 4), which can be seen on exemplar time courses shown in (b) TASK-1 and (c) TASK-3

3.1.6 Lanthanum

Lanthanum is a trivalent cation that has been shown to interact with a range of ion channels and G-protein coupled receptors, inhibiting T-type and L-type Ca^{2+} channels by pore occlusion at Ca^{2+} binding sites, and voltage gated K^+ channels by altering gating and kinetics (Enyeart *et al.*, 2002; Mlinar & Enyeart, 1993; Lansman, 1990). In their 1996 characterization of the standing outward potassium current of rat cerebellar granule neurons, $I_{K(SO)}$, Watkins and Mathie observed a significant inhibition in whole cell current size (about 50%) upon application of 10μM lanthanum. As TASK-1 channels have been suggested to underlie $I_{K(SO)}$, (Brickley *et al.*, 2001; Maingret *et al.*, 2001; Millar *et al.*, 2000), an analysis of the comparative block by lanthanum of pure, heterologously expressed TASK-1 and TASK-3 currents was needed.

Typical recordings are shown in figure 3-13. Lanthanum block of both TASK-1 and TASK-3 was dose dependent and reversible on washout. Maximal block for both channels was less than 50% (TASK-1 La^{3+} V_{max} = -35.3 ± 18.8%, TASK-3 La^{3+} V_{max} = -36.7 ± 5.0%) and of a similar order. The two means are not significantly different, making lanthanum an unsuitable blocker to differentiate between the two currents. Figure 3-12 shows the comparative responses of TASK-1 current amplitude at pH 7.4 (-18.3 ± 4%, n = 3) and 8.4 (-9.0 ± 1%, n = 4) to 300μM lanthanum.

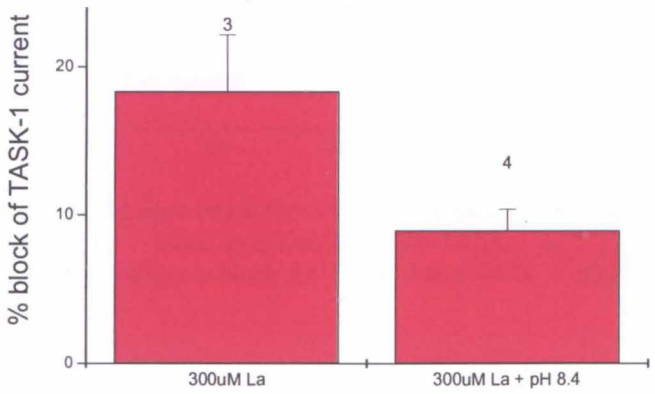

Figure 3-12 High concentrations of Lanthanum blocks TASK-1 at pH 8.4. The mean block at pH 8.4 (-9.0 ± 1%, n = 4) and pH 7.4 (-18.3 ± 4%, n = 3) were not significantly different.

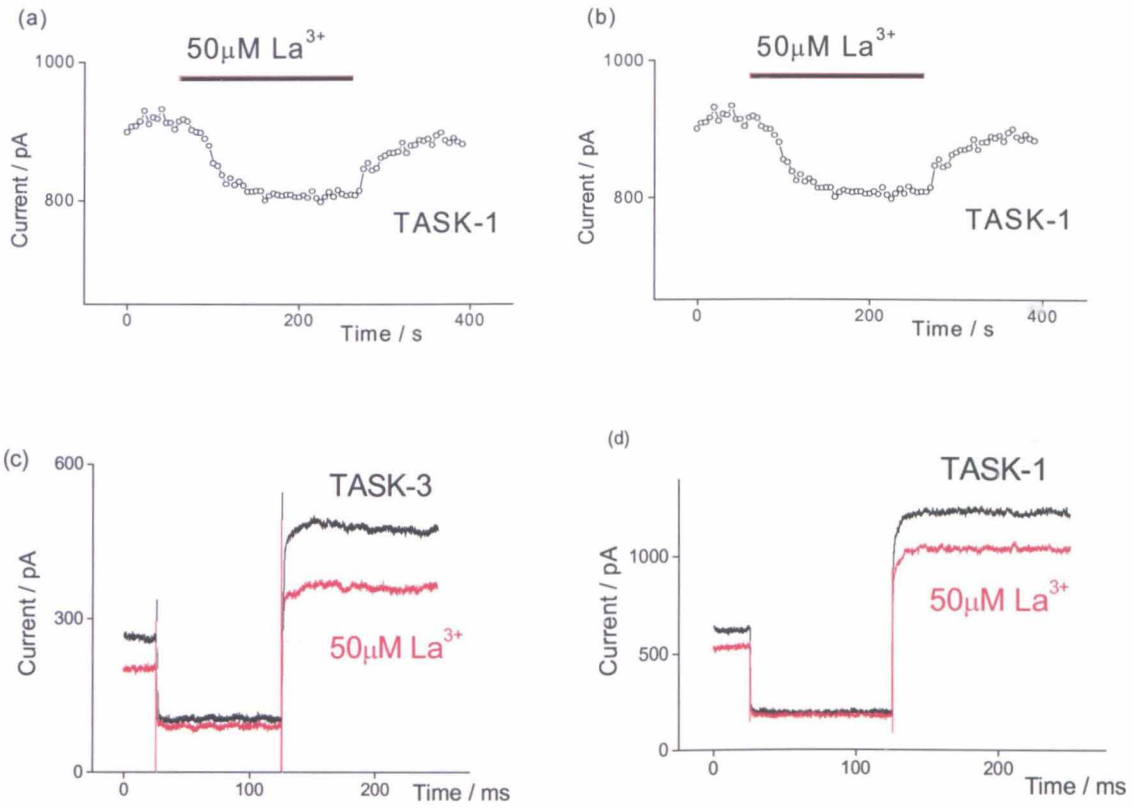

Figure 3-13 Lanthanum blocks TASK-1 and TASK-3 whole cell (a) and (b) depict exemplar time courses of La^{3+} block on a TASK-3 and a TASK-1 cell, (c) and (d) show exemplar raw traces before and during lanthanum block for TASK-3 and TASK-1 expressing cells respectively.

3.1.7 Copper

Gruss *et al* (2004) identified two-pore domain potassium channel sensitivity to $\mathbf{Cu^{2+}}$ and Zn^{2+} while working with chromium-plated brass-tipped syringes in the application of general anaesthetics. Further investigations on TREK-1 and TASK-3 showed they were differentially modulated by 10μM copper ($CuCl_2$) the former being potently activated (149 ± 60%, n = 4 for outside-out patches) while the latter was potently inhibited (93 ± 6%, n = 3 for outside-out patches).

Extending this investigation to whole cell recordings for TASK-1 and TASK-3 currents, I have found that both of the channels are inhibited by copper ions, but to significantly different extents at the 5% level. At 10μM Cu^{2+} (using $Cu(II)Cl_2$), TASK-3 currents were inhibited most potently (-77.7 ± 2.6%, n = 34) with less extensive block of TASK-1 currents (-40.6 ± 3.3%, n = 8) (Figures 3-14 and 3-15).

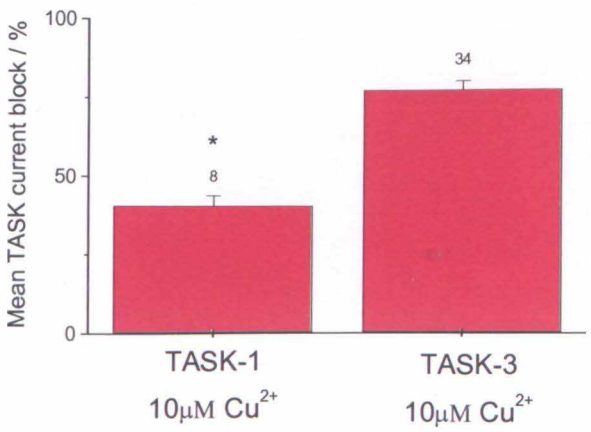

Figure 3-14 Cu^{2+} is a potent blocker of TASK-3 currents, but not of TASK-1 currents. This figure depicts mean block by Cu^{2+} of TASK-1 and TASK-3 transfected HEK cell currents. Error bars are SEMs.

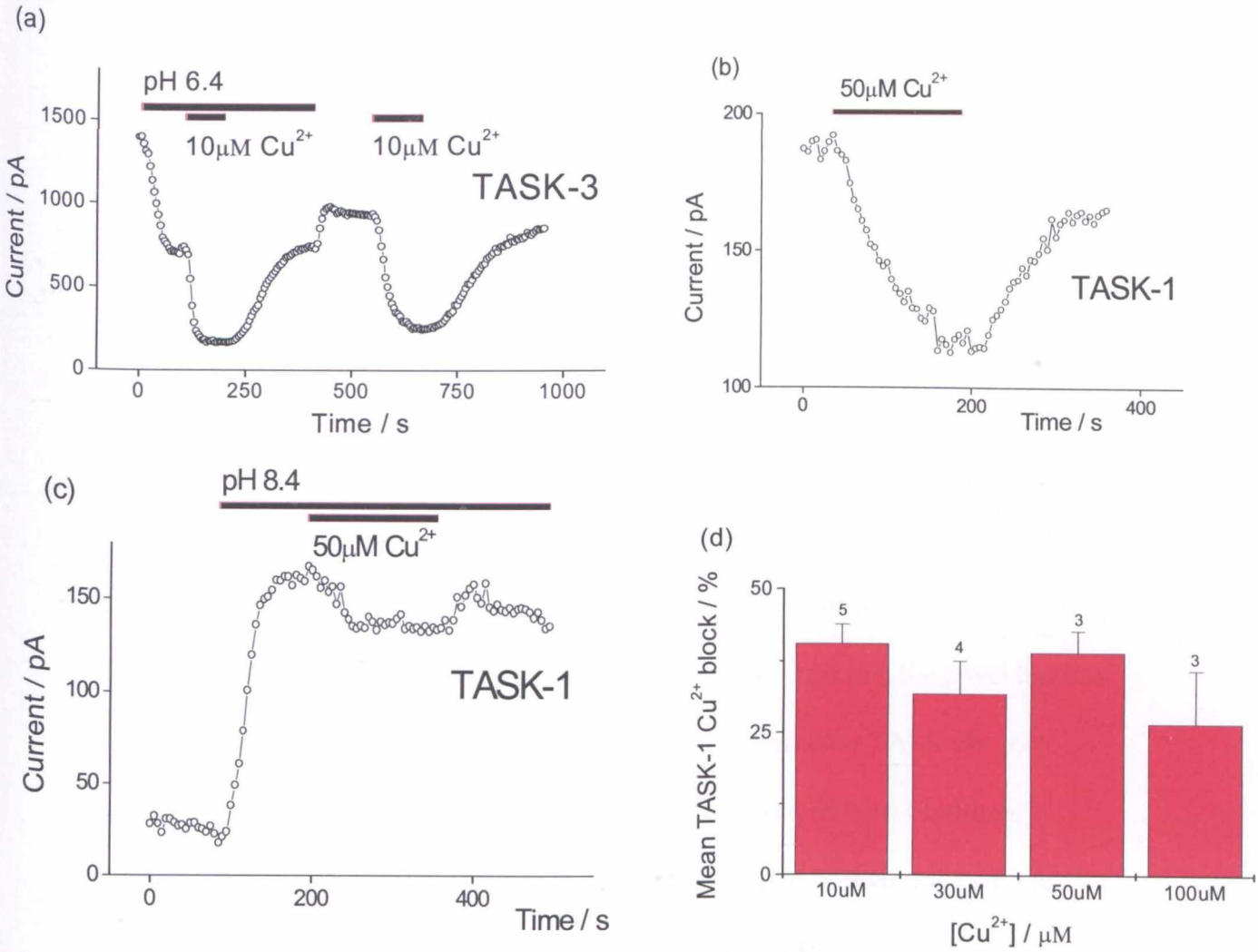

Figure 3-15 TASK-1 and TASK-3 current responses to Cu^{2+} application (a) Reduction of overall whole cell current size in TASK-3 expressing HEK cells by a unit decrease in external pH (from 7.4 to 6.4) (a) Time course plot of TASK-3 currents responding to 10μM Cu^{2+} at pH 6.4 and pH 7.4. (b) and (c) are time courses of high concentration copper block (50μM) of TASK-1, (b) at pH 7.4, (c) at pH 8.4. Cells were held at -60mV for all three traces. (d) Bar chart of mean TASK-1 whole cell current responses to Cu^{2+}. Error bars are SEMs, n numbers noted on chart.

Copper block was reversible on washout for both TASK-1 and TASK-3, with maximal block usually achieved between 10 and 15 sweeps (50 – 75 seconds). Extent of block was also concentration dependent (figure 3-15), for TASK-1 currents, this was maximal around 10μM Cu (V_{MAX} = 34.9 ± 9.2% when fitted to the Hill equation), while TASK-3 currents could be blocked to a greater extent (V_{MAX} = 85.0 ± 7.9% when fitted to the Hill equation).

These initial experiments demonstrated that copper could be used to discern leak current contributions attributable to homodimeric TASK-1 channels from those of homodimeric TASK-3 channels. In conjunction with Zn^{2+} and pH, the novel block of TASK-1 currents by Cu^{2+} could be used to identify an unknown TASK channel current as either of the aforementioned subtypes. However, *in vitro* (in primary neurone culture, for example), key to this usefulness would be a contrast with further two pore domain potassium channels. For this, acid sensitive, outwardly rectifying TASK-2 channels currents (Morton *et al.*, 2005; Kang & Kim, 2004; Reyes *et al.*, 1998) provide a suitable comparison owing to their sharing a number of pharmacological and biophysical characteristics with TASK-1 and TASK-3. Their sensitivity to copper, like TASK-1 channels, also remains to be characterised.

3.2 *Investigation of copper effect*

Copper is the third most abundant metallic element in the human body after iron and zinc (Schumann *et al.*, 2002), the average human adult male of 70kg containing 80-110mg of this essential nutrient. Copper is distributed chiefly amongst the liver (10mg), brain (8.8mg), blood (6mg), skeletal muscle (26mg) and skeleton and bone marrow (46mg) (Linder *et al.*, 1998). In the cerebrospinal fluid, it is found at an average concentration of 70μM, while in the synaptic cleft, after neurotransmitter release, it can reach concentrations in the order of 250μM and beyond that in states of neurodegenerative disease (Mathie *et al.*, 2006; Tapiero *et al.*, 2003; Schumann *et al.*, 2002; Linder *et al.*, 1998). These high concentrations are associated with exocytosis of synaptic vesicles which act as a store for copper ions (Mathie *et al.*, 2006; Horning & Trombley, 2001). Indeed, since the 1980s, several groups have described the calcium dependent release of copper after depolarization consistent with vesicular release (Hartter & Barnea, 1988; Kardos *et al.*, 1989). Most copper is protein-bound (the bulk to transcuprein[4], ceruloplasmin[5] and albumin) with an estimated concentration of free copper ions in the order of 10^{-13} M in human blood plasma , but generally, very little appears to be stored, because it is easily absorbed and excreted.

Copper is essential for development in the CNS, but is also cytotoxic at high concentrations (Tapiero *et al.*, 2003). Largely associated with glutamatergic or adrenergic neurons, copper is differentially distributed across the brain, with several

[4] Transcuprein- a copper transport macroglobulin (Liu *et al.*, 2007; Linder *et al.*, 1998)
[5] Ceruloplasmin – a single polypeptide chain involved in copper delivery to cells, excretion from the body and oxidation of Fe(II) (Tapiero *et al.*, 2003)

studies identifying its highest concentrations in the olfactory bulb, corpus striatum and locus cerulus (Tarohda *et al.*, 2004; Kardos *et al.*, 1989; Hartter & Barnea, 1988).

3.2.1 TASK-1, TASK-2 and TASK-3 at 10μM Copper

The initial comparative study of copper effects has identified it as a pharmacological agent that differently blocks TASK-1 and TASK-3 currents. TALK channel, TASK-2, shares key biophysical and pharmacological characteristics with both of the TASK channels and as yet, has not had its sensitivity to copper tested. Sequence differences of TASK-2 subunits compared with TASK-1 and TASK-3 may also be used to determine the likely mechanism of action of copper on the tested TASK channels.

10μM and 100μM $Cu(II)Cl_2$ were applied to the bath solution while the transiently transfected tsA cell expressing TASK-2 was subjected to the standard step-ramp protocol with a holding potential of -60mV. TASK-3 currents were potently blocked (figure 3-16 and figure 3-17), TASK-1 less so, while TASK-2 currents remained unaltered in the presence of copper at both 10 and 100μM (10μM Cu^{2+} block of TASK-3 channel currents = 77.8 ± 2.6%, n=34, 10μM Cu^{2+} block of TASK-1 channel currents = 40.6 ± 3.3%, n=8, 100μM Cu^{2+} block of TASK-2 channel currents = 1.7 ± 1.7%, n=7). All three responses are significantly different from each other (See appendix III, 5.1.1 - independent pair-wise t tests with Bonferroni correction (to compensate for multiple comparison (type 1) errors)). The extent of the maximal Cu^{2+} block in TASK-3 and TASK-1, combined with their differences to TASK-2 Cu^{2+} response suggest that Cu^{2+} could be used to experimentally distinguish the current contribution from each TASK channel to the potassium leak current.

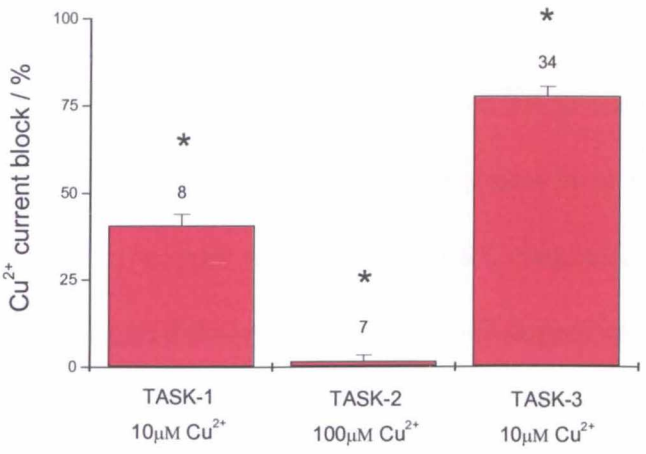

Figure 3-16 Cu^{2+} block of TASK currents at 10μM and 100μM TASK-2 was found to be insensitive to Cu^{2+} block even at 10x concentration of 100μM. TASK-3 currents were most sensitive to Cu^{2+}. Labels refer to n numbers, 10μM Cu^{2+} block of TASK-3 = 77.8 ± 2.6%, 10μM Cu^{2+} block of TASK-1 = 40.6 ± 3.3%, 100μM Cu^{2+} block of TASK-2 = 1.7 ± 1.7%.

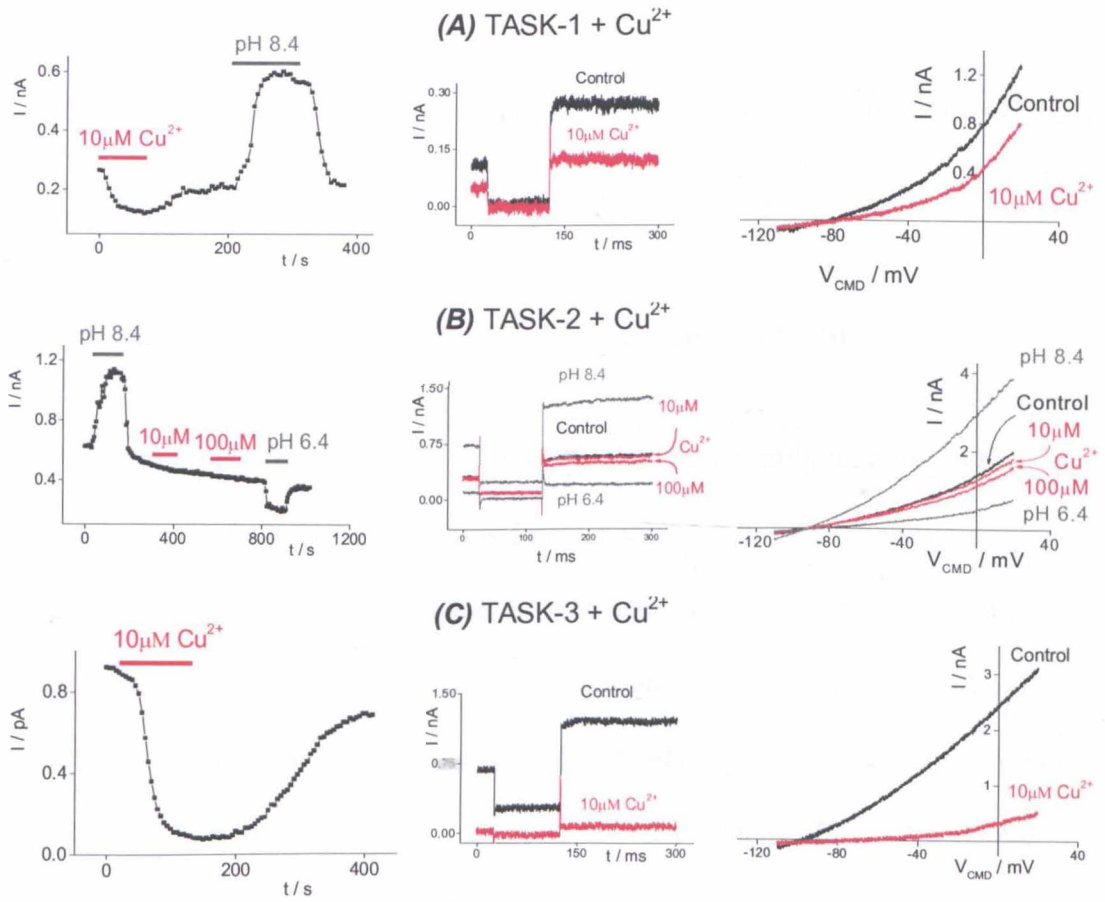

Figure 3-17 Exemplar TASK channel responses to Cu^{2+} Exemplar traces for Cu^{2+} block at 10μM or 100μM (TASK-2 only) showing current time course, raw step data and IV traces for (A) TASK-1 channels, (B) TASK-2 channels and (C) TASK-3 channels. pH test solutions were applied to confirm normal functionality, and compare potentiation and or block of channel currents where appropriate.

3.2.2 Mechanisms of copper action

The lack of sensitivity of TASK-2 to copper ions applied extracellularly suggests that sequences common to both TASK-1 and TASK-3 but absent from TASK-2 are likely to underlie the mechanism of copper action on the TASK channels. A recent review (Mathie *et al.*, 2006) highlighted three methods by which copper can alter protein function. Copper can, through its redox states, catalyse the production of free radicals. It can also oxidise cysteine residues facilitating the formation of disulphide bonds between thiol containing residues, or it can bind directly with amino acid residues, chiefly cysteine, histidine or glutamic acid.

In order to identify which mechanism underlies the copper sensitivity of TASK-1 and TASK-3 channels, each method will be considered in turn.

3.2.3 Copper as a redox agent – copper and mannitol

With a single *s* electron outside of the filled 3*d* shell, Cu readily oxidizes to the Cu^{+} (cuprous) state and can be found in this form as well as the Cu^{2+} (cupric) state in all living organisms. The ability of copper to exist in more than one stable oxidation state makes it eminently suitable as a catalyst for biological processes requiring the transfer of electrons. It is thus an integral part of a number of enzymes, including the oxido-reductase family where is sits in the catalytic site as a cofactor. Examples are the cytochrome-*c* oxidase (electron-transport and oxidative phosphorylation), superoxide dismutase (catalyses the disproportionation of superoxide into oxygen and hydrogen peroxide), protein-lysine 6-oxidase (matures and cross-links elastin and collagen fibres) among others (Linder *et al.*, 1998).

As well as acting as a catalyst in the biochemistry of the cell, copper, in both its cuprous and cupric states, can generate free radicals, and so induce oxidative stress through the *Fenton Reaction* (Mathie *et al.*, 2006; Haigh & Brown, 2006; Halliwell, 2006, 1992; Schumann *et al.*, 2002):

$$Cu^{+} + H_2O_2 \rightarrow Cu^{2+} + \bullet OH + OH^{-}$$

Hydrogen peroxide is produced endogenously through a number of cellular processes including the respiratory burst (inflammation) and during oxidative phosphorylation (Lee *et al.*, 2002). The hydroxyl radical (•OH) produced is highly potent, reacting with almost any molecule in its vicinity. Once created, it starts a cycle of further free radical production that increases the damage to biological molecules through the *Haber-Weiss reaction*:

$$H_2O_2 + \bullet OH \rightarrow H_2O + O_2^{-} + H^{+}$$

$$H_2O_2 + O_2^{-} \rightarrow O_2 + OH^{-} + \bullet OH$$

Coupled with the reduction of Cu^{2+} to Cu^{+};

$$Cu^{2+} + O_2^{-} \rightarrow Cu^{+} + O_2$$

this cycle can continue issuing cellular damage until the cell's antioxidant defences overcome free radical production.

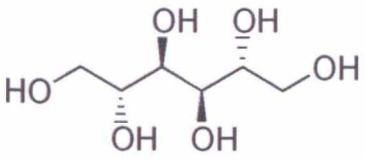

Figure 3-18 Molecular schematic of mannitol. Mannitol acts as a hydroxyl radical scavenger. •OH reacts with it according to: •OH + RH → H_2O + R• (Goldstein & Czapski, 1984)

Mannitol (fig. 4.2-3), or hexan-1,2,3,4,5,6-hexol ($C_6H_8(OH)_6$), is a known scavenger of hydroxyl radicals (Kocha *et al.*, 1997; Shen *et al.*, 1997; Goldstein & Czapski, 1984). In order to test our initial hypothesis of Cu^{2+} action on TASK channels being via free radical production, mannitol (10mM) was applied concurrently with 10μM Cu^{2+}. No significant difference (Student's two population independent t test, fig 4.2-4) was seen between the block by copper in the presence or absence of mannitol, suggesting that copper block of TASK-3 was not dependent on hydroxyl radical formation.

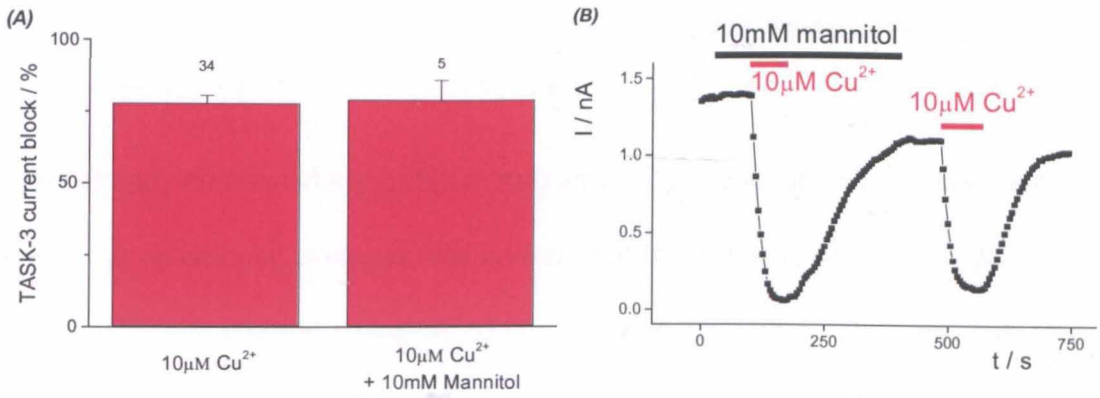

Figure 3-19 Copper block of TASK-3 currents remain unaltered in the presence of mannitol. There was no significant difference between the copper block of TASK-3 when 10mM mannitol was perfused with 10μM copper onto the cell. (A) shows bar chart of mean data (10μM Cu^{2+} block of TASK-3 = 77.8 ± 2.6%, n=34, 10μM Cu^{2+} block of TASK-3 in presence of 10mM mannitol = 79.1 ± 6.8 %, n=5) (B) shows exemplar time course of copper block of TASK-3 channel currents in the presence of mannitol followed by a copper block without mannitol after wash off.

3.2.4 DTT and DTNB

The data suggests that block of TASK-3 currents is unlikely to be a consequence of hydroxyl radical formation and interaction with the channel. A second way that copper can modify TASK-3 channel currents is through oxidation of thiol (-SH) groups on cysteine residues.

It has long been established that copper may act as a catalyst in the oxidation of thiols. In the late 1960s, Doriano Cavallini (Cavallini *et al.*, 1969) uncovered the first layers of the complex processes underlying the interaction of thiols and Cu^{2+} ions, establishing the formation of a Cu^{2+}-cysteine intermediary in cysteine oxidation with concurrent reduction of Cu(II) to Cu(I). Since then, a two-phased cycle mechanism of copper-catalyzed oxidation of cysteine has been explored extensively, taking into consideration the generation of several intermediates, including the cysteinyl radical, hydrogen peroxide, the hydroxyl radical and the chelation of copper itself by cysteine (Munday *et al.*, 2004; Rigo *et al.*, 2004; Kachur *et al.*, 1999; Salama *et al.*, 1992).

Having already eliminated a significant role for the hydroxyl radical, the oxidation of thiol groups on external cysteines was investigated by perfusion of the transfected tsA-201 cells with Cleland's reagent, $_{D,L}$–dithiothreitol (DTT), a sulphydryl reducing agent and Ellman's reagent, 5',5'-dithio-bis (2 nitrobenzoic acid) (DTNB), a sulphydryl oxidant (Figure 3-20). DTT completely reduces disulphide bonds to thiol groups and is therefore commonly used as a thiol group 'protectant' (Andrey *et al.*, 2005; Redondo *et al.*, 2004; Kr *et al.*, 2001).

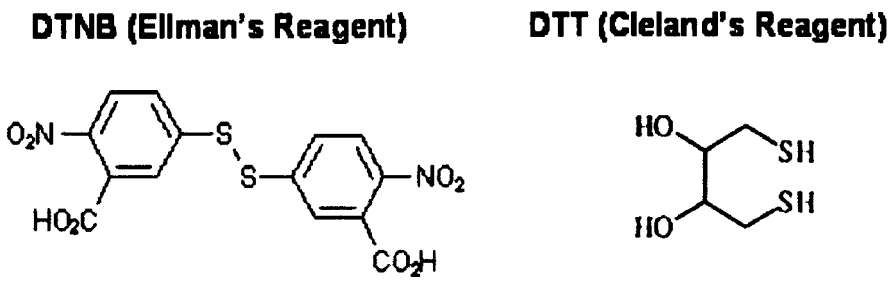

Figure 3-20 Schematic representation of the structures of Ellman Reagent, DTNB, and Cleland's reagent, DTT. DTNB is a yellow powder with a moderate solubility in water which was found to require 20minutes sonication to go into solution. DTT dissolved much more readily in external solution.

DTT and DTNB test solutions were prepared at concentrations of 5mM and 2mM respectively in external solution from stock solution of 10mM in Milli-Q water. DTNB was found to form a suspension unless sonicated; 20mins was sufficient to dissolve the solid. Both DTT and DTNB were stored at -4°C when not in use, as were the 10mM stock solutions (in foil wrapped glass vials). Careful handling of the DTNB was needed owing to the light sensitive nature of the compound. Before application an appropriate volume of stock solution was drawn into a Gilson pipette and added to 50mls of external solution in a volumetric flask. This was then dispersed by inversion and added immediately to a perfusion chamber. Solution was perfused straight away, onto the patched cell as usual.

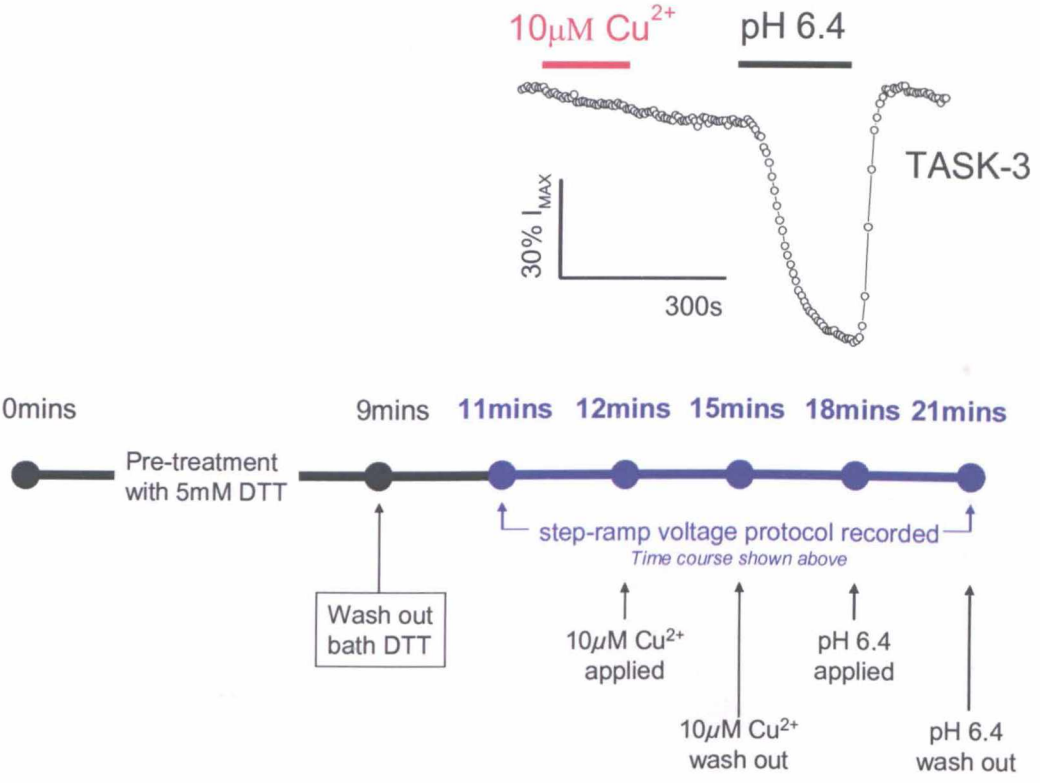

Figure 3-21 Exemplar DTT pre-treatment timeline and time course. Cells were found to be poorly tolerant of being subjected simultaneously to both the standard step-ramp protocol and 5mM DTT alone. A 'pre-treatment' protocol was devised. Cells were held at a membrane potential of -60mVwhile DTT was applied, in this case, for 9minutes. When the cell was stable, a two minute washout occurred (to minimise chelation of Cu^{2+} in bath by DTT solution), then recording began with the standard 10μM Cu^{2+} application and finally a test solution of external solution adjusted to pH 6.4 to check TASK-3 channel functionality.

5mM DTT did not change the size of the TASK-3 current itself although it was found to be poorly tolerated by the cell if applied alone while also running the step-ramp protocol. It was found that a 4 minute pretreatment at a holding potential of -60mV, followed immediately by a 2 minute washout before Cu^{2+} test solution application was necessary (Figure 3-21). When applied to the cell before 10μM Cu^{2+} in such a way DTT prevented Cu^{2+} inhibition (Figure 3-23 (b)). Application of DTT directly after copper perfusion caused a rapid reversal of copper block (Figure 3-22(a)). If copper was then applied again, no further block could be achieved (Figure 3-22(a)). Inhibition of Cu^{2+} block by DTT (whether applied before or after Cu^{2+} application) was reversible over time (10μM Cu^{2+} block of TASK-3 = 77.8 ± 2.6%, n=34, 10μM

Cu^{2+} block of TASK-3 in the presence of 5mM DTT = 0.5 ± 0.6%, n = 9). A second application of 10μM Cu^{2+} after a pH change (to 6.4) or simply a prolonged Cu^{2+} application was found to recover TASK-3 channel sensitivity to the ion, although channel currents rarely recovered on washout from this further onslaught (Figure 3-23 (b)).

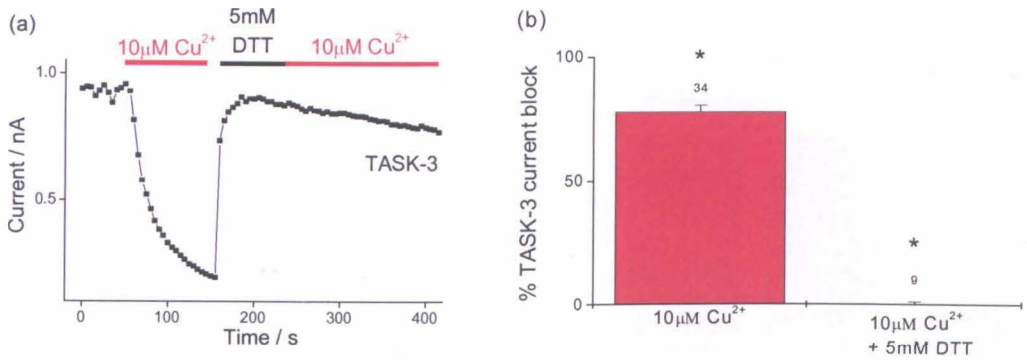

Figure 3-22 DTT prevents and reverses copper block of TASK-3 channel currents (a) Time course of exemplar TASK-3 channel current with standard block in response to 10μM Cu^{2+} application initially, reversed by 5mM DTT application, which in turn prevents block of the TASK-3 channel current by a second application of 10μM Cu^{2+}. (b) Mean Cu^{2+} block under standard conditions compared to 10μM Cu^{2+} block in the presence of 5mM DTT. Error bars are S.E.M., numbers shown are n numbers, 10μM Cu^{2+} block of TASK-3 = 77.8 ± 2.6%, n=34, 10μM Cu^{2+} block of TASK-3 in the presence of 5mM DTT = 0.5 ± 0.6%, n = 9

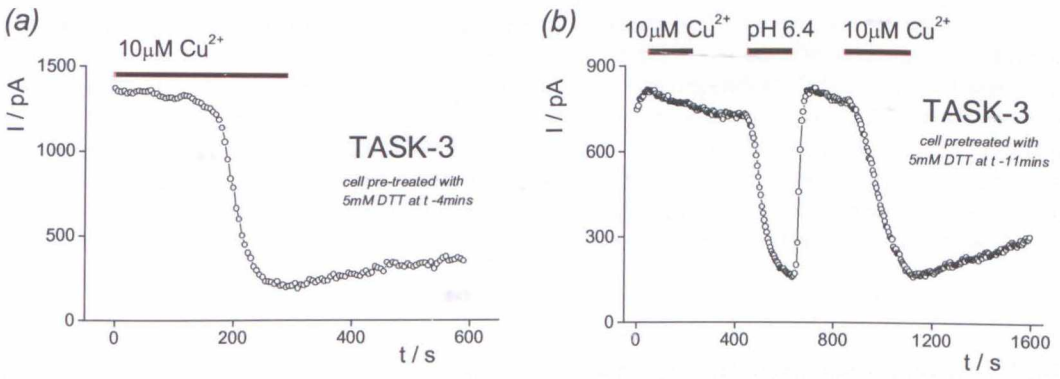

Figure 3-23 DTT effects were reversible (a) Time course showing recovery of Cu^{2+} block by prolonging application. Block typically manifests in 10 sweeps (50ms) from start of application. Here, a DTT pre-treated (DTT applied before step-ramp protocol was applied, while holding the cell at -60mV) cell took approximately 150s to respond to 10μM Cu^{2+}. (b) Time course showing TASK-3 channel currents regaining sensitivity to Cu^{2+} after a pH change (to 6.4) after initial Cu^{2+} elicited no block.

Initial investigations were carried out using 0.5mM DTNB. At first, little response could be discerned for TASK-3 channel currents (0.5mM DTNB block of TASK-3 channel currents = 8.9 ± 1.7%, n=6) but observation of a consistent small dip in current amplitude in response to DTNB indicated an increase in test solution concentration was needed.

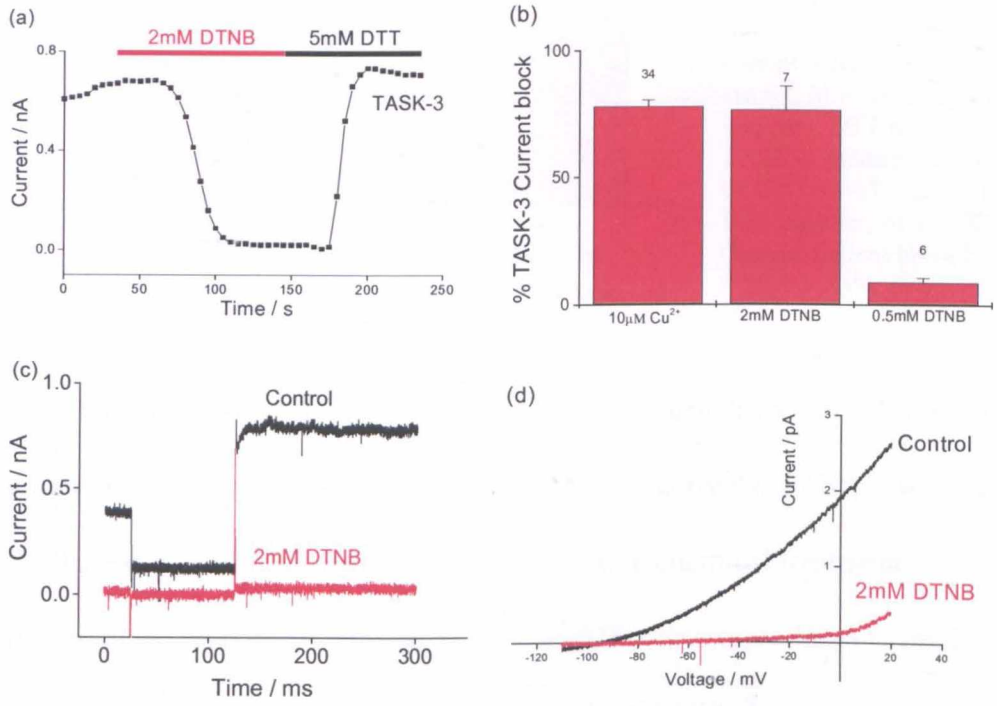

Figure 3-24 2mM DTNB blocks TASK-3 channel currents (a) Time course plot showing DTNB block (2mM) of TASK-3 currents being reversed by 5mM DTT. (b) Bar chart comparing DTNB and Cu^{2+} block of TASK-3 channel currents. DTNB block is dose dependent- 0.5mM DTNB was found to block TASK-3 channel currents much less than 2mM which blocked the TASK-3 channel currents to a similar extent as 10μM Cu^{2+} (10μM Cu^{2+} block of TASK-3 = 77.8 ± 2.6%, n=34, 0.5mM DTNB block of TASK-3 channel currents = 8.9 ± 1.7%, n=6, 2mM DTNB block of TASK-3 channel currents = 76.4 ± 9.2, n=7). Error bars shown here are S.E.M., columns are labelled with n numbers. (c) and (d) show an example raw data trace and the current voltage relation of a 2mM DTNB block of TASK-3 currents

The 2mM DTNB block of TASK-3 channel currents was significant and reversible by perfusion with DTT, mimicking these characteristics of copper block, indeed 10μM Cu^{2+} and 2mM DTNB blocks were not significantly different (10μM Cu^{2+} block of TASK-3 = 77.8 ± 2.6%, n=34, 2mM DTNB block of TASK-3 currents = 76.4 ± 9.2%, n=7), and the DTT reversal of DTNB block and Cu^{2+} block of TASK-3 currents were

also not significantly different (DTT recovery of TASK-3 channel current block by Cu^{2+} = 96.7 ± 2.5%, n=5, DTT recovery of TASK-3 channel current block by DTNB = 98.4 ± 2.1%, n=6, Figure 3-25).

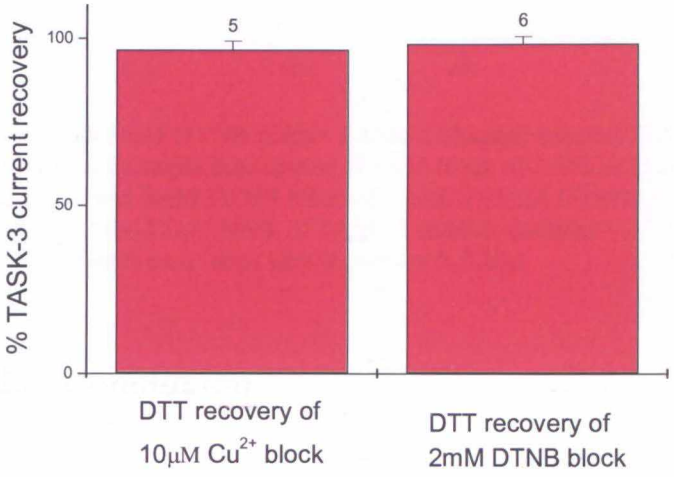

Figure 3-25 5mM DTT recovers 10μM Cu^{2+} and 2mM DTNB block equally Bar chart showing mean recovery by DTT of Cu^{2+} and DTNB sensitivity. Calculated from time courses as a % of current size after DTT recovery / current size before current block. Error bars shown are S.E.M.s, column labels are n numbers, DTT recovery of TASK-3 channel current block by Cu^{2+} = 96.7 ± 2.5%, n=5, DTT recovery of TASK-3 channel current block by DTNB = 98.4 ± 2.1%, n=6

After establishing a robust block of TASK-3 channel currents by 2mM DTNB, the study was expanded to TASK-1 and TASK-2 channel currents. TASK-1 was blocked to a similar extent as TASK-3 (-89%, n=2, aggressive chemical treatment of cells with DTNB combined with small currents made this difficult to reproduce) while TASK-2 was blocked significantly less (2mM DTNB block of TASK-2 currents = -28.5 ± 4.3%, n=3 (figure 3-26), compared to 2mM DTNB block of TASK-3 = -76.4 ± 9.2, n=7 (figure 3-24), Student's independent t-test for two populations, means are significantly different at the p = 0.05 level (Figure 3-26).

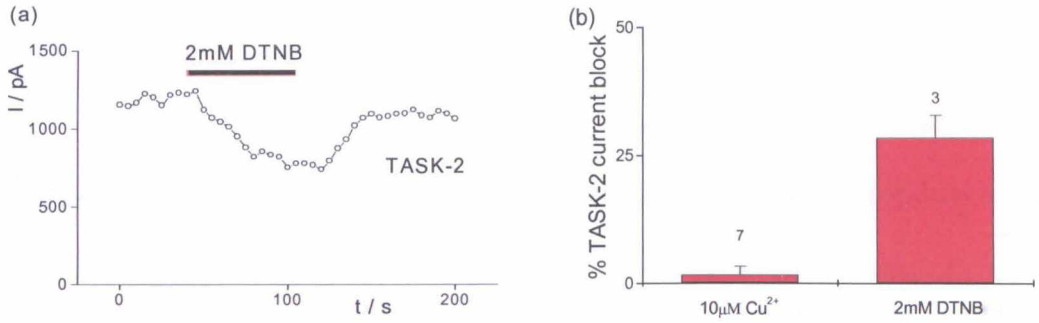

Figure 3-26 2mM DTNB blocks TASK-2 channel currents differently from TASK-3 channel currents (a) Example time course of 2mM block of TASK-2 channel currents, (b) Comparison of mean 10μM Cu^{2+} and 2mM DTNB block of TASK-2 (2mM DTNB block of TASK-2 currents = -28.5 ± 4.3%, n=3, 10μM Cu^{2+} block of TASK-2 channel currents = 1.7 ± 1.7%, n=**7** . Column labels refer to n numbers in each case, error bars shown are S.E.M.s

3.2.5 Conclusion

The copper block of the TASK-1 and 3 channel currents is significantly different from that of TASK-2 channel currents and could be used to differentiate the current contributions of the homomeric channels to a standing outward leak current. The mechanism by which copper blocks TASK-3 currents is unlikely to be due to an indirect route via hydroxyl radical formation, as shown by an unaltered block in the presence of mannitol. 2mM DTNB almost completely blocks TASK-3 currents and bears characteristics of Cu^{2+} block in that it can be reversed and prevented by application of 5mM DTT, and it is dose dependent. It should be noted, however, that DTT is able to chelate Cu^{2+} ions (Krężel *et al*, 2001). The design of the pre-treatment protocol included a bath washout between the application of DTT and that of Cu^{2+} solutions to minimise the removal of Cu^{2+} by DTT in solution, and thus retain Cu^{2+} access to the site of action at the channel. As the concentration of DTT (2mM) was much higher than that of Cu^{2+} (10μM), it is plausible that some DTT remained in solution throughout washout and influenced Cu^{2+} block of whole cell currents via co-ordination with the metal ion. Nevertheless, both Cu^{2+} and DTNB block the TASK-3

currents suggesting the involvement of cysteine residues in the block is a reasonable hypothesis to test.

The actions of DTT and DTNB suggest a significant role for cysteine residues situated on the external loops of the TASK-3 channel both for their action and that of copper. Significantly, TASK-2 channel current block by DTNB is significantly different to that of TASK-3 channel currents. This last finding puts DTNB forward as a test solution that could be used in a similar fashion to Cu^{2+} to distinguish homomeric TASK-3 channel currents from those of TASK-2.

3.3 Cysteine mutant work and TASK-2/TASK-3 Chimera

As suggested by the results in the last chapter, the commonality between copper and DTNB action on TASK-3 currents suggests that an interaction with sulphydryl (thiol) groups underlies their action. The only amino acid containing the thiol group is cysteine, and we would expect the relevant residues to be located on the outside of the membrane as both copper and DTNB responses were achieved with perfusion of the bath and not the pipette.

Thiol groups confer a number of particular chemical properties to their cysteine residues that influence structure and function of the protein. They can form permanent structural disulphide bonds with other cysteine residues in their locality or co-ordinate with metals ions (generally Cu^{2+}, Zn^{2+} or Fe^{2+}). They can also exist in a permanently reduced state or be subject to reversible oxidation (Sanchez *et al.* 2008).

The sulphurs in the side chains of two cysteine (cys) residues can form covalent bonds, endowing a protein fold with a specific, local stabilization. These structural disulphide bonds can be enzymatically formed during protein folding (e.g. by protein isulphide isomerise in eukaryotes). Covalently bonded cysteine residues combine becoming a cystine. The distance between the carbons (to which the SH group is bound) in a disulphide bond can vary, depending on the angle of bond connections. X-ray crystallography derived structures of various cystine molecules has shown that the chi1 angles are often close to 60 degrees, with the C-C distance ranging from 4 and 9 Angstroms, although more commonly it is between 4.4 and 6.8 Angstroms (Richardson, 1981).

Disuphide bonds form relatively promiscuously, with no preferences for local features. They are thought not to have a role in thhe folding of proteins, playing a more significant part once the protein has adopted its final conformation. These bonds are of particular interest to this study as DTT (a thiol protectant) reduces thiol groups while DTNB binds to thiol groups by forming a disulphide bridge with them. Cu^{2+} can also co-ordinate with cysteine residues (Krężel *et al,* 2001). Given the sensitivity of TASK-3 channel currents toboth of these reagent, it is not unreasonable to hypothesise that they share a sit of action.

To determine the molecular basis for the difference in copper sensitivity between TASK-1, TASK-2 and TASK-3 channels, an exploration of cysteine residues accessible by extracellular DTNB and copper, was embarked upon by single and multiple cysteine substitutions with alanine and serine in TASK-3.

3.3.1 TASK-1, TASK-2 and TASK-3 cysteines

The defining characteristic of the TASK channels is their sensitivity to extracellular acidosis and structurally, human TASK-1 and 3 share a 58% sequence identity (Kim *et al.*, 2000) with the most dissimilar region being that of the intracellular C-terminus domain (Rajan *et al.*, 2002). Indeed, sequence homology is frequently associated with functional similarity and this premise lay behind the discovery of the entire two-pore domain potassium channel subfamily(see Introduction), by using the potassium channel P domain signature sequence, GYG. TASK-2, from the TALK family, also

shares some functional properties with TASK-1, despite a sequence homology of less than 33% (Lesage & Lazdunski, 2000).

Aligning TASK-1 and TASK-3 channel sequences, cysteine residues common to both channels occur at positions 14, 110, 167, 172 and 193, of the TASK-3 sequence, with non-identical residues in TASK-1 occurring at C181, C146 and C147 (Figure 3-27). Similarly aligned, TASK-2 has a cysteine at position 116 (equivalent to C110 in TASK-3) (see appendix II). The aforementioned TASK-3 cysteine residues between 110 to 193 are all thought to lie towards or on the extracellular side of the protein (Figure 3-27); C110 at the top of the M2 region, C181 at the top of the M3 region, C193 in the P2 domain and C167 and C172 within the M2 region. C146 and C147 sit together on the intracellular M2 M3 loop (fig 4.3-1), while C14 near the intracellular N terminus, just within the M1 region.

TASK-3 cysteine mutants and truncations were constructed using the GenEluteTM Plasmid Miniprep Kit (Sigma Aldrich) (see Methods), substituting thiol containing cysteines at 14, 110, 146, 147, 167, 172, 181, and 193 with alanine (aliphatic side chains chemically unreactive and hydrophobic) and the larger serine (polar due to the reactive hydroxyl group side chain which can participate in hydrogen bonding) (see Methods).

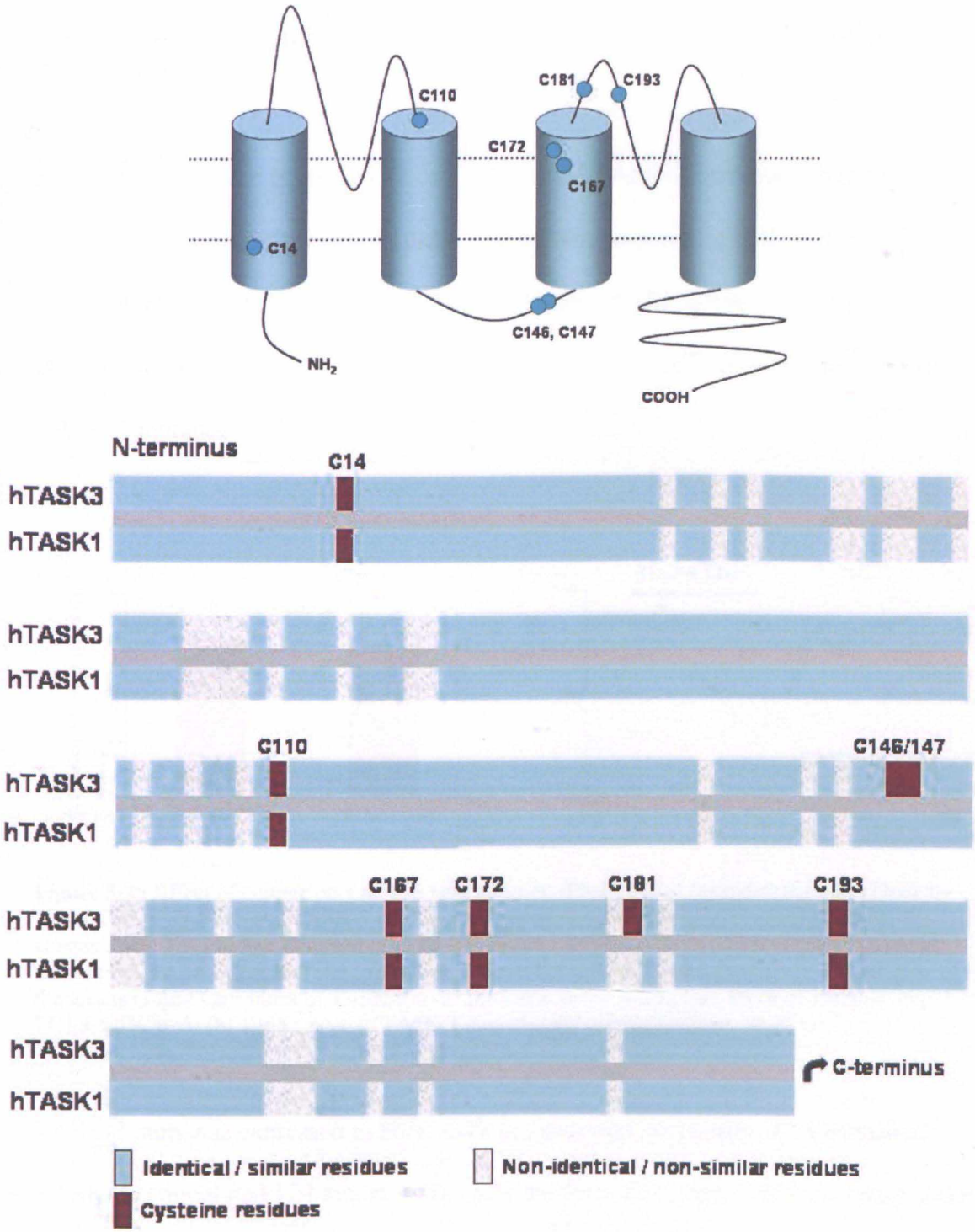

Figure 3-27 Sequence alignment of TASK-1 and TASK-3 highlights cysteine residue distribution both common and unique to each isoform. The putative locations of the cysteine residues of interest in the subunit in situ are depicted in the TASK-3 channel schematic above.

3.3.2 Copper sensitivity of TASK-3 stop, a truncated TASK-3 channel

It was found that the copper block of TASK-1 and TASK-3 currents was statistically significant at a concentration of 10μM. The current response of both of these channels was also distinguishable from that of the insensitive TASK-2 currents at this concentration, making it an ideal test concentration to explore copper sensitivity of TASK-3 mutants.

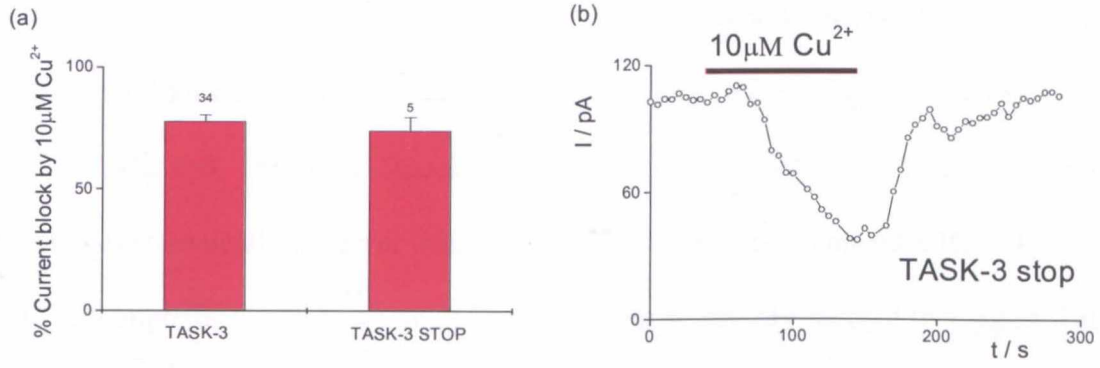

Figure 3-28 Effect of copper on TASK-3 stop compared to TASK-3 (a) shows the mean block by 10μM Cu^{2+} of TASK-3 and TASK-3 stop channel currents. TASK-3 stop is a truncated TASK-3 channel, with 124 residues removed from its C-terminus. It retains a comparable response to 10μM Cu^{2+} as WT TASK-3. Labels refer to numbers of recorded cells, error bars represent standard error of the means (10μM Cu^{2+} block of TASK-3 = -77.8 ± 2.6%, n=34, 10μM Cu^{2+} block of TASK-3 stop = -74.1 ± 5.5%, n=5) (b) Time course of TASK-3 stop channel current block by 10μM Cu^{2+}.

TASK-3 stop was expressed in HEK cells as described previously. This truncated TASK-3 channel had 124 amino acids removed from its C-terminus with a stop codon, TAG, being inserted at position 250. The whole cell currents were comparable to those of TASK-3 ($p = 0.7$, Student's t test). Application of 10μM Cu^{2+} extracellularly blocked TASK-3 stop channel currents to a similar extent as WT TASK-3 channel currents ($p = 0.6$ Student's t test, see also appendix III, 5.1.2) (Figure 3-28). Mean 10μM Cu^{2+} block of TASK-3 stop channel currents was 74.1 ± 5.5%, (n=5) (Figure

3-28). Conservation of copper sensitivity in this truncated TASK-3 mutant suggests that it is unlikely that the cysteines on the C-terminus are involved with this block.

3.3.3 Investigating copper and DTNB sensitivity of TASK-3 cysteine substitution mutants

Analysis of the aligned sequences of TASK-1 and TASK-3 showed that the cysteine residue at 181 was not present in the TASK-1 channel while C110 was shared by both sequences. It is reasonable to hypothesize, therefore, that the C181 residue may explain the differing copper sensitivities of TASK-1 and TASK-3. Point mutations of C181 and C110 to alanine yielded functional TASK channels both producing currents sensitive to block by copper ((Figure 3-29). 10μM Cu^{2+} block of TASK-3 C181A = -67.2 ± 7.4%, n=9, 10μM Cu^{2+} block of TASK-3 C110A = -79.9 ± 5.1%, n=7). Neither block was statistically different from that of WT TASK-3 (see appendix III, 5.1.2, 5.1.3), though the slight decrease in C181A copper sensitivity seemed to suggest that this avenue was worth exploring further.

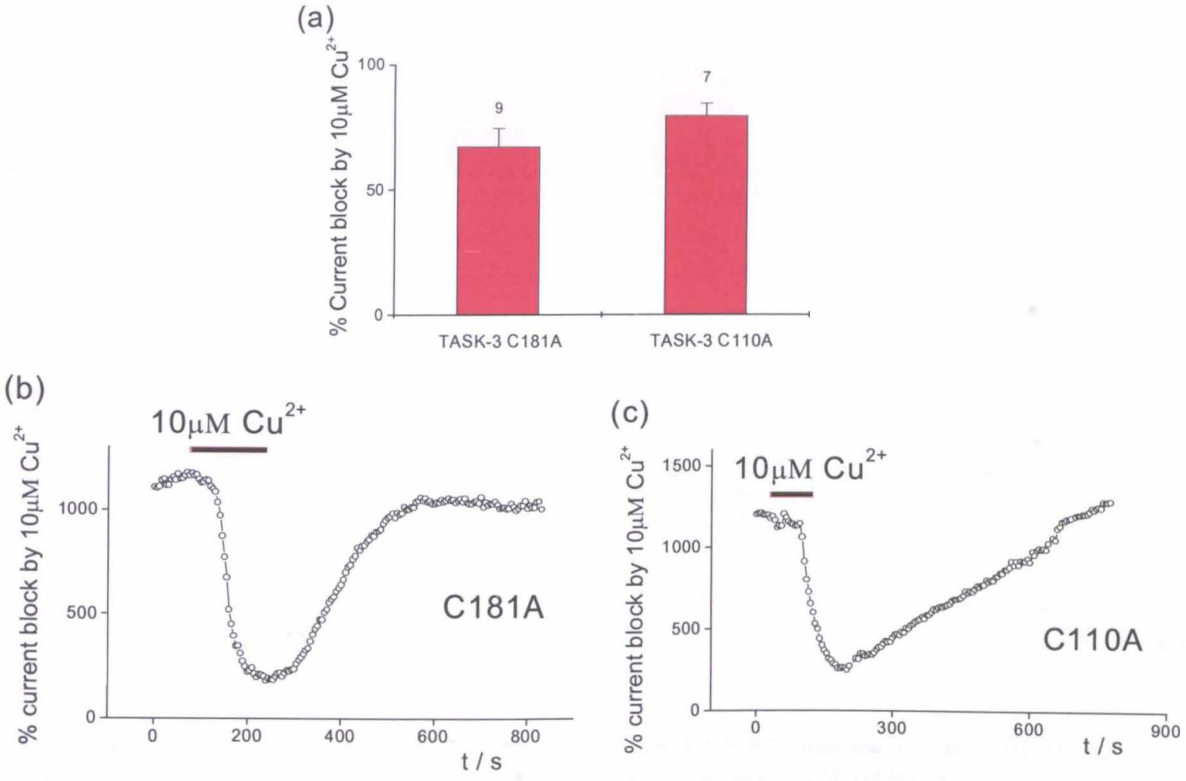

Figure 3-29 Effect of copper on TASK-3 C181A and TASK-3 C110A C181, being absent in TASK-1, but present in TASK-3 was mutated to alanine. Copper block of TASK currents is retained in both C181A and C110A mutants and while 10μM Cu^{2+} block of the C181A mutant is smaller than that of TASK-3 or TASK-3 C110A, the difference is not statistically different. Column labels are number of cells, while error bars represent standard error of the means. (10μM Cu^{2+} block of TASK-3 C181A = -67.2 ± 7.4%, n=9, 10μM Cu^{2+} block of TASK-3 C110A = -79.9 ± 5.1%, n=7) (b) and (c) show time courses of 10μM Cu^{2+} block of TASK-3 C181A and C110A current block respectively.

2mM DTNB was also applied to the cysteine to alanine TASK-3 181 and 110 mutants. The substantial block of whole cell currents by copper was mimicked by DTNB (Figure 3-30); the block of the mutant channels was of a similar magnitude to the block by 10μM Cu^{2+}, and neither was significantly different from the WT TASK-3 copper block or DTNB block. However, the slightly reduced DTNB sensitivity of TASK-3 C181A compared to that of TASK-3 C110A warranted further investigation.

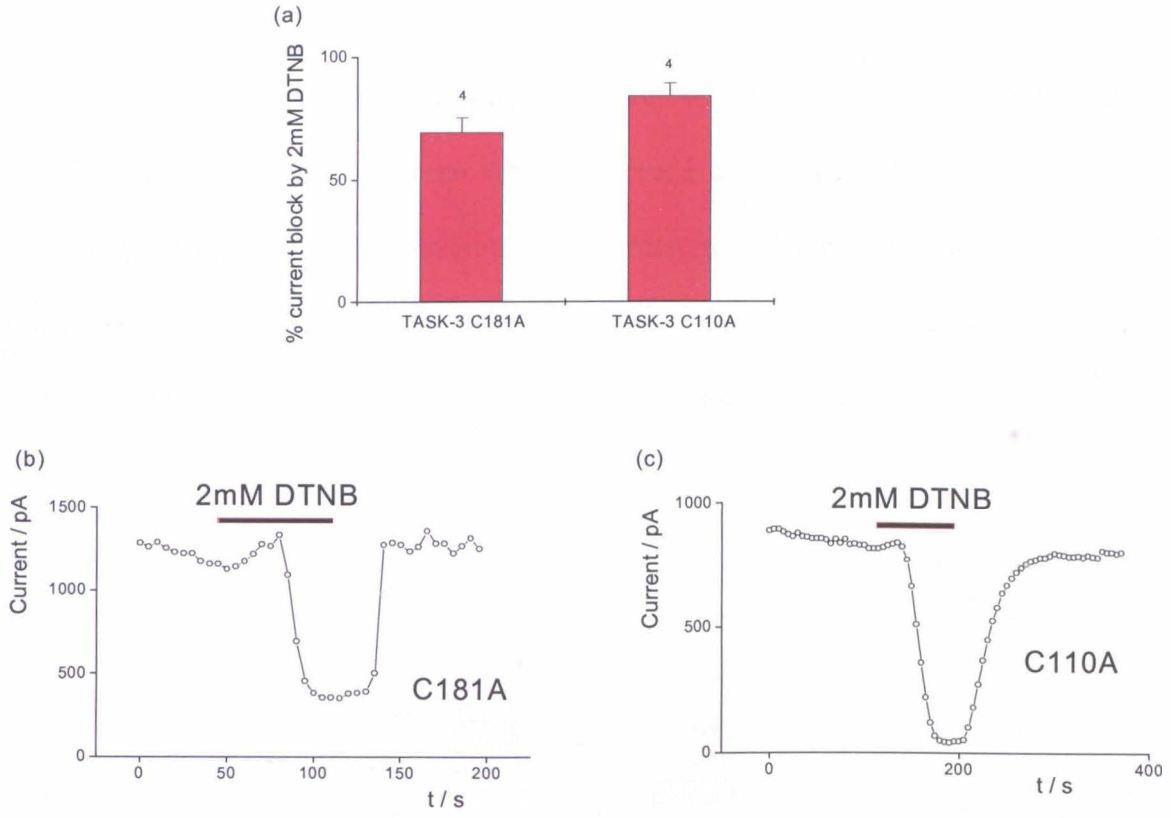

Figure 3-30 Current block of TASK-3 C181A and TASK-3 C110A channels by 2mM DTNB (a) Slight decrease in 2mM DTNB block of TASK-3 C181A compared to 2mM DTNB block of TASK-3 C110A and TASK-3 mimics copper response. 2mM DTNB block of TASK-3 C181A = -69.4 ± 6.0%, n=4, 2mM DTNB block of TASK-3 C110A = -84.35 ± 5.0%, n=4. These data are not significantly different from 2mM DTNB and 10μM Cu^{2+} block of WT TASK-3 channel currents. Column labels are number of cells, while error bars represent standard error of the means. (b) and (c) show exemplar time courses for 2mM block of TASK-3 C181A and TASK-3 C110A respectively.

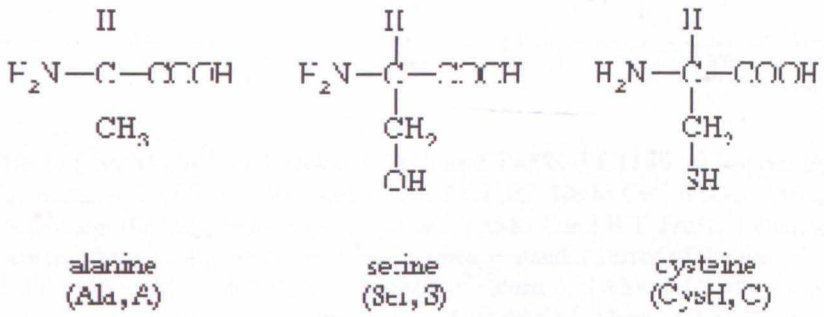

Figure 3-31 Displayed formulae of amino acids alanine, serine and cysteine (from left to right). Substitution of cysteine residues were made with both alanine a hydrophobic amino acid with aliphatic R group (molecular weight 89.1), and serine, a polar amino acid, uncharged at pH 7.4 (molecular weight 105.1). Cysteine has a molecular weight of 121.2 and is also uncharged at pH 7.4 (pK of cysteine side chain = 8.37).

The relative size of the substituted alanine was considered at this point. The molecular weight of alanine is 75% of cysteine whereas serine is a similar size, albeit slightly larger (Figure 3-31). In order to minimize conformational changes on cysteine substitution that may arise from its replacement with the smaller residue, second 181 and 110 mutants were constructed substituting serine for cysteine.

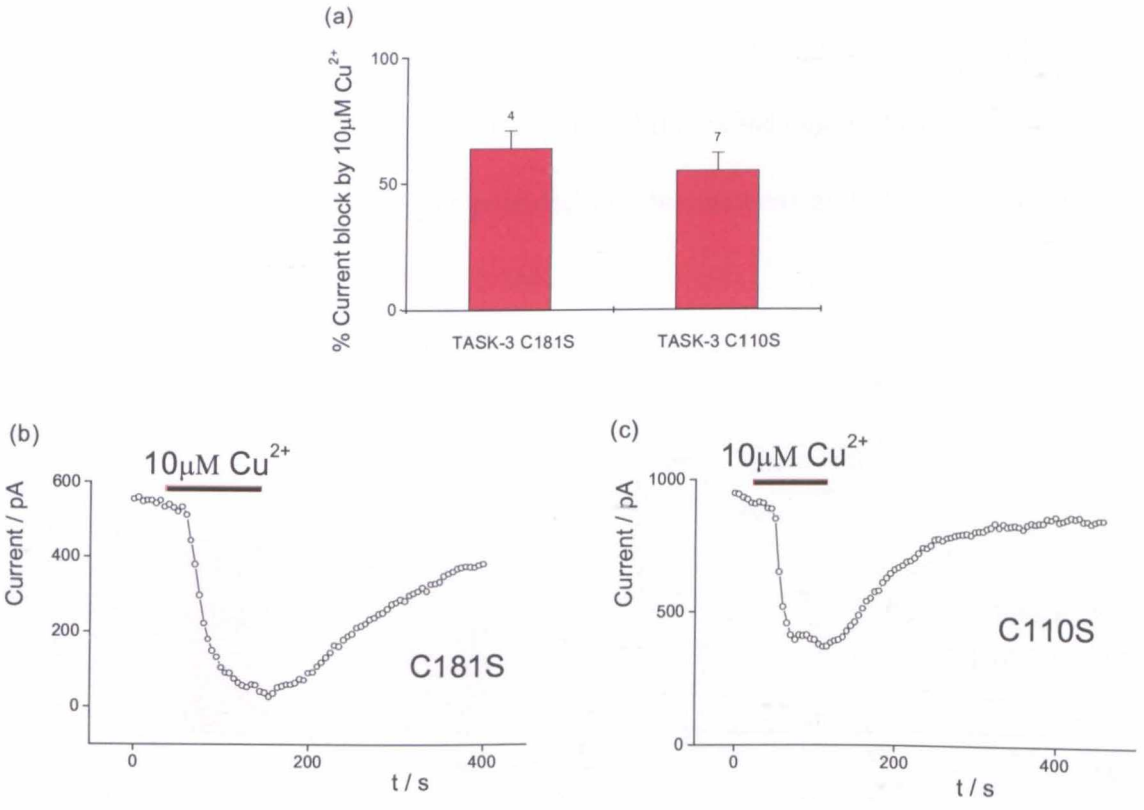

Figure 3-32 Effect of 10μM Cu^{2+} on TASK-3 C181S and TASK-3 C110S (a) Copper sensitivity retained in serine mutants, TASK-3 C181S and TASK-3 C110S. 10μM Cu^{2+} blocks TASK-3 C110S channel currents to a significantly lesser degree that WT TASK-3 and WT TASK-1 channel currents. Column labels are number of cells, while error bars represent standard error of the means. 10μM Cu^{2+} block of TASK-3 C181S = -64.1 ± 6.8 %, n=4, 10μM Cu^{2+} block of TASK-3 C110S = -55.1 ± 4.4 %, n=7 (b) and (c) show representative time course traces of 10μM Cu^{2+} block of TASK-3 C181S and TASK-3 C110S channel currents respectively.

When 10μM Cu^{2+} was applied to the serine mutants, it was found that the block of TASK-3 C181S was not significantly different from copper block of WT TASK-3 (10μM Cu^{2+} block of TASK-3 C181S = -64.1 ± 6.8 %). A pairwise t test usng the Bonferron correction for type 1 multiple comparison errors was conducted and

showed that the Cu^{2+} block of both TASK-3 C181S and TASK-3 C110S was not significantly different from the same block of WT TASK-3 channel currents (see appendix III, 5.1.2).

As neither the TASK-3 C181 nor the TASK-3 C110 mutant channel had abolished the channel copper sensitivity entirely, other cysteine residues were considered. A double TASK-3 mutant, TASK-3 C146S C147S was constructed and analysed. While these two residues were thought to lie on the intracellular M2M3 loop of the channel it was nevertheless important to test this potential involvement owing to the absence of equivalent residues in TASK-1 or TASK-2.

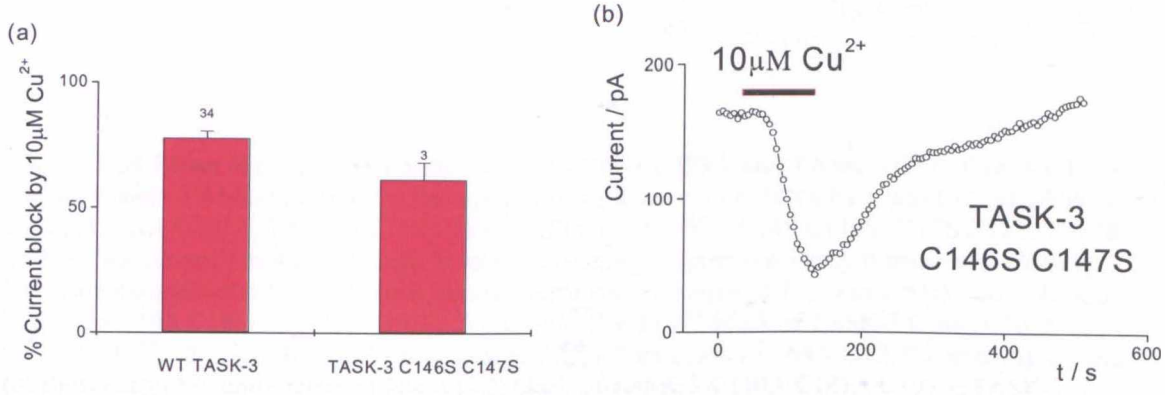

Figure 3-33 Effect of copper on TASK-3 C146S C147S (a) Bar chart comparing the copper sensitivity of WT TASK-3 with TASK-3 C146S C147S. C146 and C147 are purported to be intracellular residues. Point mutation of both of these cysteine residues did not significantly alter the copper sensitivity of the mutated channel. Column labels are number of cells, while error bars represent standard error of the means. 10μM Cu^{2+} block of TASK-3 = -77.8 ± 2.6%, n=34, 10μM Cu^{2+} block of TASK-3 C146S C147S = -61.14 ± 6.6 %, n=3 (b) Exemplar time course of 10μM Cu^{2+} block of TASK-3 C146S C147S mutant channel current.

The double mutant displayed a copper sensitivity not significantly different to that of the WT TASK-3 (see appendix III), although there was a decrease in channel current block (Figure 3-33, 10μM Cu^{2+} block of TASK-3 C146S C147S = -61.14 ± 6.6 %, n=3).

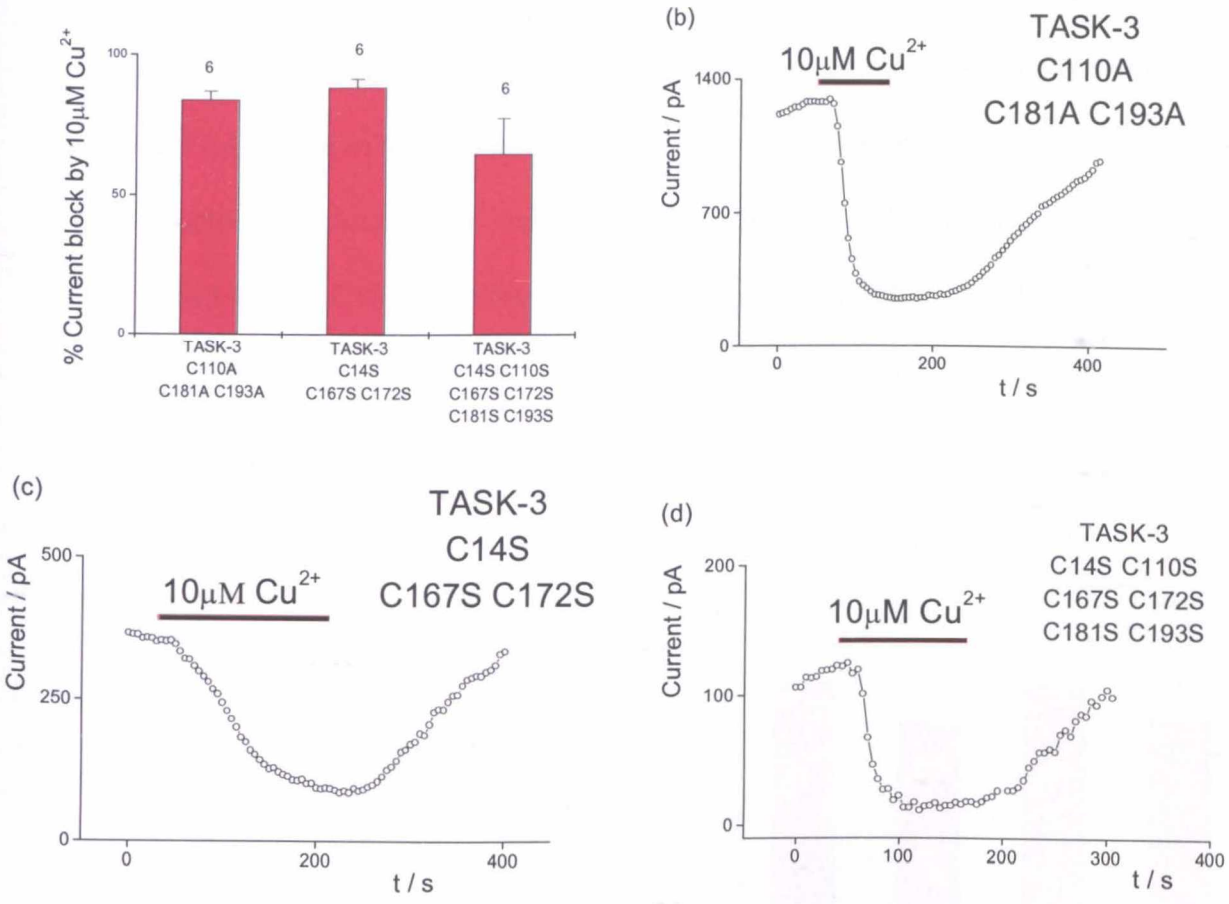

Figure 3-34 Effect of copper on TASK-3 C110A C181A C193A and TASK-3 C14S C167S C172S and six cys-ser TASK-3 mutant (a) Bar chart showing mean current block by 10μM Cu^{2+} of TASK-3 C110A C181A C193A, TASK-3 C14S C167S C172S and TASK-3 C14S C110S C167S C172S C181S C193S ('six cys-ser') mutant channels. In all three channels, copper sensitivity is preserved. Column labels are numbers of cells, while error bars represent standard error of the means. 10μM Cu^{2+} block of TASK-3 C110A C181A C193A= -79.7 ± 5.1%, n=6, 10μM Cu^{2+} block of TASK-3 C14S C167S C172S= -88.4 ± 2.9%, n=6, 10μM Cu^{2+} block of TASK-3 six cys-ser = -64.7 ± 12.7%, n=6. (b), (c) and (d) show exemplar time courses of 10μM Cu^{2+} block of TASK-3 C110A C181A C193A, TASK-3 C14S C167S C172S and TASK-3 six cys mutant channel currents respectively.

Having tested the cysteine residues absent in TASK-1 but present in TASK-3, but finding no single residue abolished copper sensitivity, multiple mutants were constructed substituting for all of the remaining cysteine residues purported to be accessible by extracellularly applied copper and DTNB.

TASK-3 C110A C181A C193A and TASK-3 C14S C167S C172S and a six cysteine-serine TASK-3 mutant (TASK-3 C14S C110S C167S C172S C181S C193S) were constructed and each mutant produced functional channels. 10μM Cu^{2+} was applied

extracellularly and it was found that copper sensitivity was retained for all mutants, though a decrease in the copper block of the TASK-3 six cys-ser was again observed (Figure 3-34). None of the mutant channel currents showed a significant difference in their sensitivity to block by Cu^{2+} compared to that of WT TASK-3 (10μM Cu^{2+} block of TASK-3 C110A C181A C193A= -79.7 ± 5.1%, n=6, 10μM Cu^{2+} block of TASK-3 C14S C167S C172S= -88.4 ± 2.9%, n=6, 10μM Cu^{2+} block of TASK-3 six cys-ser = -64.7 ± 12.7%, n=6).

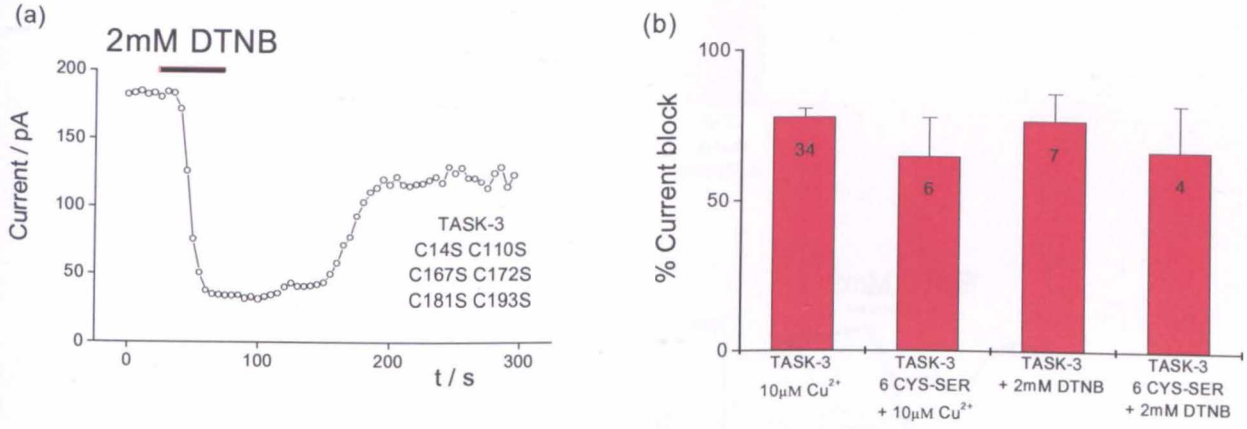

Figure 3-35 Comparing WT TASK-3 channel copper and DTNB sensitivity to TASK-3 six cys-ser mutant channel current responses (a) Exemplar time course of TASK-3 six cys-ser (C14S C110S C167S C172S C181S C193S) mutant channel current block by 2mM DTNB. (b) Summary bar chart comparing copper and DTNB block of WT TASK-3 and TASK-3 six cys mutant channel currents. Neither the copper nor the DTNB current block was significantly different in the six cys-ser TASK-3 mutant channel compared to that of WT TASK-3 channel currents. Column labels are numbers of cells, while error bars represent standard error of the means. 10μM Cu^{2+} block of TASK-3 = -77.8 ± 2.6%, n=34, 10μM Cu^{2+} block of TASK-3 six cys-ser = -64.7 ± 12.7%, n=6, 2mM DTNB block TASK-3 = -76.4 ± 9.2%, n=7, 2mM DTNB block of TASK-3 six cys-ser = -66.4 ± 15.3%, n=4

2mM DTNB was also applied to the six cys-ser TASK-3 mutant channel to determine whether a difference in the extent of DTNB block from that of the WT or with copper could be found. Such a separation of copper and DTNB sensitivity on this multiple cysteine mutant would indicate an alternative mechanism for copper block would need to be uncovered. However, 2mM DTNB block of the TASK-3 six cys-ser channel current was only slightly reduced (-66.4 ± 15.3%, n=4) from that of the WT

TASK-3 channel current block by 10μM Cu^{2+} or by 2mM DTNB (Figure 3-35). It was also found not to be statistically different from the 10μM Cu^{2+} block of the mutant channel current. These data suggest it is unlikely that the mutated cysteine residues underlie the effect of copper or DTNB.

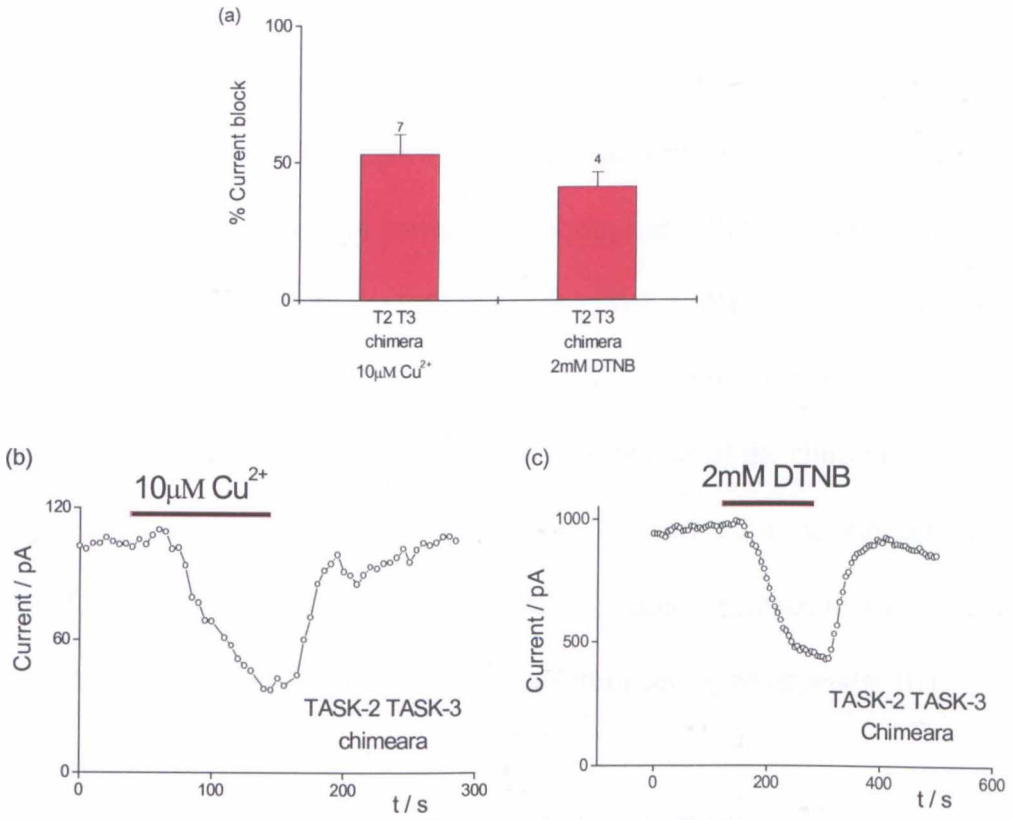

Figure 3-36 Effect of copper and DTNB on TASK-2 TASK-3 chimera (a) Bar chart comparing mean copper and DTNB blocks of whole cell currents of the TASK-2, TASK-3 chimera (T2T3) with DTNB block (2mM) of T2T3 channel currents. Column labels are numbers of cells, while error bars represent standard error of the means. 10μM Cu^{2+} block of TASK-2 TASK-3 chimera = -53.3 ± 6.9%, n=7, 2mM DTNB block of TASK-2 TASK-3 chimera = -41.4 ± 5.2%, n=4.

Having completed the analysis of cysteine residues of TASK-3, the next step was to consider the lack of copper sensitivity exhibited by TASK-2 channel currents. A functional TASK-2 TASK-3 chimeric channel became available, and was kindly gifted for this study by Dr Catherine Clarke, University of New South Wales, Australia. This channel had the M1P1 loop (glutamate 28 to glycine 77) from

wildtype human TASK-2 in place of the TASK-3 M1P1 loop from serine 31 to proline 71. When expressed in tsA-201 cells, the test concentrations of Cu^{2+} and DTNB (10μM and 2mM respectively) both elicited a current block (10μM Cu^{2+} block of TASK-2 TASK-3 chimera = -53.3 ± 6.9%, n=7, 2mM DTNB block of TASK-2 TASK-3 chimera = -41.4 ± 5.2%, n=4, (Figure 3-36)).

A comparison of DTNB block of the chimeric channel currents with that of the WT TASK-3 channels revealed no significant difference when analysed using independent pair-wise t tests with Bonferroni correction (see appendix III). No significant difference was found between the DTNB block of WT TASK-2 channel currents compared to the chimera channel (independent t test), nor was there a statistical difference between the size of the Cu^{2+} and DTNB blocks of the chimeric channel itself. The Cu^{2+} inhibition of the TASK-2 TASK-3 chimeric channel currents was also compared with the Cu^{2+} of TASK-2 and TASK-3 channel currents, using the same analysis, and found to be significantly different from each (see appendix III).

These data show that replacements of the M1P1 loop in TASK-3 with that of TASK-2 alters the TASK-3 channel DTNB sensitivity towards that of WT TASK-2 in terms of mean % current block.

3.3.4 Altered current amplitude and pH sensitivity of TASK-3 cysteine mutant channels

While all of the TASK-3 cysteine mutant channels were functional, a steady reduction in whole cell current amplitude with additional cysteine substitutions was observed (Figure 3-37). The truncated TASK-3 stop (124 C-terminal amino acids removed) did not significantly reduce the current amplitude from mean WT TASK-3 (Table 1 and Figure 3-37).

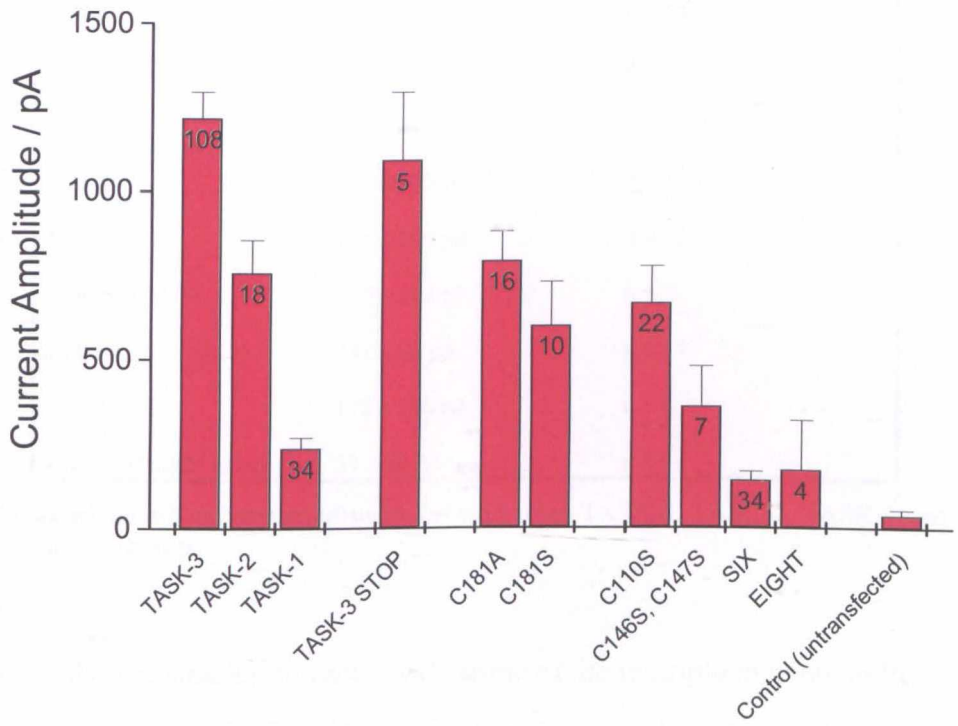

Figure 3-37 Whole cell current amplitudes (at -60mV) for wild type TASK-1, TASK-2, TASK-3, TASK-3-stop and cysteine mutant TASK-3 channels Increasing numbers of point mutations were accompanied by a steady reduction in whole cell current amplitude. 'Six' refers to TASK-3 with cysteines substituted for serine at C14, C110, C167, C172, C181 and C193. 'Eight' refers to the six cys-ser multiple mutant with additional cysteine-serine exchanges at C146 and C147. Column labels are numbers of cells, while error bars represent standard error of the means. See table 1 for mean data values.

Analysis of mean whole cell current amplitudes of wild type TASK 1, 2 and 3 and the TASK-3 mutants was conducted using Independent pair-wise t tests with Bonferroni correction (see appendix III, 5.1.4). WT TASK-3 whole cell current amplitude was significantly higher than TASK-1, TASK-3 C110S, TASK-3 C146S C147S, the six cysteine-serine TASK-3 mutant, and the eight cysteine-serine TASK-3 mutant (see fig 3-37).

Channel	Mean amplitude	n
TASK-3	1220 ± 76 pA	n = 108
TASK-2	800 ± 96 pA	n = 18
TASK-1	239 ± 31 pA	n = 34
TASK-3 STOP	1091 ± 201 pA	n = 5
C181A	794 ± 86 pA	n = 16
C181S	600 ± 129 pA	n = 10
C110S	665 ± 109 pA	n = 22
C146S, C147S	360 ± 118 pA	n = 7
SIX	141 ± 25 pA	n = 34
EIGHT	172 ± 146 pA	n = 4
Control ('blank' cells)	39 ± 14 pA	n = 9

Table 1 Mean whole cell current amplitudes for wild types TASK-1, TASK-2, TASK-3 and TASK-3 channel mutants.

Experimentally, the smaller currents made some of the multiple mutants more challenging to work with. Previous experience from initial characterisation studies of homomeric TASK-1 channel currents had demonstrated that an application and wash out of pH 8.4 had a stabilising effect on the cell. Potentiation of channel current with the alkaline extracellular bathing solution was followed by a return to the resting current amplitude upon wash out, which would remain stable if previously variable. The TASK-3 six cys-ser mutant channel exhibited small whole cell current amplitudes

similar to TASK-1 channel currents. Application of pH 8.4 was attempted- and was found to potentiate the mutant TASK-3 channel current in the same way as TASK-1 (pH 8.4 whole cell current change for TASK-3 six cys-ser = 219.4 ± 21.0%, n = 10,Figure 3-38).

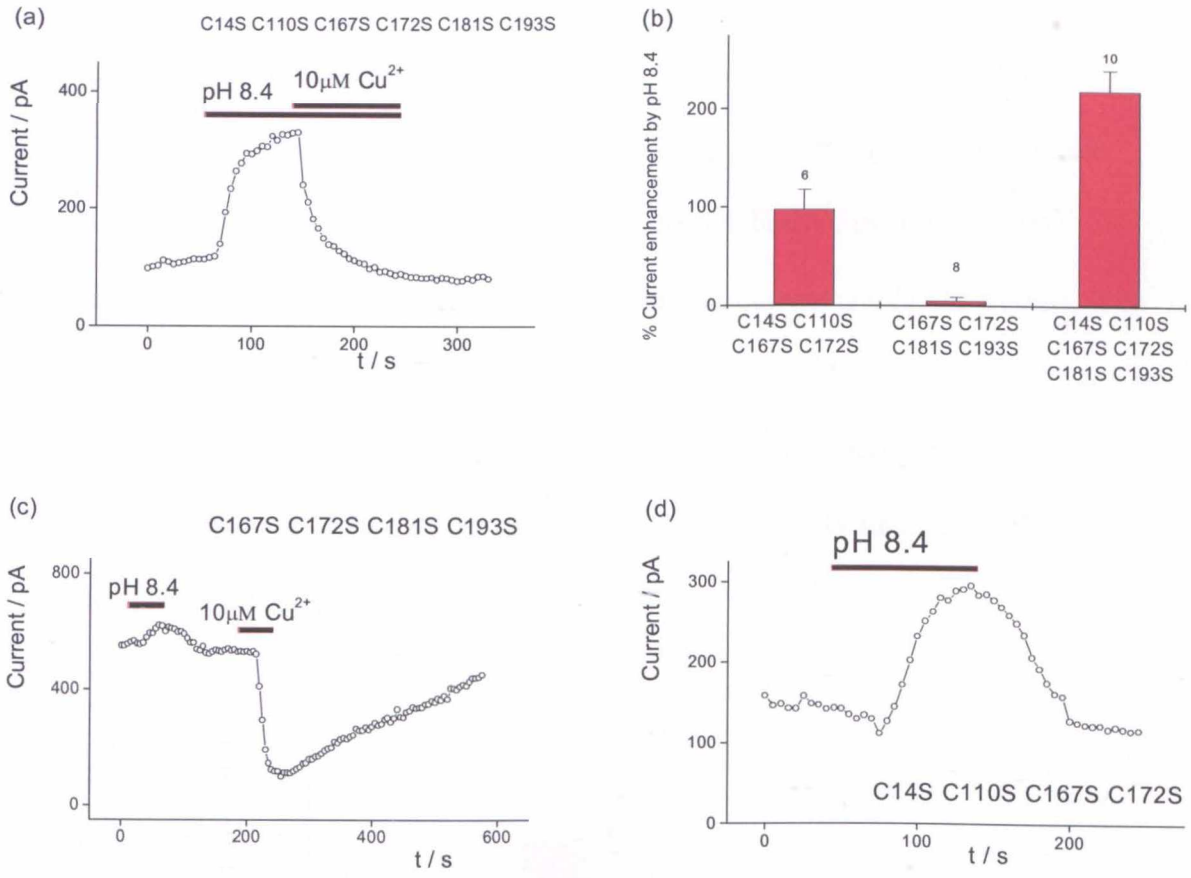

Figure 3-38 Whole cell current changes in response to pH 8.4 bathing (external) solution application for multiple cysteine mutants of TASK-3 (a) pH8.4 applied to the bath potentiated TASK-3 six cys-ser channel currents potently. Exemplar time course (b) substantial pH 8.4 enhancement of whole cell currents only occurred when applied to TASK-3 mutants with cysteine substitution at C110. pH 8.4 TASK-3 C14S C110S C167S C172S channel current enhancement = 97.6 ± 20%, n=6, pH 8.4 TASK-3 C167S C172S C181S C193S channel current enhancement = 4.9 ± 3.5%, n=8, pH 8.4 TASK-3 six cys-ser channel current enhancement = 219 ± 21%, n=10 (c) and (d) exemplar time courses of pH 8.4 responses of TASK-3 C167S C172S C181S C193S and TASK-3 C14S C110S C167S C172S channel currents

Working backwards along the list of cysteine mutants, pH 8.4 was applied to two quadruple cysteine mutants to identify which residue in particular conferred the new pH 8.4 sensitivity. Two quadruple cysteine substitution mutants were assayed first; TASK-3 C167S C172S C181S C193S and TASK-3 C14S C110S C167S C172S. pH

8.4 sensitivity appeared to be dependent on the presence of a C110 substitution (Figure 3-38, pH 8.4 TASK-3 C14S C110S C167S C172S channel current enhancement = 97.6 ± 20%, n=6, pH 8.4 TASK-3 C167S C172S C181S C193S channel current enhancement = 4.9 ± 3.5%, n=8).

Single cysteine substitution mutants, TASK-3 C181A, TASK-3 C181S, TASK-3 C110A and TASK-3 C110S were reconsidered (Figure 3-39, Figure 3-40). While neither of the C181 mutants were sensitive to pH 8.4, both of the C110 mutant channel currents were potentiated (Mean percentage current amplitude increase with pH 8.4 for C110A = 39.8 ± 7.3%, n=10, C110S = 61.3 ± 11%, n=16). Therefore, it is unlikely that C181 is responsible for different pH sensitivity between TASK-3 and TASK-1; however, C110 did seem to influence pH sensitivity making TASK-3 sensitive to alkaline pH.

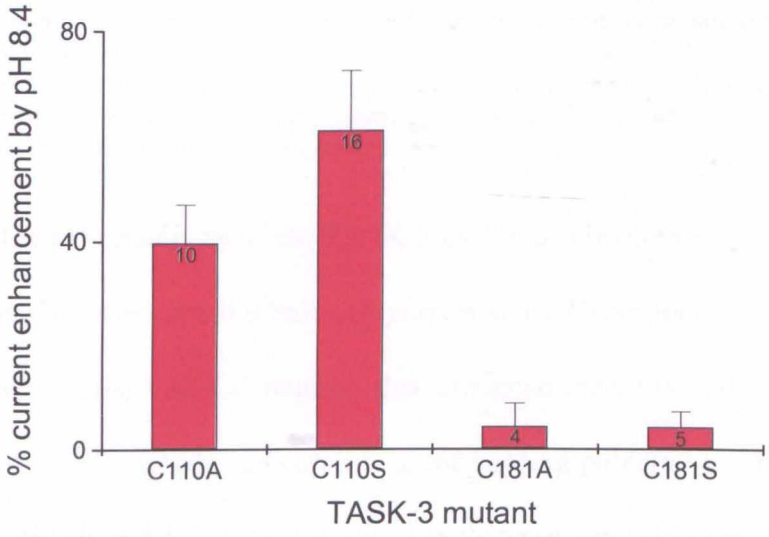

Figure 3-39 pH 8.4 enhancement of C181A, C181S, C110A and C110S Point mutations at C181 to alanine or serine from cysteine did not confer any changes in channel pH sensitivity. Both TASK-3 C181A and TASK-3 C181S were insensitive to pH 8.4. Single point mutations at C110 however induced a marked sensitivity to pH 8.4, the enhancement in current size being greater with cysteine to serine mutation over the cysteine to alanine mutation at residue 110. Column labels are numbers of cells, while error bars represent standard error of the means. Mean percentage current amplitude increase with pH 8.4 for C110A = 39.8 ± 7.3%, n=10, C110S = 61.3 ± 11%, n=16, C181A = 4.4 ± 4.4%, n =4, C181S = 4.2 ± 2.9%, n=5

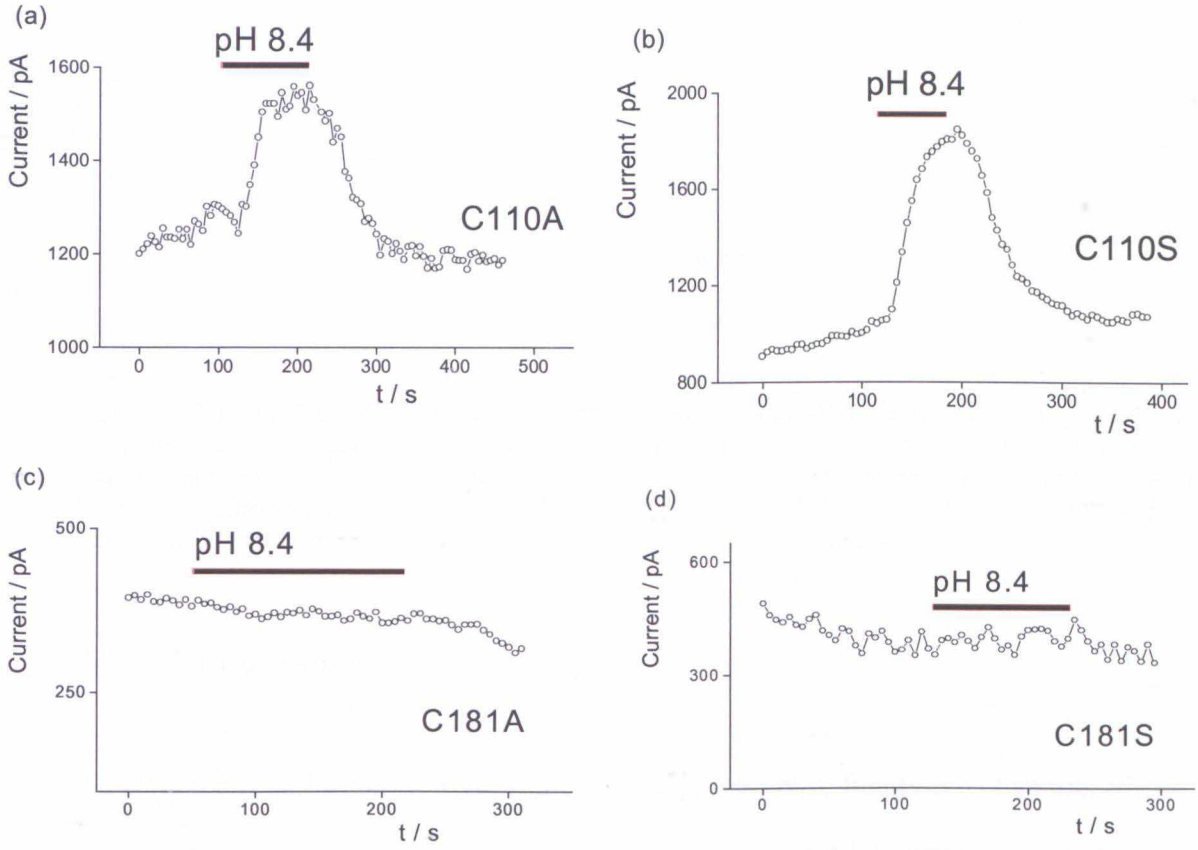

Figure 3-40 Exemplar time courses of C110 and C181 alanine and serine mutant channel current responses to pH 8.4 (a) and (b) depict exemplar time courses of TASK-3 C110A and C110S mutant channel currents. Application of pH 8.4 bathing (external) solution potentiates whole cell currents. (c) and (d) show applications of pH 8.4 bathing solutions on TASK-3 C181A and C181S mutant channel respectively. No potentiation of whole cell currents occurred.

Analysis of the pH sensitivity of the TASK-3 cysteine substitution mutants started by trying to overcome very small whole cell current sizes. Experimentally a general trend was observed with the TASK-3 mutants that contained the C110 substitution. Cells that displayed smaller whole cell currents at the holding potential of -60mV tended to be more sensitive to pH 8.4- in that these currents were potentiated more (Figure 3-41).

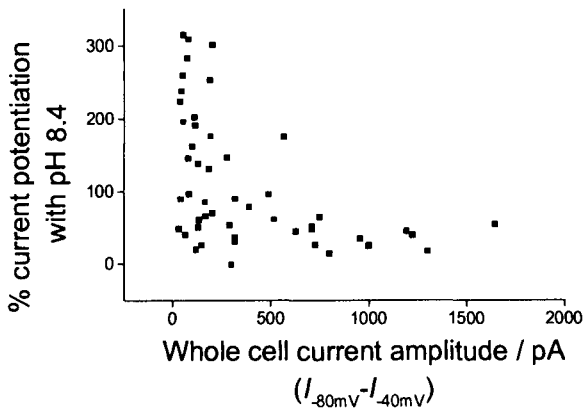

Figure 3-41 Predicting a trend between current amplitude and pH 8.4 potentiation Individual whole cell (current size calculated as previously described ($I_{-80mV} - I_{-40mV}$)) of TASK-3 cysteine substitution mutants plotted against % current amplitude increases in response to pH 8.4. Data included from mutant channels that contained C110 substitution only (TASK-3 C110S, C110A, C14S C110S C167S C172S, C110S C167S C172S C181S C193S and TASK-3 six cys-ser

3.3.5 Conclusion

All cysteine substitutions (single and multiple points) bore functional channels when expressed in tsA-201 cells and were tested for copper sensitivity. The truncated TASK-3 stop channel was equally as sensitive to copper block as the WT TASK-3, implying the C-terminus is unlikely to play a major role in copper block.

Single cysteine substitutions with serine and alanine were made comparing the effect of altering a cysteine shared by TASK-1 and TASK-3 (C110) and a non-identical cysteine (181). Both retained copper sensitivity (Figure 3-29, Figure 3-32). Multiple substitutions were also made and while Cu^{2+} sensitivity remained, whole-cell current size decreased (Figure 3-37). DTNB sensitivity was also conserved with a significant difference between the DTNB block of TASK-3 C110A and TASK-2 channel currents, Replacements of the M1P1 loop in TASK-3 with that of TASK-2 significantly altered the DTNB % block of the chimeric channel currents, away from

the WT TASK-3 phenotype, towards that of WT TASK-2, suggesting that the mechanism of action of DTNB is likely to reside within the M1P1 loop.

The small whole cell current of the 6 cys substitution mutant was comparable to the whole cell current seen in WT TASK-1 (Figure 3-37). Both currents are difficult to work with as a consequence and confirmation of the presence of TASK-1 currents experimentally necessitates the application of pH 8.4 bathing medium to observe its potentiation. pH 8.4 was also applied to the 6 cys substitution mutant. A potentiation comparable to that seen with TASK-1 currents was observed (Figure 3-32).

3.4 $I_{K(SO)}$ in Murine Cerebellar Granule Neurones

The voltage independent, standing outward potassium current ($I_{K(SO)}$) found in cerebellar granule neurones (CGNs) was first identified by Watkins and Mathie in 1996, in primary cultures of Sprague-Dawley rats (Watkins & Mathie, 1996). A key determinant of CGN resting membrane potential, considerable interest in the K_{2P} like nature of the potassium leak current has lead to characterisation of the rat CGN $I_{K(SO)}$ in recent years by several groups (see Introduction). Particular interest around the pH sensitive component of $I_{K(SO)}$ has brought the TASK channels to the fore (Han *et al.*, 2002; Millar *et al.*, 2000) and *in situ* hybridization studies have confirmed that TASK-1 and (to a lesser extent, TASK-3) gene expression occurs in the CGNs (Aller *et al.*, 2005; Rusznak *et al.*, 2004; Brickley *et al.*, 2001; Medhurst *et al.*, 2001; Talley *et al.*, 2001).

Generation of a TASK-1 knockout mouse for a recent collaboration (Aller *et al.*, 2005) necessitated a comparative study of WT murine CGN $I_{K(SO)}$ with that of the published data from the rat and the tsA-201 expressed hTASK channels. The study assessed the K_{2P} expression distributions and analysed the biophysical characteristics of murine WT and TASK-1 knockout CGN $I_{K(SO)}$. To date, the biophysical and pharmacological properties of the leak currents of cerebellar granule cells have focussed on the rat (Clarke *et al.*, 2004; Watkins & Mathie, 1996a-b). In this chapter I describe the initial electrophysiological analysis of the macroscopic biophysical characteristics of murine $I_{K(SO)}$ for comparison with the available literature on both hTASK currents and rat $I_{K(SO)}$. The development and optimisation of the primary culture for murine CGNs took place over a number of weeks resulting in the method previously described. Test

compounds from the earlier work on DTNB and copper were used as having quantified hTASK channels sensitivities of them in the tsA-201 expression system, it was of interest to assess their usefulness in dissecting the K_{2P} channel current contribution to the WT murine $I_{K(SO)}$.

3.4.1 Current amplitude development of murine CGN $I_{K(SO)}$

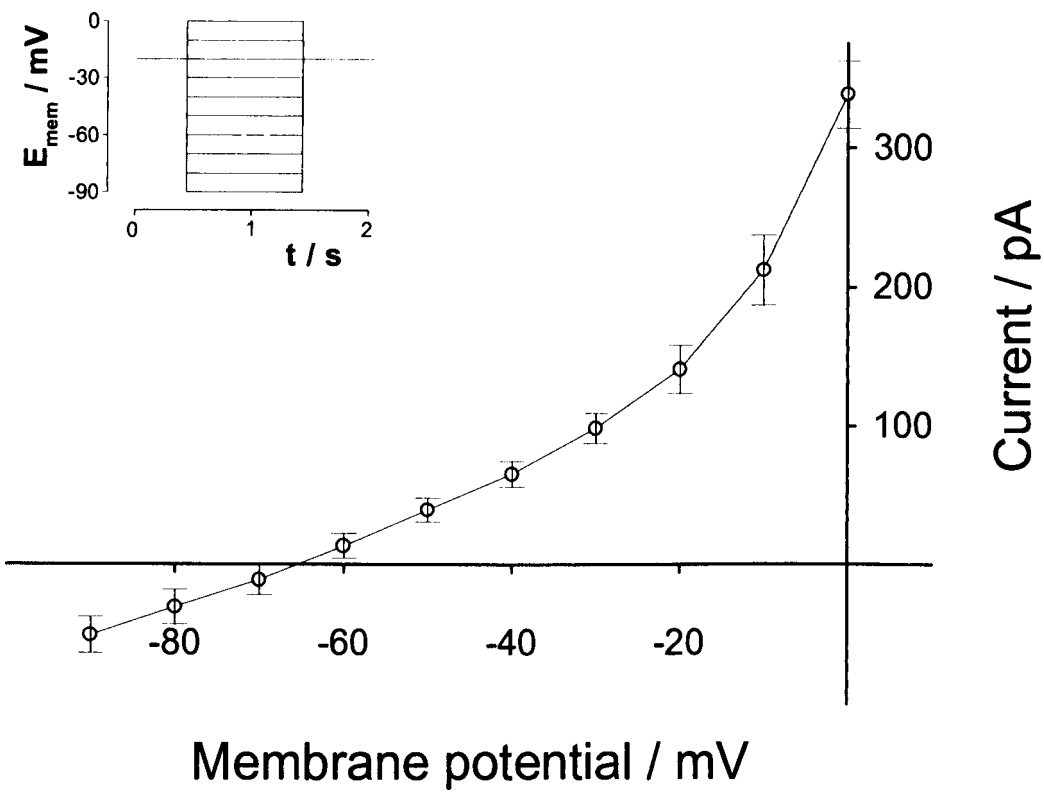

Figure 3-42 Current voltage relationship of standing outward potassium current exhibited by murine cerebella granule neurones. Mean data presented for n=6 cells with 7 days in culture, showing the current-voltage (I-V) relationship of the standing outward potassium current (IK_{SO}) of the neurones. Error bars are standard error of the mean, reversal potential (E_{rev}) = -66.9 ± 9.5mV. *Inset* 'IK_{SO} I-V' Stimulus waveform – cells were held at a potential of -20mVfor 430ms, stepped to -90mV for 1000ms before being returned to holding potential of -20mV. Sweep repeated every 2064ms for 10 sweeps. Epoch B (the step from -20mV) increased by 10mV with every sweep, the entire protocol covering recording current flow from -90mV to 0mV in the ten sweeps.

Patched cells from primary cultures of murine cerebellar granule neurones exhibited a TASK like, voltage-independent, standing outward potassium current. This was

present in all neurones patched and when subjected to a stepped voltage clamp protocol '$I_{K(SO)}$ I-V' (Figure 3-42) it exhibited a mean reversal potential of -66.9 ± 9.5mV close to reported resting membrane potentials of CGNs *in vivo* (-64 ± 1mV, n = 75, (Chadderton *et al.*, 2004). Cultured CGNs had two important variables; age of pup at culture and number of days cells were in culture before patching. Early cultures were found to be robust enough to remain suitable for electrophysiology as late as 14 days in culture, and as early as 2. Currents were recorded with a one step voltage protocol, holding at -20mV then stepping down to -60mV for 1s every 2 seconds (Figure 3-43) to assess how variability in whole cell current size could be accounted for.

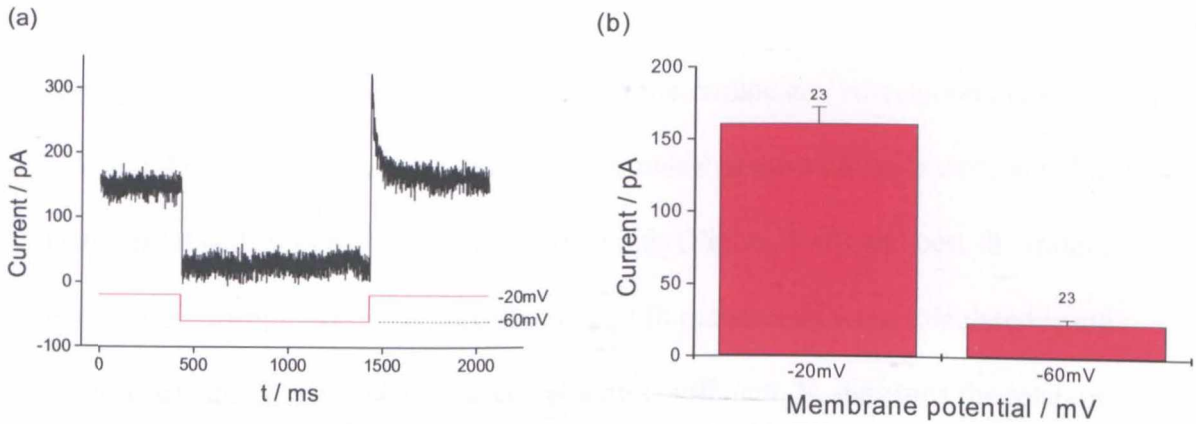

Figure 3-43 Mean current amplitude of murine IK_{SO} (a) Exemplar trace of CGN current recording with stimulus waveform. Cerebella granule neurones were patched and membrane potentials were controlled using a voltage step protocol. Cells were held at -20mV for 1.43s, voltage was stepped to -60mV for 1s followed by a return to a holding potential of -20mV (b) Mean current amplitude at -60mV = 23.7 ± 2.97%, n=23, mean current amplitude at -20mV = 161 ± 10.8%, n=23. Error bars represent standard error of the mean. Cells were in culture from between 7 and 10 days and were plated at P3, P4 or P6.

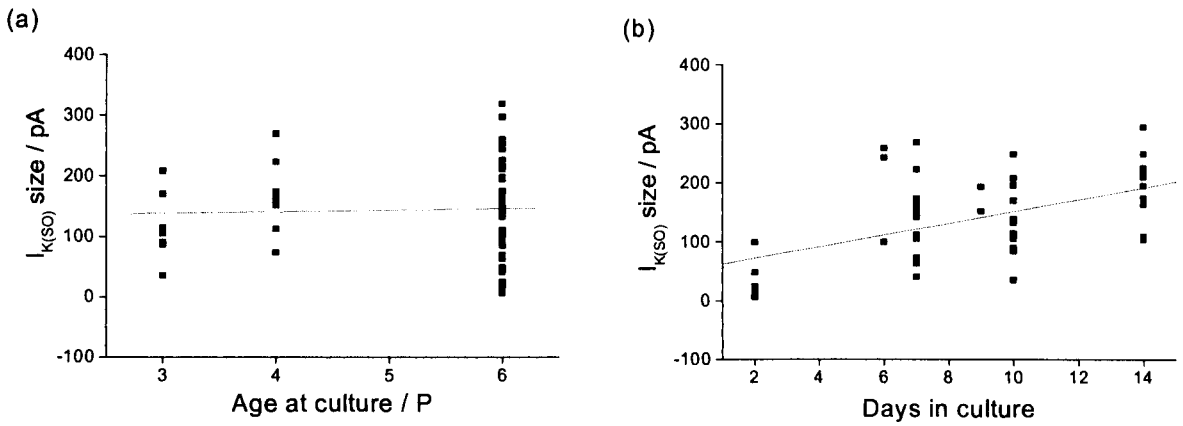

Figure 3-44 Summary of murine CGN $I_{K(SO)}$ amplitudes plotted against (a) age at culture and (b) days in culture at -20mV Linear regression was used to fit the data to a straight line, y =A + Bx, to determine correlation. When plotted against age at culture (a) no correlation was found for current amplitude (R, the correlation coefficient, = 0.37 with a probability, P, of no correlation being 0.8. A=130.5 ± 7, B=2.4 ± 0.3, n=50) (b) A positive correlation between number of days in culture and CGN $I_{K(SO)}$ size was found when fitting the dataset to a straight line where A=51.0 ± 3, B=10.1 ± 0.4. R=0.5, P=1.9 x 10^{-4}. All errors are stated as standard errors of the mean.

Data analysis software Origin 5.0 was used to determine any correlation between $I_{K(SO)}$ size and the age of the pup at culture or the number of days the cells were in culture. Data for 50 cells was plotted as scatter diagrams (Figure 3-44) and best fit straight lines (of the form $y = A + Bx$), correlation and fit parameters were calculated using linear least square regression. The correlation coefficient, R, indicates the relation between x and y and has a value, positive or negative, between 0 and 1, 0 being no correlation, the polarity indicating the change in size of y with respect to an increasing x. The significance of the calculated correlation coefficient, R, can be tested against statistical tables of correlation coefficients with $n-2$ degrees of freedom[6]. R is statistically significant when it is numerically as large as the value in the table. A further parameter p, given by Origin™ 5.0, is the probability that there is no correlation between x and y, that R=0.

[6] Table IV *'Values of the correlation coefficient, ρ, which differ significantly from 0 at the 5%, 1% and 0.1% levels'* from *'Statistics and Experimental Design'*, 2nd Edition, Geoffrey M Clarke, 1990

With a value of 0.37, the correlation of $I_{K(SO)}$ size and age at culture (Figure 3-44(a)) is close to zero and significant at the 1% level when compared to the statistical tables. There is also a high probability of no correlation as p = 0.8. An increasing age of the CGN at culture can only weakly be associated with an increase in $I_{K(SO)}$ amplitude, therefore. The data set was fit to a straight line of the form $y = A + Bx$ where A = 130.5 ± 7, B=2.4 ± 0.3. 50 cells were used.

In contrast, there was a positive correlation between $I_{K(SO)}$ size and days in culture. R was calculated to be 0.5, significant at the 0.1% level. The probability that there is no correlation is extremely small ($p = 1.9 \times 10^{-4}$). The dataset (of 50 cells) was fitted to a straight line with A = 51.0 ± 3, B = 10.1 ± 0.4.

These data suggest that $I_{K(SO)}$ size increases with days in culture; irrespective of the age at which the cells are initially cultured.

3.4.2 pH and zinc sensitivity of murine CGN $I_{K(SO)}$

Comparison of $I_{K(SO)}$ with established tests of TASK channel currents was done by looking at pH and zinc sensitivity of murine $I_{K(SO)}$ (Figure 3-45)..

Zinc (100μM) was applied to patched CGNs and was found to elicit a 46.1 ± 3% block (n=5). Exchange of the bathing solution at pH 7.4 with the more acidic pH 6.4 decreased $I_{K(SO)}$ (21.4 ± 5%, n=4), while increasing the alkalinity if the bathing solution to pH 8.4 increased $I_{K(SO)}$ size by 21.0 ± 5% (n=7). Sensitivity to zinc and pH was tested on cells plated at P6, and had been in culture for 14 days.

While the zinc and pH 6.4 sensitivity is consistent with the presence of TASK-3 channel currents, both pH 6.4 and zinc blocks are significantly different from hTASK-3 channel current block expressed previously, in tsA-201 cells. Using the Student's t test for two independent populations tested at the 0.05 level, zinc block is significantly different in the two cell types with a probability, p, of the difference arising by chance, of 1.5×10^{-6}. Using the same statistical analysis, a similar outcome is found for the pH 6.4 block, p = 3.5 x 10-4. This is also true for the potentiation caused by pH 8.4 application. Although this sensitivity is indicative of a TASK-1 channel current contribution, its magnitude is significantly different at the 0.05 level from the tsA-201 model ($p = 2.7 \times 10^{-6}$).

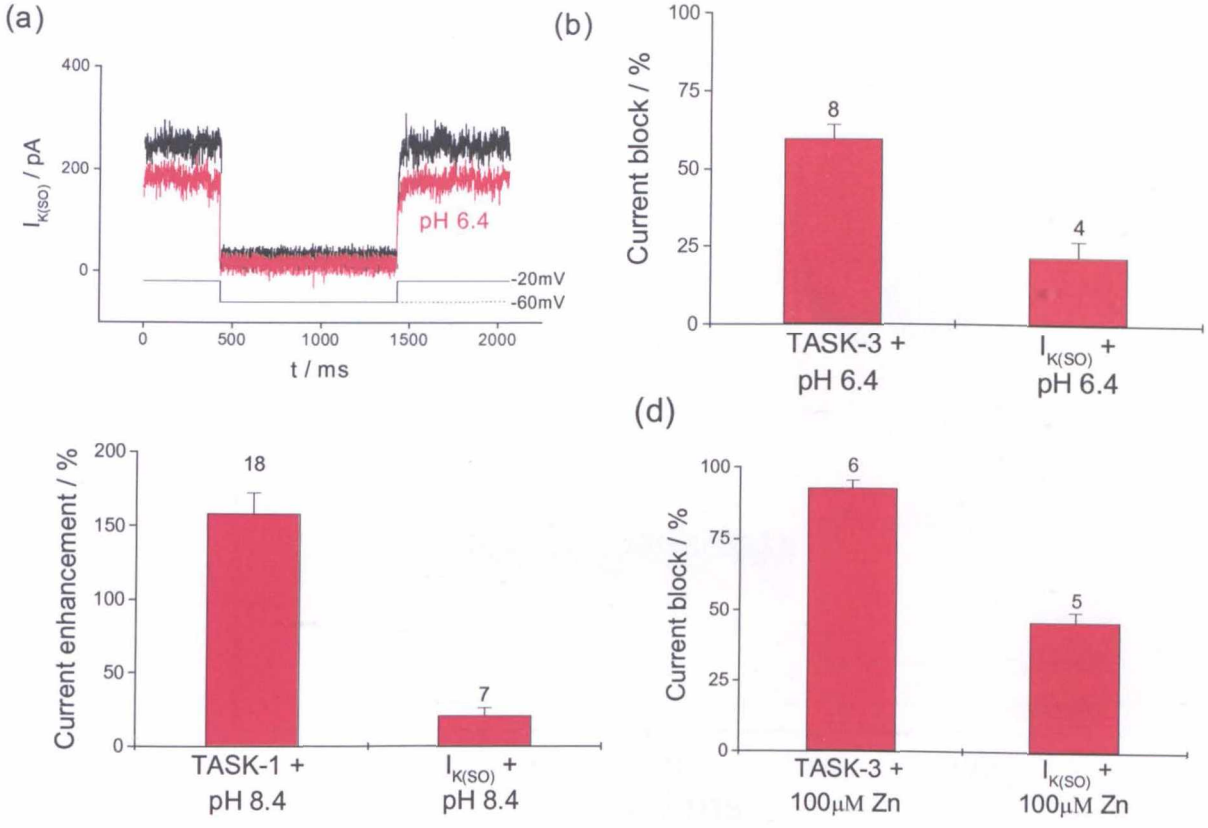

Figure 3-45 Comparison of murine $I_{K(SO)}$ pharmacology from cultured cerebella granule neurones with hTASK-1 and hTASK-3 channel current sensitivity to pH and zinc Exemplar traces of channel $I_{K(SO)}$ sensitivity to (a) pH 6.4 (b) and (c) show mean responses to pH 8.4 and pH 6.4 (d) 100μM zinc. Bar graphs show mean $I_{K(SO)}$ size changes compared to equivalent data from the hTASK-1 and hTASK-3 channels expressed in tsA-201 cells (b) hTASK-3, $I_{K(SO)}$ and pH 6.4 (TASK-3 mean block = -59.9 ± 5%, n=8, $I_{K(SO)}$ mean block = 21.4 ± 5%, n=4), (c) hTASK-1, $I_{K(SO)}$ and pH8.4 (TASK-1 mean potentiation = 158.6 ± 14%, $I_{K(SO)}$ mean potentiation = 21.0 ± 5%, n=7), (d) hTASK-3, $I_{K(SO)}$ and 100μM Zn^{2+} (TASK-3 block = -92.8 ± 3%, n=6, $I_{K(SO)}$ mean block = 46.1 ± 3%, n=5). The patched CGNs were subjected to the standard -20mV to -60mV step voltage protocol, with mean current changes at -20mV being calculated. $I_{K(SO)}$ was found to be blocked by both pH 6.4 and zinc, but was potentiated by pH 8.4. CGNs were plated at P6 and had been in culture for 14 days.

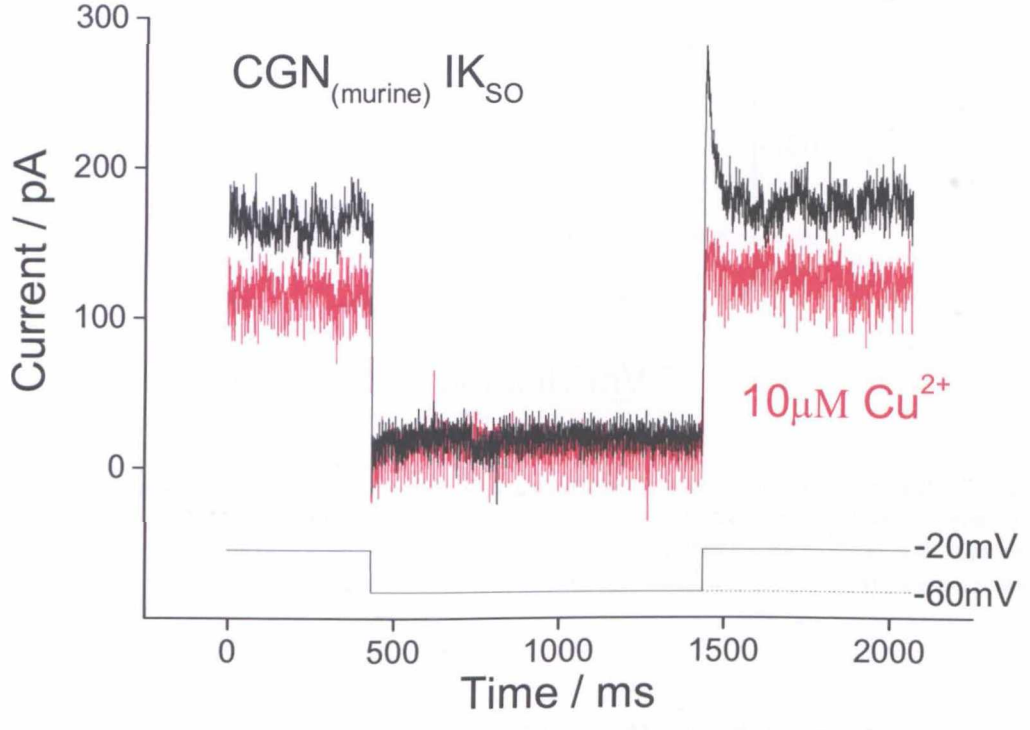

Figure 3-46 Exemplar trace of copper block of standing outward potassium current of cerebella granule neurone Control current (black) plotted with same current in the presence of extracellular 10μM Cu2+ (red). Voltage protocol stimulus waveform appended below the trace.

The test dose of 10μM Cu^{2+} was applied to CGNs while whole cell $I_{K(SO)}$ was measured. The patched cell was held at -20mV with a single step to -60mV every two seconds for 1s, as previously described. Two apparent populations of CGNs were uncovered; one that displayed Cu^{2+} sensitive $I_{K(SO)}$ currents that were blocked (Figure 3-46, Figure 3-47), the other displayed Cu^{2+} sensitive currents that were potentiated (Figure 3-48) by 10μM Cu^{2+}.

Mean Cu^{2+} block of CGN $I_{K(SO)}$ was more TASK-1 like than TASK-3 like at -29.8 ± 5.1% (n=6 cells). Blocked channel currents exhibited no significant shift in the reversal potential (E_{rev} = -62.5 ± 2.7mV).

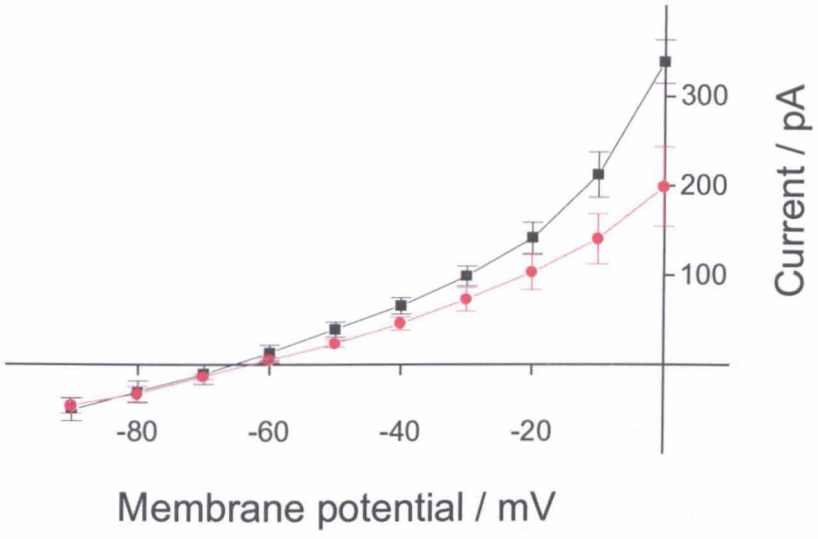

Figure 3-47 Copper block of standing outward potassium current of murine cerebellar granule neurones (red). Black trace is control I-V, 'IK_{SO} I-V' Stimulus waveform protocol used to record both traces (Figure 3-42). Control I-V is for n=6 cells, copper block IV (red) is for n=4 cells. A rightward shift in reversal potential from the control trace is present, E_{rev} = -62.5 ± 2.7mV. Error bars are standard error of the mean.

Cu^{2+} sensitive potentiation of CGN $I_{K(SO)}$ (79.8 ± 24%, n = 4, Figure 3-47) was found to be in the order of previously published data on copper activation of TREK-1 channels (V_{max} TREK-1 activation by Cu^{2+} (10μM Cu^{2+} and above) = 83 ± 11%) (Gruss *et al.*, 2004).

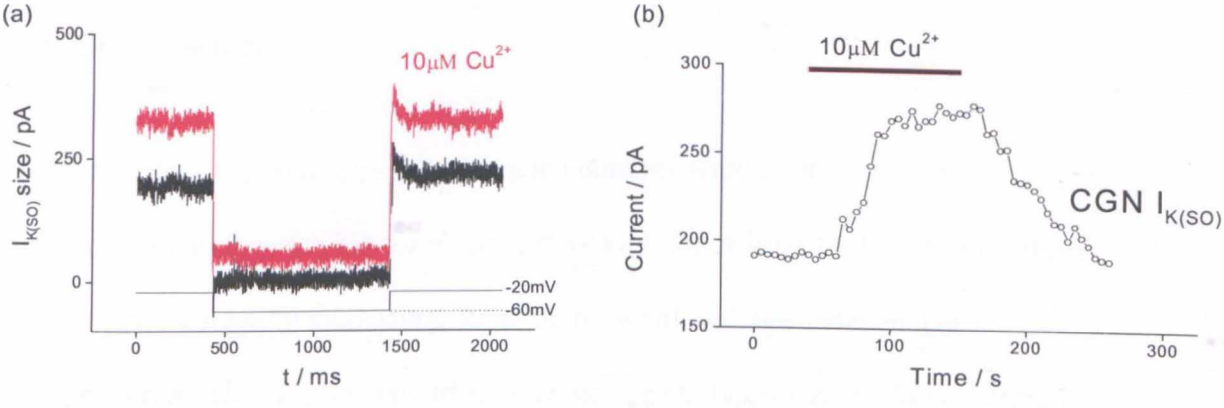

Figure 3-48 Copper enhances voltage-independent potassium leak current of murine CGNs For a small number of cerebella granule neurones (n=4), application of 10μM Cu^{2+} in the normal way significantly enhanced the CGN $I_{K(SO)}$. (a) Raw data trace showing potentiation of CGN $I_{K(SO)}$ by 10μM Cu^{2+}. Voltage step protocol used in recording is appended below the trace (b) Exemplar trace of whole cell current recorded from CGN cultured at P3, culture day 10.

3.4.3 DTNB sensitivity of $I_{K(SO)}$

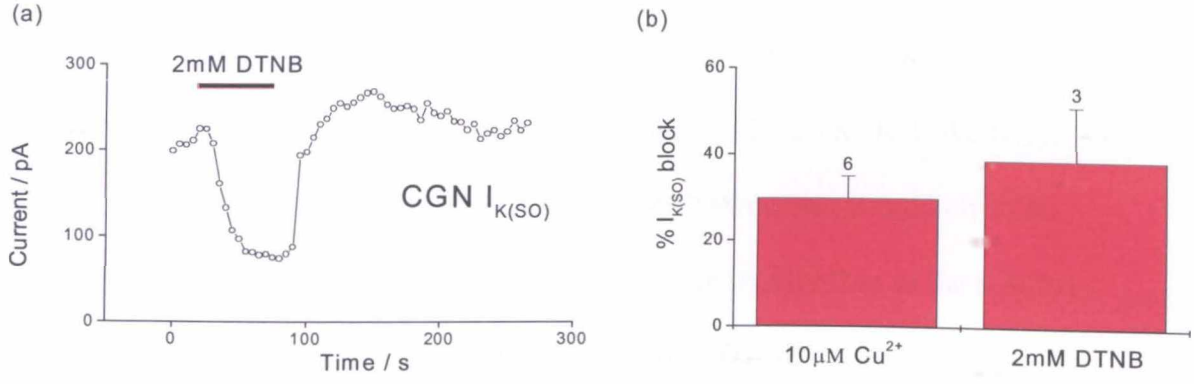

Figure 3-49 CGN $I_{K(SO)}$ can be blocked by 2mM DTNB (a) Exemplar trace of CGN $I_{K(SO)}$ block by 2mM DTNB, whole cell current recorded from day 10 of CGN cultured at P6 (b) Comparison of mean $I_{K(SO)}$ block by 10μM Cu^{2+} (-29.8±5%, n=6) and 2mM DTNB (-38.7±12.3%, n=3) Error bars are standard errors of the mean. Recordings were made of cells plated at P3 to P6 with 6-10 days in culture (Cu^{2+} responses) or P6 with 9-10 days n culture (DTNB responses).

The copper sensitivity of $I_{K(SO)}$ indicated a potential for DTNB sensitivity and the CGN $I_{K(SO)}$ was tested in the standard way. 2mM DTNB solution replaced the bath solution once a suitable granule neurone had been patched. While the cells were poorly tolerant to DTNB, a block of $I_{K(SO)}$, reversible on wash out was observed (-38.7 ± 12.3%, n=3). The block was much more variable than that exhibited by the tsA-201 cells expressing hTASK-3 channels.

3.4.4 Conclusion

Primary cultures of murine cerebella granule neurones were established and maintained, remaining suitable for electrophysiology for at least 14 days from plating. Over that time, a steadily increasing, standing outward, voltage-independent potassium current ($I_{K(SO)}$) was recorded. The increase in $I_{K(SO)}$ size could not strongly be associated with the age of the mouse pup at culture, but instead appeared to be dependant on the number of days in culture.

Murine $I_{K(SO)}$ was found to exhibit a zinc and pH 6.4 sensitivity akin to previously described hTASK-3 channel currents, but further studies demonstrated a potentiation of the current with pH 8.4 found with TASK-1. Furthermore, the TASK-3 like copper sensitivity demonstrated by $I_{K(SO)}$ block was accompanied by a TREK-1 like $I_{K(SO)}$ potentiation (Gruss *et al.*, 2004), suggesting that the CGN current is unlikely to be solely TASK-3. Further to this, all current changes were smaller than in the tsA-201 model whole cell currents, including the block by 2mM DTNB.

4 Discussion

In this study the initial assessment of novel and known pharmacological properties of TASK-1 and TASK-3 has lead to the identification of copper as a robust blocker of the TASK channel currents. Comparison of the copper sensitivity of the TALK channel, TASK-2, has demonstrated the ion to be a suitable pharmacological agent to differentiate the currents. Multiple cysteine mutations, a truncation and a chimaeric mutant of TASK-3 channels have revealed copper sensitivity is modulated by several residues in combination which also brought about a TASK-1 like pH sensitivity but none of them abolished copper effects. Copper sensitivity is maintained in murine cerebellar granule cells, although the TASK like inhibition is accompanied by a TREK like potentiation of the standing outward potassium current, $I_{K(SO)}$.

4.1 TASK-1 and TASK-3 channel current size, pH and zinc sensitivity

As previously discussed in the introduction, the distinguishing feature of the TASK channels from other two pore domain potassium channels was, initially, their sensitivity to extracellular acidification. It was later found that this property was not exclusive to the subfamily but was also exhibited by all TALK channel isoforms (of which TASK-2 is one) (Kang & Kim, 2004) as well as deSUMOylated TWIK-1 (Rajan *et al.*, 2005). TASK-1 and TASK-3 channels have also been shown to exhibit some differences in pH sensitivity with TASK-1 channel currents being both potentiated and inhibited by increasing and decreasing pH respectively, while TASK-

3 channel currents do not increase with extracellular alkalinisation but are inhibited with acidification (Kim *et al.*, 2000; Duprat *et al.*, 1997).

Initial characterisation of heterologously expressed TASK-1 and TASK-3 channels corroborated published data with TASK-3 currents being inhibited by extracellular pH 6.4 and insensitive to extracellular pH 8.4. TASK-1 currents were potentiated by extracellular pH 8.4 while they, like TASK-3 channel currents, were inhibited at pH 6.4.

Whole cell current amplitude could also be used to differentiate cells transfected with the two TASK channels. TASK-1 transfected cells exhinited smaller whole cell currents on average than those of TASK-3. This difference in whole cell current size matched reported data (Renigunta *et al.*, 2006).

The difference in current amplitude in the heterologously expressed TASK channels has been examined in a number of studies and has been ascribed to differences in single channel conductance, larger in TASK-3 (Kang *et al.*, 2004; Han *et al.*, 2002; Kim *et al.*, 2000), as well as higher mean open probability of the TASK-3 channels compared to TASK-1 (Kang *et al.*, 2004; Han *et al.*, 2002; Kim *et al.*, 2000), and the interaction of the two channels with auxiliary trafficking or endoplasmic reticulum (ER) retention / retrieval proteins. Of particular interest are the p11 and 14-3-3 proteins.

TASK-3 and TASK-1 differ in their association with p11, a member of the S100 gene family, it is a small cytosolic protein involved in vesicular trafficking. Results of a

recent study (Renigunta *et al.*, 2006) suggests that p11 binding to TASK-1 reduces surface expression of the channel acting as a retention factor that localises the channel to the ER. Indeed knockdown of p11 using small interfering RNA increased surface expression of TASK-1. Further to this the replacement of the TASK-1 C-terminus with that of TASK-3 (TASK-3 does not normally interact with p11) gave rise to larger current compares to TASK-1 wild-type. Conversely, TASK-3 with a TASK-1 C-terminus exhibited reduced current amplitude compared to wild-type TASK-3.

Two conserved sequences in TASK channels have been proposed to be involved in trafficking; the N terminus dibasic sequence KR[7] and the C-terminus RRSSV motif. The RRSSV motif is thought to interact with both p11 and 14-3-3 proteins. 14-3-3, unlike p11 is thought to promote surface expression to the membrane (Renigunta *et al.*, 2006; Plant *et al.*, 2005; O'Kelly *et al.*, 2002).

Binding of 14-3-3 to the channel is facilitated by phoshorylation of a C-terminus residue. Once 14-3-3 has bound, its mechanism of action has been proposed to lie in either the facilitation of binding a further accessory protein to allow trafficking to the cell membrane or, 14-3-3 may mask an ER retention signal (possible the KR residues of the N terminus), preventing the binding of ER retention/retrieval protein such as p11 (Renigunta *et al.*, 2006; Plant *et al.*, 2005 Rajan *et al.*, 2002).

The current voltage (I-V) properties of TASK-1 and TASK-3 channels also closely matched previously reported data with macroscopic currents exhibiting outward rectification in the physiological K^+ gradients used and reversal potentials of around -

[7] Basic amino acids R and K are often found in pairs and can, alone or in triplets also, serve as recognition motifs for 'coatamer proteins'. These proteins, such as β-COP, mediate vesicular transport towards the endoplasmic reticulum (Plant *et al.*, 2005)

70mV (see fig 3.2). Clarke and others previously reported reversal potentials for TASK-1 and TASK-3 channels of -70 ± 3mV and -78 ± 3mV in *Xenopus* oocytes while a transfection of tsA-201 cells with a separate two pore domain potassium channel, TREK-1, exhibited a reversal potential of around -85mV (Clarke *et al.*, 2004; Gruss *et al.*, 2004).

As with the entire subfamily of two pore domain channels, attribution of contributory channel currents to heterogenous potassium background conductances has been the goal for the pharmacological and biophysical characterisation studies. Zinc sensitivity has been proposed as a suitable pharmacological agent to meet this end with a much lower sensitivity being reported for TASK-1 channel currents than for TASK-3 channel currents (Clarke *et al.*, 2004). TASK-3 channels exhibited a zinc sensitivity being blocked almost completely by 100μM Zinc and a fit to the Hill equation gave a half-maximal inhibitory concentration (IC_{50}) of 5.7 ± 0.4μM, in the region of that reported by Gruss and others (12.7 ± 1μM) (Gruss *et al.*, 2004). hTASK-1 channel currents have previously been described as insensitive to zinc (Clarke *et al.*, 2004) while mouse TASK-1 has been potentiated 15% by 10μM zinc (Czirjak & Enyedi, 2006) and inhibited 10% by 100μM zinc (Aller *et al.*, 2005). The test concentration in this study was higher than previously used (200μM) and as a consequence zinc block of TASK-1 channels occurred (-52%, n=2). This is likely to be a maximal effect. It was hard to reproduce with the small currents of the TASK-1 transfected tsA cells and would require further assessment in the system used to determine the significance of the finding.

4.2 TASK-1 and TASK-3 Ruthenium Red and Ru-360 sensitivity

Another pharmacological agent reported to be selective for TASK-3 over TASK-1 is ruthenium red, a polycationic dye (Aller *et al.*, 2005; Czirjak & Enyedi, 2002, 2003). With little effect on TASK-1 ((murine) -4 ± 5%, (Aller *et al*, 2005)), the key residue thought to underlie TASK-3 sensitivity to the compound was found to be E70 (Czirjak & Enyedi, 2003, see sections 1.2.6 and 3.1.5). In this study, both TASK channels exhibited a ruthenium red sensitivity, though again, owing to the small currents of TASK-1 transfected cells this sensitivity was poorly reproducible. Block of TASK-1 channel currents was found to be -17% (n=2) by 10μM ruthenium red, while TASK-3 channel currents were more robustly blocked with the same dose (-73.2 ± 3.3 %, n=6). TASK-3 block matched that found for murine TASK-3 channel currents also expressed in tsA-201 cells (-65 ± 2%, n=10, (Aller et al, 2005)). Fitting my data to the Hill equation gave an IC_{50} of 3.5μM, implying a slightly lower sensitivity of the human TASK-3 channel tested here compared to the rat adrenal glomerulosa cloned TASK-3 channels used in Czirjak and Enyedi's study of 2003 (rTASK-3 ruthenium red IC_{50} = 0.7μM).

The use of ruthenium red is hampered by its blocking of multiple ion channel types including TREK channel, TRAAK (Czirjak & Enyedi, 2006, 2002) and Ca^{+} release ryanodine channels (Xu *et al.*, 1999). It has also been reported to block sodium currents in isolated guinea-pig ventricular heart cells (Malecot *et al.*, 1998) and a review of 1997 describes "administration of ruthenium red into the cerebrospinal fluid induces intensive convulsive activity" (Velasco & Tapia, 1997).

A ruthenium red derivative, Ru360, initially found to block mitochondrial calcium ion transport *in vivo* (Ying *et al.*, 1991) was tested with TASK-3 and TASK-1 channel currents in the hope of identifying it as a more specific blocker (see section 3.1.5). It had also been reported to block a mitoplast inwardly rectifying calcium current, I_{MiCa}, more potently than ruthenium red (Kirichok *et al.*, 2004). However, TASK-1 channel block was less significant than that seen for ruthenium red (-5.175 ± 0.9%, n = 4) as was the case for TASK-3 channel currents (-13.3%, n = 2). Such small perturbations in whole cell currents of TASK-1 and TASK-3 transfected tsA-201 cells indicated that it would be a poor pharmacological agent to test on a native conductance which could have multiple potassium channel current contributions. In addition to this, the friability of the compound (hygroscopic, light sensitive and unstable in solution (Calbiochem ® Ru360 safety and product information sheets No 557440)) also added to the unsuitability of Ru-360.

4.3 TASK channel current block by lanthanum

In the initial characterisation of the standing outward potassium current of rat cerebellar granule neurones, $I_{K(SO)}$, Watkins and Mathie reported a significant lanthanum ion sensitivity (10μM La^{3+}, -51 ± 11%, n=4, Watkins and Mathie, 1996a). $I_{K(SO)}$ was largely ascribed to TASK-1 channel currents in the rat (Millar *et al.*, 2000a), it was logical to hypothesize that human TASK-1 currents were also likely to be sensitive to extracellularly applied concentrations of the trivalent cation. Human TASK-3 channel responses also remained to be determined. In this study the novel block of both TASK-1 and TASK-3 channel currents have been described. In a similar fashion to zinc, lanthanum block of both channels was concentration dependent and reversible with maximal block in TASK-3 being similar to that in TASK-1. Lanthanum was also tested at pH 8.4 in TASK-1 channels at high concentrations (300μM) and was found to block at pH 8.4.

These findings are of particular interest not only because they show La^{3+} to be a novel blocker of TASK currents, but because the inhibitions are both smaller than that seen with the native conductance. Differences of the cloned human channel data from the rat $I_{K(SO)}$ can be attributed in part to species (a number of two pore domain potassium channels do exhibit significant species variation in terms of sequence and sometimes phenotype; see introduction). It is also reasonable to hypothesize that lanthanum may be acting on other channels that contribute to $I_{K(SO)}$ such as any other potassium channel that may be open (test membrane potential in Watkins and Mathie 1996a

paper was -30mV) (Goldstein *et al.*, 2001), or other expressed two pore domain potassium channels (e.g. TREK-2c (Aller *et al*, 2005)).

4.4 Na replacement inhibited TASK channel currents; choline and NMDG

An interesting property reported for rat TASK channel currents and human TREK-1 channel currents early in their characterisation is the apparent sensitivity of the channel currents to extracellular sodium ions (Leonoudakis *et al.*, 1998; Fink *et al.*, 1996). More recently a sensitivity of $I_{K(SO)}$ to extracellular sodium replacement was reported in primary culture of rat cerebellar granule neurones (Millar *et al.*, 2000). The correlation between the rat TASK (-1) sensitivity and $I_{K(SO)}$ to sodium replacement served, in part, to the attribution of TASK-1 channel currents to be the functional molecular correlate of the native conductance. Human TASK-1 and TASK-3 channel currents were assessed here to examine whether the same sodium sensitivity would manifest across species and be present in the previously untested TASK-3 channel. Sodium substitution was made with *N*- methyl $_D$-glucamine (NMDG) and choline for both channels. Both substitutions elicited a reversible inhibition of channel currents. NMDG substitution of extracellular sodium inhibited both TASK-1 and TASK-3 channel currents at physiological pH. Increasing the whole cell current of TASK-1 transfected cells by raising the extracellular pH to 8.4 aided the stability of the cells and was also found to be reversibly inhibited by application of NMDG. These data are in line with human TREK-1 inhibition by NMDG substitution (-28 ± 2%, Leonoudakis *et al.*, 1998) though smaller than that of $I_{K(SO)}$ (-55 ± 4%, n=7, Millar *et al.*, 2000). Again a species difference may be manifest here. Choline

substitution elicited a larger reversible inhibition, closer to that found in $I_{K(SO)}$ of both TASK-1 and TASK-3 channel currents.

From these data it can be hypothesized that the removal of sodium is key in the TASK current inhibition, rather than a direct effect of NMDG or choline on the channel. Na^+ substitution was not tested on TALK channel TASK-2. ORK1, a *Drosophila melanogaster* two-pore domain potassium channel with four transmembrane regions was found to be insensitive to sodium substitution (Goldstein *et al.*, 1996) but at this time it remains unknown as to whether the remaining two pore domain potassium channels exhibit the same sensitivity as TASK channels shown here.

4.5 Copper block of TASK1, 2 and 3

TASK-3 channel currents were reported to be inhibited by copper ions (93 ± 6%, n = 3 for outside-out patches (Gruss *et al.*, 2004)) which contrasted with TREK-1 potentiation (149 ± 60%, n = 4 for outside-out patches) by the ion. TASK-1 channel current responses to the ion had not, however, been assessed, nor had the underlying mechanism of block of TASK-3 channel currents. Initial characterisation of TASK-3 channel responses corroborated Gruss's data, with a 10μM extracellular application of copper (II) chloride eliciting a potent block of whole cell, while TASK-2 channel currents were insensitive to the ion, even at 10x concentration. The statistical differences in copper block between TASK-1, TASK-3 and TALK channel, TASK-2, in conjunction with the published data for TREK-1 channels revealed that Cu^{2+} was a suitable pharmacological agent to differentiate the currents and potentially could provide a valuable tool for analysis of native background potassium conductances.

4.5.1 Mechanism of copper action does not rely on free radical formation

A review of zinc and copper modulation of neuronal excitability (Mathie *et al.*, 2006) outlined three mechanisms of copper-protein interaction; direct binding of copper to amino acid residues, generation of reactive oxygen species (ROS) and oxidation of cysteine residues. Copper block by generation of reactive oxygen species was assessed by comparing the extent of TASK-3 channel current block by copper in the presence of mannitol, a hydroxyl ion scavenger. No change in the amplitude of copper strongly suggested that copper mediated generation of ROS was not involved in the inhibition of the TASK channel currents.

4.5.2 TASK-3 DTT and DTNB sensitivity; a role for cysteine residues

The role of the cysteine residues was then considered with application of DTT and DTNB, agents known to reduce and oxidise respectively the free thiols of cysteine residues (Krężel *et al.*, 2001; Gozlan & Ben-Ari, 1995).

Whole cell TASK-3 channel currents were found to be insensitive to extracellularly applied DTT (5mM) and the cells poorly tolerant of long exposure to the reagent. To minimize the experimental insult to the transfected cells and prolong their electrophysiological viability, a 'pretreatment' protocol was devised, involving application of DTT for a minimum of 4mins at a constant holding potential of -60mV. This was followed by a brief wash out and initiation of the test voltage protocol (see 3.2.4). This protocol greatly increased the tsA-201 cell survival, and increased cell tolerance of the reagents in combination with the recording step-ramp voltage

protocol. It was also implemented to minimize the chelation of Cu^{2+} by DTT in the bath solution. After DTT application and before applying Cu^{2+}, the bath solution was washed out and replaced to reduce the free DTT in the bath. Cu^{2+}, as well as a number of other heavy metals, such as Zn^{2+}, Cd^{2+}, Ni^{2+} and Pb^{2+}, can all form stable complexes with DTT (Krężel *et al*, 2001). Owing to the large difference in concentration of the DTT relative to Cu^{2+} applied, this co-ordination of the metal ion by DTT remaining in the bath solution must be taken into account.

2mM DTNB potently blocked TASK-3 channel currents. As expected, DTNB block of TASK-3 channel currents could be reversed by application of DTT. DTT was also found to both reverse and prevent 10μM Cu^{2+} block although this was not insurmountable. Test applications of pH 6.4 were applied to ensure that the whole cell current was still sensitive to perturbation. After full wash on and wash off of the pH 6.4 solution or after a prolonged application of 10μM Cu^{2+}, copper sensitivity of the channel was restored.

The reversal of both Cu^{2+} and DTNB block by DTT strongly suggested that they were likely to be acting through similar (if not the same) mechanisms. With comparable inhibition of TASK-3 channel currents with extracellular application, and known interactions with cysteine residues of both reagents (Rigo *et al.*, 2004; Kachur *et al.*, 1999; Cavallini *et al.*, 1969) it was reasonable to hypothesize that extracellular cysteine residues were the site of action for copper.

The different blocks of TASK-3 and TASK-2 channel currents by Cu^{2+} ions suggested that cysteine residues present in TASK-3 and absent in TASK-2 would be key targets

to reduce copper sensitivity of TASK-3. Those absent in TASK-1 but present in TASK-3 could also explain the difference in sensitivities of the two channels. Retained copper sensitivity in a truncated TASK-3 channel, TASK-3-STOP, eliminated the C-terminus as a prime site of action by copper.

Sequential and multiple cysteine substitutions were made of 6 cysteine residues thought to lie on the extracellular surface of the TASK-3 channel; C14, C110, C167, C172, C181 and C193. All mutants produced functional channels. Cysteine substitutions were initially made with alanine and compared to serine mutants. Serine residues share polarity and a comparable molecular weight with cysteine while alanine is much smaller and has an aliphatic, uncharged side chain. Both sets of mutated channels with single or multiple cysteine substitutions retained a copper sensitivity.

2mM DTNB sensitivity in TASK-3 C110A was not significantly different from that found with the WT TASK-3 channel currents, indeed both 2mM DTNB and 10μM copper blocked the multiple cys-ser mutant with all six residues substituted. Returning to the channel sequence alignments (see appendices) the remaining cysteine residues that were not present in TASK-1 or TASK-2 were intracellular, purported to be on the M2M3 loop. But the double mutation still exhibited copper sensitive currents with inhibition by the ion being comparable to the wild type TASK-3.

The same was true for TASK-2 TASK-3 chimeric channel currents also. Replacement of the M1P1 loop of TASK-3 with that of TASK-2 exhibited copper sensitive whole

cell currents. However, both 2mM DTNB current block and 10μM Cu^{2+} block of TASK-2 channel currents were significantly different from that of WT TASK-3.

From these data it is unlikely that the cysteine residues identified and tested in this study underlie the copper block of TASK-3. Indeed when tested on TASK-2 and TASK-1 tsA-201 transfected cells, 2mM DTNB inhibited both whole cell currents. TASK-1 was blocked to a similar extent as TASK-3 while TASK-2 was blocked significantly less .The divergence of DTNB sensitivity from that of copper for these two channels suggests that copper and DTNB are unlikely to act on TASK-2 in the same way. Available literature states that DTNB oxidises free thiols (see 3.2.4) and the only amino acid to contain these is cysteine. The difference in DTNB block of TASK-2 channel currents compared to TASK-1 and TASK-3 suggests that cysteine residues in equivalent positions in all three channels at least partially mediate DTNB inhibition of whole cell currents, and additional cysteines common to both TASK-1 and TASK-3 serve to increase that block.

A preliminary working hypothesis of action for DTNB at the level of the channel may be deduced from its chemical structure Figure 4-1. DTNB oxidises cysteine free thiol groups by the displacement of hydrogen. DTNB is divided into two identical components of 2-nitro-5-thiobenzoic acid, one remaining bound to the cysteine residue while the other remains free in solution Figure 4-1. The addition of the bulky, nucleophilic benzene side chain to cysteine thiol groups may decrease TASK channel current in two ways; mechanically or electrostatically. Physical occlusion of the channel pore or obstruction of K^+ co-ordination residues that mediate the ion transit may occur in conjunction to or as an alternative of disruption local structural

electrostatic interactions bringing about a conformational change. The introduction of the large electron dense, nucleophilic force near the pore region may also retard K^+ ion transit through the channel by acting as an attractive force for the cations at the pore entrance. It may be possible to attribute DTNB block to one mechanism over the

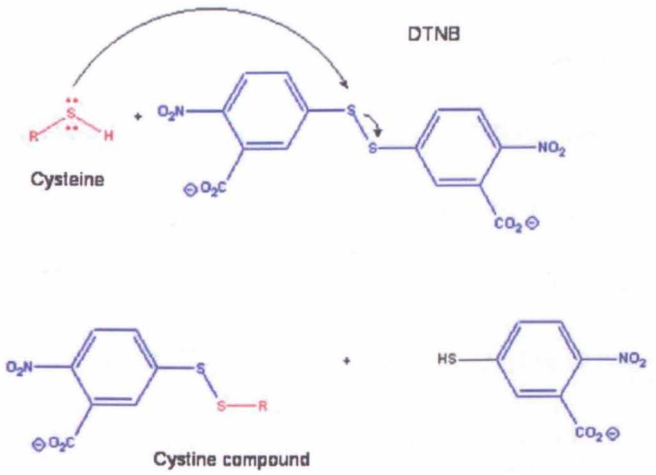

other by assessing the current-voltage dependence of block. I would predict a constant percentage inhibition at all membrane potentials with a mechanically occluded channel while it is possible that a variation in DTNB inhibition may occur with varying membrane potentials. However the nature of the electrostatic interaction is its proximity of effect; a whole cell voltage clamp may not be influenced significantly by local forces.

Figure 4-1 DTNB oxidation of cysteine residues (Adapted from *http://employees.csbsju.edu/hjakubowski/classes/ch331/protstructure/olprotein-aminoacid.html*)

Alternative residues for copper action need to be sought. The reversal of copper block of TASK-3 channel currents by disulphide bond reducing agent DTT certainly provided a compelling argument for the cysteine based mechanism of action for the ion. It is reasonable to hypothesize therefore that copper may be acting more than one way; on cysteine residues other than the ones examined in this study (which may

require Cu^{2+} penetration across the membrane or into the pore regions) and/or it may catalyse the formation of disulphide bonds on other residues.

The only other sulphur containing amino acid is methionine. Interestingly TASK-3 methionine residues may be found close to the cysteine residues tested here which may account for the similar magnitude of DTNB and Cu^{2+} block. Methionines present in TASK-3 but absent in TASK-1 may be found at positions 35, 132, 168 and 226. Methionines at positions 111, 124, 149, 160 and 249 have very close if not matching residues in TASK-1. This would corroborate the theory that while methionines mediate copper sensitivity, the magnitude of the current block is different in the two channels. Further to this, the TALK channel TASK-2 almost completely lacks corresponding methionine residues- fitting the observed lack of copper sensitivity in this channel.

I would therefore hypothesize that a multiple methionine-cysteine substitution mutant of TASK-2 would exhibit currents that could be blocked by Cu^{2+} ions, while a multiple methionine-serine amino acid substitution mutant of TASK-3 channels would abolish copper sensitivity. Further to this, the reduced (TASK-1 like) whole cell current inhibition by copper of the TASK-2 TASK-3 M1P1 chimeric channel suggests that a number of the residues Cu^{2+} ions interacted with are present in the M1P1 loop of TASK-3 but absent, or reduced in number in the M1P1 region of TASK-2.

4.6 pH sensitivity of TASK-3 cys-ser multiple mutant

With increasing numbers of cysteine substitutions of TASK-3, it was observed that whole cell current amplitude decreased steadily from a mean of 1220 ± 76 pA (n=108) for WT TASK-3 to a minimum of 141 ± 25 pA (n=34) with the six cysteine substitution mutant. An increase in pH to 8.4 was tested with the smallest currents and was found to increase whole cell current. Returning to the mutant channels with fewer cysteine substitutions, the TASK-1 like pH 8.4 sensitivity was found to be present in multiple mutants which included replacement of C110S. Comparison of the pH 8.4 sensitivity of single alanine and serine cysteine substitution mutants of residues 110 and 181 identified C110 as the key residue, with whole cell currents of C181 mutants displaying only a small potentiation at pH 8.4.

The decreasing current amplitudes with increasing cysteine substitutions suggest a co-ordinated cysteine rich environment may be required for normal function of the channel. Application of DTT elicited no change in current size implying that the accessible cysteine residues bore no disulphide bonds and at physiological pH 7.4 were in their fully reduced, free thiol state. It could therefore be argued that the cysteine residues removed in this study were either; involved in maintaining structural integrity of the channel with disulphide bridges but located in a position inaccessible by DTT, or cysteine residues interact directly with the pore increasing single channel conductance or P_{open}. It is unlikely, though not irrefutable (from these data), that the cysteine residues have a direct effect on expression levels as C-terminus residues are thought to largely be responsible for this (see above).

pH sensitivity of TASK-1 and TASK-3 channels has been shown to be dependent on a histidine residue in position 98 in a number of studies (Lopes *et al.*, 2001; Rajan *et al.*, 2000). A study in 2003 showed that H98 mutants did retain a pH sensitivity for TASK-1 channels suggesting the residue was not solely responsible for current modulation in response to changing extracellular proton concentrations (Morton *et al.*, 2003). Induction of a TASK-1 like pH 8.4 sensitivity in C110A/S mutants of TASK-3 channels supports this multi-residue hypothesis. Potentiation with pH 8.4 was greater in the multiple mutant than with the single cysteine substitution at position 110 (see above) which supports a contribution of the cysteine residues in determining the TASK-3 pH sensitivity phenotype. This novel potentiation of TASK-3 channel currents suggests that TASK-3 H98 mediates both the inhibitory effect of extracellular acidification as well as the potentiation in response to extracellular alkalinisation functioning in the same way as in TASK-1. I hypothesize that in the wild type TASK-3 channel the histidine residue is shielded by all or some of the cysteine residues tested here, with C110 playing a key role. Their removal reveals the underlying TASK-1 like pH 8.4 sensitivity.

4.7 Copper sensitivity of native conductance IK_{SO}

In the final results chapter of this study, copper block was assessed in the murine cerebellar granule neurone in primary culture. A standing outward potassium current, $I_{K(SO)}$, had been characterised and attributed to TASK channels through shared pharmacological and biophysical phenotypes (Millar *et al.*, 2000; Watkins & Mathie, 1996) with *in situ* hybridisation studies confirming the presence of TASK-1 and TASK-3 in the granule cells of the cerebellum (Rusznak *et al.*, 2004; Karschin *et al.*,

2001; Bayliss *et al.*, 2001) thereafter. With the generation of a TASK-1 knockout mouse for a collaborative study (Aller *et al.*, 2005), murine $I_{K(SO)}$ came under investigation. Cerebellar granule cells (CGNs) exhibited mean reversal potentials (-66.9 ± 9.5mV, n = 6) close to that of their counterparts *in vivo* (-64 ± 1mV, n = 75, Chadderton *et al.*, 2004). There was also an increase in current size with increasing days in culture. Zinc and pH sensitivity of murine $I_{K(SO)}$ was also examined and found to be present; Zinc (100μM) and pH 6.4 blocked chanel currents while pH 8.4 increased $I_{K(SO)}$ size.

CGN $I_{K(SO)}$ sensitivity to 10μM Cu^{2+} and 2mM DTNB was also tested. Although the cells were poorly tolerant of the thiol oxidising agent, DTNB, an $I_{K(SO)}$ inhibition was found. $I_{K(SO)}$ also proved sensitive to Cu^{2+} with a TASK-1 like block of the native current. In conjunction with this block however, some cells exhibited a potentiation of $I_{K(SO)}$ in response to copper.

Pharmacological profiling of the native conductance of murine cerebellar granule cells as completed here shows some deviation from the cloned human TASK channel data generated in this study as well as reported elsewhere. This cannot only be attributed to species differences, profiling of cloned murine TASK channels showed that they did not display properties different from their human counterparts (Aller *et al.*, 2005). The current voltage relation of the channel was close to that reported *in vivo* (-64 ± 1mV, n = 75, Chadderton *et al.*, 2004) and differences in reversal potential from primary culture of rat CGNs (-90 ± 4mV, Millar *et al.*, 2000) can be accounted for by differences in species and age at culture.

In situ hybridization and other localisation work has, as previously mentioned, identified the presence of TASK-1 and TASK-3 mRNA in cerebellar granule neuones (see above). In addition to these channels, TREK-2c has also been localised to these cells (Aller *et al.*, 2005; Medhurst *et al.*, 2001; Talley *et al.*, 2001). It has been hypothesized that $I_{K(SO)}$ is made up of currents from heterodimeric channels with subunits of all or some of two pore domain potassium channel subunits expressed (Aller *et al.*, 2005; Berg *et al.*, 2004). Indeed, the availability of different subtypes would confer additional regulatory control of excitability.

The $I_{K(SO)}$ potentiation and inhibition by extracellular pH changes observed in the cultured CGNs are suggestive of TASK-1 channels over TASK-3. However, the extent of the potentiation and inhibition is much reduced from the cloned human channel sensitivities here (see above). They are also different from cloned murine TASK-1 and TASK-3 channels sensitivities (Aller *et al.*, 2005) which closely match the cloned human data. This can be explained in two ways; the presence of heterodimeric TASK-1 TASK-3 channels with intermediate properties or the contribution of a mixed population of homodimeric TASK-1, TASK-3 or TREK-2 channels. In actuality some combination of both hypotheses may be true. The reduced DTNB sensitivity was more TASK-2 like than TASK-1 or TASK-3 but the presence of TASK-2 channels in cerebellar granule cells is a matter of current debate with a TASK-2 like conductance being proposed (Cotten *et al.*, 2004; Han *et al.*, 2002) but other groups reporting a lack of TASK-2 expression in these cells (Aller *et al.*, 2005; Talley *et al.*, 2001; Medhurst *et al.*, 2001). Furthermore, a native conductance may well have some small contribution from other potassium channels partially or sporadically open at the voltages used which may be differently sensitive to DTNB

and contribute to the whole cell current. Interestingly, the DTNB sensitivity of TREK-2 channels has only very recently been identified and an unquantified inhibition by DTNB specific to TREK-2 over TREK-1 has been tentatively reported (Kim *et al.*, 2007). Further assessment of DTNB block of TREK-2 and TASK-1 TASK-3 heterodimers may help unravel the channels underlying the DTNB sensitive component of $I_{K(SO)}$ in murine cerebellar granule cells.

Testing Cu^{2+} sensitivity of $I_{K(SO)}$ has yielded the most surprising result with both a potentiation and an inhibition being recorded for the cultured cerebellar granule neurones. A correlation between the occurrences of both responses was sought with days in culture or age at culture but none could be identified at this stage (n=7). Additional experiments in this area may provide further evidence for the regulation of two-pore domain channel availability during CGN development. The inhibition of $I_{K(SO)}$ by copper was more TASK-1 channel like than TASK-3, while the potentiation was very similar to that reported for TREK-1 channels (83 ± 11%, Gruss *et al.*, 2004). TREK-1 and TREK-2 channels share a number biophysical and pharmacological properties (Lotshaw, 2007) and a Cu^{2+} sensitivity of TREK-2 channel currents (potentiated) has been reported (unquantified, (Kim *et al.*, 2005)) so it is reasonable to hypothesize that TREK-2 channels may underlie the potentiation of $I_{K(SO)}$ seen here. Indeed, TREK-2 channels are also activated by extracellular Zn^{2+} (Czirjak & Enyedi, 2006; Kim *et al.*, 2005) which may account for the difference between zinc sensitivity of the homodimeric channels studied here in tsA-201 cells and the $I_{K(SO)}$ Zn^{2+} sensitivity; a TASK-1 or TASK-3 like block could be masked by a TREK-2 like potentiation of the potassium background conductance.

From this data it is clear that there remains some questions about the two-pore domain channels underlying $I_{K(SO)}$ in murine cerebellar granule neurones. My data strongly suggest a contribution from TREK-2 channel currents and quantification of TREK-2 DTNB and copper sensitivity is needed for comparison. TASK-1 TASK-3 heterodimer sensitivities would similarly be useful.

The heterogeneity in Cu^{2+} response also requires further investigation. No correlation could be determined here between mouse pup age and days in culture. Assuming this was representative, this would reveal a non-time-dependent regulation of two-pore domain potassium channel expression that occurs before P6-7 (the median age at culture) that leaves a 'stamp' on a cell that restricts its expression patterns (e.g. a TREK-2c dominant expression phenotype). Locality plays an important role in embryological development (Larsen,1998) and a brain slice study of pharmacological heterogeneity of γ-aminobutyric acid (GABA) receptors has suggested distinct classes of rat cerebellar granule neurones exist *in vivo* (Hevers & Luddens, 2002). It would not be unreasonable therefore to propose such a mechanism exists for two-pore domain potassium channels, especially considered the proposed compensation mechanisms between the $GABA_A$ and two pore domain potassium channels proposed by Brickley *et al* (2001).

The physiological implications of Cu^{2+} and DTNB block are significant both on the macroscopic and microscopic scale. DTNB-like oxidation-induced inhibition of TASK channel mediated background conductances such as $I_{K(SO)}$ would increase the cell excitability as the resting membrane potential would move toward the threshold for action potential firing. The most common endogenous free thiol is in the form of

glutathione which plays a central role in cellular defence against oxidative damage (Biswas *et al.*, 2006). The addition of glutathione to a cysteine thiol via creation of a disulphide bond (S-glutathiolation) was demonstrated by Dominici and colleagues to occur in response to oxidative stress in lymphoma cells (Biswas *et al.*, 2006). Glutathione therefore may provide a functional endogenous correlate of DTNB.

An increased excitability of cerebellar granule neurones would have a number of outcomes. Increased action potential firing would statistically increase the probability of concurrent activation of Purkinje cells by CGN parallel fibres and climbing fibres. This could potentiate LTD of Purkinje cells (see introduction) and therefore influence (motor) learning. It is interesting to reflect upon the selective resistance to LTD that ascending portions of the cerebellar granule axon have been reported to exhibit (Sims & Hartell, 2005). Cu^{2+} has been found to be released from putative vesicular storage after neuronal depolarisation (for review see (Mathie *et al.*, 2006)). Greater transmitter release at a higher frequency (see introduction) could be mediated by a Cu^{2+} induced increase in CGN excitability.

Granule cell responses (repetitive firing, spike bursting, oscillations, resonance (see introduction)) may be influenced by varying the available two pore domain potassium channel conductances that contribute to $I_{K(SO)}$. Differential block of TASK and TREK channel by the same ion may reversibly alter $I_{K(SO)}$ amplitude and therefore modulate firing patterns.

In this study I have identified novel pharmacological sensitivities of TASK-1, TASK-3 and TASK-2 channels and assessed the effects of DTNB and copper on the native

background potassium conductance of cerebellar granule neurones, $I_{K(SO)}$. This study contributes to the available pharmacological toolkit used to differentiate two pore domain potassium channel conductances and has identified potential mechanisms of action of copper on TASK-3 as well as a number of putative physiological effects of such modulation of background potassium currents.

5 Appendices

Sequences of TASK channels TASK-1 and TASK-3 and TALK channel, TASK-2, were aligned using Blosum 62 Similarity matrix.

I. TASK-1, TASK-3 sequence alignments

```
TASK-3  MKRQNVRTLS LIVCTFTYLL VGAAVFDALE SDHEMREEEK LKAEEIRIKG KYNISSEDYR QLELVILQSE
TASK-1  .........A .......... .......... .EP.LI.RQR .ELRQQELRA R..L.QGG.E E..R.V.RLK

TASK-3  PHRAGVQWKF AGSFYFAITV ITTIGYGHAA PGTDAGKAFC MFYAVLGIPL TLVMFQSLGE RMNTFVRYLL
TASK-1  ..K.....R. .......... .......... .S..G..V.. ....L..... .......... .I..L.....

TASK-3  KRIKKCCGMR NTDVSMENMV TVGFFSCMGT LCIGAAAFSQ CEEWSFFHAY YYCFITLTTI GFGDYVALQT
TASK-1  H.A..GL... RA....A... LI.....IS. .........H Y.H.T..Q.. .......... .........K

TASK-3  KGALQKKPLY VAFSFMYILV GLTVIGAFLN LVVLRFLTMN SEDERRDAEE RASL-----A ----GNRNSM
TASK-1  DQ...TQ.Q. .....V...T .......... ......M... A...K....H ..L.TRNGQ. GGGG.GGSAH

TASK-3  VIHIPEEPRP S-----RPRY KADVPDLQSV CSCTCYRSQD ---YGGRSVA PQNSFSAKLA PHYFHSISYK
TASK-1  TTDTASSTAA AGGGGF.NV. -.E.LHF..M ...LW.K.RE KLQ.SIPMII .RDLSTSDTC VEQS..SPGG

TASK-3  IEEISPSTLK NSLF---P-S PISSISPGLH SFTDHQRLMK RRKSV
TASK-1  GGRY.DTPSR RC.CSGA.R. A...V.T... .LSTFRG... ..S..
```

II. TASK-3, TASK-2 sequence alignments

```
TASK-3  MKRQNVRTLS LIVCTFTYLL VGAAVFDALE SDHEMREEEK LKAEEIRIKG KYN-ISSEDY RQLELVILQS
TASK2   .VDRGPLLT. A.I--.-..A I...I.EV.. EP.WKEAKKN YYTQKLHLLK EFPCLGQ.GL DKILE.VSDA

TASK-3  EPHRAGV--- ----QWKFAG SFYFAITVIT TIGYGHAAPG TDAGKAFCMF YAVLGIPLTL VMFQSLGERM
TASK2   AGQGVAITGN QTFNN.NWPN AMI..A.... .....NV..K .P..RL..V. .GLF.V..C. TWISA..-K-

TASK-3  NTFVRYLLKR IKKCCGMRNT DVSMENMVTV GFFSCMGTLC ---IGAAAFS QCEEWSFFHA YYYCFITLTT
TASK2   --.FGGRA.. LGQFLTK.GV SLRKAQITCT VI.IVW.V.V HLV.PPFV.M VT.G.NYIEG L..S...IS.

TASK-3  IGFGDYVALQ TKGALQKKPL YVAFSFMYIL VGLTVIGAFL NLVVLRFLTM N--------- -------SED
TASK2   .....F..GV NPS.-NYHA. .RY.VELW.Y L..AWLSL.V .WK.SM.VEV HKAIKKRRRR RKESFES.PH

TASK-3  ERR------- D-AEE-RA-S -LAGN--R-N SMVIHI---- ---------- ------PEE- --PR--PSR-
TASK2   S.KALQVKGS TASKDVNIF. F.SKKEETY. DLIKQ.GKKA MKTSGGGETG PGPGLG.QGG GL.ALP..LV

TASK-3  PR--Y-KADV PDLQSVCSCT CYRSQDYGGR S---------V ------APQ- --NS---FSA KL----AP--
TASK2   .LVV.S.NR. .T.EE.-.Q. L-..KGHVS. .PDEEAVARA PEDSSP..EV FM.QLDRI.E ECEPWD.QDY

TASK-3  HY--FH--SI SY-------K IEEISPSTLK NSL------- ---------- ---FPSPISS ISPGLHS--F
TASK2   .PLI.QDA.. TFVNTEAGLS D..T.K.S.E DN.AGEESPQ QGAEAKAPLN MGE...SSE. TFTSTE.ELS

TASK-3  TDHQRLM--- -KR-R-KSV
TASK2   VPYEQ..NEY N.ANSP.GT
```

III. T-tests with Bonferroni corrections for type 1, multiple comparison errors

5.1.1 Comparison of Cu^{2+} block of TASK-1, TASK-2, TASK-3 and chimeric TASK-2/TASK-3 channel currents

Cu^{2+} block of currents of TASK-1, TASK-2, TASK-3 and TASK-2/TASK-3 chimera transfected cells were each compared with each other. Statistical software SPSS (version 16) was used to test a null hypothesis of no difference between Cu^{2+} block of all channel currents. The findings are tabulated below. Copper block was found to be statistically different between all wild-type channel currents (*Mean difference I-J). The Cu^{2+} block of TASK-1 channel currents was, however, statistically comparable to Cu^{2+} TASK-2/TASK-3 chimera channel currents.

(I) V1	(J) V1	Mean Difference (I-J)	Std. Error	Sig.	95% Confidence Interval	
					Lower Bound	Upper Bound
TASK-1	TASK-2	-38.902*	7.385	.000	-59.16	-18.65
	TASK-3	37.195*	5.607	.000	21.82	52.57
	TASK-2/3	12.735	7.385	.543	-7.52	32.99
TASK-2	TASK-1	38.902*	7.385	.000	18.65	59.16
	TASK-3	76.097*	5.922	.000	59.85	92.34
	TASK-2/3	51.637*	7.627	.000	30.72	72.56
TASK-3	TASK-1	-37.195*	5.607	.000	-52.57	-21.82
	TASK-2	-76.097*	5.922	.000	-92.34	-59.85
	TASK-2/3	-24.459*	5.922	.001	-40.70	-8.21
TASK-2/3	TASK-1	-12.735	7.385	.543	-32.99	7.52
	TASK-2	-51.637*	7.627	.000	-72.56	-30.72
	TASK-3	24.459*	5.922	.001	8.21	40.70

*. The mean difference is significant at the 0.05 level.

5.1.2 Comparison of Cu^{2+} block of TASK-3 and TASK-3 cysteine mutant channel currents

To assess the statistical significance of variations of Cu^{2+} block of WT TASK-3 channels and its substitution mutants, a one-way ANOVA test was performed. The test rejected the null hypothesis of mean current block by 10uM Cu^{2+} being the same for wild-type TASK-3 and its single and multiple mutants. The F statistic (2.6) was higher than the expected value for p = 0.05 (2.0). This value is the ratio of variance between group means and variance within the groups (see below).

TASK-3 and TASK-3 cys substitution channel currents Cu^{2+} block- ANOVA analysis

	Sum of Squares	df	Mean Square	F	Sig.
Between Groups	6435.941	9	715.105	2.619	.011
Within Groups	21023.157	77	273.028		
Total	27459.097	86			

To determine where the significant difference between Cu^{2+} current block occurred in the TASK-3 mutant channel population, Independent pair-wise t tests with Bonferroni correction (to compensate for multiple comparison (type 1) errors) was performed. There was no significance difference found between wild type and any of the mutant TASK-3 channels. However, a significant difference was found (p=0.024) between Cu^{2+} block of TASK-3 C110S and C14S C167S C172S channel currents hence the rejection of the null hypothesis in the ANOVA. Data are below.

TASK-3 cysteine mutant channel current block by Cu^{2+} - Multiple Comparisons – t test with Bonferroni corrections.

(I) V1	(J) V1	Mean Difference (I-J)	Std. Error	Sig.	95% Confidence Interval	
					Lower Bound	Upper Bound

TASK-3	TASK-3 STOP	-3.702	7.914	1.000	-30.52	23.11
	TASK-3 C181A	-10.538	6.194	1.000	-31.53	10.45
	TASK-3 C110A	2.089	6.858	1.000	-21.15	25.33
	TASK-3 C181S	-13.707	8.734	1.000	-43.30	15.89
	TASK-3 C110S	-22.637	6.858	.066	-45.87	.60
	TASK-3 C146,147S	-16.316	9.952	1.000	-50.04	17.40
	TASK-3 C110,181,193A	1.901	7.317	1.000	-22.89	26.69
	TASK-3 C14,167,172S	10.634	7.317	1.000	-14.16	35.43
	TASK-3 6 cys	-13.066	7.317	1.000	-37.86	11.73
TASK-3 STOP	TASK-3	3.702	7.914	1.000	-23.11	30.52
	TASK-3 C181A	-6.836	9.216	1.000	-38.06	24.39
	TASK-3 C110A	5.791	9.675	1.000	-26.99	38.57
	TASK-3 C181S	-10.005	11.084	1.000	-47.56	27.55
	TASK-3 C110S	-18.934	9.675	1.000	-51.72	13.85
	TASK-3 C146,147S	-12.613	12.067	1.000	-53.50	28.27
	TASK-3 C110,181,193A	5.603	10.006	1.000	-28.30	39.50
	TASK-3 C14,167,172S	14.337	10.006	1.000	-19.56	48.24
	TASK-3 6 cys	-9.363	10.006	1.000	-43.26	24.54
TASK-3 C181A	TASK-3	10.538	6.194	1.000	-10.45	31.53
	TASK-3 STOP	6.836	9.216	1.000	-24.39	38.06
	TASK-3 C110A	12.627	8.327	1.000	-15.59	40.84
	TASK-3 C181S	-3.169	9.929	1.000	-36.81	30.47
	TASK-3 C110S	-12.099	8.327	1.000	-40.31	16.12
	TASK-3 C146,147S	-5.778	11.016	1.000	-43.10	31.55
	TASK-3 C110,181,193A	12.439	8.709	1.000	-17.07	41.95
	TASK-3 C14,167,172S	21.172	8.709	.782	-8.34	50.68
	TASK-3 6 cys	-2.528	8.709	1.000	-32.04	26.98
TASK-3 C110A	TASK-3	-2.089	6.858	1.000	-25.33	21.15
	TASK-3 STOP	-5.791	9.675	1.000	-38.57	26.99
	TASK-3 C181A	-12.627	8.327	1.000	-40.84	15.59
	TASK-3 C181S	-15.796	10.357	1.000	-50.89	19.29
	TASK-3 C110S	-24.726	8.832	.291	-54.65	5.20
	TASK-3 C146,147S	-18.405	11.402	1.000	-57.04	20.23
	TASK-3 C110,181,193A	-.188	9.193	1.000	-31.34	30.96

	TASK-3 C14,167,172S	8.545	9.193	1.000	-22.60	39.69
	TASK-3 6 cys	-15.155	9.193	1.000	-46.30	15.99
TASK-3 C181S	TASK-3	13.707	8.734	1.000	-15.89	43.30
	TASK-3 STOP	10.005	11.084	1.000	-27.55	47.56
	TASK-3 C181A	3.169	9.929	1.000	-30.47	36.81
	TASK-3 C110A	15.796	10.357	1.000	-19.29	50.89
	TASK-3 C110S	-8.929	10.357	1.000	-44.02	26.16
	TASK-3 C146,147S	-2.608	12.620	1.000	-45.37	40.15
	TASK-3 C110,181,193A	15.608	10.666	1.000	-20.53	51.75
	TASK-3 C14,167,172S	24.342	10.666	1.000	-11.80	60.48
	TASK-3 6 cys	.642	10.666	1.000	-35.50	36.78
TASK-3 C110S	TASK-3	22.637	6.858	.066	-.60	45.87
	TASK-3 STOP	18.934	9.675	1.000	-13.85	51.72
	TASK-3 C181A	12.099	8.327	1.000	-16.12	40.31
	TASK-3 C110A	24.726	8.832	.291	-5.20	54.65
	TASK-3 C181S	8.929	10.357	1.000	-26.16	44.02
	TASK-3 C146,147S	6.321	11.402	1.000	-32.31	44.96
	8	24.538	9.193	.417	-6.61	55.69
	TASK-3 C14,167,172S	33.271*	9.193	.024	2.12	64.42
	TASK-3 6 cys	9.571	9.193	1.000	-21.58	40.72
TASK-3 C146,147S	TASK-3	16.316	9.952	1.000	-17.40	50.04
	TASK-3 STOP	12.613	12.067	1.000	-28.27	53.50
	TASK-3 C181A	5.778	11.016	1.000	-31.55	43.10
	TASK-3 C110A	18.405	11.402	1.000	-20.23	57.04
	TASK-3 C181S	2.608	12.620	1.000	-40.15	45.37
	TASK-3 C110S	-6.321	11.402	1.000	-44.96	32.31
	TASK-3 C110,181,193A	18.217	11.684	1.000	-21.37	57.80
	TASK-3 C14,167,172S	26.950	11.684	1.000	-12.64	66.54
	TASK-3 6 cys	3.250	11.684	1.000	-36.34	42.84
TASK-3 C110,181,193A	TASK-3	-1.901	7.317	1.000	-26.69	22.89
	TASK-3 STOP	-5.603	10.006	1.000	-39.50	28.30
	TASK-3 C181A	-12.439	8.709	1.000	-41.95	17.07
	TASK-3 C110A	.188	9.193	1.000	-30.96	31.34
	TASK-3 C181S	-15.608	10.666	1.000	-51.75	20.53

	TASK-3 C110S	-24.538	9.193	.417	-55.69	6.61
	TASK-3 C146,147S	-18.217	11.684	1.000	-57.80	21.37
	TASK-3 C14,167,172S	8.733	9.540	1.000	-23.59	41.06
	TASK-3 6 cys	-14.967	9.540	1.000	-47.29	17.36
TASK-3 C14,167,172S	TASK-3	-10.634	7.317	1.000	-35.43	14.16
	TASK-3 STOP	-14.337	10.006	1.000	-48.24	19.56
	TASK-3 C181A	-21.172	8.709	.782	-50.68	8.34
	TASK-3 C110A	-8.545	9.193	1.000	-39.69	22.60
	TASK-3 C181S	-24.342	10.666	1.000	-60.48	11.80
	TASK-3 C110S	-33.271*	9.193	.024	-64.42	-2.12
	TASK-3 C146,147S	-26.950	11.684	1.000	-66.54	12.64
	TASK-3 C110,181,193A	-8.733	9.540	1.000	-41.06	23.59
	TASK-3 6 cys	-23.700	9.540	.682	-56.02	8.62
TASK-3 6 cys	TASK-3	13.066	7.317	1.000	-11.73	37.86
	TASK-3 STOP	9.363	10.006	1.000	-24.54	43.26
	TASK-3 C181A	2.528	8.709	1.000	-26.98	32.04
	TASK-3 C110A	15.155	9.193	1.000	-15.99	46.30
	TASK-3 C181S	-.642	10.666	1.000	-36.78	35.50
	TASK-3 C110S	-9.571	9.193	1.000	-40.72	21.58
	TASK-3 C146,147S	-3.250	11.684	1.000	-42.84	36.34
	TASK-3 C110,181,193A	14.967	9.540	1.000	-17.36	47.29
	TASK-3 C14,167,172S	23.700	9.540	.682	-8.62	56.02

*. The mean difference is significant at the 0.05 level.

5.1.3 Comparison of 2mM DTNB block of TASK-3 and TASK-3 cysteine mutant channel currents

The same pairwise t-test with Bonferroni was used to seek out significant differences between channel current block by 2mM DTNB. TASK-3 and TASK-2 channel currents were blocked to significantly different amounts. There was also a significant

difference between the DTNB block of TASK-3 C110A and TASK-2 channel currents.

Multiple Comparisons

(I) V1	(J) V1	Mean Difference (I-J)	Std. Error	Sig.	95% Confidence Interval	
					Lower Bound	Upper Bound
TASK-3	TASK-2	-47.9286*	13.4322	.029	-92.667	-3.191
	TASK-2/3	-35.0536	12.2004	.141	-75.689	5.582
	TASK-3 C181A	-7.0036	12.2004	1.000	-47.639	33.632
	TASK-3 C110A	7.9214	12.2004	1.000	-32.714	48.557
	6 CYS	-10.0786	12.2004	1.000	-50.714	30.557
TASK-2	TASK-3	47.9286*	13.4322	.029	3.191	92.667
	TASK-2/3	12.8750	14.8668	1.000	-36.641	62.391
	TASK-3 C181A	40.9250	14.8668	.184	-8.591	90.441
	TASK-3 C110A	55.8500*	14.8668	.019	6.334	105.366
	6 CYS	37.8500	14.8668	.289	-11.666	87.366
TASK-2/3	TASK-3	35.0536	12.2004	.141	-5.582	75.689
	TASK-2	-12.8750	14.8668	1.000	-62.391	36.641
	TASK-3 C181A	28.0500	13.7639	.825	-17.793	73.893
	TASK-3 C110A	42.9750	13.7639	.080	-2.868	88.818
	6 CYS	24.9750	13.7639	1.000	-20.868	70.818
TASK-3 C181A	TASK-3	7.0036	12.2004	1.000	-33.632	47.639
	TASK-2	-40.9250	14.8668	.184	-90.441	8.591
	TASK-2/3	-28.0500	13.7639	.825	-73.893	17.793
	TASK-3 C110A	14.9250	13.7639	1.000	-30.918	60.768
	6 CYS	-3.0750	13.7639	1.000	-48.918	42.768
TASK-3 C110A	TASK-3	-7.9214	12.2004	1.000	-48.557	32.714
	TASK-2	-55.8500*	14.8668	.019	-105.366	-6.334

	TASK-2/3	-42.9750	13.7639	.080	-88.818	2.868
	TASK-3 C181A	-14.9250	13.7639	1.000	-60.768	30.918
	6 CYS	-18.0000	13.7639	1.000	-63.843	27.843
6 CYS	TASK-3	10.0786	12.2004	1.000	-30.557	50.714
	TASK-2	-37.8500	14.8668	.289	-87.366	11.666
	TASK-2/3	-24.9750	13.7639	1.000	-70.818	20.868
	TASK-3 C181A	3.0750	13.7639	1.000	-42.768	48.918
	TASK-3 C110A	18.0000	13.7639	1.000	-27.843	63.843

*. The mean difference is significant at the 0.05 level.

5.1.4 Comparison of whole cell current amplitudes of TASK-3 and TASK-3 cysteine mutant channel currents

WT TASK-3 whole cell current amplitude was found to be significantly higher than TASK-1, TASK-3 C110S, TASK-3 C146S C147S, the six cysteine-serine TASK-3 mutant, and the eight cysteine-serine TASK-3 mutant (see 3.3.4).

Multiple Comparisons of WT and TASK-3 mutant channel whole cell currents

(I) V1	(J) V1	Mean Difference (I-J)	Std. Error	Sig.	95% Confidence Interval	
					Lower Bound	Upper Bound
TASK-3	TASK-2	460.911	145.282	.077	-18.41	940.23
	TASK-1	1001.882*	113.505	.000	627.40	1376.36
	TASK-3 STOP	128.734	261.045	1.000	-732.52	989.99
	TASK-3 C181A	426.344	152.867	.256	-78.00	930.69
	TASK-3 C181S	620.294	188.627	.052	-2.03	1242.62
	TASK-3 C110S	563.032*	128.778	.001	138.16	987.91
	TASK-3 C146, 147S	860.023*	222.568	.006	125.72	1594.33

	6 cys	1097.667*	112.219	.000	727.43	1467.91
	8 CYS	1118.344*	290.563	.007	159.70	2076.99
TASK-2	TASK-3	-460.911	145.282	.077	-940.23	18.41
	TASK-1	540.971	167.211	.062	-10.70	1092.64
	TASK-3 STOP	-332.177	288.480	1.000	-1283.95	619.60
	TASK-3 C181A	-34.567	196.073	1.000	-681.46	612.33
	TASK-3 C181S	159.383	225.069	1.000	-583.18	901.95
	TASK-3 C110S	102.121	177.933	1.000	-484.93	689.17
	TASK-3 C146, 147S	399.112	254.190	1.000	-439.53	1237.75
	6 cys	636.756*	166.341	.007	87.95	1185.56
	8 CYS	657.433	315.442	1.000	-383.29	1698.16
TASK-1	TASK-3	-1001.882*	113.505	.000	-1376.36	-627.40
	TASK-2	-540.971	167.211	.062	-1092.64	10.70
	TASK-3 STOP	-873.148	273.857	.073	-1776.67	30.38
	TASK-3 C181A	-575.538*	173.842	.048	-1149.09	-1.99
	TASK-3 C181S	-381.588	205.992	1.000	-1061.21	298.03
	TASK-3 C110S	-438.850	153.091	.203	-943.94	66.24
	TASK-3 C146, 147S	-141.859	237.464	1.000	-925.31	641.60
	6 cys	95.785	139.449	1.000	-364.29	555.86
	8 CYS	116.462	302.126	1.000	-880.33	1113.25
TASK-3 STOP	TASK-3	-128.734	261.045	1.000	-989.99	732.52
	TASK-2	332.177	288.480	1.000	-619.60	1283.95
	TASK-1	873.148	273.857	.073	-30.38	1776.67
	TASK-3 C181A	297.610	292.374	1.000	-667.01	1262.23
	TASK-3 C181S	491.560	312.561	1.000	-539.66	1522.78
	TASK-3 C110S	434.298	280.532	1.000	-491.25	1359.84
	TASK-3 C146, 147S	731.289	334.141	1.000	-371.13	1833.71
	6 cys	968.933*	273.326	.021	67.16	1870.71
	8 CYS	989.610	382.807	.464	-273.37	2252.59
TASK-3 C181A	TASK-3	-426.344	152.867	.256	-930.69	78.00
	TASK-2	34.567	196.073	1.000	-612.33	681.46
	TASK-1	575.538*	173.842	.048	1.99	1149.09
	TASK-3 STOP	-297.610	292.374	1.000	-1262.23	667.01
	TASK-3 C181S	193.950	230.038	1.000	-565.01	952.91

	TASK-3 C110S	136.688	184.178	1.000	-470.96	744.34
	TASK-3 C146, 147S	433.679	258.600	1.000	-419.51	1286.87
	6 cys	671.323*	173.005	.006	100.53	1242.11
	8 CYS	692.000	319.006	1.000	-360.48	1744.48
TASK-3 C181S	TASK-3	-620.294	188.627	.052	-1242.62	2.03
	TASK-2	-159.383	225.069	1.000	-901.95	583.18
	TASK-2	381.588	205.992	1.000	-298.03	1061.21
	TASK-3 STOP	-491.560	312.561	1.000	-1522.78	539.66
	TASK-3 C181A	-193.950	230.038	1.000	-952.91	565.01
	TASK-3 C110S	-57.263	214.787	1.000	-765.90	651.37
	TASK-3 C146, 147S	239.729	281.222	1.000	-688.10	1167.55
	6 CYS	477.373	205.287	.938	-199.92	1154.67
	8 CYS	498.050	337.604	1.000	-615.79	1611.89
TASK-3 C110S	TASK-3	-563.032*	128.778	.001	-987.91	-138.16
	TASK-2	-102.121	177.933	1.000	-689.17	484.93
	TASK-1	438.850	153.091	.203	-66.24	943.94
	TASK-3 STOP	-434.298	280.532	1.000	-1359.84	491.25
	TASK-3 C181A	-136.688	184.178	1.000	-744.34	470.96
	TASK-3 C181S	57.263	214.787	1.000	-651.37	765.90
	TASK-3 C146, 147S	296.991	245.132	1.000	-511.76	1105.74
	6 CYS	534.635*	152.140	.024	32.69	1036.58
	8 CYS	555.312	308.189	1.000	-461.48	1572.11
TASK-3 C146, 147S	TASK-3	-860.023*	222.568	.006	-1594.33	-125.72
	TASK-2	-399.112	254.190	1.000	-1237.75	439.53
	TASK-1	141.859	237.464	1.000	-641.60	925.31
	TASK-3 STOP	-731.289	334.141	1.000	-1833.71	371.13
	TASK-3 C181A	-433.679	258.600	1.000	-1286.87	419.51
	TASK-3 C181S	-239.729	281.222	1.000	-1167.55	688.10
	TASK-3 C110S	-296.991	245.132	1.000	-1105.74	511.76
	6 CYS	237.644	236.852	1.000	-543.79	1019.08
	8 CYS	258.321	357.677	1.000	-921.75	1438.39
6 CYS	TASK-3	-1097.667*	112.219	.000	-1467.91	-727.43
	TASK-2	-636.756*	166.341	.007	-1185.56	-87.95
	TASK-1	-95.785	139.449	1.000	-555.86	364.29

	TASK-3 STOP	-968.933*	273.326	.021	-1870.71	-67.16
	TASK-3 C181A	-671.323*	173.005	.006	-1242.11	-100.53
	TASK-3 C181S	-477.373	205.287	.938	-1154.67	199.92
	TASK-3 C110S	-534.635*	152.140	.024	-1036.58	-32.69
	TASK-3 C146, 147S	-237.644	236.852	1.000	-1019.08	543.79
	8 CYS	20.677	301.645	1.000	-974.53	1015.88
8 CYS	TASK-3	-1118.344*	290.563	.007	-2076.99	-159.70
	TASK-2	-657.433	315.442	1.000	-1698.16	383.29
	TASK-1	-116.462	302.126	1.000	-1113.25	880.33
	TASK-3 STOP	-989.610	382.807	.464	-2252.59	273.37
	TASK-3 C181A	-692.000	319.006	1.000	-1744.48	360.48
	TASK-3 C181S	-498.050	337.604	1.000	-1611.89	615.79
	TASK-3 C110S	-555.312	308.189	1.000	-1572.11	461.48
	TASK-3 C146, 147S	-258.321	357.677	1.000	-1438.39	921.75
	6 CYS	-20.677	301.645	1.000	-1015.88	974.53

*. The mean difference is significant at the 0.05 level.

6 References

Aidley D J, (1998) *The Physiology of Excitable Cells.* 4th Edition. Cambridge University Press

Albus JS. A theory of cerebellar function. *Mathematical Biosciences* **10**, 25-61. 1971.

Aller MI, Veale EL, Linden AM, Sandu C, Schwaninger M, Evans LJ, Korpi ER, Mathie A, Wisden W, & Brickley SG (2005). Modifying the subunit composition of TASK channels alters the modulation of a leak conductance in cerebellar granule neurons. *J Neurosci* **25**, 11455-11467.

Andrey F, Tsintsadze T, Volkova T, Lozovaya N, & Krishtal O (2005). Acid sensing ionic channels: modulation by redox reagents. *Biochim Biophys Acta* **1745**, 1-6.

Arrighi I, Lesage F, Scimeca JC, Carle GF, & Barhanin J (1998). Structure, chromosome localization, and tissue distribution of the mouse twik K+ channel gene. *FEBS Lett* **425**, 310-316.

Ashmole I, Goodwin PA, & Stanfield PR (2001). TASK-5, a novel member of the tandem pore K+ channel family. *Pflugers Arch* **442**, 828-833.

Assaf SY & Chung SH (1984). Release of endogenous Zn2+ from brain tissue during activity. *Nature* **308**, 734-736.

Barbour B (1993). Synaptic currents evoked in Purkinje cells by stimulating individual granule cells. *Neuron* **11**, 759-769.

Barriere H, Belfodil R, Rubera I, Tauc M, Lesage F, Poujeol C, Guy N, Barhanin J, & Poujeol P (2003). Role of TASK2 potassium channels regarding volume regulation in primary cultures of mouse proximal tubules. *J Gen Physiol* **122**, 177-190.

Batard P, Jordan M, & Wurm F (2001). Transfer of high copy number plasmid into mammalian cells by calcium phosphate transfection. *Gene* **270**, 61-68.

Bayliss DA, Sirois JE, & Talley EM (2003). The TASK family: two-pore domain background K+ channels. *Mol Interv* **3**, 205-219.

Bayliss DA, Talley EM, Sirois JE, & Lei Q (2001). TASK-1 is a highly modulated pH-sensitive 'leak' K(+) channel expressed in brainstem respiratory neurons. *Respir Physiol* **129**, 159-174.

Berg AP, Talley EM, Manger JP, & Bayliss DA (2004a). Motoneurons express heteromeric TWIK-related acid-sensitive K+ (TASK) channels containing TASK-1 (KCNK3) and TASK-3 (KCNK9) subunits. *J Neurosci* **24**, 6693-6702.

Bernstein J (1902). Untersuchungen zur Thermodynamik der bioelektrischen Ströme. Erster Theil. *Plugers Arch.* 92:521-562.

Biswas S, Chida AS, & Rahman I (2006). Redox modifications of protein-thiols: emerging roles in cell signaling. *Biochem Pharmacol* **71**, 551-564.

Bockenhauer D, Zilberberg N, & Goldstein SA (2001). KCNK2: reversible conversion of a hippocampal potassium leak into a voltage-dependent channel. *Nat Neurosci* **4**, 486-491.

Braitenberg V & Atwood RP (1958). Morphological observations on the cerebellar cortex. *J Comp Neurol* **109**, 1-33.

Brickley SG, Aller MI, Sandu C, Veale EL, Alder FG, Sambi H, Mathie A, & Wisden W (2007). TASK-3 two-pore domain potassium channels enable sustained high-frequency firing in cerebellar granule neurons. *J Neurosci* **27**, 9329-9340.

Brickley SG, Revilla V, Cull-Candy SG, Wisden W, & Farrant M (2001). Adaptive regulation of neuronal excitability by a voltage-independent potassium conductance. *Nature* **409**, 88-92.

Buckler KJ, Williams BA, & Honore E (2000). An oxygen-, acid- and anaesthetic-sensitive TASK-like background potassium channel in rat arterial chemoreceptor cells. *J Physiol* **525 Pt 1**, 135-142.

Campanucci VA, Brown ST, Hudasek K, O'Kelly IM, Nurse CA, & Fearon IM (2005). O2 sensing by recombinant TWIK-related halothane-inhibitable K+ channel-1 background K+ channels heterologously expressed in human embryonic kidney cells. *Neuroscience* **135**, 1087-1094.

Cavallini D, De MC, Dupre S, & Rotilio G (1969a). The copper catalyzed oxidation of cysteine to cystine. *Arch Biochem Biophys* **130**, 354-361.

Chadderton P, Margrie TW, & Hausser M (2004). Integration of quanta in cerebellar granule cells during sensory processing. *Nature* **428**, 856-860.

Chalfie M, Tu Y, Euskirchen G, Ward WW, & Prasher DC (1994). Green fluorescent protein as a marker for gene expression. *Science* **263**, 802-805.

Chapman CG, Meadows HJ, Godden RJ, Campbell DA, Duckworth M, Kelsell RE, Murdock PR, Randall AD, Rennie GI, & Gloger IS (2000). Cloning, localisation and functional expression of a novel human, cerebellum specific, two pore domain potassium channel. *Brain Res Mol Brain Res* **82**, 74-83.

Chavez RA, Gray AT, Zhao BB, Kindler CH, Mazurek MJ, Mehta Y, Forsayeth JR, & Yost CS (1999). TWIK-2, a new weak inward rectifying member of the tandem pore domain potassium channel family. *J Biol Chem* **%19;274**, 7887-7892.

Chemin J, Girard C, Duprat F, Lesage F, Romey G, & Lazdunski M (2003). Mechanisms underlying excitatory effects of group I metabotropic glutamate receptors via inhibition of 2P domain K+ channels. *EMBO J* **22**, 5403-5411.

Chemin J, Patel A, Duprat F, Zanzouri M, Lazdunski M, & Honore E (2005a). Lysophosphatidic acid-operated K+ channels. *J Biol Chem* **280**, 4415-4421.

Chemin J, Patel AJ, Duprat F, Lauritzen I, Lazdunski M, & Honore E (2005b). A phospholipid sensor controls mechanogating of the K+ channel TREK-1. *EMBO J* **24**, 44-53.

Chen C & Okayama H (1987). High-efficiency transformation of mammalian cells by plasmid DNA. *Mol Cell Biol* **7**, 2745-2752.

Chen X, Talley EM, Patel N, Gomis A, McIntire WE, Dong B, Viana F, Garrison JC, & Bayliss DA (2006). Inhibition of a background potassium channel by Gq protein alpha-subunits. *Proc Natl Acad Sci U S A* **103**, 3422-3427.

Choe S. (2002) Potassium channel structures *Nat Rev Neurosci.* **3**, 115 - 121

Clarke G M, (1990) *'Statistics and Experimental Design'*, 2nd Edition, Edward Arnold

Clarke CE, Veale EL, Green PJ, Meadows HJ, & Mathie A (2004). Selective block of the human 2-P domain potassium channel, TASK-3, and the native leak potassium current, IKSO, by zinc. *J Physiol* **560**, 51-62.

Cole KS & Curtis HJ. Electrical Impedance of the squid giant axon during activity. J.Gen.Physiol 22, 649-670. 1939.
Ref Type: Generic

Cotten JF, Zou HL, Liu C, Au JD, & Yost CS (2004a). Identification of native rat cerebellar granule cell currents due to background K channel KCNK5 (TASK-2). *Brain Res Mol Brain Res* **128**, 112-120.

Czirjak G & Enyedi P (2002a). Formation of functional heterodimers between the TASK-1 and TASK-3 two-pore domain potassium channel subunits. *J Biol Chem* **277**, 5426-5432.

Czirjak G & Enyedi P (2002b). TASK-3 dominates the background potassium conductance in rat adrenal glomerulosa cells. *Mol Endocrinol* **16**, 621-629.

Czirjak G & Enyedi P (2003). Ruthenium red inhibits TASK-3 potassium channel by interconnecting glutamate 70 of the two subunits. *Mol Pharmacol* **63**, 646-652.

Czirjak G & Enyedi P (2006). Zinc and mercuric ions distinguish TRESK from the other two-pore-domain K+ channels. *Mol Pharmacol* **69**, 1024-1032.

Czirjak G, Fischer T, Spat A, Lesage F, & Enyedi P (2000). TASK (TWIK-related acid-sensitive K+ channel) is expressed in glomerulosa cells of rat adrenal cortex and inhibited by angiotensin II. *Mol Endocrinol* **14**, 863-874.

Czirjak G, Petheo GL, Spat A, & Enyedi P (2001). Inhibition of TASK-1 potassium channel by phospholipase C. *Am J Physiol Cell Physiol* **281**, C700-C708.

Czirjak G, Toth ZE, & Enyedi P (2004). The two-pore domain K+ channel, TRESK, is activated by the cytoplasmic calcium signal through calcineurin. *J Biol Chem* **279**, 18550-18558.

D'Angelo E, De FG, Rossi P, & Taglietti V (1995). Synaptic excitation of individual rat cerebellar granule cells in situ: evidence for the role of NMDA receptors. *J Physiol* **484 (Pt 2)**, 397-413.

D'Angelo E, Nieus T, Maffei A, Armano S, Rossi P, Taglietti V, Fontana A, & Naldi G (2001). Theta-frequency bursting and resonance in cerebellar granule cells: experimental evidence and modeling of a slow k+-dependent mechanism. *J Neurosci* **21**, 759-770.

Decher N, Maier M, Dittrich W, Gassenhuber J, Bruggemann A, Busch AE, & Steinmeyer K (2001). Characterization of TASK-4, a novel member of the pH-sensitive, two-pore domain potassium channel family. *FEBS Lett* **492**, 84-89.

Doyle D, Cabral JM, Pfuetzner RA, Kuo A, Gulbis JM, Cohen SL, Chait BT, MacKinnon R (1998) The Structure of the Potassium Channel: Molecular Basis of K1 Conduction and Selectivity. *Science* **280**; 69-77

Duprat F, Girard C, Jarretou G, & Lazdunski M (2005). Pancreatic two P domain K+ channels TALK-1 and TALK-2 are activated by nitric oxide and reactive oxygen species. *J Physiol* **562**, 235-244.

Duprat F, Lesage F, Fink M, Reyes R, Heurteaux C, & Lazdunski M (1997a). TASK, a human background K+ channel to sense external pH variations near physiological pH. *EMBO J* **16**, 5464-5471.

Eccles JC, Llinas R, & Sasaki K (1966). The mossy fibre-granule cell relay of the cerebellum and its inhibitory control by Golgi cells. *Exp Brain Res* **1**, 82-101.

Engelman DM, (2005). Membranes are more mosaic than fluid. *Nature* **438,** 578-580.

Enyeart JJ, Xu L, & Enyeart JA (2002). Dual actions of lanthanides on ACTH-inhibited leak K(+) channels. *Am J Physiol Endocrinol Metab* **282**, E1255-E1266.

Feliciangeli S, Bendahhou S, Sandoz G, Gounon P, Reichold M, Warth R, Lazdunski M, Barhanin J, & Lesage F (2007). Does sumoylation control K2P1/TWIK1 background K+ channels? *Cell* **130**, 563-569.

Fink M, Duprat F, Lesage F, Reyes R, Romey G, Heurteaux C, & Lazdunski M (1996). Cloning, functional expression and brain localization of a novel unconventional outward rectifier K+ channel. *EMBO J* **15**, 6854-6862.

Fink M, Lesage F, Duprat F, Heurteaux C, Reyes R, Fosset M, & Lazdunski M (1998). A neuronal two P domain K+ channel stimulated by arachidonic acid and polyunsaturated fatty acids. *EMBO J* **17**, 3297-3308.

Frederickson CJ & Moncrieff DW (1994). Zinc-containing neurons. *Biol Signals* **3**, 127-139.

Gabbiani F, Midtgaard J, & Knopfel T (1994). Synaptic integration in a model of cerebellar granule cells. *J Neurophysiol* **72**, 999-1009.

Gerstin KM, Gong DH, Abdallah M, Winegar BD, Eger EI, & Gray AT (2003). Mutation of KCNK5 or Kir3.2 potassium channels in mice does not change minimum alveolar anesthetic concentration. *Anesth Analg* **96**, 1345-9, table.

Ghez C (1991) The Cerebellum in Kandel ER, Schwarz JH, Jessel TM, *Principles of Neural Science* 3rd edition, Appleton and Lange pp 626 – 626.

Girard C, Duprat F, Terrenoire C, Tinel N, Fosset M, Romey G, Lazdunski M, & Lesage F (2001). Genomic and functional characteristics of novel human pancreatic 2P domain K(+) channels. *Biochem Biophys Res Commun* **282**, 249-256.

Goldstein S & Czapski G (1984). Mannitol as an OH. scavenger in aqueous solutions and in biological systems. *Int J Radiat Biol Relat Stud Phys Chem Med* **46**, 725-729.

Goldstein SA, Bayliss DA, Kim D, Lesage F, Plant LD, & Rajan S (2005). International Union of Pharmacology. LV. Nomenclature and molecular relationships of two-P potassium channels. *Pharmacol Rev* **57**, 527-540.

Goldstein SA, Bockenhauer D, O'Kelly I, & Zilberberg N (2001). Potassium leak channels and the KCNK family of two-P-domain subunits. *Nat Rev Neurosci* **2**, 175-184.

Goldstein SA, Price LA, Rosenthal DN, & Pausch MH (1996). ORK1, a potassium-selective leak channel with two pore domains cloned from Drosophila melanogaster by expression in Saccharomyces cerevisiae. *Proc Natl Acad Sci U S A* **93**, 13256-13261.

Gozlan H & Ben-Ari Y (1995). NMDA receptor redox sites: are they targets for selective neuronal protection? *Trends Pharmacol Sci* **16**, 368-374.

Graham FL, Smiley J, Russell WC, & Nairn R (1977). Characteristics of a human cell line transformed by DNA from human adenovirus type 5. *J Gen Virol* **36**, 59-74.

Gray AT, Winegar BD, Leonoudakis DJ, Forsayeth JR, & Yost CS (1998). TOK1 is a volatile anesthetic stimulated K+ channel. *Anesthesiology* **88**, 1076-1084.

Gray AT, Zhao BB, Kindler CH, Winegar BD, Mazurek MJ, Xu J, Chavez RA, Forsayeth JR, & Yost CS (2000). Volatile anesthetics activate the human tandem pore domain baseline K+ channel KCNK5. *Anesthesiology* **92**, 1722-1730.

Gruss M, Mathie A, Lieb WR, & Franks NP (2004). The two-pore-domain K(+) channels TREK-1 and TASK-3 are differentially modulated by copper and zinc. *Mol Pharmacol* **66**, 530-537.

Gu W, Schlichthorl G, Hirsch JR, Engels H, Karschin C, Karschin A, Derst C, Steinlein OK, & Daut J (2002). Expression pattern and functional characteristics of two novel splice variants of the two-pore-domain potassium channel TREK-2. *J Physiol* **539**, 657-668.

Haigh CL & Brown DR (2006). Prion protein reduces both oxidative and non-oxidative copper toxicity. *J Neurochem* **98**, 677-689.

Halliwell B (2006). Oxidative stress and neurodegeneration: where are we now? *J Neurochem* **97**, 1634-1658.

Halliwell B (1992). Reactive oxygen species and the central nervous system. *J Neurochem* **59**, 1609-1623.

Hamill OP, Marty A, Neher E, Sakmann B, & Sigworth FJ (1981). Improved patch-clamp techniques for high-resolution current recording from cells and cell-free membrane patches. *Pflugers Arch* **391**, 85-100.

Han J, Gnatenco C, Sladek CD, & Kim D (2003a). Background and tandem-pore potassium channels in magnocellular neurosecretory cells of the rat supraoptic nucleus. *J Physiol* **546**, 625-639.

Han J, Kang D, & Kim D (2003b). Functional properties of four splice variants of a human pancreatic tandem-pore K+ channel, TALK-1. *Am J Physiol Cell Physiol* **285**, C529-C538.

Han J, Truell J, Gnatenco C, & Kim D (2002a). Characterization of four types of background potassium channels in rat cerebellar granule neurons. *J Physiol* **542**, 431-444.

Harkins AB & Fox AP (2002). Cell death in weaver mouse cerebellum. *Cerebellum* **1**, 201-206.

Hartter DE & Barnea A (1988). Evidence for release of copper in the brain: depolarization-induced release of newly taken-up 67copper. *Synapse* **2**, 412-415.

Hevers W & Luddens H (2002). Pharmacological heterogeneity of gamma-aminobutyric acid receptors during development suggests distinct classes of rat cerebellar granule cells in situ. *Neuropharmacology* **42**, 34-47.

Hille B (2001) *Ion Channels of Excitable Membranes*. 3rd Edition. Sinauer Associates, Inc

Hodgkin AL & Huxley AF (1952a). Movement of sodium and potassium ions during nervous activity. *Cold Spring Harb Symp Quant Biol* **17:43-52.**, 43-52.

Hodgkin AL & Huxley AF (1952b). Currents carried by sodium and potassium ions through the membrane of the giant axon of Loligo. *J Physiol* **116**, 449-472.

Hodgkin AL & Huxley AF (1952c). The components of membrane conductance in the giant axon of Loligo. *J Physiol* **116**, 473-496.

Hodgkin AL & Huxley AF (1952d). The dual effect of membrane potential on sodium conductance in the giant axon of Loligo. *J Physiol* **116**, 497-506.

Hodgkin AL & Huxley AF (1952e). A quantitative description of membrane current and its application to conduction and excitation in nerve. *J Physiol* **117**, 500-544.

Hodgkin AL & Huxley AF (1952f). Propagation of electrical signals along giant nerve fibers. *Proc R Soc Lond B Biol Sci* **140**, 177-183.

Hodgkin AL, Huxley AF, & Katz B (1952). Measurement of current-voltage relations in the membrane of the giant axon of Loligo. *J Physiol* **116**, 424-448.

Horning MS & Trombley PQ (2001). Zinc and copper influence excitability of rat olfactory bulb neurons by multiple mechanisms. *J Neurophysiol* **86**, 1652-1660.

Ito M (2006). Cerebellar circuitry as a neuronal machine. *Prog Neurobiol* **78**, 272-303.

Ito M (1970). Neurophysiological aspects of the cerebellar motor control system. *Int J Neurol* **7**, 162-176.

Ito M & Kano M (1982). Long-lasting depression of parallel fiber-Purkinje cell transmission induced by conjunctive stimulation of parallel fibers and climbing fibers in the cerebellar cortex. *Neurosci Lett* **33**, 253-258.

Kachur AV, Koch CJ, & Biaglow JE (1999a). Mechanism of copper-catalyzed autoxidation of cysteine. *Free Radic Res* **31**, 23-34.

Kang D, Choe C, Cavanaugh E, & Kim D (2007). Properties of single two-pore domain TREK-2 channels expressed in mammalian cells. *J Physiol* **583**, 57-69.

Kang D, Choe C, & Kim D (2005). Thermosensitivity of the two-pore domain K+ channels TREK-2 and TRAAK. *J Physiol* **564**, 103-116.

Kang D, Han J, Talley EM, Bayliss DA, & Kim D (2004a). Functional expression of TASK-1/TASK-3 heteromers in cerebellar granule cells. *J Physiol* **554**, 64-77.

Kang D & Kim D (2004). Single-channel properties and pH sensitivity of two-pore domain K+ channels of the TALK family. *Biochem Biophys Res Commun* **315**, 836-844.

Kang D, Mariash E, & Kim D (2004b). Functional expression of TRESK-2, a new member of the tandem-pore K+ channel family. *J Biol Chem* **279**, 28063-28070.

Kardos J, Kovacs I, Hajos F, Kalman M, & Simonyi M (1989). Nerve endings from rat brain tissue release copper upon depolarization. A possible role in regulating neuronal excitability. *Neurosci Lett* **103**, 139-144.

Karschin C, Wischmeyer E, Preisig-Muller R, Rajan S, Derst C, Grzeschik KH, Daut J, & Karschin A (2001). Expression pattern in brain of TASK-1, TASK-3, and a tandem pore domain K(+) channel subunit, TASK-5, associated with the central auditory nervous system. *Mol Cell Neurosci* **18**, 632-648.

Kase M, Miller DC, & Noda H (1980). Discharges of Purkinje cells and mossy fibres in the cerebellar vermis of the monkey during saccadic eye movements and fixation. *J Physiol* **300**, 539-555.

Keshavaprasad B, Liu C, Au JD, Kindler CH, Cotten JF, & Yost CS (2005). Species-specific differences in response to anesthetics and other modulators by the K2P channel TRESK. *Anesth Analg* **101**, 1042-9, table.

Ketchum KA, Joiner WJ, Sellers AJ, Kaczmarek LK, & Goldstein SA (1995). A new family of outwardly rectifying potassium channel proteins with two pore domains in tandem. *Nature* **376**, 690-695.

Kim D (2005). Physiology and pharmacology of two-pore domain potassium channels. *Curr Pharm Des* **11**, 2717-2736.

Kim D & Gnatenco C (2001). TASK-5, a new member of the tandem-pore K(+) channel family. *Biochem Biophys Res Commun* **284**, 923-930.

Kim JS, Park JY, Kang HW, Lee EJ, Bang H, & Lee JH (2005). Zinc activates TREK-2 potassium channel activity. *J Pharmacol Exp Ther* **314**, 618-625.

Kim Y, Bang H, Gnatenco C, & Kim D (2001a). Synergistic interaction and the role of C-terminus in the activation of TRAAK K+ channels by pressure, free fatty acids and alkali. *Pflugers Arch* **442**, 64-72.

Kim Y, Bang H, & Kim D (2000). TASK-3, a new member of the tandem pore K(+) channel family. *J Biol Chem* **275**, 9340-9347.

Kim Y, Bang H, & Kim D (1999). TBAK-1 and TASK-1, two-pore K(+) channel subunits: kinetic properties and expression in rat heart. *Am J Physiol* **277**, H1669-H1678.

Kim Y, Gnatenco C, Bang H, & Kim D (2001b). Localization of TREK-2 K+ channel domains that regulate channel kinetics and sensitivity to pressure, fatty acids and pHi. *Pflugers Arch* **442**, 952-960.

Kim Y, Lee SH, & Ho WK (2007). Hydrogen peroxide selectively increases TREK-2 currents via myosin light chain kinases. *Front Biosci* **12**, 1642-1650.

Kirichok Y, Krapivinsky G, & Clapham DE (2004). The mitochondrial calcium uniporter is a highly selective ion channel. *Nature* **427**, 360-364.

Kocha T, Yamaguchi M, Ohtaki H, Fukuda T, & Aoyagi T (1997). Hydrogen peroxide-mediated degradation of protein: different oxidation modes of copper- and iron-dependent hydroxyl radicals on the degradation of albumin. *Biochim Biophys Acta* **1337**, 319-326.

Koh SD, Monaghan K, Sergeant GP, Ro S, Walker RL, Sanders KM, & Horowitz B (2001). TREK-1 regulation by nitric oxide and cGMP-dependent protein kinase. An essential role in smooth muscle inhibitory neurotransmission. *J Biol Chem* **276**, 44338-44346.

Kozma M, Szerdahelyi P, & Kasa P (1981). Histochemical detection of zinc and copper in various neurons of the central nervous system. *Acta Histochem* **69**, 12-17.

Krężel A, Lesniak W, Jezowska-Bojczuk M, Mlynarz P, Brasun J, Kozlowski H, & Bal W (2001). Coordination of heavy metals by dithiothreitol, a commonly used thiol group protectant. *J Inorg Biochem* **84**, 77-88.

Lansman JB (1990). Blockade of current through single calcium channels by trivalent lanthanide cations. Effect of ionic radius on the rates of ion entry and exit. *J Gen Physiol* **95**, 679-696.

Larsen WJ (1998), *Essentials of Human Embryology* 1st Edition, Churchill Livingstone Inc.

Lee DH, O'Connor TR, & Pfeifer GP (2002). Oxidative DNA damage induced by copper and hydrogen peroxide promotes CG-->TT tandem mutations at methylated CpG dinucleotides in nucleotide excision repair-deficient cells. *Nucleic Acids Res* **30**, 3566-3573.

Leonoudakis D, Gray AT, Winegar BD, Kindler CH, Harada M, Taylor DM, Chavez RA, Forsayeth JR, & Yost CS (1998). An open rectifier potassium channel with two pore domains in tandem cloned from rat cerebellum. *J Neurosci* **18**, 868-877.

Lesage F, Guillemare E, Fink M, Duprat F, Lazdunski M, Romey G, & Barhanin J (1996). TWIK-1, a ubiquitous human weakly inward rectifying K+ channel with a novel structure. *EMBO J* **15**, 1004-1011.

Lesage F, Lauritzen I, Duprat F, Reyes R, Fink M, Heurteaux C, & Lazdunski M (1997). The structure, function and distribution of the mouse TWIK-1 K+ channel. *FEBS Lett* **402**, 28-32.

Lesage F & Lazdunski M (2000). Molecular and functional properties of two-pore-domain potassium channels. *Am J Physiol Renal Physiol* **279**, F793-F801.

Lesage F, Terrenoire C, Romey G, & Lazdunski M (2000). Human TREK2, a 2P domain mechano-sensitive K+ channel with multiple regulations by polyunsaturated fatty acids, lysophospholipids, and Gs, Gi, and Gq protein-coupled receptors. *J Biol Chem* **275**, 28398-28405.

Linden AM, Aller MI, Leppa E, Vekovischeva O, itta-Aho T, Veale EL, Mathie A, Rosenberg P, Wisden W, & Korpi ER (2006). The in vivo contributions of TASK-1-containing channels to the actions of inhalation anesthetics, the alpha(2) adrenergic sedative dexmedetomidine, and cannabinoid agonists. *J Pharmacol Exp Ther* **317**, 615-626.

Linder MC, Wooten L, Cerveza P, Cotton S, Shulze R, & Lomeli N (1998). Copper transport. *Am J Clin Nutr* **67**, 965S-971S.

Liu C, Au JD, Zou HL, Cotten JF, & Yost CS (2004). Potent activation of the human tandem pore domain K channel TRESK with clinical concentrations of volatile anesthetics. *Anesth Analg* **99**, 1715-22, table.

Liu N, Lo LS, Askary SH, Jones L, Kidane TZ, Nguyen TT, Goforth J, Chu YH, Vivas E, Tsai M, Westbrook T, & Linder MC (2007). Transcuprein is a macroglobulin regulated by copper and iron availability. *J Nutr Biochem.*

Llinás RR, Walton, KD (1998) Cerebellum in Shepard G M (ed), *Synaptic Organisation of the Brain: An Introduction*, 4th edition, Oxford University Press, pp 255-288

Lopes CM, Gallagher PG, Buck ME, Butler MH, & Goldstein SA (2000b). Proton block and voltage gating are potassium-dependent in the cardiac leak channel Kcnk3. *J Biol Chem* **275**, 16969-16978.

Lopes CM, Rohacs T, Czirjak G, Balla T, Enyedi P, & Logothetis DE (2005). PIP2 hydrolysis underlies agonist-induced inhibition and regulates voltage gating of two-pore domain K+ channels. *J Physiol* **564**, 117-129.

Lopes CM, Zilberberg N, & Goldstein SA (2001). Block of Kcnk3 by protons. Evidence that 2-P-domain potassium channel subunits function as homodimers. *J Biol Chem* **276**, 24449-24452.

Lotshaw DP (2007). Biophysical, pharmacological, and functional characteristics of cloned and native mammalian two-pore domain K+ channels. *Cell Biochem Biophys* **47**, 209-256.

Lotshaw DP (2006). Biophysical and pharmacological characteristics of native two-pore domain TASK channels in rat adrenal glomerulosa cells. *J Membr Biol* **210**, 51-70.

MacKinnon R (1991). Determination of the subunit stoichiometry of a voltage-activated potassium channel. *Nature* 350, 232

Maingret F, Fosset M, Lesage F, Lazdunski M, & Honore E (1999a). TRAAK is a mammalian neuronal mechano-gated K+ channel. *J Biol Chem* **274**, 1381-1387.

Maingret F, Honore E, Lazdunski M, & Patel AJ (2002). Molecular basis of the voltage-dependent gating of TREK-1, a mechano-sensitive K(+) channel. *Biochem Biophys Res Commun* **292**, 339-346.

Maingret F, Lauritzen I, Patel AJ, Heurteaux C, Reyes R, Lesage F, Lazdunski M, & Honore E (2000). TREK-1 is a heat-activated background K(+) channel. *EMBO J* **19**, 2483-2491.

Maingret F, Patel AJ, Lazdunski M, & Honore E (2001). The endocannabinoid anandamide is a direct and selective blocker of the background K(+) channel TASK-1. *EMBO J* **20**, 47-54.

Maingret F, Patel AJ, Lesage F, Lazdunski M, & Honore E (1999b). Mechano- or acid stimulation, two interactive modes of activation of the TREK-1 potassium channel. *J Biol Chem* **274**, 26691-26696.

Malecot CO, Bito V, & Argibay JA (1998). Ruthenium red as an effective blocker of calcium and sodium currents in guinea-pig isolated ventricular heart cells. *Br J Pharmacol* **124**, 465-472.

Marr D (1969). A theory of cerebellar cortex. *J Physiol* **202**, 437-470.

Mathie A, Sutton GL, Clarke CE, & Veale EL (2006). Zinc and copper: pharmacological probes and endogenous modulators of neuronal excitability. *Pharmacol Ther* **111**, 567-583.

Matlib MA, Zhou Z, Knight S, Ahmed S, Choi KM, Krause-Bauer J, Phillips R, Altschuld R, Katsube Y, Sperelakis N, & Bers DM (1998). Oxygen-bridged dinuclear ruthenium amine complex specifically inhibits Ca2+ uptake into mitochondria in vitro and in situ in single cardiac myocytes. *J Biol Chem* **273**, 10223-10231.

Maylie J & Adelman JP (2001). Beam me up, Scottie! TREK channels swing both ways. *Nat Neurosci* **4**, 457-458.

Meadows HJ, Chapman CG, Duckworth DM, Kelsell RE, Murdock PR, Nasir S, Rennie G, & Randall AD (2001). The neuroprotective agent sipatrigine (BW619C89) potently inhibits the human tandem pore-domain K(+) channels TREK-1 and TRAAK. *Brain Res* **892**, 94-101.

Meadows HJ & Randall AD (2001). Functional characterisation of human TASK-3, an acid-sensitive two-pore domain potassium channel. *Neuropharmacology* **40**, 551-559.

Medhurst AD, Rennie G, Chapman CG, Meadows H, Duckworth MD, Kelsell RE, Gloger II, & Pangalos MN (2001). Distribution analysis of human two pore domain potassium channels in tissues of the central nervous system and periphery. *Brain Res Mol Brain Res* **86**, 101-114.

Millar JA, Barratt L, Southan AP, Page KM, Fyffe RE, Robertson B, & Mathie A (2000). A functional role for the two-pore domain potassium channel TASK-1 in cerebellar granule neurons. *Proc Natl Acad Sci U S A* **97**, 3614-3618.

Miller C (2000). An overview of the potassium channel family. *Genome Biol* Vol **1** pt 4 1-5

Mlinar B & Enyeart JJ (1993). Block of current through T-type calcium channels by trivalent metal cations and nickel in neural rat and human cells. *J Physiol* **469**, 639-652.

Morton MJ, Abohamed A, Sivaprasadarao A, & Hunter M (2005). pH sensing in the two-pore domain K+ channel, TASK2. *Proc Natl Acad Sci U S A* **102**, 16102-16106.

Morton MJ, O'Connell AD, Sivaprasadarao A, & Hunter M (2003). Determinants of pH sensing in the two-pore domain K(+) channels TASK-1 and -2. *Pflugers Arch* **445**, 577-583.

Munday R, Munday CM, & Winterbourn CC (2004). Inhibition of copper-catalyzed cysteine oxidation by nanomolar concentrations of iron salts. *Free Radic Biol Med* **36**, 757-764.

Musset B, Meuth SG, Liu GX, Derst C, Wegner S, Pape HC, Budde T, Preisig-Muller R, & Daut J (2006). Effects of divalent cations and spermine on the K+ channel TASK-3 and on the outward current in thalamic neurons. *J Physiol* **572**, 639-657.

Neher E & Sakmann B (1976). Single-channel currents recorded from membrane of denervated frog muscle fibres. *Nature* **260**, 799-802.

Nicholls JG, Martin AR, Wallace BG (1992) *From Neuron to brain* 3rd edition.

Niemeyer MI, Cid LP, Barros LF, & Sepulveda FV (2001). Modulation of the two-pore domain acid-sensitive K+ channel TASK-2 (KCNK5) by changes in cell volume. *J Biol Chem* **276**, 43166-43174.

O'Kelly I, Butler MH, Zilberberg N, & Goldstein SA (2002). Forward transport. 14-3-3 binding overcomes retention in endoplasmic reticulum by dibasic signals. *Cell* **111**, 577-588.

Ono S, Koropatnick DJ, & Cherian MG (1997). Regional brain distribution of metallothionein, zinc and copper in toxic milk mutant and transgenic mice. *Toxicology* **124**, 1-10.

Orias M, Velazquez H, Tung F, Lee G, & Desir GV (1997). Cloning and localization of a double-pore K channel, KCNK1: exclusive expression in distal nephron segments. *Am J Physiol* **273**, F663-F666.

Ozaita A & Vega-Saenz de ME (2002). Cloning of two transcripts, HKT4.1a and HKT4.1b, from the human two-pore K+ channel gene KCNK4. Chromosomal localization, tissue distribution and functional expression. *Brain Res Mol Brain Res* **102**, 18-27.

Patel AJ, Honore E, Lesage F, Fink M, Romey G, & Lazdunski M (1999). Inhalational anesthetics activate two-pore-domain background K+ channels. *Nat Neurosci* **2**, 422-426.

Patel AJ, Honore E, Maingret F, Lesage F, Fink M, Duprat F, & Lazdunski M (1998). A mammalian two pore domain mechano-gated S-like K+ channel. *EMBO J* **17**, 4283-4290.

Patel AJ, Lazdunski M, & Honore E (2001). Lipid and mechano-gated 2P domain K(+) channels. *Curr Opin Cell Biol* **13**, 422-428.

Phillips W D, (1997) Transfection in Cell Cultures, In Martin, R (ed) *Neuroscience Methods; A Guide for Advanced Students,* Harwood Academic Publishers. pp 192-202

Plant LD, Rajan S, & Goldstein SA (2005). K2P channels and their protein partners. *Curr Opin Neurobiol* **15**, 326-333.

Rajan S, Plant LD, Rabin ML, Butler MH, & Goldstein SA (2005). Sumoylation silences the plasma membrane leak K+ channel K2P1. *Cell* **121**, 37-47.

Rajan S, Preisig-Muller R, Wischmeyer E, Nehring R, Hanley PJ, Renigunta V, Musset B, Schlichthorl G, Derst C, Karschin A, & Daut J (2002). Interaction with 14-3-3 proteins promotes functional expression of the potassium channels TASK-1 and TASK-3. *J Physiol* **545**, 13-26.

Rajan S, Wischmeyer E, Karschin C, Preisig-Muller R, Grzeschik KH, Daut J, Karschin A, & Derst C (2001). THIK-1 and THIK-2, a novel subfamily of tandem pore domain K+ channels. *J Biol Chem* **276**, 7302-7311.

Rajan S, Wischmeyer E, Xin LG, Preisig-Muller R, Daut J, Karschin A, & Derst C (2000). TASK-3, a novel tandem pore domain acid-sensitive K+ channel. An extracellular histiding as pH sensor. *J Biol Chem* **275**, 16650-16657.

Redondo PC, Salido GM, Rosado JA, & Pariente JA (2004). Effect of hydrogen peroxide on Ca2+ mobilisation in human platelets through sulphydryl oxidation dependent and independent mechanisms. *Biochem Pharmacol* **67**, 491-502.

Renigunta V, Yuan H, Zuzarte M, Rinne S, Koch A, Wischmeyer E, Schlichthorl G, Gao Y, Karschin A, Jacob R, Schwappach B, Daut J, & Preisig-Muller R (2006). The retention factor p11 confers an endoplasmic reticulum-localization signal to the potassium channel TASK-1. *Traffic* **7**, 168-181.

Reyes R, Duprat F, Lesage F, Fink M, Salinas M, Farman N, & Lazdunski M (1998). Cloning and expression of a novel pH-sensitive two pore domain K+ channel from human kidney. *J Biol Chem* **273**, 30863-30869.

Rigo A, Corazza A, di Paolo ML, Rossetto M, Ugolini R, & Scarpa M (2004). Interaction of copper with cysteine: stability of cuprous complexes and catalytic role of cupric ions in anaerobic thiol oxidation. *J Inorg Biochem* **98**, 1495-1501.

Rusznak Z, Pocsai K, Kovacs I, Por A, Pal B, Biro T, & Szucs G (2004). Differential distribution of TASK-1, TASK-2 and TASK-3 immunoreactivities in the rat and human cerebellum. *Cell Mol Life Sci* **61**, 1532-1542.

Sakurai M (1987). Synaptic modification of parallel fibre-Purkinje cell transmission in in vitro guinea-pig cerebellar slices. *J Physiol* **394**, 463-480.

Salama G, Abramson JJ, & Pike GK (1992). Sulphydryl reagents trigger Ca2+ release from the sarcoplasmic reticulum of skinned rabbit psoas fibres. *J Physiol* **454**, 389-420.

Salinas M, Reyes R, Lesage F, Fosset M, Heurteaux C, Romey G, & Lazdunski M (1999). Cloning of a new mouse two-P domain channel subunit and a human homologue with a unique pore structure. *J Biol Chem* **274**, 11751-11760.

Sanchez R, Riddle M, Woo J, Momand J (2008) Prediction of reversibly oxidized protein cysteine thiols using protein structure properties *Protein Science* **17**, 473-481

Sano Y, Inamura K, Miyake A, Mochizuki S, Kitada C, Yokoi H, Nozawa K, Okada H, Matsushime H, & Furuichi K (2003). A novel two-pore domain K+ channel, TRESK, is localized in the spinal cord. *J Biol Chem* **278**, 27406-27412.

Schumann K, Classen HG, Dieter HH, Konig J, Multhaup G, Rukgauer M, Summer KH, Bernhardt J, & Biesalski HK (2002). Hohenheim consensus workshop: copper. *Eur J Clin Nutr* **56**, 469-483.

Sejnowski TJ (1977). Statistical constraints on synaptic plasticity. *J Theor Biol* **69**, 385-389.

Seyfarth EA (2006). Julius Bernstein (1839-1917): pioneer neurobiologist and biophysicist. *Biol Cybern* **94**, 2-8.

Shen B, Jensen RG, & Bohnert HJ (1997). Mannitol Protects against Oxidation by Hydroxyl Radicals. *Plant Physiol* **115**, 527-532.

Sims RE & Hartell NA (2005). Differences in transmission properties and susceptibility to long-term depression reveal functional specialization of ascending axon and parallel fiber synapses to Purkinje cells. *J Neurosci* **25**, 3246-3257.

Singer SJ & Nicolson GL (1972). The fluid mosaic model of the structure of cell membranes. *Science* **175**, 720-731.

Sirois JE, Lei Q, Talley EM, Lynch C, III, & Bayliss DA (2000). The TASK-1 two-pore domain K+ channel is a molecular substrate for neuronal effects of inhalation anesthetics. *J Neurosci* **20**, 6347-6354.

Szabadkai G, Varnai P, & Enyedi P (1999). Selective inhibition of potassium-stimulated rat adrenal glomerulosa cells by ruthenium red. *Biochem Pharmacol* **57**, 209-218.

Takeda A (2000). Movement of zinc and its functional significance in the brain. *Brain Res Brain Res Rev* **34**, 137-148.

Talley EM & Bayliss DA (2002). Modulation of TASK-1 (Kcnk3) and TASK-3 (Kcnk9) potassium channels: volatile anesthetics and neurotransmitters share a molecular site of action. *J Biol Chem* **277**, 17733-17742.

Talley EM, Lei Q, Sirois JE, & Bayliss DA (2000). TASK-1, a two-pore domain K+ channel, is modulated by multiple neurotransmitters in motoneurons. *Neuron* **25**, 399-410.

Talley EM, Sirois JE, Lei Q, & Bayliss DA (2003). Two-pore-Domain (KCNK) potassium channels: dynamic roles in neuronal function. *Neuroscientist* **9**, 46-56.

Talley EM, Solorzano G, Lei Q, Kim D, & Bayliss DA (2001). Cns distribution of members of the two-pore-domain (KCNK) potassium channel family. *J Neurosci* **21**, 7491-7505.

Tan JH, Liu W, & Saint DA (2002). Trek-like potassium channels in rat cardiac ventricular myocytes are activated by intracellular ATP. *J Membr Biol* **185**, 201-207.

Tapiero H, Townsend DM, & Tew KD (2003). Trace elements in human physiology and pathology. Copper. *Biomed Pharmacother* **57**, 386-398.

Tarohda T, Yamamoto M, & Amamo R (2004). Regional distribution of manganese, iron, copper, and zinc in the rat brain during development. *Anal Bioanal Chem* **380**, 240-246.

Terrenoire C, Lauritzen I, Lesage F, Romey G, & Lazdunski M (2001). A TREK-1-like potassium channel in atrial cells inhibited by beta-adrenergic stimulation and activated by volatile anesthetics. *Circ Res* **89**, 336-342.

Veale EL, Buswell R, Clarke CE, & Mathie A (2007a). Identification of a region in the TASK3 two pore domain potassium channel that is critical for its blockade by methanandamide. *Br J Pharmacol* . **152** (5): 778 - 786

Veale EL, Kennard LE, Sutton GL, Mackenzie G, Sandu C, & Mathie A (2007b). G(alpha)q-mediated regulation of TASK3 two-pore domain potassium channels: the role of protein kinase C. *Mol Pharmacol* **71**, 1666-1675.

Vega-Saenz de ME, Lau DH, Zhadina M, Pountney D, Coetzee WA, & Rudy B (2001). KT3.2 and KT3.3, two novel human two-pore K^{+a} channels closely related to TASK-1. *J Neurophysiol* **86**, 130-142.

Velasco I & Tapia R (1997). Ruthenium red neurotoxicity and interaction with gangliosides in primary cortical cultures. *J Neurosci Res* **49**, 72-79.

Verkhratsky A, Krishtal OA, & Petersen OH (2006). From Galvani to patch clamp: the development of electrophysiology. *Pflugers Arch* **453**, 233-247.

Voogd J (2003). The human cerebellum. *J Chem Neuroanat* **26**, 243-252.

Warth R, Barriere H, Meneton P, Bloch M, Thomas J, Tauc M, Heitzmann D, Romeo E, Verrey F, Mengual R, Guy N, Bendahhou S, Lesage F, Poujeol P, & Barhanin J (2004). Proximal renal tubular acidosis in TASK2 K+ channel-deficient mice reveals a mechanism for stabilizing bicarbonate transport. *Proc Natl Acad Sci U S A* **101**, 8215-8220.

Washburn CP, Sirois JE, Talley EM, Guyenet PG, & Bayliss DA (2002). Serotonergic raphe neurons express TASK channel transcripts and a TASK-like pH- and halothane-sensitive K+ conductance. *J Neurosci* **22**, 1256-1265.

Watkins CS & Mathie A (1996a). A non-inactivating K+ current sensitive to muscarinic receptor activation in rat cultured cerebellar granule neurons. *J Physiol* **491 (Pt 2)**, 401-412.

Watkins CS & Mathie A (1996b). Effects on K+ currents in rat cerebellar granule neurones of a membrane-permeable analogue of the calcium chelator BAPTA. *Br J Pharmacol* **118**, 1772-1778.

Williams BA & Buckler KJ (2004). Biophysical properties and metabolic regulation of a TASK-like potassium channel in rat carotid body type 1 cells. *Am J Physiol Lung Cell Mol Physiol* **286**, L221-L230.

Xu L, Tripathy A, Pasek DA, & Meissner G (1999). Ruthenium red modifies the cardiac and skeletal muscle Ca(2+) release channels (ryanodine receptors) by multiple mechanisms. *J Biol Chem* **274**, 32680-32691.

Ying WL, Emerson J, Clarke MJ, & Sanadi DR (1991). Inhibition of mitochondrial calcium ion transport by an oxo-bridged dinuclear ruthenium ammine complex. *Biochemistry* **30**, 4949-4952.

Zagon IS, McLaughlin PJ, & Smith S (1977). Neural populations in the human cerebellum: estimations from isolated cell nuclei. *Brain Res* **127**, 279-282.

Zigmond, M (1999) *Fundamental Neuroscience*, Academic Press